TAMPEREEN TEKNILLINEN YLIOPISTO

JANNE KOIVUMÄKI

VIRTUAL DECOMPOSITION CONTROL OF A HYDRAULIC MANIPULATOR

Masters of Science Thesis

Examiner: Professor Jouni Mattila
Examiner and topic approved in the Faculty of Automation, Mechanical and Material Engineering Council meeting on 15th of August 2012

ABSTRACT

TAMPERE UNIVERSITY OF TECHNOLOGY
Master's Degree Program in Automation
KOIVUMÄKI, JANNE:
Master of Science Thesis, 73 pages, 50 Appendix pages
November 2012
Major: Hydraulic Engineering
Examiner: Professor Jouni Mattila
Keywords: Robotics, Model-Based Control, Subsystem Dynamics Based Control, Virtual Stability, Rigid Body Dynamics, Hydraulic Cylinder, Cartesian Motion Control.

The controller design and modelling of hydraulically driven robots is a challenging task. This comes inter alia due to inherent nonlinear dynamics associated with hydraulic actuators, highly nonlinear characteristic of the robot dynamics and various uncertainties and disturbances of mathematical models.

In this master's thesis a new control theory, namely Virtual Decomposition Control (VDC), is studied. The VDC approach is developed especially for precision control of complex robots. In VDC approach the robotic system to be controlled is first virtually decomposed into subsystems. Then, the subsystems dynamics based control can be applied, to make each subsystem qualified to be virtually stable. Finally, the virtual stability of every subsystem results in the stability and convergence of entire robot. An effectiveness of this approach comes from the fact that no matter how complicated a robotic system is the dynamics of the subsystems remain relatively simple with fixed dynamic structures invariant to target systems.

The purpose of this thesis was to study and implement VDC into hydraulic 2-DOF manipulator actuated with hydraulic cylinders. The parameter adaptation for uncertain parameters was not studied in scope of this thesis. The objective of this thesis was also test performance of VDC-controller in practice and compare achieved results to corresponding PID-controller results.

The theory of VDC approach was successfully applied into studied manipulator and the L_2 and L_∞ stability of subsystems were mathematically guaranteed leading to stability of entire system. In experimental measurements certain Cartesian motion trajectory was driven with both VDC- and PID-controller. With VDC- controller roughly 7 times better piston position tracking performance was achieved for first cylinder and about 4.4 times better performance for second cylinder was achieved. Moreover, the very same Cartesian motion trajectory was driven with twice faster and half slower execution times. The stability of PID-controller was lost in both of these cases, whereas VDC-controller managed to drive these trajectories without problems.

TIIVISTELMÄ

TAMPEREEN TEKNILLINEN YLIOPISTO
Automaatiotekniikan koulutusohjelma
KOIVUMÄKI, JANNE:
Diplomityö, 73 sivua, 50 liitesivua
Marraskuu 2012
Pääaine: Hydraulitekniikka
Tarkastaja: Professori Jouni Mattila
Avainsanat: Robotiikka, Mallipohjainen säätö, Alijärjestelmien dynamiikkaan perustuva säätö, Virtuaalinen stabiilius, Jäykän kappaleen dynamiikka, Hydraulisylinteri, Karteesisen asema säätö.

Hydraulisten robottien säädön suunnittelu ja mallintaminen on tunnetusti haastava tehtävä. Tähän vaikuttavat muun muassa voimakkaat epälineaarisuudet hydraulisten toimilaitteiden ja robottien dynaamisessa käyttäytymisessä sekä käytettyjen matemaattisten mallien ja parametrien epävarmuus ja häiriötekijät.

Tässä diplomityössä keskitytään tarkastelemaan uutta mallipohjaista säätömenetelmää nimeltä Virtual Decomposition Control (VDC). VDC menetelmä on kehitetty erityisesti rakenteellisesti monimutkaisten robottien säätöön. Kyseinen menetelmä perustuu tutkittavan järjestelmän virtuaaliseen ”hajottamiseen” alijärjestelmiksi. Tämän jälkeen järjestelmälle suoritetaan mallipohjainen alijärjestelmien dynamiikkaan perustuva säädön toteutus, jonka päämääränä on alijärjestelmien virtuaalinen stabiilius. Kaikkien alijärjestelmien virtuaalinen stabiilius takaa lopulta koko järjestelmän stabiiliuden. Käytetyn menetelmän tehokkuus perustuu siihen, että todella monimutkaisetkin järjestelmät kyetään pilkkomaan rakenteeltaan yksinkertaisiin alijärjestelmiin, jolloin koko järjestelmän dynaamisten mallien käsittely helpottuu huomattavasti.

Diplomityön päämääränä oli soveltaa VDC menetelmää kahden vapausasteen hydrauliseen manipulaattoriin. Parametrien sovittaminen (parameter adaptation) jätettiin tässä diplomityössä tarkastelujen ulkopuolelle. VDC-säätimen suorituskyky testattiin käytännössä ja saatuja tuloksia verrattiin PID-säätimellä saatuihin vastaaviin tuloksiin.

VDC menetelmää käsittelevä teoria kyettiin onnistuneesti soveltamaan tutkimusvälineenä olleeseen manipulaattoriin. Manipulaattorin alijärjestelmät kyettiin matemaattisesti todistamaan L_2 and L_∞ stabiilisiksi, tämän taaten lopulta koko järjestelmän stabiiliuden. Kokeellisissa mittauksissa manipulaattorilla ajettiin sekä VDC- että PID-säätimellä sama määrätty Karteesinen rata. VDC-säätimellä saavutettiin noin seitsemän kerta tarkempi sylinterin männän aseman seurantatarkkuus toiselle järjestelmän sylintereistä ja noin neljä ja puoli kertaa tarkempi sylinterin männän aseman seurantatarkkuus toiselle järjestelmän sylintereistä. Mittauksissa ajettiin edellä mainittu Karteesinen rata myös puolet nopeammalla ja puolet hitaammalla suoritusajalla. Molemmissa tapauksissa PID-säätimen stabiilius menetettiin. VDC-säätimellä kyseiset radat kyettiin suorittamaan ilman ongelmia.

PREFACE

This Master of Science Thesis has been undertaken at Tampere University of Technology (TUT) at the Department of Intelligent Hydraulics and Automation (IHA).

First at all, I would like to thank Prof. Jouni Mattila for the opportunity to work in IHA and also for his leading me into this challenging but still fascinating world of robotics. I would also like express my gratitude for Prof. Mattila for his support and guidance during this thesis. I am also honestly grateful for Dr. Wen-Hong Zhu from Canada Space Agency for his valuable comments and guidance related to this thesis. I want also thank M.Sc. Janne Honkakorpi for his help and guidance related to use of dSpace and ControlDesk.

Special thanks I would like to address to my parents, Irmeli and Kalevi, for their constant support and encourage during my whole life. Especially, I would like to thank my wife Maratee with her support, love and understanding during these years.

At the end, I want to give thanks to Janne, Juho and Miika for this seven years of journey in TUT and also all my colleagues in room K2442B for fruitful and relaxing atmosphere.

Tampere, 14.11.2012

Janne Koivumäki

CONTENTS

NOMENCLATURE AND ABBREVIATIONS

The following notations are applied throughout this thesis unless otherwise specified:

- An italic letter in lower case represents scalar.
- A bold letter in lower case with an overhead right arrow, such as $\vec{\mathbf{v}}$, represents a directed (physical) vector; a bold letter in lower case, such as **v**, represents a valued vector.
- A bold letter in upper case, such as **U**, represents a matrix.
- A bold letter in upper case surrounded by a pair of braces, such as {**A**}, represents a coordinate frame.

$\dot{\square}$	The dot notation for derivative operator
$\int$	Integral operator
$\frac{d}{dt}$	Leibniz's notation for derivative operator
$(\boldsymbol{s}\times) \in \mathbb{R}^{3\times3}$	A skew-symmetric matrix operator from vector $\boldsymbol{s} \in \mathbb{R}^3$
$\{\mathbf{A}\}$	A coordinate system (frame)
β	Bulk modulus of fluid
Δp	Pressure drop across the orifice
λ	VDC-controller position error feedback gain
∂	Partial differentiator operator
$\boldsymbol{\theta_A} \in \mathbb{R}^{13}$	Parameter vector of rigid body related to frame $\{\mathbf{A}\}$
$\boldsymbol{\theta_f} \in \mathbb{R}^{7}$	Parameter vector of applied friction model
$\boldsymbol{\theta_v} \in \mathbb{R}^{4}$	Parameter vector of servo valve control equation
θ	Manipulator joint angle
$\varphi(F)$	A monotonic function with force input
$\phi(\dot{x})$	Bounded and differentiable function characterizing the profile of the Stribeck and viscous friction
${}^{\boldsymbol{A}}\boldsymbol{\omega} \in \mathbb{R}^3$	Angular velocity vector of frame $\{\mathbf{A}\}$
$\mathbf{0_{3\times3}} \in \mathbb{R}^{3\times3}$	Empty 3x3 square matrix
A_a	Piston area of cylinder in chamber A
$\boldsymbol{A}^{-1}$	Inverse of matrix **A**
$\boldsymbol{A}^{T}$	Transpose of matrix **A**
$\boldsymbol{C_A}\left({}^{A}\omega\right) \in \mathbb{R}^{6\times6}$	A vector of centrifugal and Coriolis terms of rigid body related to frame $\{\mathbf{A}\}$
c_n	Valve flow coefficient from chamber to return
c_p	Valve flow coefficient from supply to chamber
${}^{\boldsymbol{A}}\boldsymbol{F} \in \mathbb{R}^6$	Force/moment vector of frame $\{\mathbf{A}\}$
${}^{\boldsymbol{A}}\boldsymbol{F}^{*} \in \mathbb{R}^6$	Net force/moment vector of frame $\{\mathbf{A}\}$

$^{A}\boldsymbol{f} \in \mathbb{R}^3$	Force vector of frame **{A}**
f_c	The actuation force of cylinder piston
f_f	Friction force of cylinder piston
f_p	Net pressure force of cylinder piston
$\boldsymbol{G_A} \in \mathbb{R}^6$	A vector of gravity terms of rigid body related to frame **{A}**
$g(z, z_{ss})$	A function characterizing behavior of cylinder seal bristles in cylinder friction model
$\boldsymbol{I}_0(t)$	The moment of inertia matrix around the center of mass
$\boldsymbol{I}_3 \in \mathbb{R}^{3\times3}$	A 3×3 identity matrix
$\boldsymbol{J}_q$	Geometric Jacobian matrix
$\boldsymbol{K_A} \in \mathbb{R}^{6\times6}$	Positive definite gain matrix of rigid body related to frame **{A}**
k_D	Derivative gain of PID-controller
k_{fp}	Piston force feedback gain of VDC-controller
k_I	Integral gain of PID-controller
k_P	Proportional gain of PID-controller
k_u	Ultimate gain of PID-controller
k_x	Velocity feedback gain of VDC-controller
$\mathcal{L}(t)$	Differentiable switching function
L_p	Lebesgue space
l_0	Effective length of cylinder
l_j	Number of joints within the *open chain*
$\boldsymbol{M_A} \in \mathbb{R}^{6\times6}$	Mass matrix of rigid body related to frame **{A}**
$^{A}\boldsymbol{m} \in \mathbb{R}^3$	Moment vector of frame **{A}**
m_A	A mass of rigid body related to frame **{A}**
n_c	Number of *open chains* in virtually decomposed system
n_o	Number of *objects* in virtually decomposed system
p_A	Virtual power flow with respect to frame {**A**}
p_a	Pressure in cylinder chamber A
p_s	Supply pressure
p_t	Pressure of return line
Q_a	Flow rate entering in cylinder chamber A
q_d	Desired position in joint space
q_r	Required position in joint space
$\dot{q}_d$	Desired velocity in joint space
$\dot{q}_r$	Required velocity in joint space
$^{A}\boldsymbol{R}_B \in \mathbb{R}^{3\times3}$	Rotation matrix of frame {**B**} with respect to frame {**A**}
$^{A}\boldsymbol{r}_m \in \mathbb{R}^3$	Vector pointing from the origin of frame {**A**} toward the center of mass and expressed in frame {**A**}
$\mathcal{S}(x)$	Selective function
t_f	Transition time between two points defined in Cartesian frame

t_u	Oscillation period of asymptotically stable PID-controller
${}^{\boldsymbol{A}}\boldsymbol{U}_{\boldsymbol{B}} \in \mathbb{R}^{6\times6}$	Force/moment transformation matrix from frame {**A**} to frame {**B**}
u	Control voltage of servo valve
u_f	Control term of servo valve control voltage
${}^{\boldsymbol{A}}\boldsymbol{V} \in \mathbb{R}^{6}$	Linear/angular velocity vector of frame {**A**}
${}^{\boldsymbol{A}}\boldsymbol{v} \in \mathbb{R}^{3}$	Linear velocity vector of frame {**A**}
$\vartheta(\Delta p)$	Pressure drop related function
$v(t)$	Non-negative accompanying function
X_0	Initial Cartesian position along x-axis of Cartesian frame
X_d	Desired Cartesian position along x-axis of Cartesian frame
$\dot{X}_d$	Desired Cartesian velocity in Cartesian frame
X_f	Final Cartesian position along x-axis of Cartesian frame
x_d	Desired position given in actuator space
$\dot{x}_d$	Desired velocity given in actuator space
x_r	Required position given in actuator space
$\dot{x}_r$	Required velocity given in actuator space
$\boldsymbol{Y}_{\boldsymbol{A}} \in \mathbb{R}^{6\times13}$	Regressor matrix of rigid body related to frame {**A**}
$\boldsymbol{Y}_{\boldsymbol{f}} \in \mathbb{R}^{1\times7}$	Regressor matrix of applied friction model
$\boldsymbol{Y}_{\boldsymbol{v}} \in \mathbb{R}^{1\times4}$	Regressor matrix of servo valve control equation
Y_0	Initial Cartesian position along x-axis of Cartesian frame
Y_d	Desired Cartesian position along x-axis of Cartesian frame
$\dot{Y}_d$	Desired Cartesian velocity in Cartesian frame
Y_f	Final Cartesian position along x-axis of Cartesian frame

CAD	Computer Aided Design
DOF	Degree Of Freedom
IHA	Department of Intelligent Hydraulics and Automation
PID	Proportional, Integral, Derivative
TUT	Tampere University of Technology
VDC	Virtual Decomposition Control
VPF	Virtual Power Flow

1 INTRODUCTION

The robots and robotic manipulators have been used in industry for many decades. The first programmable robot was designed as early as 1954, by George Devol, and first commercially available robot appeared in markets already in 1959. Robotic manipulators were used in industries after 1960, and saw sky rocketing growth in the 80*s*. Rapid growth of robot industry in 80*s* occurs primarily because of the huge investments by the automotive industry. (Jazar 2010, p.2).

The first industrial robots were nothing but numerical control of mechanical linkages that were basically designed to do some simple material handling tasks (Jazar 2010, p.2). In addition to material handling tasks, industrial robots are nowadays designed to accomplish also different manipulation and measurement task. (Sciavicco 2001, p.4-5). It is quite obvious that today's highly automated industrial targets of robotic applications, such as welding, milling, assembling and object inspections to name a few, require much more motion capability and sensing. Moreover, many of today's industrial robotics applications demands high accuracy, forces and repeatability that they are hardly attainable without robots (Jazar 2010, p.2-3).

Apart from industry, more and more advanced robots are needed in extreme and hostile environments, such space, nuclear and underwater. In these applications, whole new level of autonomy of robots is required. Also complexity of these systems has usually significantly increased and more versatile operations are demanded. (Jazar 2010, p.2-3) (Sciavicco 2001, p.4-5).

In the view of the above, it is quite clear that nowadays robotics is very interdisciplinary field of science. According to books concerning into field of robotics, such as (Craig 2005), (Jazar 2010), (Sciavicco 2001), the robotics can be seen as a fusion of different branches of science such as mechanics, electronics, information theory, automation theory, mathematics and computer science.

1.1 Hydraulics in View of Control System

Hydraulic actuators are well-known of their high power-to-weight ratio, compactness and reliable performance. In (Watton 1989), it is said that in applications where high power is needed with a requirement from good-to-precision control, it is inevitable that fluid power systems will be used. Furthermore, the relatively high power-to-weight ratio of hydraulics together with advantages of electronic signal processing produces a flexible and efficient means of power transfer and control. Usage of hydraulic components is also said to provide a rapid system response (Sirouspour 2001).

However, the inherent nonlinear dynamics associated with hydraulics actuators substantially challenge the controller design (Zhu 2005), (Zhu 2010, p.169), (Niksefat 1999). In view of (Linjama 1998), turbulent flow equations to model flow through valves is also significantly nonlinear. Also, determination of the parameters of mathematical models of hydraulic systems, such as system compliances and valve characteristics, can be difficult and time-consuming task (Niksefat 1999).

1.2 Special Characteristics of Control in Robotics

The primary purpose of robot manipulators is to perform certain manipulation tasks in its environment (Muhammad 2011, p.26). Completion of a generic task requires the execution of a specific motion prescribed to the manipulator's end-effector. The correct execution of the end-effector motion is entrusted to the control system which shall provide the joint actuators of the manipulator with the commands consistent with the desired motion trajectory. (Sciavicco 2001, p.14)

Control of end-effector motion demands an accurate analysis of the characteristics of the mechanical structure of manipulator. Modeling a manipulator is therefore a necessary premise to finding motion control strategies. Modeling of a robotic manipulator can be divided to kinematic and dynamic analysis. Kinematic analysis of a manipulator structure concerns the description of the manipulator motion with respect to fixed reference Cartesian frame by ignoring the forces and moments that causes motion of the structures. (Sciavicco 2001, p.14-15)

The kinematics of a manipulator represents the basis of a systematic, general derivation of manipulators dynamics, i.e., the equations of motion of the manipulator as a function of the forces and moments acting on it (Sciavicco 2001, p.15). The dynamics of rigid robot is also well-known to be modeled by a set of coupled highly nonlinear differential equations (Huang 2010, p.83). The dynamic model of manipulator is used for mechanical design of the structure, choice of actuators, determination of control strategies, and computer simulation of manipulator motion (Sciavicco 2001, p.15).

The control systems are essential to robots, as they produce desired behavior, maximize potential performances, and deliver achievable accuracy, subject to robustness requirements (Zhu 2010, p.4). The problem of manipulator control is to find the time behavior of the forces and torques to be delivered by the joint actuators so as to ensure the execution of the reference trajectories. This problem is quite complex, since a manipulator is an articulated system and thus the motion of one link influences the motion of the others. (Sciavicco 2001, p.15-16) Also highly nonlinear characteristic of the robot dynamics increases largely the difficulty of the controller design. The controller design of robot is generally said to be not easy even when the dynamic model of system is precisely known. This comes from the various uncertainties and disturbances of mathematical models. (Huang 2010, p.83).

1.3 Towards Virtual Decomposition Control

Robot manipulators have been widely used in the industrial applications in the past decades. However, most of these applications are restricted to slow-motion operations without interactions with the environment. This is mainly due to limited performance of the available controllers in the market that are based on simplified system models. Thus, more advanced control strategies are needed to increase the operation speed with more servo accuracy. (Huang 2010, p.1)

The most widely used control scheme for industrial robots is based on the joint Proportional, Integral, and Derivative (PID) servo control. While this scheme is easy to implement and is able to move a robot to its desired position in steady state, the dynamic properties of the robot can be vitiate this approach, since the dynamic coupling among the joints and the mass matrix variations can invalidate the PID control. A typical second-order system, representing a one Degree Of Freedom (DOF) robot *G(s)*, subject to a PID controller *C(s)*, is illustrated in Figure 1. (Zhu 2010, p.5)

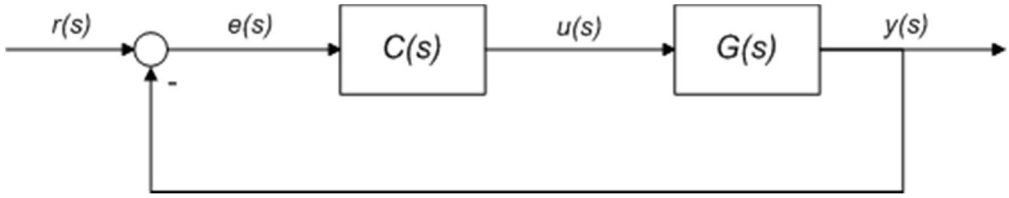

Figure 1: A PID feedback controlled system.

With this kind of arrangement, a PID controller is able to deliver acceptable control performances at low frequencies, but it is unable to produce adequate control performances at high frequencies beyond the cut-off frequency, i.e. bandwidth of controller is poor. Also, in order to prevent overshoots in contact motion, the joint PID controllers are designed to be over-damped in most circumstances. As a result, these robots are capable only of performing regulation tasks that require accuracies only in the steady state. For task requiring tracking accuracies the joint PID control is generally inadequate. (Zhu 2010, p.5)

Due to the limitations of PID control, researchers have long been seeking advanced control approaches that are able to achieve higher control performances. One solution is to use so called dynamic based feedforward plus PID feedback control (simply called dynamics based control), as illustrated in Figure 2.

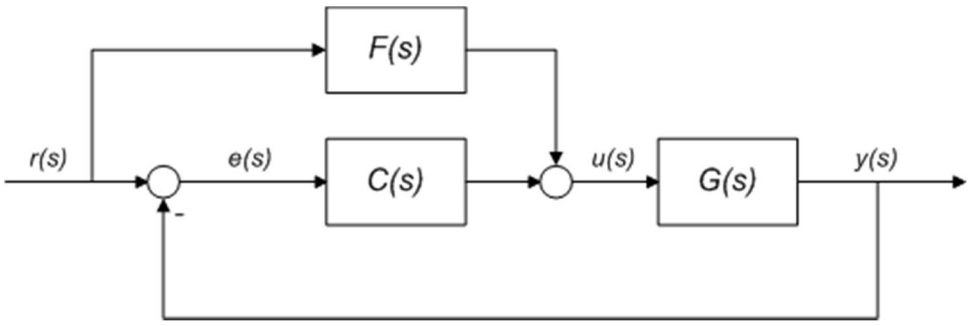

Figure 2: Dynamic based control.

In dynamics based control a new feedforward block *F(s)* is added. If the feedforward transfer function *F(s)* takes exactly the inverse dynamics of the system *G(s)* to be controlled, subject to that *F(s) = 1/ G(s)* holds indefinitely, then the ideal transfer function $\frac{x(j\omega)}{r(j\omega)} = 1, \forall\omega \in [0, \infty)$, can be achieved. This result implies that "infinite" control bandwidth is possible as long as a proper feedforwad control is designed. Having high bandwidth allows accurate execution of dynamically challenging tasks, which would be otherwise impossible by using PID controlled robots. High bandwidth also allows rapid executions of tasks which were previously executed by PID controlled robots by much slower speed. (Zhu 2010, p.6-7)

In dynamic based control approach, the feedforward term *F(s)* mainly contributes to high control accuracies, whereas the feedback term is primarily used to overcome uncertainties, to maintain stability, and to address transition issues. The design of *F(s)* is completely based on the robot inverse dynamics and can thus be obtained independently from the feedback controller *C(s)*. The dynamics based control approach is also generally applicable to highly coupled nonlinear systems such as robots. Due to these advantages of the dynamic based control approach, it has been taken as baseline approach from which the Virtual Decomposition Control (VDC) has originally evolved. (Zhu 2010, p.6-7)

Control of complex systems, such as robots, has long been a challenging topic for the past five decades (Zhu 2011). In complex robotic systems the uncertainties, high nonlinearity, and strong couplings in the dynamics becomes even far more challenging to model precisely than aforementioned in chapter 1.2 and this obviously makes the control problem even more complicated and difficult to solve (Zhu 1997).

One of the major technical challenges of dynamic based control in complex robotic systems is that the control design is based on the complete dynamic models of robots. This same control design feature occurs also in most of the books on control of robotics, such as (Craig 2005), (Sciavicco 2001), and (Lewis 2004) to name a few. Usually, robots with two or three DOF were taken as examples in simulations or experiments in order to make control implementations manageable. However, substantial technical challenges in control implementations arise when the number of DOF of motion is well over six. This is due to fact that the complexity (computational burden) of robot dynamics is proportional to the fourth power of the number of DOF of motion. (Zhu 2010, p.8)

The Virtual Decomposition Control (VDC) is one of the most efficient approaches toward precision control of complex robots (Zhu 2011). With respect to the technical challenges arisen from the application of dynamics based control to complex robots, one possible solution is to base control directly on subsystem dynamics, rather than on the complete dynamics of the robot with hyper degrees of freedom. Thus, the essence of the VDC approach is the use of each subsystem dynamics rather than dynamics of the entire system. In view the fact that no matter how complicated a robotic system is, the dynamics of the subsystems (rigid links and joints) remain relatively simple with fixed dynamic structures invariant to target system. This means that control

computations are proportional to number of subsystems. (Zhu 2010, p.9). The VDC approach is included with parametric uncertainty to construct model-based feedforward compensation terms and guarantees the stability of the entire complex robot with mathematical certainty, leading to precise motion/force tracking control with the control bandwidth being independent of the feedback control gains (Zhu 2011).

The VDC is capable of accomplishing a variety of control objectives such as motion control, internal force control, and optimizations, without restrictions on target systems. Furthermore, one of the advantages of using VDC approach is that the change of the dynamics of s subsystem only affects the respective local control equations associated with this subsystem, while keeping the control equations associated with the rest of the system unchanged. For example, when an electrical motor is replaced by hydraulic actuator, only the control equations for this particular joint change, whereas the control equations for the rest of the system keep unchanged. (Zhu 2010, p.9)

1.4 Objectives of Thesis

According to (Linjama 1998, p.12), the modeling and control of hydraulic cranes (manipulators) incur difficult problems which arise from the strong nonlinearities, the complexity of the system and uncertainties of physical parameters. On the other hand, the VDC introduced in previous section, has been reported to achieved significant control results, as in (Zhu 2002), (Zhu 2005) and (Zhu 2011), in various different applications.

In view of challenges towards control issues arisen in sections 1.1 and 1.2, hydraulic manipulators serves a fruitful and challenging application to study the VDC in practice. The objectives of this thesis are:

- Implement theory of VDC into hydraulically operated 2-DOF manipulator.
- Carry out measurements with hydraulically operated 2-DOF manipulator.
- Compare achieved VDC-controller results to corresponding results achieved with PID-controller.

1.5 Restrictions

The generic formulation for *Virtual Decomposition Control* (VDC) approach is represented in (Zhu 2010). However, this complete generic formulation is far too profound to deal with in scope of this thesis. Thus, only essential and inevitable parts of theory of VDC approach are represented.

This thesis restricts to cover only 2-DOF in motion. Due to this fact, some simplifications are made. Firstly, for convenience, in robotics well-known and broadly used Denavit-Hartenberg convention to attach body frames is not used. Also regressor matrices $\boldsymbol{Y_A} \in \mathbb{R}^{6\times 13}$ and parameter vectors $\boldsymbol{\theta_A} \in \mathbb{R}^{13}$ covering 6-DOF in motion and defined in section 2.6 are simplified to cover only 2-DOF in motion.

As mentioned in (Linjama 1998, p.13) and (Mattila 2000, p.10), the control problem of hydraulic manipulators is very wide-ranging and challenging field. Thus, it is obvious that only some parts of this control problem of hydraulic manipulators are considered herein. This thesis concentrates only on free space motion studies, i.e. all contacts and interactions between manipulator and environment are neglected and left to future studies. Also parameter adaptation is neglected and left out in scope of this thesis.

In scope of this thesis, only control of prismatic hydraulically actuated joints (hydraulic cylinders) are studied. This comes due to fact that all rotational joints appearing in this thesis are unactuated. In view of (Zhu 2010, p.169), in hydraulic cylinder actuated systems, the friction in the motion is usually dominated by the piston friction between the piston seal and the cylinder. Therefore, the bearing frictions of all rotational unactuated joints are neglected and assumed to be zero.

To make general presentation and mathematical formulation more manageable, all *objects* and *links* of *open chains*[1] are handled as a rigid body and thus all flexibilities of system are neglected and left to future studies.

1.6 Structure of Thesis

This thesis is divided into seven different chapters. First, in the next chapter all the mathematical preliminaries to be used later on VDC are given. Then, in chapter 3 a general formulation of the VDC is given. This chapter introduces only the essential formulation and theory of VDC approach to be applied later into studied system. In chapter 4, studied hydraulic manipulator, namely HIAB 031, is introduced. This chapter covers formulation of direct kinematics, inverse kinematics, and differential kinematics of studied manipulator. In chapter 5, a theory of the VDC is applied into studied system. In chapter 6, first an experimental implementation is discussed and then measured results with VDC- and PID-controller are given. Finally, in chapter 7 conclusions about the results and observations of this thesis are given. Also, future work is discussed in this chapter.

[1] *objects* and *open chains* will be specified more detailed in subsections 3.1.2 and 3.1.1, respectively.

2 MATHEMATICAL PRELIMINARIES

In this chapter the necessary mathematical preliminaries, which are essential to understand and apply the VDC approach into studied system, are defined. Mathematical preliminaries to be presented in this chapter are based on the (Zhu 2010).

First, in section 2.1 coordinate systems applied in this thesis are introduced. Then, in section 2.2 rotation matrix for describing orientation is introduced. In section 2.3, linear/angular velocity vector and force/moment vector of body frame are defined, leading to the duality of linear/angular velocity and force/moment transformations, which is to represented in section 2.4. After that, equations describing rigid body dynamics are given in section 2.5 and in section 2.6 linear parametrizised expression for rigid body dynamics is defined. In section 2.7, the definitions for *virtual power flow* and simple oriented graph are given. Finally, definition and mathematical background for the concept of *virtual stability* is given in section 2.8.

2.1 Coordinate Systems

Coordinate systems (called frames for simplicity) defined in (Zhu 2010, p.24) and used in this thesis are constructed by three mutually orthogonal three-dimensional unit vectors as base. By this definition, frame {**A**} can be represented as follows:

$$\{\boldsymbol{A}\} = [\vec{\boldsymbol{x}}_a,\ \vec{\boldsymbol{y}}_a,\ \vec{\boldsymbol{z}}_a\ ] \tag{2.1}$$

where $\vec{\boldsymbol{x}}_a,\ \vec{\boldsymbol{y}}_a,\ \vec{\boldsymbol{z}}_a$ are axis of frame {**A**}.

An illustrated example of orthogonal three-dimensional frame {**A**} defined in (2.1) is represented in Figure 3.

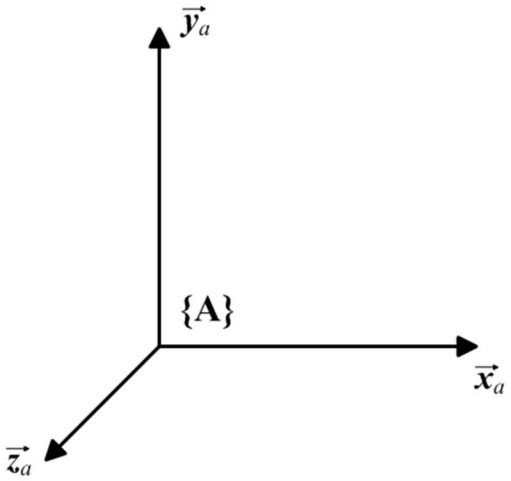

Figure 3: Orthogonal three-dimensional coordinate system {A}.

2.2 Description of Orientation by Rotation Matrix

In scope of this thesis, the rotation matrices are used to transforms a physical vector expressed in frame {**A**} to the same physical vector expressed in frame {**B**}. The rotation matrix ${}^{A}\boldsymbol{R}_{B} \in \mathbb{R}^{3\times3}$, denoting the rotation of frame {**B**} with respect to frame {**A**}, is defined in (Zhu 2010, p.25) as

$$\{\boldsymbol{B}\} = {}^{A}\boldsymbol{R}_{B}\{\boldsymbol{A}\} \tag{2.2}$$

In scope of this thesis, all frames are applied such a way that rotation between two frames, namely {**A**} and {**B**}, is able to be described only about $\vec{z}$-axis. In view of (Sciavicco 2001, p.23), the rotation about $\vec{z}$-axis can be described as

$${}^{A}\boldsymbol{R}_{B} = \begin{bmatrix} \cos\alpha & -\sin\alpha & 0 \\ \sin\alpha & \cos\alpha & 0 \\ 0 & 0 & 1 \end{bmatrix}, \tag{2.3}$$

where angle α denotes the rotation of frame {**B**} with respect to frame {**A**} and about $\vec{\boldsymbol{z}}_{a}$-axis.

2.3 Expressions of Velocities and Forces in Body Frame

In view of (Zhu 2010, p.29), the linear velocity vector ${}^{A}\boldsymbol{v} \in \mathbb{R}^{3}$ of frame {**A**}, expressed in frame {**A**}, and the angular velocity vector ${}^{A}\boldsymbol{\omega} \in \mathbb{R}^{3}$ of frame {**A**}, expressed in frame {**A**}, are wanted to integrate to facilitate the transformations of velocities between different frames. Thus, the linear/angular velocity vector of frame {**A**} can be defined as

Definition 2.1. *Let* ${}^{A}\boldsymbol{v} \in \mathbb{R}^{3}$ *be the linear velocity vector of frame {**A**}, expressed in frame {**A**}, and* ${}^{A}\boldsymbol{\omega} \in \mathbb{R}^{3}$ *be the angular velocity vectors of frame {**A**}, expressed in frame {**A**}. The linear/angular velocity vector of frame {**A**} is defined by* (Zhu 2010, p.29) *as*

$${}^{A}V \stackrel{\text{def}}{=} \begin{bmatrix} {}^{A}\boldsymbol{v} \\ {}^{A}\boldsymbol{\omega} \end{bmatrix} \in \mathbb{R}^{6}. \tag{2.4}$$

Similar to Definition 2.1., the force vector ${}^{A}\boldsymbol{f} \in \mathbb{R}^{3}$ applied to the origin of frame a {**A**}, expressed in frame {**A**}, and the moment vector ${}^{A}\boldsymbol{m} \in \mathbb{R}^{3}$ applied to the origin of frame a {**A**}, expressed in frame {**A**}, are wanted to integrate to facilitate the transformations of velocities between different frames. In view of (Zhu 2010, p.29), the force/moment vector of frame {**A**} can be defined as

Definition 2.2. *Let* ${}^{A}\boldsymbol{f} \in \mathbb{R}^3$ *be the force vector that is being measured and expressed in frame {**A**} and* ${}^{A}\boldsymbol{m} \in \mathbb{R}^3$ *be the moment vector that is being measured and expressed in frame {**A**}. The force/moment vector of frame {**A**} is defined by* (Zhu 2010, p.29) *as*

$$ {}^{A}F \stackrel{\text{def}}{=} \begin{bmatrix} {}^{A}\boldsymbol{f} \\ {}^{A}\boldsymbol{m} \end{bmatrix} \in \mathbb{R}^6. \tag{2.5} $$

2.4 The Duality of Linear/Angular Velocity and Force/Moment Transformations

As defined in (Zhu 2010, p.29), if two given frames, denoted as {**A**} and {**B**}, are being fixed to a common rigid body moving freely and subject to a pair of physical force and moment vectors defined in (2.4) and (2.5), the duality between the linear/angular velocity transformations and the force/moment transformations can be written as

$$ {}^{B}V = {}^{A}\boldsymbol{U}_{\boldsymbol{B}}^{T}\, {}^{A}V \tag{2.6} $$

$$ {}^{A}F = {}^{A}\boldsymbol{U}_{\boldsymbol{B}}\, {}^{B}F \ . \tag{2.7} $$

In equation (2.7)

$$ {}^{A}\boldsymbol{U}_{\boldsymbol{B}} = \begin{bmatrix} {}^{A}\boldsymbol{R}_{\boldsymbol{B}} & \boldsymbol{0}_{3\times3} \\ ({}^{A}\boldsymbol{r}_{\boldsymbol{AB}}\times)\, {}^{A}\boldsymbol{R}_{\boldsymbol{B}} & {}^{A}\boldsymbol{R}_{\boldsymbol{B}} \end{bmatrix} \in \mathbb{R}^{6\times6} \tag{2.8} $$

denotes a force/moment transformation matrix that transforms the force/moment vector measured and expressed in frame {**B**} to the same force/moment vector measured and expressed in frame {**A**} and in equation (2.6) ${}^{A}\boldsymbol{U}_{\boldsymbol{B}}^{T} \in \mathbb{R}^{6\times6}$denotes a linear/angular velocity transformation matrix that transforms the linear/angular velocity vector measured and expressed in frame {**A**} to the same linear/angular velocity vector measured and expressed in frame {**B**}.

Furthermore, in (2.8) $\boldsymbol{0}_{3\times3} \in \mathbb{R}^{3\times3}$ denotes an empty 3×3 square matrix and cross product $({}^{A}\boldsymbol{r}_{\boldsymbol{AB}}\times) \in \mathbb{R}^{\boldsymbol{3\times3}}$ is understood to be skew-symmetric matrix operator defined as

$$ ({}^{A}\boldsymbol{r}_{\boldsymbol{AB}}\times) = \begin{bmatrix} 0 & -r_z & r_y \\ r_z & 0 & -r_x \\ -r_y & r_x & 0 \end{bmatrix} \tag{2.9} $$

where r_x, r_y, and r_z are the distances from origin of frame {**A**} to origin of frame {**B**}, along the axes of frame {**A**}.

By applying formulation of taking inverse from transformation matrix introduced in (Craig 2005, p.158), the transformation matrix defined in (2.7) can be inversely written as

$$ {}^{A}\boldsymbol{U}_{B}^{-1} = \begin{bmatrix} {}^{A}\boldsymbol{R}_{B}^{T} & \mathbf{0}_{3\times3} \\ -{}^{A}\boldsymbol{R}_{B}^{T}({}^{A}\boldsymbol{r}_{AB}\times) & {}^{A}\boldsymbol{R}_{B}^{T} \end{bmatrix} \in \mathbb{R}^{6\times6} \tag{2.10} $$

Thus, in view of (2.10), the equations (2.6) and (2.7) can be inversely written as

$$ {}^{A}V = {}^{A}\boldsymbol{U}_{B}^{-T}\,{}^{B}V \tag{2.11} $$

$$ {}^{B}F = {}^{A}\boldsymbol{U}_{B}^{-1}\,{}^{A}F, \tag{2.12} $$

respectively.

2.5 Rigid Body Dynamics in a Body Frame

Similar to Definition 2.2., the net force/moment vector ${}^{A}\boldsymbol{F}^{*} \in \mathbb{R}^{6}$ applied to the origin of frame a {**A**}, expressed in frame {**A**}, can be defined in view of (Zhu 2010, p.30) as

Definition 2.3. *Let* ${}^{A}\boldsymbol{f}^{*} \in \mathbb{R}^{3}$ *be the net (summation) force vector that is being measured and expressed in frame {**A**} and* ${}^{A}\boldsymbol{m}^{*} \in \mathbb{R}^{3}$ *be the net (summation) moment vector that is being measured and expressed in frame {**A**}. The net (summation) force/moment vector of frame {**A**} is defined in (Zhu 2010, p.29) as*

$$ {}^{A}F^{*} \stackrel{\text{def}}{=} \begin{bmatrix} {}^{A}\boldsymbol{f}^{*} \\ {}^{A}\boldsymbol{m}^{*} \end{bmatrix} \in \mathbb{R}^{6}. \tag{2.13} $$

According to (Zhu 2010, pp.30-31), if two frames, denoted as {**A**} and {**B**}, are fixed to a rigid body and frame {**A**} is used to express the rigid body dynamics, and frame {**B**} is assumed to be located at the center of mass, the dynamic equation of the rigid body in free motion, expressed in the inertial frame {**I**}, can be written as

$$ \mathbf{M}_{\mathbf{A}}\frac{d}{dt}\left({}^{\mathbf{A}}V\right) + \mathbf{C}_{\mathbf{A}}\left({}^{\mathbf{A}}\omega\right){}^{\mathbf{A}}V + \mathbf{G}_{\mathbf{A}} = {}^{\mathbf{A}}F^{*} \tag{2.14} $$

where

$$ \mathbf{M}_{\mathbf{A}} = \begin{bmatrix} m_{A}\boldsymbol{I}_{3} & -m_{A}({}^{A}\boldsymbol{r}_{AB}\times) \\ m_{A}({}^{A}\boldsymbol{r}_{AB}\times) & \boldsymbol{I}_{A} - m_{A}({}^{A}\boldsymbol{r}_{AB}\times)^{2} \end{bmatrix} \in \mathbb{R}^{6\times6} \tag{2.15} $$

denotes the mass matrix of rigid body,

$$\mathbf{C_A}\left({}^{A}\omega\right) = \begin{bmatrix} m_A\left({}^{A}\boldsymbol{\omega}\times\right) & -m_A\left({}^{A}\boldsymbol{\omega}\times\right)\left({}^{A}\boldsymbol{r_{AB}}\times\right) \\ m_A\left({}^{A}\boldsymbol{r_{AB}}\times\right)\left({}^{A}\boldsymbol{\omega}\times\right) & \left({}^{A}\boldsymbol{\omega}\times\right)\boldsymbol{I_A} + \boldsymbol{I_A}\left({}^{A}\boldsymbol{\omega}\times\right) - m_A\left({}^{A}\boldsymbol{r_{AB}}\times\right)\left({}^{A}\boldsymbol{\omega}\times\right)\left({}^{A}\boldsymbol{r_{AB}}\times\right) \end{bmatrix} \in \mathbb{R}^{6\times 6} \quad (2.16)$$

denotes the matrix of centrifugal and Coriolis terms, and

$$\mathbf{G_A} = \begin{bmatrix} m_A\,{}^{A}\boldsymbol{R_I}\,\boldsymbol{g} \\ m_A\left({}^{A}\boldsymbol{r_{AB}}\times\right){}^{A}\boldsymbol{R_I}\,\boldsymbol{g} \end{bmatrix} \in \mathbb{R}^{6\times 1} \quad (2.17)$$

denotes the gravity terms.

Furthermore, in (2.15) – (2.17) $\boldsymbol{I}_3 \in \mathbb{R}^{3\times 3}$ denotes the identity matrix, m_A denotes the mass of rigid body, $\left({}^{A}\boldsymbol{\omega}\times\right) \in \mathbb{R}^{3\times 3}$ is skew-symmetric angular velocity matrix, $\boldsymbol{g} \in \mathbb{R}^3$ denotes the gravitational vector, and $\boldsymbol{I_A} \in \mathbb{R}^{3\times 3}$ is defined as

$$\boldsymbol{I_A} = {}^{A}\boldsymbol{R_I}\,\boldsymbol{I}_0(t)\,{}^{A}\boldsymbol{R_I}\,, \quad (2.18)$$

where $\boldsymbol{I}_0(t) \in \mathbb{R}^{3\times 3}$ denotes the moment of inertia matrix around the center of mass. (Zhu 2010, pp. 30-31)

2.6 Linear Parametrization Expression

If parameter uncertainties in dynamic equation of the rigid body in free motion defined in (2.14) is wanted to take into account, the parameter adaptation is required. Even though parameter estimation is not incorporated in the control equations in scope of this thesis, the linear parametrization expression for rigid body dynamics, defined in (2.14), is wanted to be applied in the view of the further studies.

The linear parametrizised dynamic equation for the rigid body in free motion with design vector ${}^{A}\boldsymbol{V}_r \in \mathbb{R}^6$ is defined in (Zhu 2010, p.32) as

$$\boldsymbol{Y_A\theta_A} \stackrel{\text{def}}{=} \mathbf{M_A}\frac{d}{dt}\left({}^{A}V_r\right) + \mathbf{C_A}\left({}^{A}\omega\right){}^{A}V_r + \mathbf{G_A} \quad (2.19)$$

The detail expressions of the regressor matrix $\boldsymbol{Y_A} \in \mathbb{R}^{6\times 13}$ and the parameter vector $\boldsymbol{\theta_A} \in \mathbb{R}^{13}$ are given in Appendix A.

2.7 Virtual Cutting Points and Simple Oriented Graph

A concept of *virtual cutting point* is central to the VDC approach. *Virtual cutting points* allow a robotic system to be conceptually “broken down” into subsystems. The *cutting*

points are virtual in the sense that the robotic system is cut conceptually rather than physically. Definition for virtual cutting point is given in (Zhu 2010, p.34) as

Definition 2.4. *A cutting point is a directed separation interface that conceptually cuts through a rigid body. At the cutting point, the two parts resulting from the virtual cut maintain equal position and orientation. The cutting point is interpreted as a driving cutting point by one part and is simultaneously interpreted as a driven cutting point by another part. A force vector* $\boldsymbol{f} \in \mathbb{R}^3$ *and a moment vector* $\boldsymbol{m} \in \mathbb{R}^3$*are exerted from one part to which the cutting point is interpreted as a driving cutting point to the other part to which the cutting point is interpreted as a driven cutting point.*

Simple oriented graphs will be used to represent the topological structure and control relations of a complex robot. A following definition for simple oriented graph is given in (Zhu 2010, p.34) as

Definition 2.5. *A graph consists of nodes and edges. A directed graph is a graph in which all the edges have direction. An oriented graph is a directed graph in which each edge has a unique direction. A simple oriented graph is an oriented graph in which no loop is formed.*

In simple oriented graph, each subsystem is represented by a node, while each *cutting point* is represented by a directed edge defining the reference direction of these forces and moments passing through this cutting point. The forces and moments at a *cutting point* are exerted from the subsystem to which the *cutting point* is interpreted as a *driving cutting point* to the adjacent subsystem to which the *cutting point* is interpreted as a *driven cutting point*. Some nodes are called *source nodes* that have pointing-away edges only, and some nodes are called *sink nodes* that have pointing-to edges only. (Zhu 2010, p.35)

2.8 Virtual Stability

After a system is virtually decomposed into subsystems, a natural concern in on the properties of each subsystem should have in order to maintain the stability of the entire system. These properties are being addressed in this section around the central concept of the *virtual stability* to be defined below.

2.8.1 Lebesgue Space

Lebesgue spaces, more precisely L_2 and L_∞ spaces, are in significant role in the concept of *virtual stability*. Following two definitions given in (Zhu 2010, p.15) and represented below are essential on scope of this thesis.

Definition 2.6. *Lebesgue space, denoted as L_p with p being positive integer, contains all Lebesgue measurable and integrable functions f(t) subject to*

$$\|f\|_p = \lim_{T\to\infty}\left[\int_0^T |f(t)|^p\, d\tau\right]^{\frac{1}{p}} < +\infty \tag{2.20}$$

Two particular cases are given:

(a) A Lebesgue measurable function *f(t)* belongs to L_2 if and only if $\lim_{T\to\infty}\int_0^T |f(t)|^2\, d\tau < +\infty$

(b) A Lebesgue measurable function *f(t)* belongs to L_∞ if and only if $\max_{t\in[0,\infty)}|f(t)| < +\infty$

Definition 2.7. *A vectored Lebesgue measurable function* $\boldsymbol{f}(t) = [f_1(t), f_2(t), \dots, f_n(t)]^T \in L_p,\ p = 1,2,\cdots,\infty,$ *implies* $f_i(t) \in L_p$ *for all* $i \in \{1, n\}$.

2.8.2 Non-negative Accompanying Functions

In this thesis, every subsystem or a node in simple oriented graph is assigned a non-negative accompanying function to conduct the stability and convergence analysis. A non-negative accompanying function $v(t)$ is defined (Zhu 2010, p35) as

Definition 2.8. *A non-negative accompanying function* $v(t) \in \mathbb{R}$ *is a piecewise differentiable function possessing the following properties*

(i) $v(t) \geq 0\ for\ t > 0, and$
(ii) $\dot{v}(t)\ exists\ almost\ everywhere.$

2.8.3 Virtual Power Flow

The *Virtual power flows* (VPFs) are used to characterize the dynamic interactions among subsystems. The *Virtual power flow* (VPF) is defined in (Zhu 2010, p.35) as

Definition 2.9. *With respect to frame {**A**}, the virtual power flow (VPF) is defined as the inner product of the linear/angular velocity vector error and force/moment vector error, that is*

$$p_{\boldsymbol{A}} = \left({}^{\boldsymbol{A}}\boldsymbol{V}_r - {}^{\boldsymbol{A}}\boldsymbol{V}\right)^T\left({}^{\boldsymbol{A}}\boldsymbol{F}_r - {}^{\boldsymbol{A}}\boldsymbol{F}\right) \tag{2.21}$$

where ${}^{\boldsymbol{A}}\boldsymbol{V}_r \in \mathbb{R}^6$ *and* ${}^{\boldsymbol{A}}\boldsymbol{F}_r \in \mathbb{R}^6$ *represents the required (design) vectors of* ${}^{\boldsymbol{A}}\boldsymbol{V} \in \mathbb{R}^6$ *and* ${}^{\boldsymbol{A}}\boldsymbol{F} \in \mathbb{R}^6$*, respectively.*

Now, let two frames, denoted as {**A**} and {**B**}, be attached to a common rigid body. If the required linear/angular velocity vectors and the required force/moment vectors are subject to the same constraints as that imposed on the linear/angular velocity vectors and on the force/moment vectors, that is

$$^{B}\boldsymbol{V}_{r} = {}^{A}\boldsymbol{U}_{B}^{T}\,{}^{A}\boldsymbol{V}_{r} \tag{2.22}$$

$$^{A}\boldsymbol{F}_{r} = {}^{A}\boldsymbol{U}_{B}\,{}^{B}\boldsymbol{F}_{r} \tag{2.23}$$

then it follows from (2.4), (2.5) and (2.21) − (2.23) that

$$p_{A} = p_{B} \tag{2.24}$$

holds. (Zhu 2010, p.36)

Accordint to (Zhu 2010, p.36), equation (2.24) indicates that the VPF defined by (2.21) is invariant to frames fixed to a common rigid body.

2.8.4 Virtual Stability

Based on the above definitions about Lebesgue space, non-negative accompanying function and VPFs, the definition for *virtual stability* of subsystem is given in (Zhu 2010, p.35) as

Definition 2.10. *A subsystem that is virtually decomposed from complex robot is said to be virtually stable with its affiliated vector* $\boldsymbol{x}(t)$ *being a virtual function in* L_{∞} *and its affiliated vector* $\boldsymbol{y}(t)$ *being a virtual function in* L_{2}*, if and only if there exists a non-negative accompanying function*

$$v(t) \geq \tfrac{1}{2}\boldsymbol{x}(t)^{T}\boldsymbol{P}\boldsymbol{x}(t) \tag{2.25}$$

such that

$$\dot{v}(t) \leq -\boldsymbol{y}(t)^{T}\boldsymbol{Q}\boldsymbol{y}(t) + \sum_{\{A\}\in\Phi} p_{A} + \sum_{\{C\}\in\Psi} p_{C} \tag{2.26}$$

holds, where $\boldsymbol{P}$ *and* $\boldsymbol{Q}$ *are two block-diagonal positive-definite matrices, set* Φ *contains frames being placed at the driven cutting point of this subsystem and set* Ψ *contains frames being placed at the driving cutting points of this subsystem, and* p_{A} *and* P_{C} *denote the virtual power flows in Definition 2.9.*

The following lemma represented in (Zhu 2012, p.37) shows that two adjacent subsystems that are *virtually stable* are equivalent to a single subsystem that is *virtually stable*.

Lemma 2.1. *Every two adjacent subsystems that are virtually stable can be equivalent to a single subsystem that is virtually stable in the sense of Definition 2.*10.*. Every virtual function in L_p affiliated with any one of the two adjacent subsystems remains to be a virtual function in L_p affiliated with the equivalent subsystem for $p = 2, \infty$.*

Finally, when every subsystem is guaranteed to be virtually stable in the sense of Definition 2.10., the following theorem given in (Zhu 2010, p.38) ensures that the L_2 and L_∞ stability of the system can be guaranteed.

Theorem 2.1. *Consider the system that is virtually decomposed into subsystems and is represented by a simple oriented graph. If every subsystem is virtually stable in the sense of Definition 2.*10.*, then all virtual functions in L_2 are functions in L_2 and all virtual functions in L_∞ are functions in L_∞.*

3 VIRTUAL DECOMPOSITION CONTROL APPROACH

The general formulation for *Virtual Decomposition Control* (VDC) approach is represented in (Zhu 2010). However, this complete general formulation is far too profound to deal with in scope of this thesis. In view of this fact, only the essential formulation and theory from (Zhu 2010) to apply VDC into studied system will be introduced in this chapter.

First in section 3.1, virtual decomposition is illustrated by conceptually "breaking" complex robotic system into subsystems, namely into *objects* and *rigid links*. In section 3.2, kinematics of decomposed subsystems is covered. In sections 3.3, dynamics and control of *objects* completed with virtual stability analysis are explored in more detail and respectively, dynamics and control of *rigid links* completed with virtual stability analysis are explored in sections 3.4. After the dynamics and control issues of *objects* and *rigid links* has been addressed, first in section 3.5, the required force/moment vector computations of the entire system are given, and then, in section 3.6, the dynamics and control issues of joints are to be addressed. Finally, in section 3.7, the joint/actuator position control implementation is given.

3.1 Virtual Decomposition

The VDC approach is based on the concept of a virtual decomposition. A complex robotic system, represented in (Zhu 2010, p.65), is illustrated in Figure 4 and is used here as an illustrative example to clarify virtual decomposition process.

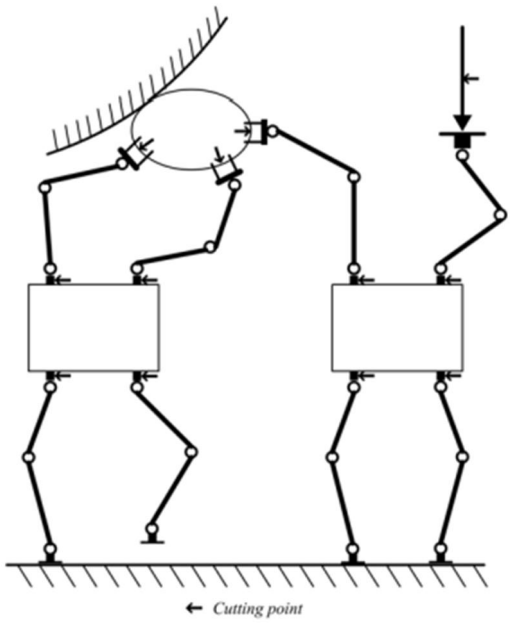

Figure 4: Example of some complex robotic system. (Zhu 2010, p.65)

As represented in (Zhu 2010, p.65), in a virtual decomposition, system is first virtually decomposed into n_o *objects* and n_c *open chains* by placing conceptual *virtual cutting points* defined in Definition 2.4. After being virtually decomposed, a complex robotic system, represented in Figure 4, can be represented as a simple oriented graph defined in Definition 2.5. Simple oriented graph of complex robotic system is illustrated in Figure 5.

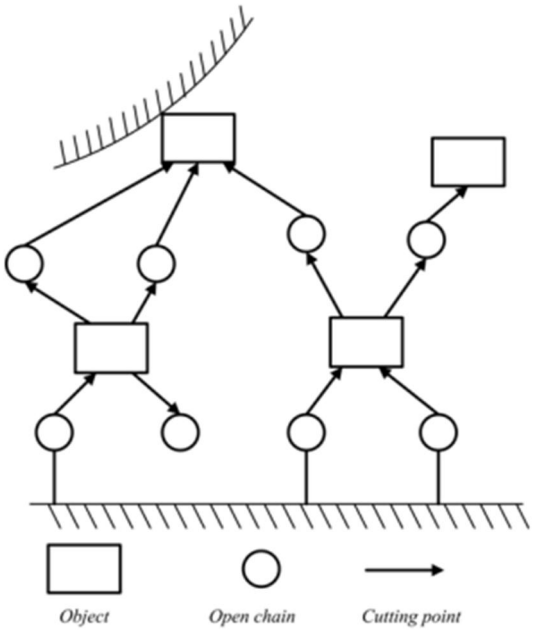

Figure 5: Simple oriented graph of complex robotic system represented in Figure 4. (Zhu 2010, p.66)

In next subsections 3.1.1 and 3.1.2, a nodes (or subsystems) of simple oriented graph, namely *open chains* and *objects*, are to be defined and examined in more detailed.

3.1.1 One-DOF Open Chains

According to (Zhu 1997), an *open chain* is a base floating free-motion single chain constructed by a series of rigid links connected one by one through one-DOF joints. All joints of original system must be included in the *open chains*.

In studied system (to be represented in chapter 4) all decomposed *open chains* contains only one-DOF. In view of this fact, in this chapter the theory covering only one-DOF *open chains* will be represented.

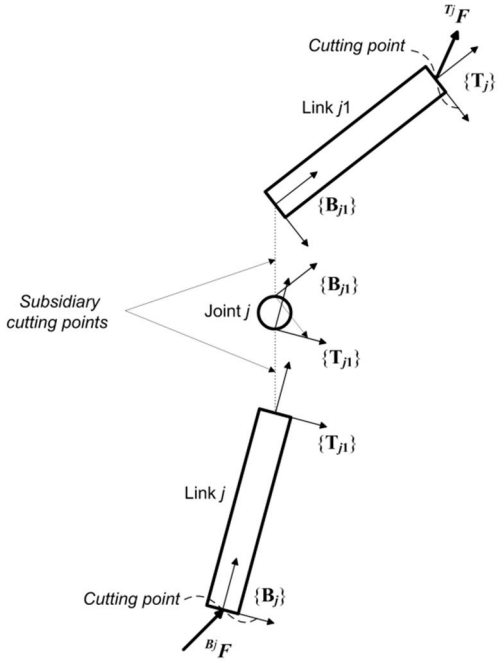

Figure 6: *j*th one-DOF decomposed *open chain*.

In Figure 6 is illustrated the *j*th decomposed one-DOF *open chain*, $j \in \{1, n_c\}$. The *j*th one-DOF *open chain*, comprises of *2* rigid links, namely link *j* and link *j*1, connected by one joint, namely joint *j*. The *j*th *open chain* has two *cutting points* located at both ends. The *driven cutting point* is located at the bottom of the link *j* and the *driving cutting point* at the top of link *j*1. Frame $\{\mathbf{B}_j\}$ is fixed to the *driven cutting point* in link *j* and frame $\{\mathbf{T}_j\}$ is fixed to the *driving cutting point* in link *j*1. The force/moment vector ${}^{B_j}\boldsymbol{F}$ in frame $\{\mathbf{B}_j\}$ is exerted (directed) toward the *j*th *open chain*, and the force/moment vector ${}^{T_j}\boldsymbol{F}$ in frame $\{\mathbf{T}_j\}$ is exerted (directed) away from the *j*th *open chain*. (Zhu 2010, p.65)

In Figure 6 there are also two so called *subsidiary cutting points*. Aim of *subsidiary cutting points* is at virtually isolate the joints from the rigid links. For joint *j* a pair of frames, denoted as $\{\mathbf{B}_{j1}\}$ and $\{\mathbf{T}_{j1}\}$, is located to the joint *j* with frame $\{\mathbf{B}_{j1}\}$ being fixed to link *j* and frame $\{\mathbf{T}_{j1}\}$ being fixed to link *j*1. (Zhu 2010, p.65)

In view of Definition 2.4, the *cutting point* associated with frame $\{\mathbf{B}_j\}$ is called the *driven cutting point* of link *j*. The *subsidiary cutting point* associated with frame $\{\mathbf{B}_{j1}\}$, is called the *driving cutting point* of joint *j* and is simultaneously called the *driven cutting point* of link *j*1. The *subsidiary cutting point* associated with frame $\{\mathbf{T}_{j1}\}$ is

called the *driving cutting point* of link *j* and is simultaneously called the *driven cutting point* of joint 1. Finally, the *cutting point* associated with frame {**T**$_j$} is called the *driving cutting point* of link *j*1.

3.1.2 Objects

An *object* is a rigid body on which the motion and force control specifications are given. (Zhu 2010, p.68) In *object* there can be a several *driven* and *driving cutting points* with at least one *driven cutting point*. An *object* may or may not be contact with environment. A rigid link with three or more joints must be handled as an *object*, because it cannot form a single chain and thus it cannot be included in an open chain. Also all rigid bodies which are in contact with the environment must be taken as *objects*. (Zhu 1997) In scope of this thesis, only contactless situations are to be considered.

In Figure 7 is illustrated the *i*th *object*, $i \in \{1, n_0\}$, of decomposed system.

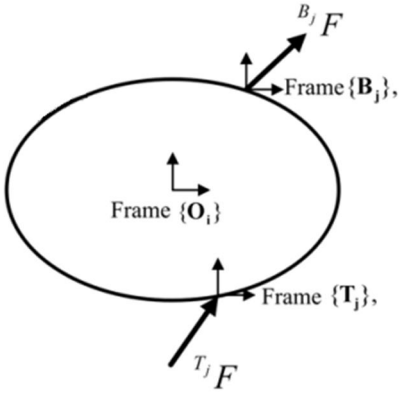

Figure 7: The ith object of decomposed system. (Zhu 2010, p.69)

In *i*th *object* frame {**O**$_i$} is fixed to describe the motion and force specifications. If the *j*th *open chain*, given in Figure 6, is adjacent to the *i*th object with frame {**B**$_j$} being placed at the *cutting point* between them, then this cutting point is called a *driving cutting point* of the *i*th *object*. The force/moment vector $^{\boldsymbol{B}_j}\boldsymbol{F}$ in frame {**B**$_j$} is exerted from the *i*th *object* toward the *j*th *open chain*. Alternatively, if the *j*th *open chain*, given in Figure 6, is adjacent to the *i*th *object* with frame {**T**$_j$} being placed at the *cutting point* between them, then this *cutting point* is called a *driven cutting point* of the *i*th *object*. The force/moment vector $^{\boldsymbol{T}_j}\boldsymbol{F}$ in frame {**T**$_j$} is exerted from the *j*th *open chain* toward *i*th *object*. (Zhu 2010, p.68-69)

3.2 Kinematics Computations

First, before dynamics and control issues of the system can be considered, all kinematics computations including velocity transformations among different body-attached frames are needed to be carry out by propagating from the *open chain* 1,

through *open chain j* (for all $j \in \{2, n_c\}$) and *object i* (for all $i \in \{1, n_o - 1\}$), to *object* n_o.

First, in subsections 3.2.1 and 3.2.2, velocity transformations considering to the *j*th one-DOF *open chain* (illustrated in Figure 6) and the *i*th *object* (illustrated in Figure 7), respectively, are to be given.

Then, in subsection 3.2.3, an important design vector, namely required velocity vector, is introduced and required velocity transformations considering to the *j*th one-DOF *open chain* and the *i*th *object* are given.

3.2.1 Velocity Transformations of *j*th Open Chain

Consider the fact that the linear/angular velocity vector ${}^{\boldsymbol{B_j}}\boldsymbol{V} \in \mathbb{R}^6$ at the *driven cutting point* of *j*th one-DOF *open chain* is known[2]. Hence, in the view of equation (2.6), the linear/angular velocity vector of frame $\{\boldsymbol{T}_{j1}\}$ of *j*th *open chain* (illustrated in Figure 6) can be given as

$$ {}^{\boldsymbol{T_{j1}}}\boldsymbol{V} = {}^{\boldsymbol{B_j}}\boldsymbol{U}^{T}_{\boldsymbol{T_{j1}}}\,{}^{\boldsymbol{B_j}}\boldsymbol{V} \tag{3.1} $$

The *j*th joint of *j*th one-DOF *open chain* can be either revolute joint or prismatic joint. Let $\dot{q}_j$ be the angular velocity of revolute joint and $\dot{x}_j$ be the linear velocity of prismatic joint. Now, in view of (2.6) and (3.1), the relationship between the velocity of *j*th joint and the linear/angular velocity vectors of the adjacent links can be expressed for revolute joint as

$$ \begin{aligned} {}^{\boldsymbol{B_{j1}}}\boldsymbol{V} &= \boldsymbol{z}\dot{q}_j + {}^{\boldsymbol{T_{j1}}}\boldsymbol{U}^{T}_{\boldsymbol{B_{j1}}}\,{}^{\boldsymbol{T_{j1}}}\boldsymbol{V} \\ &= \boldsymbol{z}\dot{q}_j + {}^{\boldsymbol{B_j}}\boldsymbol{U}^{T}_{\boldsymbol{B_{j1}}}\,{}^{\boldsymbol{B_j}}\boldsymbol{V} \end{aligned} \tag{3.2} $$

where $\boldsymbol{z} = [0,0,0,0,0,1]^T$. If the *j*th joint is prismatic equation (3.2) will take form of

$$ \begin{aligned} {}^{\boldsymbol{B_{j1}}}\boldsymbol{V} &= \boldsymbol{x}\dot{x}_j + {}^{\boldsymbol{T_{j1}}}\boldsymbol{U}^{T}_{\boldsymbol{B_{j1}}}\,{}^{\boldsymbol{T_{j1}}}\boldsymbol{V} \\ &= \boldsymbol{x}\dot{x}_j + {}^{\boldsymbol{B_j}}\boldsymbol{U}^{T}_{\boldsymbol{B_{j1}}}\,{}^{\boldsymbol{B_j}}\boldsymbol{V} \end{aligned} \tag{3.3} $$

where $\boldsymbol{x} = [1,0,0,0,0,0]^T$.

---

[2] ${}^{\boldsymbol{B_j}}\boldsymbol{V} \in \mathbb{R}^6$ can be obtained either from velocity transformation from known inertial frame, if *j*=1, or it is corresponding with known linear/angular velocity vector ${}^{\boldsymbol{B_j}}\boldsymbol{V} \in \mathbb{R}^6$ of adjacent *i*th *object*

Finally, in view of (2.6), (3.2) and (3.3), the linear/angular velocity frame $\{\boldsymbol{T}_j\}$ can be given as

$$^{\boldsymbol{T}_j}\boldsymbol{V} = {}^{\boldsymbol{B}_{j1}}\boldsymbol{U}_{\boldsymbol{T}_j}^{T}\,{}^{\boldsymbol{B}_{j1}}\boldsymbol{V} \tag{3.4}$$

3.2.2 Velocity Transformation of *i*th Object

Consider the fact that the velocity of *driven cutting point* of *i*th *object* is now known in view of (2.6) and equation (3.4). Thus, in view of (2.6), for the *i*th *object* (illustrated in Figure 7) the following relationships hold for velocity transformations

$$\begin{aligned} ^{\boldsymbol{O}_i}\boldsymbol{V} &= {}^{\boldsymbol{T}_j}\boldsymbol{U}_{\boldsymbol{O}_i}^{T}\,{}^{\boldsymbol{T}_j}\boldsymbol{V} \\ &= {}^{\boldsymbol{B}_j}\boldsymbol{U}_{\boldsymbol{O}_i}^{T}\,{}^{\boldsymbol{B}_j}\boldsymbol{V} \end{aligned} \tag{3.5}$$

3.2.3 Required Velocities and Required Velocity Transformations

When the required velocities for the *j*th joint of *j*th one-DOF *open chain* is specified for all $j \in \{1, n_c\}$, to validate (2.22), the required velocity transformations for *j*th one-DOF *open chain* can be written in view of (3.1) − (3.4) as

$$^{\boldsymbol{T}_{j1}}\boldsymbol{V}_r = {}^{\boldsymbol{B}_j}\boldsymbol{U}_{\boldsymbol{T}_{j1}}^{T}\,{}^{\boldsymbol{B}_j}\boldsymbol{V}_r \tag{3.6}$$

in case of revolute joint

$$\begin{aligned} ^{\boldsymbol{B}_{j1}}\boldsymbol{V}_r &= \boldsymbol{z}\dot{q}_{jr} + {}^{\boldsymbol{T}_{j1}}\boldsymbol{U}_{\boldsymbol{B}_{j1}}^{T}\,{}^{\boldsymbol{T}_{j1}}\boldsymbol{V}_r \\ &= \boldsymbol{z}\dot{q}_{jr} + {}^{\boldsymbol{B}_j}\boldsymbol{U}_{\boldsymbol{B}_{j1}}^{T}\,{}^{\boldsymbol{B}_j}\boldsymbol{V}_r \end{aligned} \tag{3.7}$$

and in case of prismatic joint

$$\begin{aligned} ^{\boldsymbol{B}_{j1}}\boldsymbol{V}_r &= \boldsymbol{x}\dot{x}_{jr} + {}^{\boldsymbol{T}_{j1}}\boldsymbol{U}_{\boldsymbol{B}_{j1}}^{T}\,{}^{\boldsymbol{T}_{j1}}\boldsymbol{V}_r \\ &= \boldsymbol{x}\dot{x}_{jr} + {}^{\boldsymbol{B}_j}\boldsymbol{U}_{\boldsymbol{B}_{j1}}^{T}\,{}^{\boldsymbol{B}_j}\boldsymbol{V}_r, \end{aligned} \tag{3.8}$$

and finally,

$$^{\boldsymbol{T}_j}\boldsymbol{V}_r = {}^{\boldsymbol{B}_{j1}}\boldsymbol{U}_{\boldsymbol{T}_j}^{T}\,{}^{\boldsymbol{B}_{j1}}\boldsymbol{V}_r. \tag{3.9}$$

Note that $^{\boldsymbol{B}_j}\boldsymbol{V}_r \in \mathbb{R}^6$ in equation (3.6) is known by similar manners to $^{\boldsymbol{B}_j}\boldsymbol{V} \in \mathbb{R}^6$ (see subsection 3.2.1).

For the *i*th *object*, required velocity vectors can be written in view of (2.22), (3.9), and (3.4) as

$$\begin{aligned} {}^{O_i}\boldsymbol{V}_r &= {}^{T_j}\boldsymbol{U}_{O_i}^{T}\,{}^{T_j}\boldsymbol{V}_r \\ &= {}^{B_j}\boldsymbol{U}_{O_i}^{T}\,{}^{B_j}\boldsymbol{V}_r \end{aligned} \tag{3.10}$$

3.3 Dynamics and Control of *i*th Object

The VDC approach allows the dynamics and control issues of the *i*th *object*, represented in section 3.1.2, to be handled independently, provided that *i*th *object* combined with its respective control equations qualifies to be virtually stable in sense of Definition 2.10. In this section the dynamics and control equations for the *i*th *object*, in view of (Zhu 2010, pp.72-78), are given.

3.3.1 Dynamics of *i*th Object

Referring back to (2.14), the dynamics of the *i*th *object* can be expressed as

$$\boldsymbol{M}_{O_i}\frac{d}{dt}\left({}^{O_i}\boldsymbol{V}\right) + \boldsymbol{C}_{O_i}\left({}^{O_i}\boldsymbol{\omega}\right){}^{O_i}\boldsymbol{V} + \boldsymbol{G}_{O_i} = {}^{O_i}\boldsymbol{F}^{*} \tag{3.11}$$

where the linear/angular velocity vector ${}^{O_i}\boldsymbol{V} \in \mathbb{R}^6$ is obtained from (3.5). On the other hand, the net force/moment vector in frame $\{\mathbf{O}_i\}$ is governed by

$${}^{O_i}\boldsymbol{F}^{*} = \sum {}^{O_i}\boldsymbol{U}_{T_j}\,{}^{T_j}\boldsymbol{F} - \sum {}^{O_i}\boldsymbol{U}_{B_j}\,{}^{B_j}\boldsymbol{F} \tag{3.12}$$

3.3.2 Required Net Force/Moment Vectors of *i*th Object

After ${}^{O_i}\boldsymbol{V}_r \in \mathbb{R}^6$ is being obtained from (3.10), a new design vector, namely the required net force/moment vector, is specified as

$${}^{O_i}\boldsymbol{F}_r^{*} = \boldsymbol{Y}_{O_i}\boldsymbol{\theta}_{O_i} + \boldsymbol{K}_{O_i}\left({}^{O_i}\boldsymbol{V}_r - {}^{O_i}\boldsymbol{V}\right) \tag{3.13}$$

where $\boldsymbol{K}_{O_i} \in \mathbb{R}^{6\times 6}$ is a positive-definite gain matrix characterizing the velocity feedback control. The term $\boldsymbol{Y}_{O_i}\boldsymbol{\theta}_{O_i}$ denotes the model based feedforward compensation term by using the required velocities and their time derivatives. The regressor matrix $\boldsymbol{Y}_{O_i} \in \mathbb{R}^{6\times 13}$ and the parameter vector $\boldsymbol{\theta}_{O_i} \in \mathbb{R}^{13}$ are defined according to (2.19) and further given in Appendix A by substituting frame $\{\mathbf{O}_i\}$ for frame $\{\mathbf{A}\}$.

3.3.3 Required Force/Moment Vector Transformation of *i*th Object

Similar to (3.12), the force resultant equation is applied to the required forces. It follows that

$$ {}^{o_i}\boldsymbol{F}_r^* = \sum \left({}^{o_i}\boldsymbol{U}_{\boldsymbol{T}_j}{}^{\boldsymbol{T}_j}\boldsymbol{F}_r \right) - \sum \left({}^{o_i}\boldsymbol{U}_{\boldsymbol{B}_j}{}^{\boldsymbol{B}_j}\boldsymbol{F}_r \right) \tag{3.14} $$

holds.

3.3.4 Virtual Stability

In this subsection, it will be shown that according to (Zhu 2010, pp.76-78) each *object* combined with its respective control equations qualifies to be *virtually stable* in sense of Definition 2.10.

Lemma 3.1. *Consider the ith object described by (3.11) and combined with its respective control equation (3.13). If non-negative accompanying function for this object is chosen as*

$$ \nu_{\mathbf{O_i}} = \tfrac{1}{2}\left({}^{\mathbf{O_i}}\mathbf{V_r} - {}^{\mathbf{O_i}}\mathbf{V}\right)^{\mathrm{T}}\mathbf{M}_{\mathbf{O_i}}\left({}^{\mathbf{O_i}}\mathbf{V_r} - {}^{\mathbf{O_i}}\mathbf{V}\right) \tag{3.15} $$

then it follows that

$$ \begin{aligned} \dot{\nu}_{\mathbf{O_i}} \leq & -\left({}^{\mathbf{O_i}}\mathbf{V_r} - {}^{\mathbf{O_i}}\mathbf{V}\right)^{\mathrm{T}}\mathbf{K}_{\mathbf{O_i}}\left({}^{\mathbf{O_i}}\mathbf{V_r} - {}^{\mathbf{O_i}}\mathbf{V}\right) \\ & + \left({}^{\mathbf{O_i}}\mathbf{V_r} - {}^{\mathbf{O_i}}\mathbf{V}\right)^{\mathrm{T}}\left({}^{\mathbf{O_i}}\mathbf{F}_{\mathrm{r}}^* - {}^{\mathbf{O_i}}\mathbf{F}^*\right) \end{aligned} \tag{3.16} $$

holds.

The following theorem given in (Zhu 2010, p.81) ensures that *i*th *object* combined with its respective control equations qualifies to be *virtually stable* in the sense of Definition 2.10.

Theorem 3.1. *The ith object described by (3.5), (3.11), and (3.12), combined with its respective control equations (3.10), (3.13),and (3.14), is virtually stable with its affiliated vector* $ {}^{o_i}\boldsymbol{V_r} - {}^{o_i}\boldsymbol{V} $ *being a virtual function in both* L_2 *and* L_∞*, in the sense of Definition 2.*10.

The complete proof for above Theorem (i.e. *virtual stability* of *i*th *object*) can be found in (Zhu 2010, p. 77-78)

3.4 Dynamics and Control of Rigid Links

In this section the dynamics and control issues of the *j*th one-DOF open chain, described in section 3.1.1, will be covered in the view of (Zhu 2010, pp.78-82). Aim of this section is to represent that both links of the *j*th one-DOF *open chain* combined with its respective control equations qualifies to be virtually stable in sense of Definition 2.10.

3.4.1 Dynamics of Rigid Links

Referring back to (2.14), the dynamics of the link *j*1 and link *j* of the *i*th one-DOF *open chain* can be expressed as

$$\boldsymbol{M}_{\boldsymbol{B}_{j1}} \frac{d}{dt}\left({}^{\boldsymbol{B}_{j1}}\boldsymbol{V}\right) + \boldsymbol{C}_{\boldsymbol{B}_{j1}}\left({}^{\boldsymbol{B}_{j1}}\boldsymbol{\omega}\right){}^{\boldsymbol{B}_{j1}}\boldsymbol{V} + \boldsymbol{G}_{\boldsymbol{B}_{j1}} = {}^{\boldsymbol{B}_{j1}}\boldsymbol{F}^{*} \tag{3.17}$$

$$\boldsymbol{M}_{\boldsymbol{B}_{j}} \frac{d}{dt}\left({}^{\boldsymbol{B}_{j}}\boldsymbol{V}\right) + \boldsymbol{C}_{\boldsymbol{B}_{j}}\left({}^{\boldsymbol{B}_{j}}\boldsymbol{\omega}\right){}^{\boldsymbol{B}_{j}}\boldsymbol{V} + \boldsymbol{G}_{\boldsymbol{B}_{j}} = {}^{\boldsymbol{B}_{j}}\boldsymbol{F}^{*} \tag{3.18}$$

where the linear/angular velocity vector ${}^{\boldsymbol{B}_{j}}\boldsymbol{V} \in \mathbb{R}^{6}$ is known and ${}^{\boldsymbol{B}_{j1}}\boldsymbol{V} \in \mathbb{R}^{6}$ is obtained either from (3.2) or from (3.3), depending on the type of joint.

On the other hand, in view of (2.7) and Figure 6 the above net force/moment vectors can be further expressed as

$${}^{\boldsymbol{B}_{j1}}\boldsymbol{F}^{*} = {}^{\boldsymbol{B}_{j1}}\boldsymbol{F} - {}^{\boldsymbol{B}_{j1}}\boldsymbol{U}_{\boldsymbol{T}_{j}}{}^{\boldsymbol{T}_{j}}\boldsymbol{F} \tag{3.19}$$

$$\begin{aligned} {}^{\boldsymbol{B}_{j}}\boldsymbol{F}^{*} &= {}^{\boldsymbol{B}_{j}}\boldsymbol{F} - {}^{\boldsymbol{B}_{j}}\boldsymbol{U}_{\boldsymbol{T}_{j1}}{}^{\boldsymbol{T}_{j1}}\boldsymbol{F} \\ &= {}^{\boldsymbol{B}_{j}}\boldsymbol{F} - {}^{\boldsymbol{B}_{j}}\boldsymbol{U}_{\boldsymbol{B}_{j1}}{}^{\boldsymbol{B}_{j1}}\boldsymbol{F} \end{aligned} \tag{3.20}$$

3.4.2 Required Net Force/Moment Vectors of *j*th One-DOF Open Chain

After the required linear/angular velocity vectors ${}^{\boldsymbol{B}_{j}}\boldsymbol{V}_{\boldsymbol{r}} \in \mathbb{R}^{6}$ are ${}^{\boldsymbol{O}_{\boldsymbol{B}_{j1}}}\boldsymbol{V}_{\boldsymbol{r}} \in \mathbb{R}^{6}$ are being specified (see subsection 3.2.3), the required net force/moment vectors, can be specified as

$${}^{\boldsymbol{B}_{j}}\boldsymbol{F}_{r}^{*} = \boldsymbol{Y}_{\boldsymbol{B}_{j}}\boldsymbol{\theta}_{\boldsymbol{B}_{j}} + \boldsymbol{K}_{\boldsymbol{B}_{j}}\left({}^{\boldsymbol{B}_{j}}\boldsymbol{V}_{\boldsymbol{r}} - {}^{\boldsymbol{B}_{j}}\boldsymbol{V}\right) \tag{3.21}$$

$${}^{\boldsymbol{B}_{j1}}\boldsymbol{F}_{r}^{*} = \boldsymbol{Y}_{\boldsymbol{B}_{j1}}\boldsymbol{\theta}_{\boldsymbol{B}_{j1}} + \boldsymbol{K}_{\boldsymbol{B}_{j1}}\left({}^{\boldsymbol{B}_{j1}}\boldsymbol{V}_{\boldsymbol{r}} - {}^{\boldsymbol{B}_{j1}}\boldsymbol{V}\right), \tag{3.22}$$

where $\boldsymbol{K}_{\boldsymbol{B}_{j}} \in \mathbb{R}^{6\times6}$ and $\boldsymbol{K}_{\boldsymbol{B}_{j1}} \in \mathbb{R}^{6\times6}$ are symmetric positive-definite matrices representing the velocity feedback control gain matrices. The terms $\boldsymbol{Y}_{\boldsymbol{B}_{j}}\boldsymbol{\theta}_{\boldsymbol{B}_{j}}$ and $\boldsymbol{Y}_{\boldsymbol{B}_{j1}}\boldsymbol{\theta}_{\boldsymbol{B}_{j1}}$ denote the model-based feedforward compensation terms with the regressor matrices $\boldsymbol{Y}_{\boldsymbol{B}_{j}} \in \mathbb{R}^{6\times13}$ and $\boldsymbol{Y}_{\boldsymbol{B}_{j1}} \in \mathbb{R}^{6\times13}$ and the parameter vectors $\boldsymbol{\theta}_{\boldsymbol{B}_{j}} \in \mathbb{R}^{13}$ and

$\boldsymbol{\theta}_{\boldsymbol{B}_{j1}} \in \mathbb{R}^{13}$ being defined according to (2.19) and further given in Appendix A by substituting frames $\{\boldsymbol{B}_j\}$ and $\{\boldsymbol{B}_{j1}\}$ for frame $\{\mathbf{A}\}$, respectively.

3.4.3 Required Force/Moment Vector Transformation of *j*th One-DOF Open Chain

After ${}^{\boldsymbol{B}_j}\boldsymbol{F}_r^*$ and ${}^{\boldsymbol{B}_{j1}}\boldsymbol{F}_r^*$ are being obtained from (3.21) and (3.22), the required force/moment vectors in frame $\{\boldsymbol{B}_j\}$ and $\{\boldsymbol{B}_{j1}\}$ can be written as

$$ {}^{\boldsymbol{B}_{j1}}\boldsymbol{F}_r = {}^{\boldsymbol{B}_{j1}}\boldsymbol{F}_r^* + {}^{\boldsymbol{B}_{j1}}\boldsymbol{U}_{\boldsymbol{T}_j}{}^{\boldsymbol{T}_j}\boldsymbol{F}_r \tag{3.23} $$

$$ \begin{aligned} {}^{\boldsymbol{B}_j}\boldsymbol{F}_r &= {}^{\boldsymbol{B}_j}\boldsymbol{F}_r^* + {}^{\boldsymbol{B}_j}\boldsymbol{U}_{\boldsymbol{T}_{j1}}{}^{\boldsymbol{T}_{j1}}\boldsymbol{F}_r \\ &= {}^{\boldsymbol{B}_j}\boldsymbol{F}_r^* + {}^{\boldsymbol{B}_j}\boldsymbol{U}_{\boldsymbol{B}_{j1}}{}^{\boldsymbol{B}_{j1}}\boldsymbol{F}_r \end{aligned} \tag{3.24} $$

3.4.4 Virtual Stability

The following theorem given in (Zhu 2010, p.81) ensures that the *j*th one-DOF *open chain* combined with its respective control equations qualifies to be *virtually stable* in the sense of Definition 2.10.

Theorem 3.2. *Each rigid link of the jth open chain described by (3.18) or (3.17) subject to (3.1), (3.4), (3.19) and (3.20), combined with its respective control equations (3.6), (3.9), and (3.21) or (3.22), and (3.23) – (3.24), is virtually stable with its affiliated vector* ${}^{\boldsymbol{B}_j}\boldsymbol{V}_{\boldsymbol{r}} - {}^{\boldsymbol{B}_j}\boldsymbol{V}$ *or* ${}^{\boldsymbol{B}_{j1}}\boldsymbol{V}_{\boldsymbol{r}} - {}^{\boldsymbol{B}_{j1}}\boldsymbol{V}$*, being a virtual function in both* L_2 *and* L_∞*, in the sense of Definition 2.*10.

The complete proof for above Theorem (i.e. *virtual stability* of *i*th *open chain*) can be found in (Zhu 2010, p. 81-82).

3.5 Required Force/Moment Vector Computations of the Entire System

The required net force/moment vectors of the entire system can be computed along the opposite directions of the simple oriented graph, starting from the *sink nodes* towards the *source nodes*. Equation (3.14) is used for a node representing an *object* and equations (3.23) and (3.24) are used for a node representing a one-DOF *open chain*. The alternative connections of objects and open chains allows the alternative use of (3.14) and (3.23) and (3.24), leading to the completion of the computations. (Zhu 2010, pp.82-83)

3.6 Dynamics and Control of Joints

After the dynamics and control issues of the *i*th *object* and *j*th *open chains* has been addressed the dynamics and control issues of *j*th *joint* is to be addressed. The objective in the scope of this thesis is to show that a *j*th one-*DOF joint*, illustrated in Figure 6, combined with its control equations qualifies to be virtually stable in the sense of Definition 2.10.

Due to fact that all revolute joints in scope of this thesis are unactuated, following assumption is used throughout this thesis.

Assumption 1. *The friction torques in all unactuated rotational joints are zero.*

In view of above, in this section dynamics and control issues are addressed to cover only prismatic joints.

3.6.1 Joint Dynamics of Prismatic Joints

In view of (Zhu 2010, p.83), the dynamics of one-DOF prismatic joint can be written as

$$f_j^* \stackrel{\text{def}}{=} M_j \ddot{x}_j + \varepsilon_j(t) = f_j - \boldsymbol{z}^T {}^{\boldsymbol{B}_{j1}}\boldsymbol{F} \tag{3.25}$$

where $M_j \in \mathbb{R}$ is the equivalent mass, $x_j \in \mathbb{R}$ is the joint displacement, $f_j \in \mathbb{R}$ is the joint control force, $f_j^* \in \mathbb{R}$ represents the net force devoted to the joint dynamics, ${}^{\boldsymbol{B}_{j1}}\boldsymbol{F} \in \mathbb{R}^6$ denotes the force/moment vector in frame $\{\boldsymbol{B}_{j1}\}$ exerted from link j to link $j1$, and $\varepsilon_j(t) \in \mathbb{R}$ is the friction model for prismatic joint.

3.6.2 Control Equations

The relationship between the required velocity of the *j*th joint of the *j*th one-DOF *open chain* and the required linear/angular velocity vectors of its adjacent links in the case of prismatic joint is already defined in (3.8).

After $\dot{x}_{jr} \in \mathbb{R}$ being obtained (3.29), the joint control equations are designed as

$$f_{jr}^* = \boldsymbol{Y}_j \boldsymbol{\theta}_j + k_j\left(\dot{x}_{jr} - \dot{x}_j\right) \tag{3.26}$$

$$f_j = f_{jr}^* + \boldsymbol{z}^T {}^{\boldsymbol{B}_{j1}}\boldsymbol{F}_r \tag{3.27}$$

where $k_j > 0$ denotes the feedback gain of joint j and ${}^{\boldsymbol{B}_{j1}}\boldsymbol{F}_r \in \mathbb{R}^6$ is obtained from (3.23).

3.6.3 Virtual Stability

The following theorem ensures that a *j*th one-DOF joint combined with its respective control equations qualifies to be *virtually stable* in the sense of Definition 2.10.

Theorem 3.3. *The joint j of the jth open chain described by* (3.3) *and (3.25), combined with its respective control equations (3.8),(3.26), and (3.27), is virtually stable with its affiliated variable* $\dot{x}_{jr} - \dot{x}_j$ *being a virtual function of in both* L_2 and L_∞, in the sense of *Definition 2.*10.

The complete proof for above Theorem (i.e. *virtual stability* of joint *j* in the *jth* one-DOF *open chain*) can be found in (Zhu 2010, p. 85-86).

3.7 Joint Position Control Implementation

The VDC is based on velocity control, i.e. control objective is to make controlled actual velocities to track required velocities. In VDC objective is to design a velocity controller that takes care of all dynamics of the system. When velocity controller with L_2/L_∞ stability and asymptotic stability is designed, the required velocity can be "modified" to accomplish an ultimate control objective.

If the control objective is to make the manipulators position trajectory track to its desired position trajectory, the position control can be performed through a velocity controller by incorporating a position error term into the required velocity. In position control implementation new term namely desired velocity is introduced. A desired velocity serves the reference trajectory of a velocity with respect to time. In view of (Zhu 2010, p.51), the required velocity of the joint *j* of the *j*th *open chain* can be designed to be in a case of revolute joint as

$$\dot{q}_{jr} = \dot{q}_{jd} + \lambda[q_{jd} - q_j], \tag{3.28}$$

where $\dot{q}_{jd}$ denotes the desired joint velocity, $q_{jd} - q_j$ is a position error term, where q_{jd} denote the desired joint angle and q_j is actual measured joint angle, and $\lambda > 0$ is a control parameter.

Similar to (3.28), the respective equation for the prismatic joint, can designed to be as

$$\dot{x}_{jr} = \dot{x}_{jd} + \lambda[x_{jd} - x_j], \tag{3.29}$$

4 STUDIED HYDRAULIC MANIPULATOR

In this thesis the VDC approach is applied into hydraulically operated HIAB 031 manipulator. HIAB 031 contains two hydraulic cylinders (Cylinder 1 and Cylinder 2) which are used to operate two booms (Boom 1 and Boom 2) of manipulator. There exists also third cylinder which is used to operate the telescopic boom inside the boom 2, but in scope of this thesis telescopic cylinder is set to be fixed and non-operated. An external load, denoted as M, is attached at the tip of the manipulator. Studied manipulator is illustrated in Figure 8.

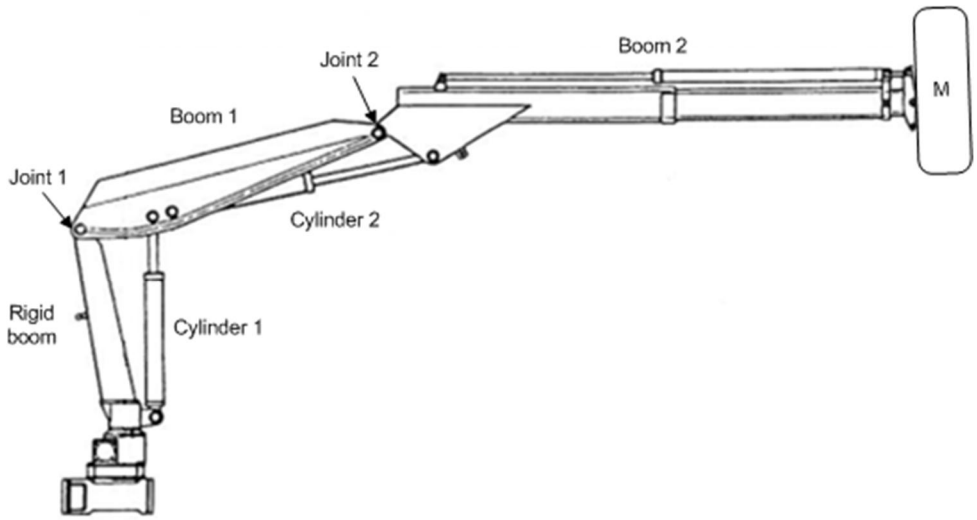

Figure 8: HIAB 031 hydraulic manipulator with attached mass.

As from Figure 8 can be seen, boom 1 is coupled with joint 1 (1-DOF rotational joint) to rigid boom from its other end and with joint 2 (1-DOF rotational joint) to boom 2 from another end. In a system a linear motion of cylinders (Cylinder 1 and Cylinder 2) is converted to rotational motion of joints (Joint 1 and Joint 2). Described construction provides 2-DOF in motion. More detailed information about structural dimensions of HIAB 031 can be found on Appendix C.

4.1 Direct Kinematics of HIAB 031

The aim of direct kinematics is to compute the position and orientation of the end-effector as a function of the joint variables (Sciavicco 2001, p.39). In our case, the tip of the boom 2 is considered as an end-effector of system.

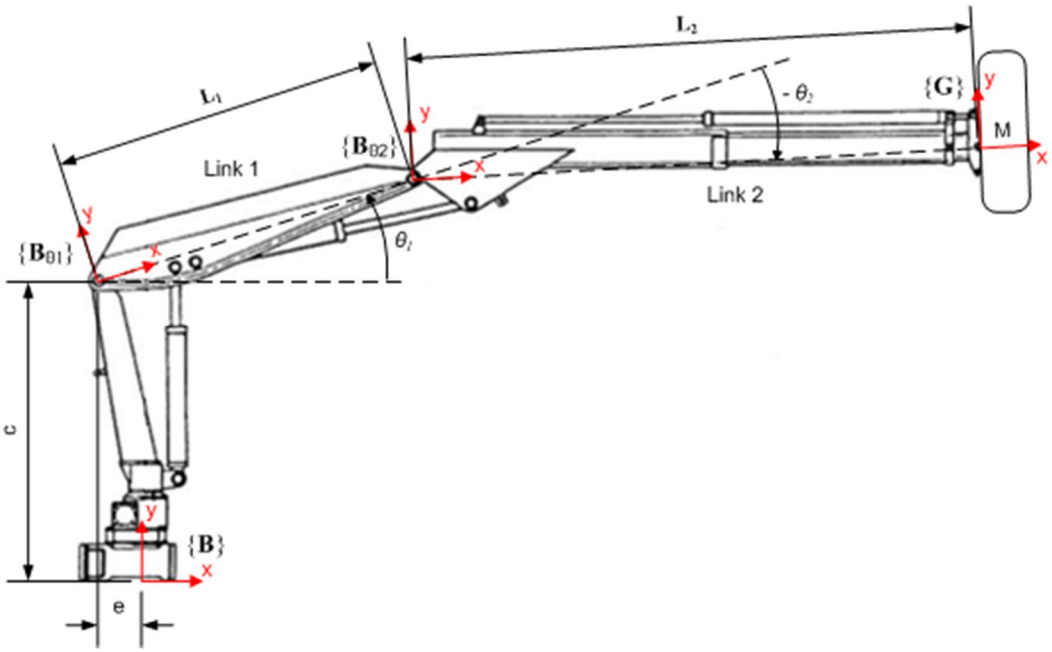

Figure 9: Frames and dimensions of manipulator to compute direct kinematics.

In order to compute direct kinematics of manipulator, four frames, namely $\{\boldsymbol{B}\}$, $\{\boldsymbol{B}_{\theta 1}\}$, $\{\boldsymbol{B}_{\theta 2}\}$ and $\{\boldsymbol{G}\}$, are attached in the assembly. Attached frames and structural dimensions needed in direct kinematics computations are represented in Figure 9. Frame $\{\boldsymbol{B}\}$ is a fixed and non-moving base frame of assembly. The *y*-axis of frame $\{\boldsymbol{B}\}$ is set to be pointing away from gravity. Frames $\{\boldsymbol{B}_{\theta 1}\}$ and $\{\boldsymbol{B}_{\theta 2}\}$ are attached to link 1 and link 2 at the location of joint 1 and joint 2, respectively, to represent a rotation of links. The rotation of link 1 and link 2 are represented with joint variables θ_1 and θ_2, respectively. Frame $\{\boldsymbol{G}\}$ is attached at the tip of link 2 and *x*-axis of frame $\{\boldsymbol{G}\}$ is set to be parallel with centerline of link 2.

In view of direct kinematic equations defined in (Sciavicco 2001), the transformation matrix from frame $\{\boldsymbol{B}\}$ to frame $\{\boldsymbol{G}\}$ can be given as

$$
\begin{aligned}
{}^{B}\boldsymbol{T}_{G} &= \begin{bmatrix} \cos(\theta_1+\theta_2) & -\sin(\theta_1+\theta_2) & 0 & L_1\cos(\theta_1)+L_2\cos(\theta_1+\theta_2)-e \\ \sin(\theta_1+\theta_2) & \cos(\theta_1+\theta_2) & 0 & L_1\sin(\theta_1)+L_2\sin(\theta_1+\theta_2)+c \\ 0 & 0 & 1 & 0 \\ 0 & 0 & 0 & 1 \end{bmatrix} \\
&= \begin{bmatrix} {}^{B}\boldsymbol{R}_{G} & \boldsymbol{p}_{G} \\ 0\ \ 0\ \ 0 & 1 \end{bmatrix}
\end{aligned} \tag{4.1}
$$

where

$$
{}^{B}\boldsymbol{R}_{G} = \begin{bmatrix} r_{11} & r_{12} & r_{13} \\ r_{21} & r_{22} & r_{23} \\ r_{31} & r_{32} & r_{33} \end{bmatrix}, \text{ and } \qquad \boldsymbol{p}_{G} = \begin{bmatrix} p_x \\ p_y \\ p_z \end{bmatrix}.
$$

In equation (4.1) ${}^{B}\boldsymbol{R}_{G}$ represents a rotation matrix from frame $\{\boldsymbol{B}\}$ to frame $\{\boldsymbol{G}\}$, describing the orientation of frame $\{\boldsymbol{G}\}$ with respect to frame $\{\boldsymbol{B}\}$. Term $\boldsymbol{p}_{G}$ represents a Cartesian position vector, describing the position of origin of frame $\{\boldsymbol{G}\}$ with respect to origin of frame $\{\boldsymbol{B}\}$ expressed in frame $\{\boldsymbol{B}\}$.

4.2 Inverse Kinematic of HIAB 031

The inverse kinematics consists of the determination of the joint variables corresponding to a given end-effector position and orientation (Sciavicco 2001, p.66). The inverse kinematic of manipulator can be derived from transformation matrix defined in (4.1) by using e.g. *algebraic solution technique* represented in (Sciavicco 2001, pp.67 - 68). Thus, the joint angles θ_2 and θ_1 can be given as a function of manipulator tip position in *x* and *y* with respect to reference frame $\{\boldsymbol{B}\}$ as

$$\theta_2(p_x, p_y) = -\cos^{-1}\left(\frac{(p_x-e)^2+(p_y-c)^2-L_1^2-L_2^2}{2L_1L_2}\right) \tag{4.2}$$

$$\theta_1(p_x, p_y) = \sin^{-1}\left(\frac{\left(L_1+L_2\cos\left(\theta_2(p_x,p_y)\right)\right)(p_y-c)-L_2\sin\left(\theta_2(p_x,p_y)\right)(p_x-e)}{L_1^2+L_2^2+2L_1L_2\cos\left(\theta_2(p_x,p_y)\right)}\right) \tag{4.3}$$

4.3 Differential Kinematics of HIAB 031

Differential kinematics defines the relationship between the joint velocities and the corresponding end-effector linear velocities in Cartesian space. This mapping is described by a matrix, termed *geometric Jacobian*. (Sciavicco 2001, p.79)

In the view of the equation (4.1), the Cartesian position of HIAB 031 with respect to frame $\{\boldsymbol{B}\}$ can be given as

$$\boldsymbol{p_G} = \begin{bmatrix} p_x \\ p_y \end{bmatrix} = \begin{bmatrix} L_1\cos(\theta_1) + L_2\cos(\theta_1+\theta_2) - e \\ L_1\sin(\theta_1) + L_2\sin(\theta_1+\theta_2) + c \end{bmatrix} \tag{4.4}$$

Note, that in (4.4) the Cartesian position $p_z = 0$ in *z* and can be thus neglected.

The geometric Jacobian of HIAB 031, can be defined in the view of (Jazar 2011, p.359) and (4.4) as

$$\boldsymbol{J_q} = \begin{bmatrix} \frac{\partial p_x}{\partial \theta_1} & \frac{\partial p_x}{\partial \theta_2} \\ \frac{\partial p_y}{\partial \theta_1} & \frac{\partial p_y}{\partial \theta_2} \end{bmatrix} = \begin{bmatrix} -L_1\sin(\theta_1) - L_2\sin(\theta_1+\theta_2) & -L_2\sin(\theta_1+\theta_2) \\ L_1\cos(\theta_1) + L_2\cos(\theta_1+\theta_2) & L_2\cos(\theta_1+\theta_2) \end{bmatrix} \tag{4.5}$$

The relationship between the joint velocities and the corresponding end-effector linear velocities of HIAB 031 can be written in the view of (Sciavicco 2001, p.79) and equation (4.5), as

$$\dot{\boldsymbol{p}}_{\boldsymbol{G}} = \boldsymbol{J_q}\dot{\boldsymbol{\theta}} \tag{4.6}$$

where $\dot{\boldsymbol{p}}_{\boldsymbol{G}} = [\dot{p}_x \quad \dot{p}_y]^T \in \mathbb{R}^2$ represents a Cartesian velocity vector, describing the velocity of origin of frame $\{\boldsymbol{G}\}$ with respect to origin of frame $\{\boldsymbol{B}\}$ expressed in frame $\{\boldsymbol{B}\}$, and $\dot{\boldsymbol{\theta}} = [\dot{\theta}_1 \quad \dot{\theta}_2]^T \in \mathbb{R}^2$ represents a respective angular velocity vector of HIAB 031 joints.

Further, the equation (4.6) can be written inversely as

$$\dot{\boldsymbol{\theta}} = \boldsymbol{J_q}^{-1}\dot{\boldsymbol{p}}_{\boldsymbol{G}} \tag{4.7}$$

where,

$$\boldsymbol{J_q}^{-1} = \frac{-1}{L_1 L_2 \sin(\theta_2)}\begin{bmatrix} -L_2\cos(\theta_1+\theta_2) & -L_2\sin(\theta_1+\theta_2) \\ L_1\cos(\theta_1)+L_2\cos(\theta_1+\theta_2) & L_1\sin(\theta_1)+L_2\sin(\theta_1+\theta_2) \end{bmatrix} \tag{4.8}$$

5 APPLYING VDC APPROACH INTO THE HIAB 031

In this chapter the VDC approach, introduced in chapter 3, is applied into HIAB 031 hydraulic manipulator, introduced in chapter 4.

5.1 Virtual Decomposition of HIAB 031

Using of hydraulic cylinders to provide a rotational movement produces *closed chains* in the kinematic structure of system. *A closed chain* means that sequence of links forms a loop in a system (Sciavicco 2001, p. 39). In our case, formed *closed chains* of a system are illustrated in Figure 10. Both *closed chains* contain three un-actuated rotational one-DOF joint and one actuated linear joint.

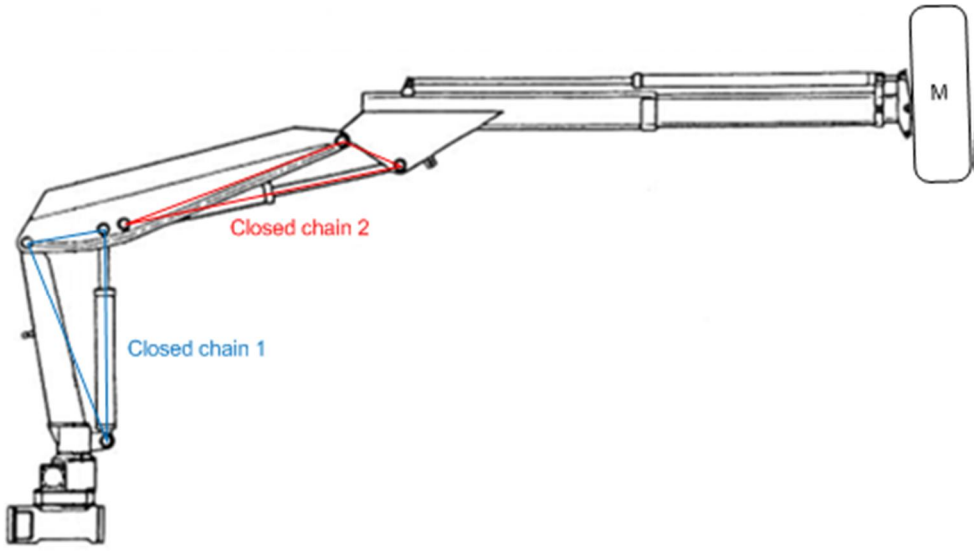

Figure 10: Closed chains of system.

As was introduced in section 3.1, in a virtual decomposition a system is first needed to be virtually decomposed into *objects* and *open chains* by placing conceptual *cutting points*. Because of existence of *closed chains*, system is first virtually decomposed into *objects* and *closed chains* by placing four cutting points to the both ends of cylinders joints (see Figure 11).

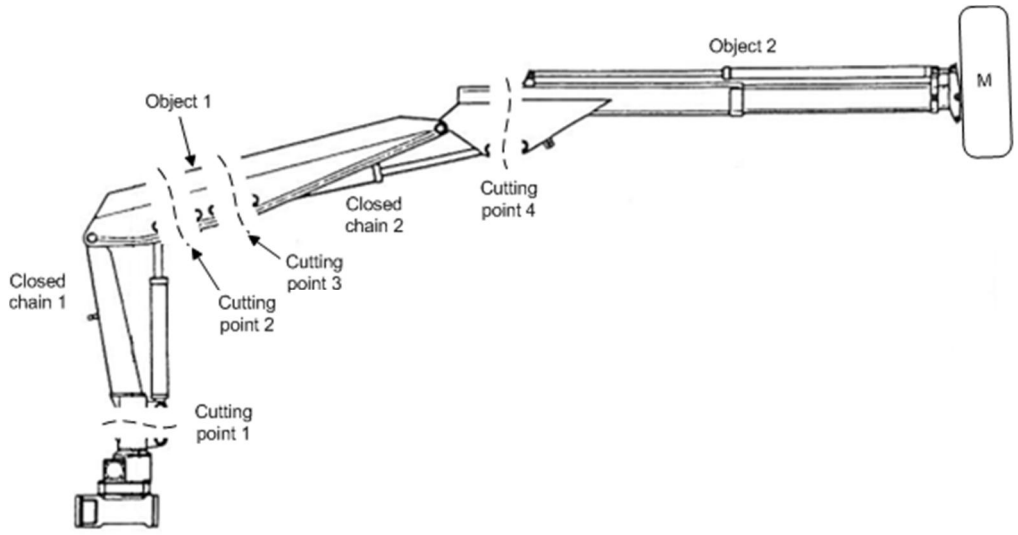

Figure 11: Placing of cutting points at HIAB 031.

In a simple oriented graph, introduced in section 2.7, there can be only *objects*, *open chains* and *cutting points*. This implies that both *closed chains* are needed to be further decomposed and expressed as a form of *open chains*. Conversion from *closed chain structure* to *open chain structures* can be seen from Figure 12 and Figure 13.

In view of the Definition 2.4, frames $\{\boldsymbol{B}_j\}$ and $\{\boldsymbol{T}_j\}$, where *j* denotes the number of open chain, are needed to attach to the *driven cutting point* and *driving cutting point* of *open chains*, respectively, to describe the motion and force specifications. Also *subsidiary cutting point*s are needed to attach. The virtual composition for the *closed chains* is made in view theory represented in subsection 3.1.2. The decomposed one-DOF open chains of system can be seen from Figure 12 and Figure 13.

As from Figure 12 and Figure 13 can be seen, there has been made one addition, into *open chains* with prismatic joint (*open chain* 2 and *open chain* 4), compared to general one-DOF *open chain* structure represented in Figure 6. This come due to fact that, in the *open chains* with prismatic joints the frames in the *driven cutting point*, namely $\{\boldsymbol{B}_2\}$ and $\{\boldsymbol{B}_4\}$, are not coincide with axis of actuation of respective joint. Thus, one "extra frame", namely $\{\boldsymbol{B}_{21}\}$ and $\{\boldsymbol{B}_{41}\}$, into *open chain* 2 and *open chain* 4, respectively, is needed to add. Function of these frames is to represent the rotation from frame in *driven cutting point* to actuation axis of respective joint. The structure of *open chain* 2 and *open chain* 4 is identical to structure represented in Figure 6, if frames $\{\boldsymbol{B}_{j1}\}$ and $\{\boldsymbol{B}_{j2}\}$, with $j = 2, 4$, in Figure 12 and Figure 13, are compare to frames $\{\boldsymbol{B}_j\}$ and $\{\boldsymbol{B}_j\}$ in Figure 6.

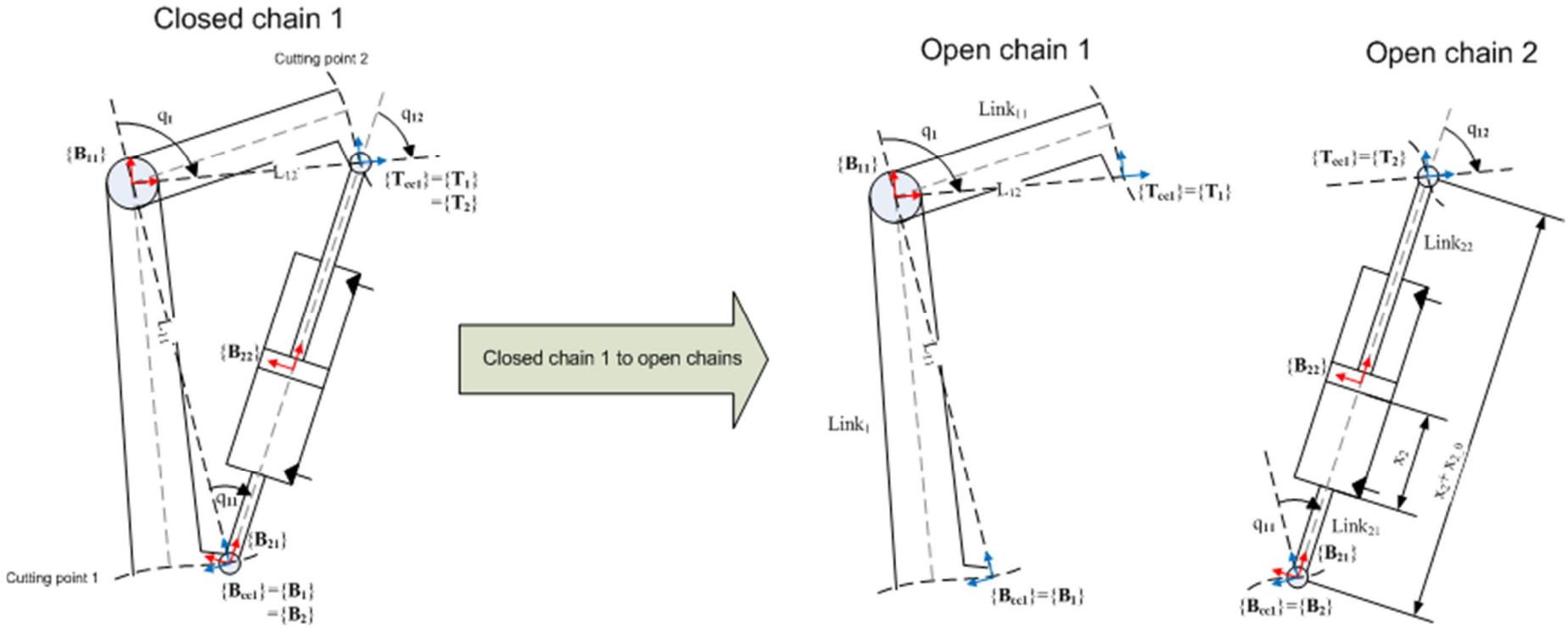

Figure 12: Closed chain 1 conversion to open chains.

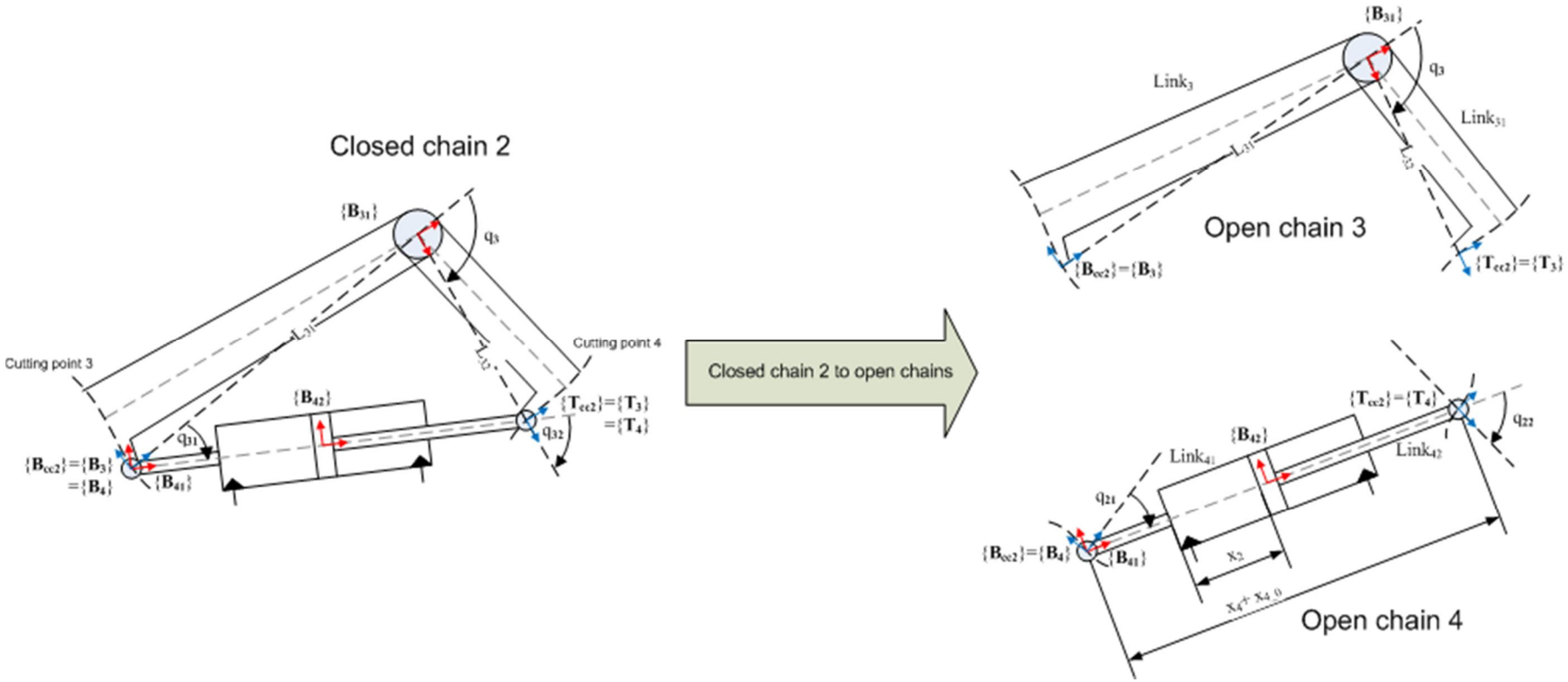

Figure 13: Closed chain 2 conversion to open chains.

As introduced in section 3.1.2, frames are also needed to attach at the *objects* of system to describe the motion and force specifications. Attached frames of *object 1* and *object 2* can be seen from Figure 14 and Figure 15, respectively.

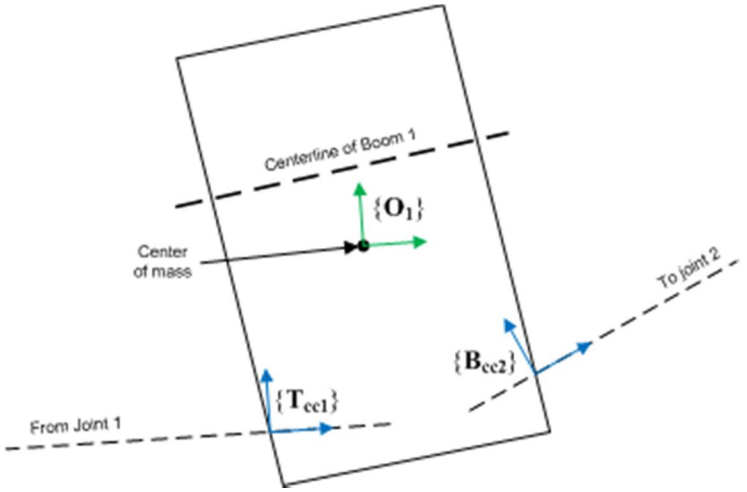

Figure 14: Frames of Object 1.

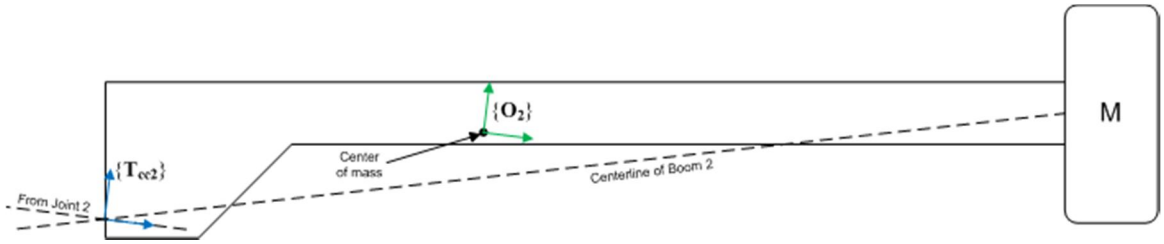

Figure 15: Frames of Object 2.

In Figure 14 and Figure 15, origins of frames $\{\boldsymbol{O}_1\}$ and $\{\boldsymbol{O}_2\}$ are fixed to the center of masses of *object 1* and *object 2*, respectively. Furthermore, frames $\{\boldsymbol{O}_1\}$ and $\{\boldsymbol{O}_2\}$ possess a same orientation with respect to frames $\{\boldsymbol{T}_{cc1}\}$ and $\{\boldsymbol{T}_{cc2}\}$, respectively.

In view of Figure 11, Figure 12, and Figure 13, a simple oriented graph can be formed and is represented in Figure 16. The rigid non-moving structure of manipulator which locates beneath *cutting point 1*, is modeled as *zero-mass object* as no motion control specification is assigned to the this part of manipulator.

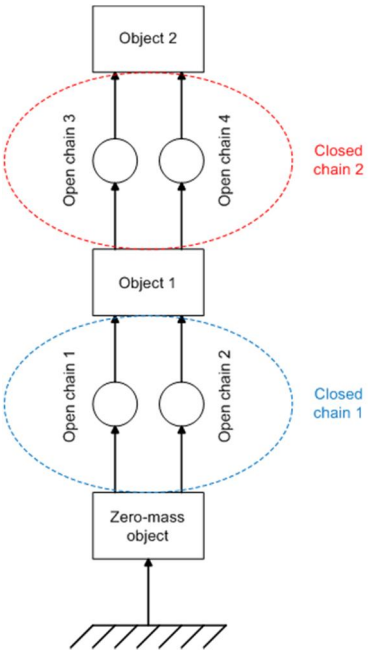

Figure 16: Simple oriented graph of HIAB 031.

In view of Figure 12, Figure 13, Figure 16, Figure 14 and Figure 15, it follows that

- The *j*th *open chain* has one *driving cutting point* associated with frame $\{\boldsymbol{T}_j\}$ and one *driven cutting point* associated with frame $\{\boldsymbol{B}_j\}$ for all $j \in \{1, 2, 3, 4\}$.
- The *open chains* with revolute joint (*open chain 1* and *open chain 3*) has one *subsidiary cutting point* associated with frame $\{\boldsymbol{B}_{j1}\}$, for $j = \{1,\ 3\}$.
- The *open chains* with prismatic joint (*open chain 2* and *open chain 4*) has one *subsidiary cutting point* associated with frame $\{\boldsymbol{B}_{j2}\}$, for $j = \{2,\ 4\}$.
- The *zero-mass object* has one *driving cutting point* associated with frame $\{\boldsymbol{B}_{cc1}\}$ and two *driven cutting points* associated with frames $\{\boldsymbol{B}_1\}$ and $\{\boldsymbol{B}_2\}$.
- The *object 1* has two *driving cutting point* associated with frame $\{\boldsymbol{B}_3\}$ and $\{\boldsymbol{B}_4\}$, and two *driven cutting points* associated with frames $\{\boldsymbol{T}_3\}$ and $\{\boldsymbol{T}_4\}$. Frame $\{\boldsymbol{O}_1\}$ is fixed at the center of mass of *object 1* to describe the force and the motion specifications.
- The *object 2* has two *driven cutting point* associated with frames $\{\boldsymbol{T}_3\}$ and $\{\boldsymbol{T}_4\}$. Frame $\{\boldsymbol{O}_2\}$ is fixed at the center of mass of *object 2* to describe the force and the motion specifications.

Finally, base frame $\{\boldsymbol{B}\}$ and goal frame $\{\boldsymbol{G}\}$, introduced in section 4.1, are attached to the system to finalize description of manipulator kinematics. All 22 attached frames of system can be seen from Figure 17.

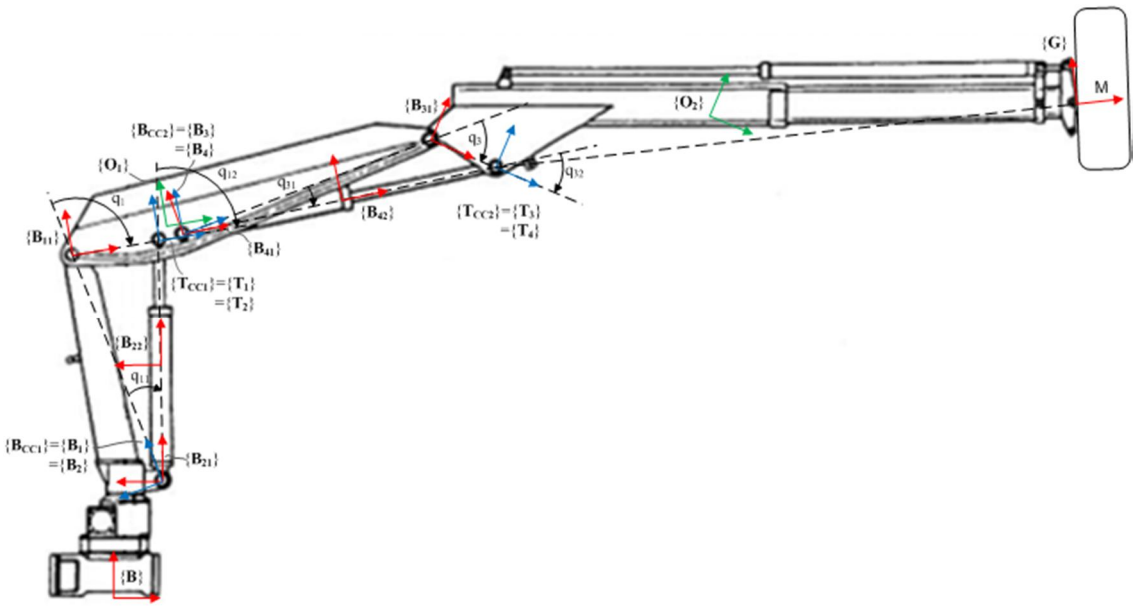

Figure 17: Attached frames of decomposed system.

5.2 Kinematic Equations of HIAB 031

In this section kinematics equations for each *open chain* and *object* of system will be given in view of theories represented in subsections 3.2.1 and 3.2.2, respectively. For a consolidate a general presentation, in following subsections a kinematic equations of *open chain 1* and *open chain 2* are elaborated under *closed chain 1*, and respectively a kinematic equations of *open chain 3* and *open chain 4* are elaborated under *closed chain 2*.

5.2.1 Joint Variables of System

The joint angles θ_1 and θ_2, represented in Figure 9, can be converted through geometry to respective *closed chain* angles q_1 and q_3, represented in Figure 17, as

$$q_1 = k_{q_1}\theta_1 \tag{5.1}$$
$$q_3 = k_{q_3}\theta_2 \tag{5.2}$$

where k_{q_1} and k_{q_3} represents conversion between joint angles and *closed chain* angles.

Joint velocities $\dot{q}_1$ and $\dot{q}_3$ can be computed by taking the time derivatives from joint angles θ_1 and θ_2, respectively.

As there was mentioned earlier, both *closed chains* of assembly contains three unactuated rotational joints and one actuated linear joint. Due to geometrical constraints of *closed chains*, by knowing joint variables q_1 and q_3, other three joint variables in the *closed chains* can be computed with the law of cosine, respectively, as

$$x_2 = \sqrt{L_{11}^2 + L_{12}^2 + 2L_{11}L_{12}\cos(q_1)} - x_{2\_0} \tag{5.3}$$

$$q_{11} = \cos^{-1}\left(\frac{{L_{12}}^2-(x_2+x_{2\_0})^2-{L_{11}}^2}{-2(x_2+x_{2\_0})L_{11}}\right) \tag{5.4}$$

$$q_{12} = \cos^{-1}\left(\frac{{L_{11}}^2-(x_2+x_{2\_0})^2-{L_{12}}^2}{-2(x_2+x_{2\_0})L_{12}}\right) \tag{5.5}$$

$$x_4 = \sqrt{L_{31}^2 + L_{32}^2 + 2L_{31}L_{32}\cos(q_3)} - x_{4\_0} \tag{5.6}$$

$$q_{31} = \cos^{-1}\left(\frac{{L_{32}}^2-(x_4+x_{4\_0})^2-{L_{31}}^2}{-2(x_4+x_{4\_0})L_{31}}\right) \tag{5.7}$$

$$q_{32} = \cos^{-1}\left(\frac{{L_{31}}^2-(x_4+x_{4\_0})^2-{L_{32}}^2}{-2(x_4+x_{4\_0})L_{32}}\right) \tag{5.8}$$

where L_{11} and L_{12} denote the link lengths of *open chain 1*, L_{31} and L_{32} denote the link lengths of *open chain 3*, and x_{2_0} and x_{4_0} denote the initial lengths of cylinder 1 and cylinder 2, respectively.

Taking the time derivatives of (5.3) - (5.8) yields

$$\dot{x}_2 = -\frac{L_{11}L_{12}\sin(q_1)}{x_2+x_{2\_0}}\dot{q}_1 \tag{5.9}$$

$$\dot{q}_{11} = -\frac{(x_2+x_{2\_0})-L_{11}\cos(q_{11})}{(x_2+x_{2\_0})L_{11}\sin(q_{11})}\dot{x}_2 \tag{5.10}$$

$$\dot{q}_{12} = -\frac{(x_1+x_{1\_0})-L_{12}\cos(q_{12})}{(x_1+x_{1\_0})L_{12}\sin(q_{12})}\dot{x}_2 \tag{5.11}$$

$$\dot{x}_4 = -\frac{L_{31}L_{32}\sin(q_3)}{x_4+x_{4\_0}}\dot{q}_3 \tag{5.12}$$

$$\dot{q}_{31} = -\frac{(x_4+x_{4\_0})-L_{31}\cos(q_{31})}{(x_4+x_{4\_0})L_{31}\sin(q_{31})}\dot{x}_4 \tag{5.13}$$

$$\dot{q}_{32} = -\frac{(x_4+x_{4\_0})-L_{32}\cos(q_{32})}{(x_4+x_{4\_0})L_{32}\sin(q_{32})}\dot{x}_4 \tag{5.14}$$

5.2.2 Linear/Angular Velocity Vectors of Closed Chain 1

The fixed and nonmoving frame $\{\boldsymbol{B}_{CC1}\}$ is attached at the *driven cutting point* of *closed chain 1* and the linear/angular velocity vector of this frame is known and can be written as

$$^{\boldsymbol{B}_{CC1}}\boldsymbol{V}=[0,0,0,0,0,0]^T \in \mathbb{R}^6 \tag{5.15}$$

In view of theory represented in subsection 3.2.1 and Figure 12, the relationships among the linear/angular velocity vectors of *closed chain 1* can be written as

$$^{\boldsymbol{B}_{CC1}}\boldsymbol{V} = {}^{\boldsymbol{B}_1}\boldsymbol{V} = {}^{\boldsymbol{B}_2}\boldsymbol{V} \tag{5.16}$$

$$^{\boldsymbol{B}_{11}}\boldsymbol{V} = {}^{\boldsymbol{B}_1}\boldsymbol{U}_{\boldsymbol{B}_{11}}^T\,{}^{\boldsymbol{B}_1}\boldsymbol{V} + \boldsymbol{z}_\tau\dot{q}_1 \tag{5.17}$$

$$^{\boldsymbol{T}_1}\boldsymbol{V} = {}^{\boldsymbol{B}_{11}}\boldsymbol{U}_{\boldsymbol{T}_1}^T\,{}^{\boldsymbol{B}_{11}}\boldsymbol{V} \tag{5.18}$$

$$^{B_{21}}\boldsymbol{V} = {}^{B_2}\boldsymbol{U}_{B_{21}}^{T}\,{}^{B_2}\boldsymbol{V} + \boldsymbol{z}_\tau \dot{q}_{11} \tag{5.19}$$

$$^{B_{22}}\boldsymbol{V} = {}^{B_{21}}\boldsymbol{U}_{B_{22}}^{T}\,{}^{B_{21}}\boldsymbol{V} + \boldsymbol{x}_f \dot{x}_2 \tag{5.20}$$

$$^{T_2}\boldsymbol{V} = {}^{B_{22}}\boldsymbol{U}_{T_2}^{T}\,{}^{B_{22}}\boldsymbol{V} + \boldsymbol{z}_\tau \dot{q}_{12} \tag{5.21}$$

$$^{T_{CC1}}\boldsymbol{V} = {}^{T_1}\boldsymbol{V} = {}^{T_2}\boldsymbol{V} \tag{5.22}$$

with

$$\boldsymbol{z}_\tau = [0,0,0,0,0,1]^T \in \mathbb{R}^6 \tag{5.23}$$

$$\boldsymbol{x}_f = [1,0,0,0,0,0]^T \in \mathbb{R}^6 \tag{5.24}$$

5.2.3 Linear/Angular Velocity Vectors of Object 1

In view of theory represented in subsection 3.2.2 and Figure 14, the relationships among the linear/angular velocity vectors of *object 1* can be written as

$$^{B_{CC2}}\boldsymbol{V} = {}^{T_{CC1}}\boldsymbol{U}_{B_{CC2}}^{T}\,{}^{T_{CC1}}\boldsymbol{V} \tag{5.25}$$

$$\begin{aligned} ^{O_1}\boldsymbol{V} &= {}^{T_{CC1}}\boldsymbol{U}_{O_1}^{T}\,{}^{T_{CC1}}\boldsymbol{V} \\ &= {}^{B_{CC2}}\boldsymbol{U}_{O_1}^{T}\,{}^{B_{CC2}}\boldsymbol{V} \end{aligned} \tag{5.26}$$

5.2.4 Linear/Angular Velocity Vectors of Closed Chain 2

Similar to *closed chain 1*, the relationships among the linear/angular velocity vectors of *closed chain 2* can be written, in view of theory represented in subsection 3.2.1 and Figure 13, as

$$^{B_{CC2}}\boldsymbol{V} = {}^{B_3}\boldsymbol{V} = {}^{B_4}\boldsymbol{V} \tag{5.27}$$

$$^{B_{31}}\boldsymbol{V} = {}^{B_3}\boldsymbol{U}_{B_{31}}^{T}\,{}^{B_3}\boldsymbol{V} + \boldsymbol{z}_\tau \dot{q}_3 \tag{5.28}$$

$$^{T_3}\boldsymbol{V} = {}^{B_{31}}\boldsymbol{U}_{T_3}^{T}\,{}^{B_{31}}\boldsymbol{V} \tag{5.29}$$

$$^{B_{41}}\boldsymbol{V} = {}^{B_4}\boldsymbol{U}_{B_{41}}^{T}\,{}^{B_4}\boldsymbol{V} + \boldsymbol{z}_\tau \dot{q}_{31} \tag{5.30}$$

$$^{B_{42}}\boldsymbol{V} = {}^{B_{41}}\boldsymbol{U}_{B_{42}}^{T}\,{}^{B_{41}}\boldsymbol{V} + \boldsymbol{x}_f \dot{x}_4 \tag{5.31}$$

$$^{T_4}\boldsymbol{V} = {}^{B_{42}}\boldsymbol{U}_{T_4}^{T}\,{}^{B_{42}}\boldsymbol{V} + \boldsymbol{z}_\tau \dot{q}_{32} \tag{5.32}$$

$$^{T_{CC2}}\boldsymbol{V} = {}^{T_3}\boldsymbol{V} = {}^{T_4}\boldsymbol{V} \tag{5.33}$$

5.2.5 Linear/Angular Velocity Vectors of Object 2

Similar to *object 1*, the relationships among the linear/angular velocity vectors of *object 2* can be written, view of theory represented in subsection 3.2.2 and Figure 14, as

$$^{G}\boldsymbol{V} = {}^{T_{CC2}}\boldsymbol{U}_{G}^{T}\,{}^{T_{CC2}}\boldsymbol{V} \tag{5.34}$$

$$^{O_2}\boldsymbol{V} = {}^{T_{CC2}}\boldsymbol{U}_{O_2}^{T}\,{}^{T_{CC2}}\boldsymbol{V} = {}^{G}\boldsymbol{U}_{O_2}^{T}\,{}^{G}\boldsymbol{V} \tag{5.35}$$

5.3 Dynamics of HIAB 031

In this section dynamic equations of studied system are represented. For a consolidate a general presentation, in following subsections a dynamic equations of *open chain 1* and *open chain 2* are elaborated under *closed chain 1*, and respectively a dynamic equations of *open chain 3* and *open chain 4* are elaborated under *closed chain 2.*

5.3.1 Dynamics of Object 2

In view theory represented in subsection 3.3.1, the dynamics of the *object 2* can be expressed as

$$\boldsymbol{M}_{O_2}\frac{d}{dt}\left({}^{O_2}\boldsymbol{V}\right) + \boldsymbol{C}_{O_2}\left({}^{O_2}\boldsymbol{\omega}\right){}^{O_2}\boldsymbol{V} + \boldsymbol{G}_{O_2} = {}^{O_2}\boldsymbol{F}^{*} \tag{5.36}$$

where $^{O_2}\boldsymbol{V} \in \mathbb{R}^6$ is obtained from (5.35). On the other hand, in view of (3.12) the net force/moment vector in frame $\{\mathbf{O}_2\}$ is governed by

$$^{O_2}\boldsymbol{F}^{*} = {}^{O_2}\boldsymbol{U}_{T_{CC2}}\,{}^{T_{CC2}}\boldsymbol{F} - {}^{O_2}\boldsymbol{U}_{G}\,{}^{G}\boldsymbol{F} \tag{5.37}$$

where $^{G}\boldsymbol{F} \in \mathbb{R}^6$ denotes the external force exerted to the tip of boom 2. As external load is incorporated into structure of *object 2* and there will be no contacts with the environment, the external force vector $^{G}\boldsymbol{F} \in \mathbb{R}^6$ is known and can be written as

$$^{G}\boldsymbol{F} = [0\ 0\ 0\ 0\ 0\ 0]^{T} \tag{5.38}$$

In view of (5.36), (5.37) and (5.38), the force resultant in *cutting point 4* can be computed as

$$^{T_{CC2}}\boldsymbol{F} = {}^{T_{CC2}}\boldsymbol{U}_{O_2}\,{}^{O_2}\boldsymbol{F}^{*} \tag{5.39}$$

5.3.2 Dynamics of Closed Chain 2

In view of theory represented in subsection 3.3.2, the dynamics of rigid bodies in *open chain 3* and *open chain 4* can be expressed as

$$\boldsymbol{M}_{B_3}\frac{d}{dt}\left({}^{B_3}\boldsymbol{V}\right) + \boldsymbol{C}_{B_3}\left({}^{B_3}\boldsymbol{\omega}\right){}^{B_3}\boldsymbol{V} + \boldsymbol{G}_{B_3} = {}^{B_3}\boldsymbol{F}^{*} \tag{5.40}$$

$$\boldsymbol{M}_{B_{31}} \frac{d}{dt}\left({}^{B_{31}}\boldsymbol{V}\right) + \boldsymbol{C}_{B_{31}}\left({}^{B_{31}}\boldsymbol{\omega}\right){}^{B_{31}}\boldsymbol{V} + \boldsymbol{G}_{B_{31}} = {}^{B_{31}}\boldsymbol{F}^{*} \tag{5.41}$$

$$\boldsymbol{M}_{B_{41}} \frac{d}{dt}\left({}^{B_{41}}\boldsymbol{V}\right) + \boldsymbol{C}_{B_{41}}\left({}^{B_{41}}\boldsymbol{\omega}\right){}^{B_{41}}\boldsymbol{V} + \boldsymbol{G}_{B_{41}} = {}^{B_{41}}\boldsymbol{F}^{*} \tag{5.42}$$

$$\boldsymbol{M}_{B_{42}} \frac{d}{dt}\left({}^{B_{42}}\boldsymbol{V}\right) + \boldsymbol{C}_{B_{42}}\left({}^{B_{42}}\boldsymbol{\omega}\right){}^{B_{42}}\boldsymbol{V} + \boldsymbol{G}_{B_{42}} = {}^{B_{42}}\boldsymbol{F}^{*} \tag{5.43}$$

where ${}^{B_3}\boldsymbol{V}$, ${}^{B_{31}}\boldsymbol{V}$, ${}^{B_{41}}\boldsymbol{V}$ and ${}^{B_{42}}\boldsymbol{V}$ are obtained from (5.27), (5.28), (5.30) and (5.31), respectively.

The force resultant of the frame $\{\boldsymbol{T}_{CC2}\}$ located at the *cutting point 4*, can be expressed with a force components exerted from *open chain 3* and *open chain 4* as

$${}^{T_{CC2}}\boldsymbol{F} = {}^{T_3}\boldsymbol{F} + {}^{T_4}\boldsymbol{F} \tag{5.44}$$

where ${}^{T_{CC2}}\boldsymbol{F} \in \mathbb{R}^6$ is obtained from (5.39).

Let ${}^{T_{CC2}}\boldsymbol{\eta} \in \mathbb{R}^6$ be the internal force vector between two *open chains* with its reference direction pointing from the cylinder 2 to the link 31, and expressed in frame $\{\boldsymbol{T}_{CC2}\}$. It follows from (5.44) that

$${}^{T_3}\boldsymbol{F} = \alpha_3 {}^{T_{CC2}}\boldsymbol{F} + {}^{T_{CC2}}\boldsymbol{\eta} \tag{5.45}$$

$${}^{T_4}\boldsymbol{F} = \alpha_4 {}^{T_{CC2}}\boldsymbol{F} - {}^{T_{CC2}}\boldsymbol{\eta} \tag{5.46}$$

hold. In (5.45) and (5.46), α_3 and α_4 represent load distribution factors, with characteristics of $\alpha_3 + \alpha_4 = 1$. Mathematical derivations for α_3 and α_4 are given in Appendix D, whereas the procedure to calculate internal force vector ${}^{T_{CC2}}\boldsymbol{\eta} \in \mathbb{R}^6$ is given in Appendix E.

Now, the force resultant equations of the two rigid bodies affiliated with the *open chain 3* can be written as

$${}^{B_{31}}\boldsymbol{F} = {}^{B_{31}}\boldsymbol{F}^{*} + {}^{B_{31}}\boldsymbol{U}_{T_3} {}^{T_3}\boldsymbol{F} \tag{5.47}$$

$${}^{B_3}\boldsymbol{F} = {}^{B_3}\boldsymbol{F}^{*} + {}^{B_3}\boldsymbol{U}_{B_{31}} {}^{B_{31}}\boldsymbol{F} \tag{5.48}$$

Furthermore, the force resultant equations of the two rigid bodies affiliated with *open chain 4* can be written as

$${}^{B_{42}}\boldsymbol{F} = {}^{B_{42}}\boldsymbol{F}^{*} + {}^{B_{42}}\boldsymbol{U}_{T_4} {}^{T_4}\boldsymbol{F} \tag{5.49}$$

$${}^{B_{41}}\boldsymbol{F} = {}^{B_{41}}\boldsymbol{F}^{*} + {}^{B_{41}}\boldsymbol{U}_{B_{42}} {}^{B_{42}}\boldsymbol{F} \tag{5.50}$$

In view of (2.7) the force resultant equation of frame $\{\boldsymbol{B_4}\}$ can be written as

$$\begin{aligned} {}^{B_4}\boldsymbol{F} &= {}^{B_4}\boldsymbol{U}_{B_{41}}{}^{B_{41}}\boldsymbol{F} \\ &= {}^{B_4}\boldsymbol{U}_{B_{41}}{}^{B_{41}}\boldsymbol{F}^* + {}^{B_4}\boldsymbol{U}_{B_{41}}{}^{B_{41}}\boldsymbol{U}_{B_{42}}{}^{B_{42}}\boldsymbol{F} \end{aligned} \tag{5.51}$$

The force resultant equation of the frame $\{\boldsymbol{B}_{CC2}\}$ located in the *cutting point 3* can be written as

$${}^{B_{CC2}}\boldsymbol{F} = {}^{B_3}\boldsymbol{F} + {}^{B_4}\boldsymbol{F}. \tag{5.52}$$

In view of (5.49), the actuating force of the cylinder 2 can be given as

$$f_{c2} = \boldsymbol{x}_f^T{}^{B_{42}}\boldsymbol{F}. \tag{5.53}$$

5.3.3 Dynamics of Object 1

In view of the theory represented in subsection 3.3.1, the dynamics of the *object 1* can be expressed as

$$\boldsymbol{M}_{O_1}\frac{d}{dt}\left({}^{O_1}\boldsymbol{V}\right) + \boldsymbol{C}_{O_1}\left({}^{O_1}\boldsymbol{\omega}\right){}^{O_1}\boldsymbol{V} + \boldsymbol{G}_{O_1} = {}^{O_1}\boldsymbol{F}^* \tag{5.54}$$

where ${}^{O_1}\boldsymbol{V} \in \mathbb{R}^6$ is obtained from (5.26).

On the other hand, in view of (3.12), the net force/moment vector of frame $\{\boldsymbol{O}_1\}$ is governed by

$${}^{O_1}\boldsymbol{F}^* = {}^{O_1}\boldsymbol{U}_{T_{CC1}}{}^{T_{CC1}}\boldsymbol{F} - {}^{O_1}\boldsymbol{U}_{B_{CC2}}{}^{B_{CC2}}\boldsymbol{F} \tag{5.55}$$

where ${}^{B_{CC2}}\boldsymbol{F} \in \mathbb{R}^6$ is obtained from (5.52).

In view of (5.54) and (5.55), the force resultant in the frame $\{\boldsymbol{T}_{CC1}\}$ locating at the *cutting point 2* can be computed as

$$\begin{aligned} {}^{T_{CC1}}\boldsymbol{F} &= {}^{O_1}\boldsymbol{U}_{T_{CC1}}^{-1}\left({}^{O_1}\boldsymbol{F}^* + {}^{O_1}\boldsymbol{U}_{B_{CC2}}{}^{B_{CC2}}\boldsymbol{F}\right) \\ &= {}^{T_{CC2}}\boldsymbol{U}_{O_1}{}^{O_1}\boldsymbol{F}^* + {}^{T_{CC1}}\boldsymbol{U}_{B_{CC2}}{}^{B_{CC2}}\boldsymbol{F} \end{aligned} \tag{5.56}$$

5.3.4 Dynamics of Closed Chain 1

Similar to *closed chain 2*, the dynamics of rigid bodies in *open chain 1* and *open chain 2* can be expressed as

$$\boldsymbol{M}_{\boldsymbol{B}_1}\frac{d}{dt}\left({}^{\boldsymbol{B}_1}\boldsymbol{V}\right)+\boldsymbol{C}_{\boldsymbol{B}_1}\left({}^{\boldsymbol{B}_1}\boldsymbol{\omega}\right){}^{\boldsymbol{B}_1}\boldsymbol{V}+\boldsymbol{G}_{\boldsymbol{B}_1}={}^{\boldsymbol{B}_1}\boldsymbol{F}^{*} \tag{5.57}$$

$$\boldsymbol{M}_{\boldsymbol{B}_{11}}\frac{d}{dt}\left({}^{\boldsymbol{B}_{11}}\boldsymbol{V}\right)+\boldsymbol{C}_{\boldsymbol{B}_{11}}\left({}^{\boldsymbol{B}_{11}}\boldsymbol{\omega}\right){}^{\boldsymbol{B}_{11}}\boldsymbol{V}+\boldsymbol{G}_{\boldsymbol{B}_{11}}={}^{\boldsymbol{B}_{11}}\boldsymbol{F}^{*} \tag{5.58}$$

$$\boldsymbol{M}_{\boldsymbol{B}_{21}}\frac{d}{dt}\left({}^{\boldsymbol{B}_{21}}\boldsymbol{V}\right)+\boldsymbol{C}_{\boldsymbol{B}_{21}}\left({}^{\boldsymbol{B}_{21}}\boldsymbol{\omega}\right){}^{\boldsymbol{B}_{21}}\boldsymbol{V}+\boldsymbol{G}_{\boldsymbol{B}_{21}}={}^{\boldsymbol{B}_{21}}\boldsymbol{F}^{*} \tag{5.59}$$

$$\boldsymbol{M}_{\boldsymbol{B}_{22}}\frac{d}{dt}\left({}^{\boldsymbol{B}_{22}}\boldsymbol{V}\right)+\boldsymbol{C}_{\boldsymbol{B}_{22}}\left({}^{\boldsymbol{B}_{22}}\boldsymbol{\omega}\right){}^{\boldsymbol{B}_{22}}\boldsymbol{V}+\boldsymbol{G}_{\boldsymbol{B}_{22}}={}^{\boldsymbol{B}_{22}}\boldsymbol{F}^{*} \tag{5.60}$$

The force resultant in the frame $\{\boldsymbol{T}_{CC1}\}$ located at the *cutting point 2*, can be expressed with a force components exerted from *open chain 1* and *open chain 2* as

$${}^{\boldsymbol{T}_{CC1}}\boldsymbol{F}={}^{\boldsymbol{T}_1}\boldsymbol{F}+{}^{\boldsymbol{T}_2}\boldsymbol{F} \tag{5.61}$$

where ${}^{\boldsymbol{T}_{CC1}}\boldsymbol{F}\in\mathbb{R}^6$ is obtained from (5.56).

Let ${}^{\boldsymbol{T}_{CC1}}\boldsymbol{\eta}\in\mathbb{R}^6$ be the internal force vector between two *open chains* with its reference direction pointing from the cylinder 1 to the link 11, expressed in frame $\{\boldsymbol{T}_{CC1}\}$. It follows from (5.61) that

$${}^{\boldsymbol{T}_1}\boldsymbol{F}=\alpha_1{}^{\boldsymbol{T}_{CC1}}\boldsymbol{F}+{}^{\boldsymbol{T}_{CC1}}\boldsymbol{\eta} \tag{5.62}$$

$${}^{\boldsymbol{T}_2}\boldsymbol{F}=\alpha_2{}^{\boldsymbol{T}_{CC1}}\boldsymbol{F}-{}^{\boldsymbol{T}_{CC1}}\boldsymbol{\eta} \tag{5.63}$$

hold. In (5.62) and (5.63), α_1 and α_2 represent the load distribution factors, given in Appendix D, whereas the procedure to calculate internal force vector ${}^{\boldsymbol{T}_{CC1}}\boldsymbol{\eta}\in\mathbb{R}^6$ is given in Appendix E.

Now, the force resultant equations of the two rigid bodies affiliated with the *open chain 1* can be written as

$${}^{\boldsymbol{B}_{11}}\boldsymbol{F}={}^{\boldsymbol{B}_{11}}\boldsymbol{F}^{*}+{}^{\boldsymbol{B}_{11}}\boldsymbol{U}_{\boldsymbol{T}_1}{}^{\boldsymbol{T}_1}\boldsymbol{F} \tag{5.64}$$

$${}^{\boldsymbol{B}_1}\boldsymbol{F}={}^{\boldsymbol{B}_1}\boldsymbol{F}^{*}+{}^{\boldsymbol{B}_1}\boldsymbol{U}_{\boldsymbol{B}_{11}}{}^{\boldsymbol{B}_{11}}\boldsymbol{F} \tag{5.65}$$

Furthermore, the force resultant equations of the two rigid bodies affiliated with *open chain 2* can be written as

$${}^{\boldsymbol{B}_{22}}\boldsymbol{F}={}^{\boldsymbol{B}_{22}}\boldsymbol{F}^{*}+{}^{\boldsymbol{B}_{22}}\boldsymbol{U}_{\boldsymbol{T}_2}{}^{\boldsymbol{T}_2}\boldsymbol{F} \tag{5.66}$$

$${}^{\boldsymbol{B}_{21}}\boldsymbol{F}={}^{\boldsymbol{B}_{21}}\boldsymbol{F}^{*}+{}^{\boldsymbol{B}_{21}}\boldsymbol{U}_{\boldsymbol{B}_{22}}{}^{\boldsymbol{B}_{22}}\boldsymbol{F} \tag{5.67}$$

In view of (2.7) the force resultant equation of frame $\{\boldsymbol{B}_2\}$ can be written as

$$
\begin{aligned}
{}^{\boldsymbol{B_2}}\boldsymbol{F} &= {}^{\boldsymbol{B_2}}\boldsymbol{U}_{\boldsymbol{B_{21}}}{}^{\boldsymbol{B_{21}}}\boldsymbol{F} \\
&= {}^{\boldsymbol{B_2}}\boldsymbol{U}_{\boldsymbol{B_{21}}}{}^{\boldsymbol{B_{21}}}\boldsymbol{F}^{*} + {}^{\boldsymbol{B_2}}\boldsymbol{U}_{\boldsymbol{B_{21}}}{}^{\boldsymbol{B_{21}}}\boldsymbol{U}_{\boldsymbol{B_{22}}}{}^{\boldsymbol{B_{22}}}\boldsymbol{F}
\end{aligned} \tag{5.68}
$$

The force resultant equation of the frame $\{\boldsymbol{B}_{CC1}\}$ locating at the *cutting point 1* can be given as

$$
{}^{\boldsymbol{B}_{CC1}}\boldsymbol{F} = {}^{\boldsymbol{B}_1}\boldsymbol{F} + {}^{\boldsymbol{B}_2}\boldsymbol{F}. \tag{5.69}
$$

In view of (5.66), the actuating force of the cylinder 1 can be written as

$$
f_{c1} = \boldsymbol{x}_f^{T}{}^{\boldsymbol{B_{22}}}\boldsymbol{F}. \tag{5.70}
$$

5.4 Control Equations of HIAB 031

In view of the theories represented in subsection 3.2.3 and sections 3.3 and 3.4, the control equations for the *objects* and *rigid links*, respectively, of studied system will be given in this section.

5.4.1 Required Velocities

By knowing the required *closed chain* velocities $\dot{q}_{1r}$ and $\dot{q}_{3r}$, similar to (5.9) - (5.14), all the remaining required joint variables of studied 2-DOF hydraulic manipulator can be represented as

$$
\dot{x}_{2r} = -\frac{L_{11}L_{12}\sin(q_1)}{x_2+x_{2\_0}}\dot{q}_{1r} \tag{5.71}
$$

$$
\dot{q}_{11r} = -\frac{(x_2+x_{2\_0})-L_{11}\cos(q_{11})}{(x_2+x_{2\_0})L_{11}\sin(q_{11})}\dot{x}_{2r} \tag{5.72}
$$

$$
\dot{q}_{12r} = -\frac{(x_2+x_{2\_0})-L_{12}\cos(q_{12})}{(x_2+x_{2\_0})L_{12}\sin(q_{12})}\dot{x}_{2r} \tag{5.73}
$$

$$
\dot{x}_{4r} = -\frac{L_{31}L_{32}\sin(q_3)}{x_4+x_{4\_0}}\dot{q}_{2r} \tag{5.74}
$$

$$
\dot{q}_{31r} = -\frac{(x_4+x_{4\_0})-L_{31}\cos(q_{31})}{(x_4+x_{4\_0})L_{31}\sin(q_{31})}\dot{x}_{4r} \tag{5.75}
$$

$$
\dot{q}_{32r} = -\frac{(x_4+x_{4\_0})-L_{32}\cos(q_{32})}{(x_4+x_{4\_0})L_{32}\sin(q_{32})}\dot{x}_{4r} \tag{5.76}
$$

5.4.2 Required Velocity Transformations

In view of (5.16), the required linear/angular velocity vector of frame $\{\boldsymbol{B}_{CC1}\}$ is known and can be written as

$$
{}^{\boldsymbol{B}_{CC1}}\boldsymbol{V}_r = [0,0,0,0,0,0]^T \in \mathbb{R}^6 \tag{5.77}
$$

Now, by knowing the required linear/angular velocity vector of frame $\{\boldsymbol{B}_{CC1}\}$ defined in (5.77) and required joint velocities defined in (5.71) - (5.76), in view of the theory represented in subsection 3.2.3, all required linear/angular velocity vectors of studied system can be written as

$$^{B_{CC1}}\boldsymbol{V}_r = {}^{B_1}\boldsymbol{V}_r = {}^{B_2}\boldsymbol{V}_r \tag{5.78}$$

$$^{B_{11}}\boldsymbol{V}_r = {}^{B_1}\boldsymbol{U}_{B_{11}}^T\, {}^{B_1}\boldsymbol{V}_r + \boldsymbol{z}_\tau \dot{q}_{1r} \tag{5.79}$$

$$^{T_1}\boldsymbol{V}_r = {}^{B_{11}}\boldsymbol{U}_{T_1}^T\, {}^{B_{11}}\boldsymbol{V}_r \tag{5.80}$$

$$^{B_{21}}\boldsymbol{V}_r = {}^{B_2}\boldsymbol{U}_{B_{21}}^T\, {}^{B_2}\boldsymbol{V}_r + \boldsymbol{z}_\tau \dot{q}_{11r} \tag{5.81}$$

$$^{B_{22}}\boldsymbol{V}_r = {}^{B_{21}}\boldsymbol{U}_{B_{22}}^T\, {}^{B_{21}}\boldsymbol{V}_r + \boldsymbol{x}_f \dot{x}_{2r} \tag{5.82}$$

$$^{T_2}\boldsymbol{V}_r = {}^{B_{22}}\boldsymbol{U}_{T_2}^T\, {}^{B_{22}}\boldsymbol{V}_r + \boldsymbol{z}_\tau \dot{q}_{12r} \tag{5.83}$$

$$^{T_{CC1}}\boldsymbol{V}_r = {}^{T_1}\boldsymbol{V}_r = {}^{T_2}\boldsymbol{V}_r \tag{5.84}$$

$$^{B_{CC2}}\boldsymbol{V}_r = {}^{T_{CC1}}\boldsymbol{U}_{B_{CC2}}^T\, {}^{T_{CC1}}\boldsymbol{V}_r \tag{5.85}$$

$$^{O_1}\boldsymbol{V}_r = {}^{T_{CC1}}\boldsymbol{U}_{O_2}^T\, {}^{T_{CC1}}\boldsymbol{V}_r = {}^{B_{CC2}}\boldsymbol{U}_{O_1}^T\, {}^{B_{CC2}}\boldsymbol{V}_r \tag{5.86}$$

$$^{B_{CC2}}\boldsymbol{V}_r = {}^{B_3}\boldsymbol{V}_r = {}^{B_4}\boldsymbol{V}_r \tag{5.87}$$

$$^{B_{31}}\boldsymbol{V}_r = {}^{B_3}\boldsymbol{U}_{B_{31}}^T\, {}^{B_3}\boldsymbol{V}_r + \boldsymbol{z}_\tau \dot{q}_{3r} \tag{5.88}$$

$$^{T_3}\boldsymbol{V}_r = {}^{B_{31}}\boldsymbol{U}_{T_3}^T\, {}^{B_{31}}\boldsymbol{V}_r \tag{5.89}$$

$$^{B_{41}}\boldsymbol{V}_r = {}^{B_4}\boldsymbol{U}_{B_{41}}^T\, {}^{B_4}\boldsymbol{V}_r + \boldsymbol{z}_\tau \dot{q}_{31r} \tag{5.90}$$

$$^{B_{42}}\boldsymbol{V}_r = {}^{B_{41}}\boldsymbol{U}_{B_{42}}^T\, {}^{B_{41}}\boldsymbol{V}_r + \boldsymbol{x}_f \dot{x}_{4r} \tag{5.91}$$

$$^{T_4}\boldsymbol{V}_r = {}^{B_{42}}\boldsymbol{U}_{T_4}^T\, {}^{B_{42}}\boldsymbol{V} + \boldsymbol{z}_\tau \dot{q}_{32r} \tag{5.92}$$

$$^{T_{CC2}}\boldsymbol{V}_r = {}^{T_3}\boldsymbol{V}_r = {}^{T_4}\boldsymbol{V}_r \tag{5.93}$$

$$^{G}\boldsymbol{V}_r = {}^{T_{CC2}}\boldsymbol{U}_{G}^T\, {}^{T_{CC2}}\boldsymbol{V}_r \tag{5.94}$$

$$^{O_2}\boldsymbol{V}_r = {}^{T_{CC2}}\boldsymbol{U}_{O_2}^T\, {}^{T_{CC2}}\boldsymbol{V}_r = {}^{G}\boldsymbol{U}_{O_2}^T\, {}^{G}\boldsymbol{V}_r \tag{5.95}$$

5.4.3 Applied Regressor Matrix and Parameter Vector for Studied 2-DOF Manipulator

Due to fact that studied system possesses only 2-DOF, regressor matrix $\boldsymbol{Y}_A \in \mathbb{R}^{6\times 13}$ and parameter vector $\boldsymbol{\theta}_A \in \mathbb{R}^{13}$ of rigid body defined in (2.19) and given in Appendix A, are simplified to form of $\boldsymbol{Y}_{2A} \in \mathbb{R}^{6\times 6}$ and $\boldsymbol{\theta}_{2A} \in \mathbb{R}^{6}$. Derivations of simplified regressor matrix $\boldsymbol{Y}_{2A} \in \mathbb{R}^{6\times 6}$ and parameter vector $\boldsymbol{\theta}_{2A} \in \mathbb{R}^{6}$ are given in Appendix B. In scope of this thesis, all regressor matrices and parameter vectors of *rigid links* and *objects* are computed according to formulation of Appendix B.

5.4.4 The Required Net Force/Moment vectors of

In the view of the theory represented in subsection 3.3.2, the required net force/moment vectors of *object1* and *object2* can be computed in view of (3.13), as

$$^{O_1}\boldsymbol{F}_r^* = \boldsymbol{Y}_{2O_1}\boldsymbol{\theta}_{2O_1} + \boldsymbol{K}_{O_1}\left(^{O_1}\boldsymbol{V}_r - {}^{O_1}\boldsymbol{V}\right) \tag{5.96}$$

$$^{O_2}\boldsymbol{F}_r^* = \boldsymbol{Y}_{2O_2}\boldsymbol{\theta}_{2O_2} + \boldsymbol{K}_{O_2}\left(^{O_2}\boldsymbol{V}_r - {}^{O_2}\boldsymbol{V}\right), \tag{5.97}$$

5.4.5 The Required Net Force/Moment Vectors of Rigid Links in Closed Chains

In view of the theory represented in subsection 3.4.2, the required net force/moment vectors for rigid links of *closed chain 1* can be computed in view (3.21) and (3.22), as

$$^{B_1}\boldsymbol{F}_r^* = \boldsymbol{Y}_{2B_1}\boldsymbol{\theta}_{2B_1} + \boldsymbol{K}_{B_1}\left(^{B_1}\boldsymbol{V}_r - {}^{B_1}\boldsymbol{V}\right) \tag{5.98}$$

$$^{B_{11}}\boldsymbol{F}_r^* = \boldsymbol{Y}_{2B_{11}}\boldsymbol{\theta}_{2B_{11}} + \boldsymbol{K}_{B_{11}}\left(^{B_{11}}\boldsymbol{V}_r - {}^{B_{11}}\boldsymbol{V}\right) \tag{5.99}$$

$$^{B_{21}}\boldsymbol{F}_r^* = \boldsymbol{Y}_{2B_{21}}\boldsymbol{\theta}_{2B_{21}} + \boldsymbol{K}_{B_{21}}\left(^{B_{21}}\boldsymbol{V}_r - {}^{B_{21}}\boldsymbol{V}\right) \tag{5.100}$$

$$^{B_{22}}\boldsymbol{F}_r^* = \boldsymbol{Y}_{2B_{22}}\boldsymbol{\theta}_{2B_{22}} + \boldsymbol{K}_{B_{22}}\left(^{B_{22}}\boldsymbol{V}_r - {}^{B_{22}}\boldsymbol{V}\right) \tag{5.101}$$

and similar to *closed chain 1*, the required net force/moment vectors for rigid links of *closed chain 2* can be computed in view (3.21) and (3.22), as

$$^{B_3}\boldsymbol{F}_r^* = \boldsymbol{Y}_{2B_3}\boldsymbol{\theta}_{2B_3} + \boldsymbol{K}_{B_3}\left(^{B_3}\boldsymbol{V}_r - {}^{B_3}\boldsymbol{V}\right) \tag{5.102}$$

$$^{B_{31}}\boldsymbol{F}_r^* = \boldsymbol{Y}_{2B_{31}}\boldsymbol{\theta}_{2B_{31}} + \boldsymbol{K}_{B_{31}}\left(^{B_{31}}\boldsymbol{V}_r - {}^{B_{31}}\boldsymbol{V}\right) \tag{5.103}$$

$$^{B_{41}}\boldsymbol{F}_r^* = \boldsymbol{Y}_{2B_{41}}\boldsymbol{\theta}_{2B_{41}} + \boldsymbol{K}_{B_{41}}\left(^{B_{41}}\boldsymbol{V}_r - {}^{B_{41}}\boldsymbol{V}\right) \tag{5.104}$$

$$^{B_{42}}\boldsymbol{F}_r^* = \boldsymbol{Y}_{2B_{42}}\boldsymbol{\theta}_{2B_{42}} + \boldsymbol{K}_{B_{42}}\left(^{B_{42}}\boldsymbol{V}_r - {}^{B_{42}}\boldsymbol{V}\right). \tag{5.105}$$

5.4.6 The Required Force/Moment Vector Transformations of Studied System

In view of the section 3.5, after all the required net force/moment vector of *objects* and *rigid links* of studied system has been defined, the required force/moment vectors of the entire system can computed along the opposite direction of the simple oriented graph.

In view of theory represented in subsections 3.3.3, the required force resultant equation of *object 2* can be written as

$$^{O_2}\boldsymbol{F}_r^* = {}^{O_2}\boldsymbol{U}_{T_{CC2}}\,{}^{T_{CC2}}\boldsymbol{F}_r - {}^{O_2}\boldsymbol{U}_G\,{}^{G}\boldsymbol{F}_r. \tag{5.106}$$

As external load is incorporated into structure of *object 2* and there will be no contacts with the environment, the required external force vector ${}^{G}\boldsymbol{F}_r \in \mathbb{R}^6$ is known and can be written as ${}^{G}\boldsymbol{F}_r = [0\ 0\ 0\ 0\ 0\ 0]^T$. Thus, the required force/moment vector in the frame $\{\boldsymbol{T}_{CC2}\}$ located *cutting point 4* can be computed from (5.106) as

$$ {}^{T_{CC2}}\boldsymbol{F}_r = {}^{T_{CC2}}\boldsymbol{U}_{O_2}\,{}^{O_2}\boldsymbol{F}_r^* \tag{5.107} $$

Similar to (5.45) and (5.46), the required force/moment vectors at the *driven cutting points* of the *Object 2* can be computed as

$$ {}^{T_3}\boldsymbol{F}_r = \alpha_3\,{}^{T_{CC2}}\boldsymbol{F}_r + {}^{T_{CC2}}\boldsymbol{\eta}_r \tag{5.108} $$

$$ {}^{T_4}\boldsymbol{F}_r = \alpha_4\,{}^{T_{CC2}}\boldsymbol{F}_r - {}^{T_{CC2}}\boldsymbol{\eta}_r \tag{5.109} $$

where, α_3 and α_4 denotes the load distribution factors defined in Appendix D, whereas ${}^{T_{CC2}}\boldsymbol{\eta}_r \in \mathbb{R}^6$ denotes the required internal force/moment vector obtained with similar procedure described in Appendix E.

Now, in view of theory represented in subsection 3.4.3, the required force/moment vectors of the *open chain 3* are computed as

$$ {}^{B_{31}}\boldsymbol{F}_r = {}^{B_{31}}\boldsymbol{F}_r^* + {}^{B_{31}}\boldsymbol{U}_{T_3}\,{}^{T_3}\boldsymbol{F}_r \tag{5.110} $$

$$ {}^{B_3}\boldsymbol{F}_r = {}^{B_3}\boldsymbol{F}^* + {}^{B_3}\boldsymbol{U}_{B_{31}}\,{}^{B_{31}}\boldsymbol{F}_r \tag{5.111} $$

and the required force/moment vectors of the *open chain 4* are computed as

$$ {}^{B_{42}}\boldsymbol{F}_r = {}^{B_{42}}\boldsymbol{F}_r^* + {}^{B_{42}}\boldsymbol{U}_{T_4}\,{}^{T_4}\boldsymbol{F}_r \tag{5.112} $$

$$ {}^{B_4}\boldsymbol{F}_r = {}^{B_4}\boldsymbol{U}_{B_{41}}\,{}^{B_{41}}\boldsymbol{F}^* + {}^{B_4}\boldsymbol{U}_{B_{41}}\,{}^{B_{41}}\boldsymbol{U}_{B_{42}}\,{}^{B_{42}}\boldsymbol{F}_r \tag{5.113} $$

Finally, the required force/moment vector in *cutting point 3* is computed as

$$ {}^{B_{CC2}}\boldsymbol{F}_r = {}^{B_3}\boldsymbol{F}_r + {}^{B_4}\boldsymbol{F}_r \tag{5.114} $$

In view of the theory represented in subsection 3.3.2 and (5.55), the required force resultant equation of *object 1* can be written as

$$ {}^{O_1}\boldsymbol{F}_r^* = {}^{O_1}\boldsymbol{U}_{T_{CC1}}\,{}^{T_{CC1}}\boldsymbol{F}_r - {}^{O_1}\boldsymbol{U}_{B_{CC2}}\,{}^{B_{CC2}}\boldsymbol{F}_r \tag{5.115} $$

The required force/moment vector in *cutting point 2* can be computed from (5.115) as

$$ {}^{T_{CC1}}\boldsymbol{F}_r = {}^{T_{CC1}}\boldsymbol{U}_{O_1}\,{}^{O_1}\boldsymbol{F}_r^* + {}^{T_{CC1}}\boldsymbol{U}_{B_{CC2}}\,{}^{B_{CC2}}\boldsymbol{F}_r \tag{5.116} $$

The required force/moment vector transformations of *closed chain 1* can be computed similar to *closed chain 2* required force/moment vector transformations by replacing frame frames $\{\boldsymbol{T_3}\}$, $\{\boldsymbol{T_4}\}$, $\{\boldsymbol{B_{31}}\}$, $\{\boldsymbol{B_3}\}$, $\{\boldsymbol{B_{42}}\}$, $\{\boldsymbol{B_{41}}\}$ and $\{\boldsymbol{B_4}\}$ to frames $\{\boldsymbol{T_1}\}$, $\{\boldsymbol{T_2}\}$, $\{\boldsymbol{B_{11}}\}$, $\{\boldsymbol{B_1}\}$, $\{\boldsymbol{B_{22}}\}$, $\{\boldsymbol{B_{21}}\}$ and $\{\boldsymbol{B_2}\}$, respectively, and distribution factors α_3 and α_4 to α_1 and α_2, respectively, leading to

$$^{\boldsymbol{T_1}}\boldsymbol{F}_r = \alpha_1 \, ^{\boldsymbol{T_{CC1}}}\boldsymbol{F}_r + ^{\boldsymbol{T_{CC1}}}\boldsymbol{\eta}_r \tag{5.117}$$

$$^{\boldsymbol{T_2}}\boldsymbol{F}_r = \alpha_2 \, ^{\boldsymbol{T_{CC1}}}\boldsymbol{F}_r - ^{\boldsymbol{T_{CC1}}}\boldsymbol{\eta}_r \tag{5.118}$$

$$^{\boldsymbol{B_{11}}}\boldsymbol{F}_r = ^{\boldsymbol{B_{11}}}\boldsymbol{F}_r^* + ^{\boldsymbol{B_{11}}}\boldsymbol{U}_{\boldsymbol{T_1}} \, ^{\boldsymbol{T_1}}\boldsymbol{F}_r \tag{5.119}$$

$$^{\boldsymbol{B_1}}\boldsymbol{F}_r = ^{\boldsymbol{B_1}}\boldsymbol{F}^* + ^{\boldsymbol{B_1}}\boldsymbol{U}_{\boldsymbol{B_{11}}} \, ^{\boldsymbol{B_{11}}}\boldsymbol{F}_r \tag{5.120}$$

$$^{\boldsymbol{B_{22}}}\boldsymbol{F}_r = ^{\boldsymbol{B_{22}}}\boldsymbol{F}_r^* + ^{\boldsymbol{B_{22}}}\boldsymbol{U}_{\boldsymbol{T_2}} \, ^{\boldsymbol{T_2}}\boldsymbol{F}_r \tag{5.121}$$

$$^{\boldsymbol{B_2}}\boldsymbol{F}_r = ^{\boldsymbol{B_2}}\boldsymbol{U}_{\boldsymbol{B_{21}}} \, ^{\boldsymbol{B_{21}}}\boldsymbol{F}^* + ^{\boldsymbol{B_2}}\boldsymbol{U}_{\boldsymbol{B_{21}}} \, ^{\boldsymbol{B_{21}}}\boldsymbol{U}_{\boldsymbol{B_{22}}} \, ^{\boldsymbol{B_{22}}}\boldsymbol{F}_r \tag{5.122}$$

$$^{\boldsymbol{B_{CC1}}}\boldsymbol{F}_r = ^{\boldsymbol{B_1}}\boldsymbol{F}_r + ^{\boldsymbol{B_2}}\boldsymbol{F}_r \tag{5.123}$$

Finally, According to (5.53) and (5.70), the required actuating forces along the cylinder axis are designed to be as

$$f_{c2r} = \boldsymbol{x}_f^T \, ^{\boldsymbol{B_{42}}}\boldsymbol{F}_r \tag{5.124}$$

$$f_{c1r} = \boldsymbol{x}_f^T \, ^{\boldsymbol{B_{22}}}\boldsymbol{F}_r \tag{5.125}$$

In view of the joint torque constraints (E.1) – (E.3) defined in Appendix E, the required torques of the three unactuated joints of closed chain 2 and closed chain 1, respectively, can be written as

$$\boldsymbol{z}_\tau^T \, ^{\boldsymbol{T_4}}\boldsymbol{F}_r = 0 \tag{5.126}$$

$$\boldsymbol{z}_\tau^T \, ^{\boldsymbol{B_{31}}}\boldsymbol{F}_r = 0 \tag{5.127}$$

$$\boldsymbol{z}_\tau^T \, ^{\boldsymbol{B_{41}}}\boldsymbol{F}_r = 0 \tag{5.128}$$

$$\boldsymbol{z}_\tau^T \, ^{\boldsymbol{T_2}}\boldsymbol{F}_r = 0 \tag{5.129}$$

$$\boldsymbol{z}_\tau^T \, ^{\boldsymbol{B_{11}}}\boldsymbol{F}_r = 0 \tag{5.130}$$

$$\boldsymbol{z}_\tau^T \, ^{\boldsymbol{B_{21}}}\boldsymbol{F}_r = 0 \tag{5.131}$$

5.5 Dynamics and Control of Hydraulic Cylinders

As represented in section 3.6, after dynamics and control issues of all *objects* and *open chains* of studied system has been addressed, the dynamics and control issues of actuated joints has still to be considered. The studied system represent in chapter 4,

contains two actuated prismatic joints (cylinder 1 and cylinder 2), while all the remaining joints are unactuated. This section concentrates on the dynamics and control issues of these actuated joints, in view of the theory represented in section 3.6.

5.5.1 Hydraulic Fluid Dynamics

In (Zhu 2010, pp.181-184) the fluid dynamics for hydraulic cylinder are given and can be applied into studied system. In this section the equations to model hydraulic fluid dynamics are to be represented.

According to (Zhu 2010, p.181), when high-bandwidth servo valve is used for a hydraulic cylinder, it is reasonable to ignore the servo valve's dynamics so that the valve position is considered to be proportional to its control voltage within a frequency range of interest.

The control arrangement of cylinder is illustrated in Figure 18.

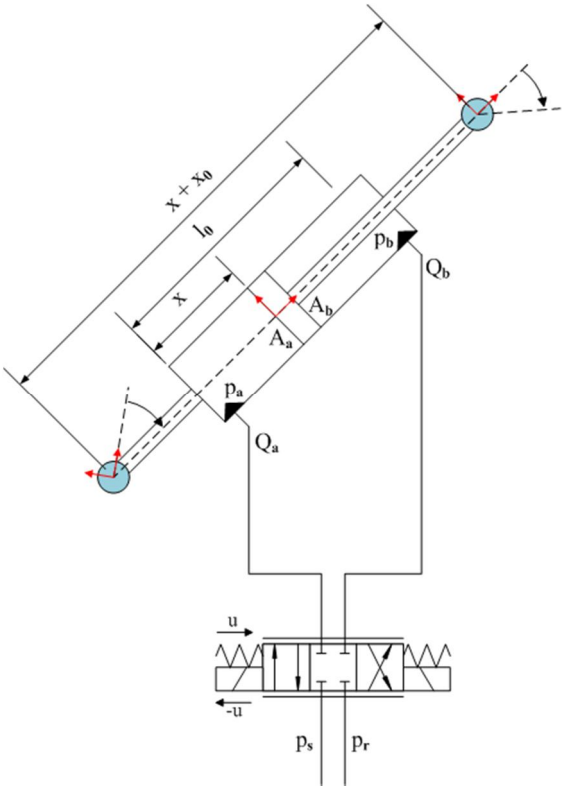

Figure 18: Control of cylinder.

Each control edge (S→A, B→R, S→B, A→R) of valve can be modeled as an orifice. Based on the Bernoulli's static flow equation, the rate of flow passing through an orifice, denoted as Q, is proportional to the product of the valve control voltage and the square root of the pressure drop across the orifice (Zhu 2010, p.182), that is

$$Q = c\sqrt{\Delta p}u \tag{5.132}$$

where $c > 0$ is a constant, $\Delta p = p_1 - p_2$ is a pressure drop across the orifice, and u is the valve control voltage.

By considering equation (5.132), it can be noticed that if direction of flow in orifice is reversed $(p_2 > p_1)$, a pressure drop across the orifice becomes negative and pressure drop related term $\sqrt{\Delta p}$ in becomes imaginary. Imaginary characteristic can be overcome by replacing pressure-drop related term with pressure-drop related function defined as

$$\vartheta(\Delta p) \stackrel{\text{def}}{=} sign(\Delta p) \cdot \sqrt{|\Delta p|} \tag{5.133}$$

where a sign function can be defined as

$$sign(\Delta p) = \begin{cases} 1 & if\ \Delta p > 0 \\ 0 & if\ \Delta p = 0 \\ -1 & if\ \Delta p < 0 \end{cases} \tag{5.134}$$

As a structure of used servo valve constrains, opening and closing of control edges occurs in pairs. Used servo valve is modeled as zero lapped, meaning that when control edges S→A and B→R are opened, control edges S→B and A→R are closed, and vice versa. This behavior of control edges can be modeled as function of control voltage u with selective function defined as

$$\mathcal{S}(u) = \begin{cases} 1, & if\ u > 0 \\ 0, & if\ u \leq 0 \end{cases} \tag{5.135}$$

As illustrated in Figure 18, let Q_a and Q_b be the flow rates entering the left and right chamber of cylinder, respectively, and let p_a and p_b be the pressures inside the left and right chamber of cylinder, respectively. It follows from (5.132), (5.133) and (5.135) that

$$Q_a = c_{p1}\vartheta(p_s - p_a)u\mathcal{S}(u) + c_{n1}\vartheta(p_a - p_r)u\mathcal{S}(-u) \tag{5.136}$$

$$Q_b = -c_{n2}\vartheta(p_b - p_r)u\mathcal{S}(u) - c_{p2}\vartheta(p_s - p_b)u\mathcal{S}(-u) \tag{5.137}$$

hold, where $c_{p1} > 0$, $c_{n1} > 0$, $c_{p2} > 0$, and $c_{n2} > 0$ are four constants and $p_s > 0$ and $p_r > 0$ denote the supply and return pressures, respectively, with $p_s \gg p_t$.

The dynamic equation for the fluid compressibility inside a cylinder chamber can be written as

$$\dot{p} = \frac{\beta}{v_c}(Q - \dot{v}_c) \tag{5.138}$$

where p denotes the specific chamber pressure, β denotes the effective bulk modulus, v_c denotes the chamber volume, and Q denotes the flow rate of fluid entering the chamber.

In view of (5.138), the pressure dynamic equations of the two chambers can be written as

$$\dot{p}_a = \frac{\beta}{A_a \cdot x}(Q_a - A_a\dot{x}) \tag{5.139}$$

$$\dot{p}_b = \frac{\beta}{A_b(l_0 - x)}(Q_b + A_b\dot{x}) \tag{5.140}$$

where $A_a > 0$ and $A_b > 0$ denotes the piston areas at both chambers of cylinder, x denotes the displacement cylinder, and l_0 is the effective length of the cylinder.

The pressures of the two chambers can be converted into net pressure force of cylinder 1 as

$$f_p = A_a p_a - A_b p_b \tag{5.141}$$

Now, by premultiplying A_a and A_b to (5.140) and (5.139), respectively, and using (5.136), (5.137), and (5.141) yields

$$\dot{f}_p = \beta\left[u_f - \left(\frac{A_a}{x} + \frac{A_b}{l_0 - x}\right)\dot{x}\right] \tag{5.142}$$

where

$$\begin{aligned} u_f &= \frac{Q_a}{x} - \frac{Q_b}{l_0 - x} \\ &= \left(\frac{c_{p1} \cdot \vartheta(p_s - p_a)}{x} + \frac{c_{n2} \cdot \vartheta(p_b - p_r)}{l_0 - x}\right) u\mathcal{S}(u) \\ &\quad + \left(\frac{c_{n1} \cdot \vartheta(p_a - p_r)}{x} + \frac{c_{p2} \cdot \vartheta(p_s - p_b)}{l_0 - x_2}\right) u\mathcal{S}(-u) \\ &\stackrel{\text{def}}{=} \boldsymbol{Y}_v(u)\boldsymbol{\theta}_v \end{aligned} \tag{5.143}$$

with

$$\boldsymbol{Y}_v(u) = \begin{bmatrix} \frac{\vartheta(p_s - p_a)}{x} u\mathcal{S}(u) \\ \frac{\vartheta(p_a - p_r)}{x} u\mathcal{S}(-u) \\ \frac{\vartheta(p_s - p_b)}{l_0 - x} u\mathcal{S}(-u) \\ \frac{\vartheta(p_b - p_r)}{l_0 - x} u\mathcal{S}(u) \end{bmatrix}^T \in \mathbb{R}^{1x4} \tag{5.144}$$

$$\boldsymbol{\theta}_v = \begin{bmatrix} c_{p1} & c_{n1} & c_{p2} & c_{n2} \end{bmatrix}^T \in \mathbb{R}^4. \tag{5.145}$$

The following assumption is made in scope of this thesis.

Assumption 3. *The following relationship holds*

$$0 < x < l_0 \tag{5.146}$$

Thus, in view of (5.143) and Assumption 3, the univalence between u and u_f exists, provided that

$$\frac{c_{p1}\cdot\vartheta(p_s-p_a)}{x} + \frac{c_{n2}\cdot\vartheta(p_b-p_r)}{l_0-x} > 0 \tag{5.147}$$

$$\frac{c_{n1}\cdot\vartheta(p_a-p_r)}{x} + \frac{c_{p2}\cdot\vartheta(p_s-p_b)}{l_0-x} > 0 \tag{5.148}$$

hold. In view of this statement, for given u_f one can find a unique valve control voltage u as

$$u = \frac{1}{\frac{c_{p1}\cdot\vartheta(p_s-p_a)}{x}+\frac{c_{n2}\cdot\vartheta(p_b-p_r)}{l_0-x}} u_f \mathcal{S}(u_f) + \frac{1}{\frac{c_{n1}\cdot\vartheta(p_a-p_r)}{x}+\frac{c_{p2}\cdot\vartheta(p_s-p_b)}{l_0-x}} u_f \mathcal{S}(-u_f) \tag{5.149}$$

when both (5.147) and (5.148) are satisfied.

5.5.2 Cylinder Control Equations

Also cylinder control equations given in (Zhu 2010, p.184-185) can be applied directly to studied system.

In view (5.149), the designed valve control voltage can be written as

$$u = \frac{1}{\frac{c_{p1}\cdot\vartheta(p_s-p_a)}{x}+\frac{c_{n2}\cdot\vartheta(p_b-p_r)}{l_0-x}} u_{fd} \mathcal{S}(-u_{fd}) + \frac{1}{\frac{c_{n1}\cdot\vartheta(p_a-p_r)}{x}+\frac{c_{p2}\cdot\vartheta(p_s-p_b)}{l_0-x}} u_{fd} \mathcal{S}(u_{fd}) \tag{5.150}$$

where

$$\begin{aligned} u_{fd} &= \left(\frac{1}{\beta}\right)\dot{f}_{pr} + \left(\frac{A_a}{x} + \frac{A_b}{l_0-x}\right)\dot{x} \\ &\quad + k_{fp}\left(f_{pr} - f_p\right) + k_x(\dot{x}_r - \dot{x}) \\ &= \boldsymbol{Y}_c\boldsymbol{\theta}_c + k_{fp}\left(f_{pr} - f_p\right) + k_x(\dot{x}_r - \dot{x}). \end{aligned} \tag{5.151}$$

By incorporating piston position control law given in (3.29) in (5.151), the above equation can be written as

$$u_{fd} = \left(\frac{1}{\beta}\right)\dot{f}_{pr} + \left(\frac{A_a}{x} + \frac{A_b}{l_0 - x}\right)\dot{x} + k_{fp}\left(f_{pr} - f_p\right) + k_x(\dot{x}_r - \dot{x}) = \boldsymbol{Y}_c\boldsymbol{\theta}_c + k_{fp}\left(f_{pr} - f_p\right) + k_x((\dot{x}_d + \lambda[x_d - x]) - \dot{x}) \quad (5.152)$$

with

$$f_{pr} = f_{cr} + f_f \quad (5.153)$$

$$\boldsymbol{Y}_c = \left[\dot{f}_{pr} \quad \frac{\dot{x}}{x} \quad \frac{\dot{x}}{l_0 - x}\right] \in \mathbb{R}^{1x3} \quad (5.154)$$

$$\boldsymbol{\theta}_c = \left[\frac{1}{\beta} \quad A_a \quad A_b\right]^T \in \mathbb{R}^3 \quad (5.155)$$

where f_{cr} is a required actuating force of cylinder obtained from (5.125), f_f is an applied piston friction model for cylinder, represented in Appendix F, f_{pr} denotes the required piston force, f_p denotes the measured piston force, $\dot{x}_d$ and x_d denotes the desired cylinder piston velocity and the desired piston position, respectively, $\dot{x}$ and x denotes the measured cylinder piston velocity and the measured piston position, respectively, $k_{fp} > 0$ and $k_x > 0$ are two feedback gains and $\lambda > 0$ is a position feedback gain.

5.6 Virtual Stability of Studied System

In the view of theory represented in subsection 3.3.4 all decomposed *objects*, illustrated in simple oriented graph in Figure 16, qualifies to be virtually stable in sense of Definition 2.10.

In the view of theory represented in subsection 3.4.4, both unactuated *open chains*, namely *open chain 1* and *open chain 3*, illustrated in simple oriented graph in Figure 16, qualifies to be virtually stable in sense of Definition 2.10.

In the view of theory represented in subsection 3.6.3, both actuated *open chains*, namely *open chain 2* and *open chain 4*, illustrated in simple oriented graph in Figure 16, qualifies to be virtually stable in sense of Definition 2.10.

Proofs of *virtual stability* of studied hydraulic manipulator are given in Appendix G and Appendix H.

6 EXPERIMENTAL IMPLEMENTATION AND RESULTS

In this chapter experimental implementation and results are given. First, in section 6.1 experiment set-up is defined. Then, in section 6.2, the control law for implemented PID-controller is given. In section 6.3, an applied Cartesian position control laws are introduced and given. Finally, in section 6.4, measured results with VDC- and PID-controller are given and discussed.

6.1 Experiment Set-Up

The experimental measurements were carried out in heavy machinery laboratory of Department of Intelligent Hydraulics and Automation (IHA) in Tampere University of Technology (TUT).

An applied theory of VDC (introduced and defined in chapter 5) into studied manipulator was implemented by using Simulink® block diagram environment developed by MathWorks®. Before moving to actual real-time measurements, the correct behavior of generated VDC model was verified with off-line simulations. For off-line simulations, a simulation model of studied manipulator was implemented by using Simulink® SimMechanics toolbox, which is a tool to model mechanical systems.

After off-line simulations, a generated VDC model was compiled to real-time code and code was uploaded into dSpace CP1103 PPC controller board. Controller board was embedded with real-time processor and comprehensive I/O, with high I/O speed and accuracy. (dSpace 2009) System was controlled and monitored with dSpace ControlDesk 3.7.1. ControlDesk was also used to capture and record system data during measurements. Sample time for control loop in dSpace was set to be 16 ms.

In the view the fact that typically used backward difference as a derivative leads easily very noisy output signal, the estimation algorithm given in (Harrison 1995) was used as a derivative throughout this thesis. The estimation algorithm uses current value of signal together with five past values as

$$\dot{x}(kh) = \frac{5x(kh)+3x(kh-h)+x(kh-2h)-x(kh-3h)-3x(kh-4h)-5x(5h)}{35h} \qquad (6.1)$$

where, x is a signal to be derived, $\dot{x}$ is a derivative of x and h denotes the sample time of system.

The uncertain parameters of an applied parameter vector $\boldsymbol{\theta}_{2A} \in \mathbb{R}^6$ (see Appendix B) of rigid bodies were found out by utilizing SolidWorks 3D mechanical

CAD program. First, all the rigid bodies (*rigid links* and *objects*) of studied system were CAD program. After 3D CAD model of all rigid bodies were realized, all unknown parameters of rigid bodies, needed to solve components of parameter vector $\boldsymbol{\theta}_{2A} \in \mathbb{R}^6$, were calculated from rigid body models. Calculated rigid body parameter vectors are given in Appendix I. Also applied valve flow coefficient parameter vector $\boldsymbol{\theta}_v \in \mathbb{R}^4$ and cylinder control parameter vector $\boldsymbol{\theta}_c \in \mathbb{R}^3$ are defined in Appendix I.

The joint angles θ_1 and θ_2 of studied manipulator (see Figure 9), were measured with SICK DGS60 incremental encoders, providing 40000 puls/rev. With given encoders an angular resolution of 0.0009 deg was obtained. Given joint angular resolution can be converted to respective cylinder piston position resolution[3]. The minimum piston position resolution for both cylinders was calculated to be about 0.005 mm.

All system pressures (supply pressure, return line pressure and chamber pressures of both cylinders) were measured with Trafag NAH (Type: 8253.74.2317) hydraulic pressure transmitters, providing a pressure range from 0 bar to 250 bar. Pressure transmitters had a pressure resolution of 0.25 bars.

Two different Bosch Rexroth servo solenoid valves were used to control cylinders. Valve 1 to control cylinder 1 (Type: 4WRPEH10-C4B-100L) with a nominal flow of 100 l/min @ Δp=35 bar per notch; and valve 2 to control cylinder 2 (Type: 4WRPEH10-C4B-50L) with a nominal flow of 50 l/min @ Δp=35 bar per notch. Both valve had the bandwidth of 100 Hz @ ± 5% signals.

6.2 Implemented PID-Controller

The results achieved with VDC controller were compared to corresponding results achieved with PID controller. Similar to VDC-control, PID-control was implemented in actuator space and thus piston position errors and piston velocity errors were used as error variables. An applied the joint PID control law can be written as

$$k_P e(t) + k_I \int_0^t e(t)dt + k_D \dot{e}(t) = 0, \tag{6.2}$$

where

$$e(t) = x_{des}(t) - x_{mes}(t) \tag{6.3}$$
$$\dot{e}(t) = \dot{x}_{des}(t) - \dot{x}_{mes}(t) \tag{6.4}$$

and $k_P > 0$ denotes the proportional gain, $k_I > 0$ denotes the integral gain and $k_D > 0$ denotes the derivative gain. Furthermore, $e(t)$ denotes the position error between desired position and measured position, and $\dot{e}(t)$ denotes the velocity error between desired velocity and measured velocity.

[3] Note that conversion between joint angular resolution and piston position resolution is not linear.

Parameters of implemented PID-controller (k_P, k_I, k_D) were tuned according to Ziegler-Nichols method. In this method integral gain k_I and derivative gain k_D are first set to be zero. Then, the ultimate gain k_u was determined by increasing proportional gain k_P until controlled output value began to oscillate and oscillation period t_u was measured. Finally, values for PID-control gains were determined according to Ziegler-Nichols tuning method (Ziegler 1942) as

$$k_P = 0.6 \cdot k_u \tag{6.5}$$

$$k_I = 2\frac{k_P}{t_u} \tag{6.6}$$

$$k_D = \frac{k_P t_u}{8} \tag{6.7}$$

6.3 Cartesian Position Control

The objective of Cartesian position control was to control end-effector, i.e. origin of frame $\{\boldsymbol{G}\}$, with respect to defined base frame $\{\boldsymbol{B}\}$ (see Figure 17). In Cartesian position control implementation, desired Cartesian motion trajectories (position trajectory and velocity trajectory) were needed convert to respective desired joint motions (in our case desired piston motions).

The desired end-effector position in Cartesian space was defined with position components X_d and Y_d, where X_d stood for desired Cartesian position with respect to *x*-axis of Cartesian base frame $\{\boldsymbol{B}\}$ and Y_d stood for desired Cartesian position with respect to *y*-axis of Cartesian base frame $\{\boldsymbol{B}\}$. Similar, the desired end-effector velocity in Cartesian space was defined with Cartesian velocity components $\dot{X}_d$ and $\dot{Y}_d$.

The desired Cartesian positions in X_d and Y_d were converted to respective desired joint space values θ_{2d} and θ_{1d} by utilizing inverse kinematics equations defined in (4.2) and (4.3). Further, the desired actuator space values (desired piston positions) x_{2d} and x_{4d} were obtained by utilizing *closed chain* geometric equations (5.3) and (5.6) through (5.1) and (5.2).

Respectively, the desired Cartesian velocities in $\dot{X}_d$ and $\dot{Y}_d$ was converted to respective desired joint space velocities $\dot{\theta}_{2d}$ and $\dot{\theta}_{1d}$ by utilizing differential kinematics equation defined in (4.7). The desired actuator space velocities (desired piston velocities) $\dot{x}_{2d}$ and $\dot{x}_{4d}$ were obtained by utilizing closed chain differential geometric equations (5.9) and (5.12)[4].

In scope of this thesis, a performance of VDC was tested by using diamond-like square Cartesian trajectory. An applied Cartesian path is given in Figure 19. In Figure 19 a reachable Cartesian workspace of HIAB 031 is outlined with red line. The driven square Cartesian path inside the reachable workspace is outlined with black line.

[4] Note, that in equations (5.9) and (5.12), $\dot{\theta}_{1d} = \dot{q}_{1d}$ and $\dot{\theta}_{2d} = \dot{q}_{3d}$holds, respectively.

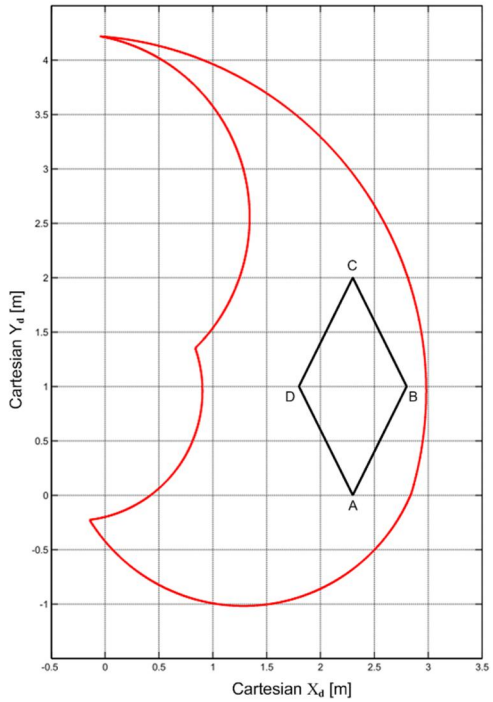

Figure 19: Square path in Cartesian workspace.

The Cartesian paths between points A, B, C and D were carried out by utilizing Quintic rest-to-rest path trajectory generator introduced in (Jazar 2010, pp.736-737) and given in (6.8) and equation of straight line given in (6.9)[5]

$$X_d(t) = a_0 + a_1 t + a_2 t^2 + a_3 t^3 + a_4 t^4 + a_5 t^5 \tag{6.8}$$

$$Y_d(t) = \frac{Y_f - Y_0}{X_f - X_0}(X_d(t) - X_0) + Y_0 \tag{6.9}$$

where, Y_0 and X_0 denotes the initial Cartesian positions and, Y_f and X_f denotes the final Cartesian positions. Six coefficients $(a_0, a_1, a_2, a_3, a_4, a_5)$ of fifth order time varying polynomial Quintic path function given in (6.8) can be solved from below equation

$$\begin{bmatrix} 1 & 0 & 0 & 0 & 0 & 0 \\ 0 & 1 & 0 & 0 & 0 & 0 \\ 0 & 0 & 2 & 0 & 0 & 0 \\ 1 & t_f & t_f^2 & t_f^3 & t_f^4 & t_f^5 \\ 0 & 1 & 2t_f & 3t_f^2 & 4t_f^3 & 5t_f^4 \\ 0 & 0 & 2 & 6t_f & 12t_f^2 & 20t_f^3 \end{bmatrix} \begin{bmatrix} a_0 \\ a_1 \\ a_2 \\ a_3 \\ a_4 \\ a_5 \end{bmatrix} = \begin{bmatrix} X_0 \\ \dot{X}_0 \\ \ddot{X}_0 \\ X_f \\ \dot{X}_f \\ \ddot{X}_f \end{bmatrix} \tag{6.10}$$

[5] In case of singularity $X_f - X_0 = 0$, desired path can be solved inversely by defining

$$X_d(t) = \frac{X_f - X_0}{Y_f - Y_0}(Y_d(t) - Y_0) + X_0$$

$$Y_d(t) = a_0 + a_1 t + a_2 t^2 + a_3 t^3 + a_4 t^4 + a_5 t^5$$

where, t_f denotes the desired transition time between two Cartesian points, X_0, $\dot{X}_0$ and $\ddot{X}_0$ denotes the initial position, velocity and acceleration, respectively, and X_f, $\dot{X}_f$ and $\ddot{X}_f$ denotes the desired final position, velocity and acceleration, respectively.

The desired Cartesian velocities were solved by taking time derivatives from equations (6.9) and (6.10), yielding to

$$\dot{X}_d(t) = a_1 + 2a_2t + 3a_3t^2 + 4a_4t^3 + 5a_5t^4 \quad (6.11)$$

$$\dot{Y}_d(t) = \frac{Y_f - Y_0}{X_f - X_0}\dot{X}_d(t) \quad (6.12)$$

An illustrative example of forms of motion trajectories (position, velocity and acceleration) generated by Quintic path generator are given in Figure 20 under the following conditions $X_0 = 0, \dot{X}_0 = 0, \ddot{X}_0 = 0, X_f = 1, \dot{X}_f = 0, \ddot{X}_f = 0$ and $t_f = 2$.

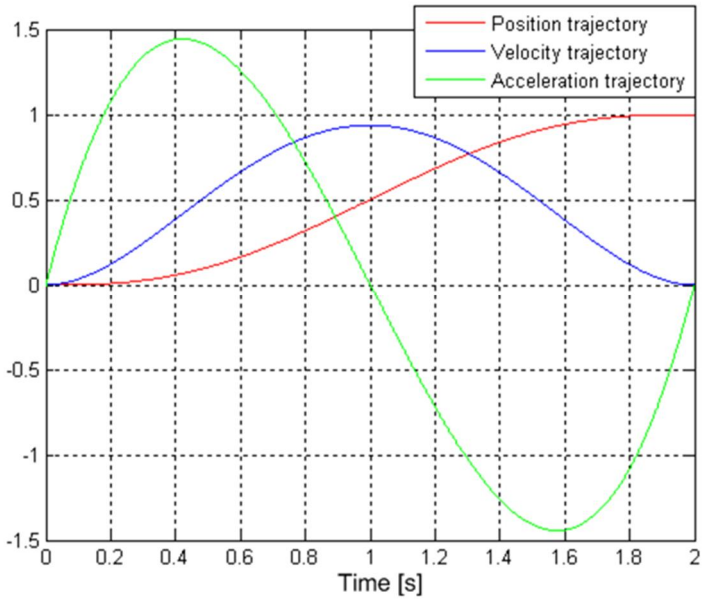

Figure 20: Motion trajectories of generated by Quintic path generator.

6.4 Results

The very same square Cartesian path was driven with both VDC- and PID-controllers. The driven Cartesian path is illustrated in Figure 19. Specific values for the Cartesian points in path were $A = (2.3,\ 0), B = (2.8,\ 1), C = (2.3,\ 2)$ and $A = (1.8,\ 1)$.

The desired piston position paths for cylinder 1 and cylinder 2, generated by Cartesian motion trajectory generator described in (6.8) and (6.9), are illustrated in Figure 21. The axis of time is intentionally left blank as different Cartesian transition times were applied. The maximum stroke for both cylinders is 0.545 m. As from Figure 21 can be seen, during Cartesian motion trajectory piston positions between 0.15 m – 0042 m are achieved for cylinder 1 and piston positions between 0.15 m – 0044 m are achieved for cylinder 2.

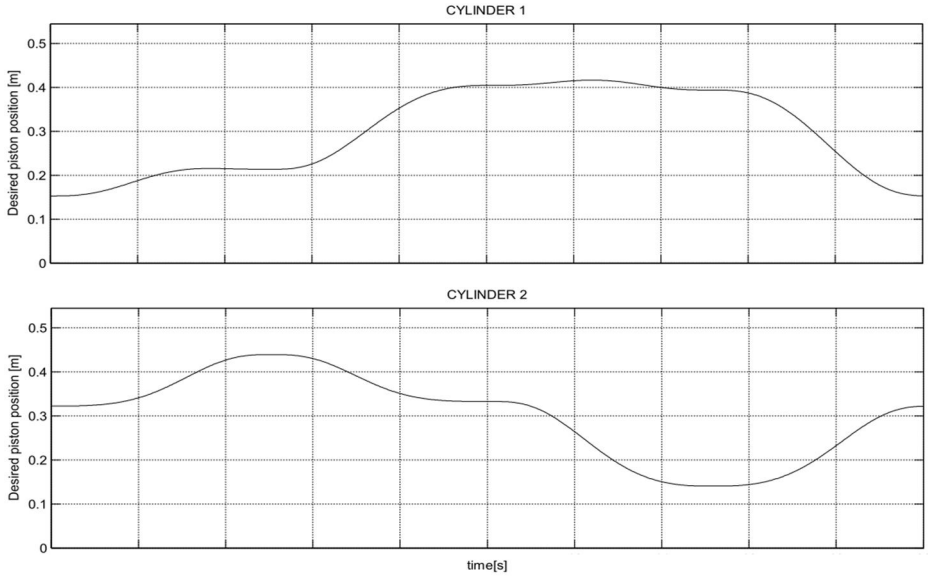

Figure 21: Desired piston positions for cylinder 1 and cylinder 2 generated by cartesian path generator.

The defined Cartesian motion trajectory was driven under three different Cartesian transition times $t_{f2.5} = 2.5\,s$, $t_{f5} = 5\,s$ and $t_{f10} = 10\,s$. In Figure 22 is illustrated the desired piston velocity trajectories generated by desired Cartesian motion trajectory generator, described in (6.11) and (6.12), under different Cartesian transition times. Note that in Figure 22 the time spans of different transition times are scaled to be same for the convenience[6].

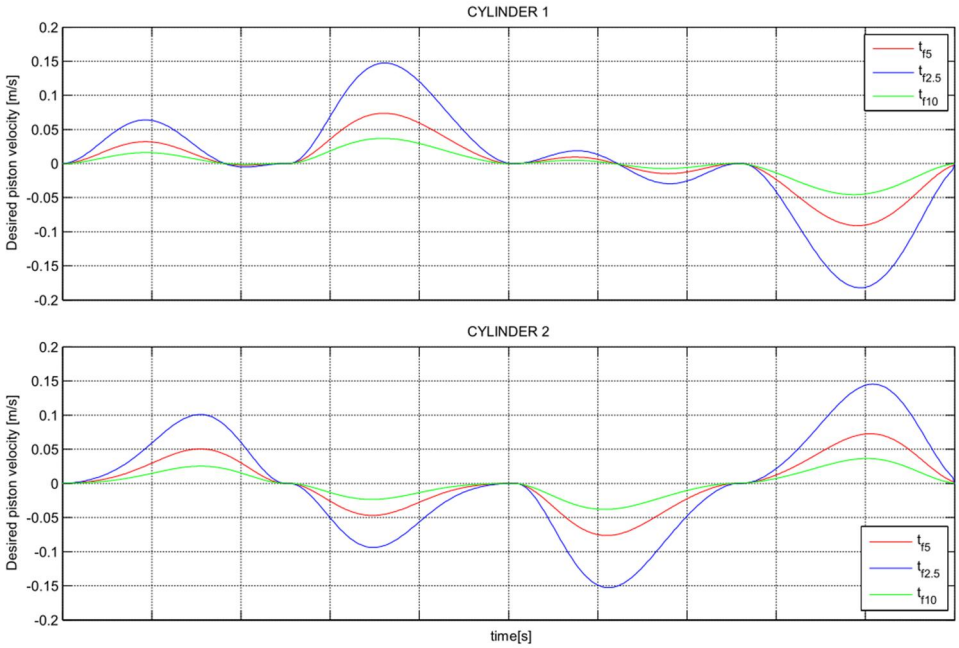

Figure 22: Desired piston velocity trajectories under different Cartesian transition times.

Cartesian transition time t_{f5}, providing a maximum piston velocity of about 0.09 m/s for cylinder 1 and 0.075 m/s for cylinder 2, was treated as a nominal condition for both VDC- and PID-controllers and controllers were tuned in the predominant

[6] In truth, time span under $t_{f2.5}$ = (time span t_{f5})/2 and
time span under t_{f10} = 2·(time span t_{f5}).

conditions of this transition time. The Cartesian transition time $t_{f2.5}$ was found out to be quite near the performance limits of system as about 70 percentages of valves full capability were utilized. On the other hand, Cartesian transition time t_{f10} can be considered to quite slow for system as only about 10 percentages of valves full capacity were utilized.

The following tuning parameters, given in Table 1, were used in measurements.

Table 1: Applied tuning parameters for VDC- and PID controllers.

	CYLINDER 1	CYLINDER 2
VDC-controller	k_x = 0.110	k_x = 0.044
	k_{fp} = $3.40 \cdot 10^{-8}$	k_{fp} = $3.00 \cdot 10^{-8}$
	λ = 11	λ = 7
	$\boldsymbol{K_A} = 500 \cdot \boldsymbol{I_6}$ for all rigid links and objects.	
PID-controller	k_P = 13.20	k_P = 19.20
	k_I = 72.53	k_I = 102.40
	k_D = 0.60	k_D = 0.90

The measured piston position tracking errors for cylinder 1 and cylinder 2 are given in Figure 23 and Figure 24, respectively. In both figures measured results with VDC-controller under three different Cartesian transition times (t_{f5}, $t_{f2.5}$ and t_{f10}) are given and with PID-controller measured results under nominal Cartesian transition time t_{f5} are given. Cartesian motion trajectory with transition times $t_{f2.5}$ and t_{f10} was not been able to driven with PID-controller as it went unstable under these conditions.

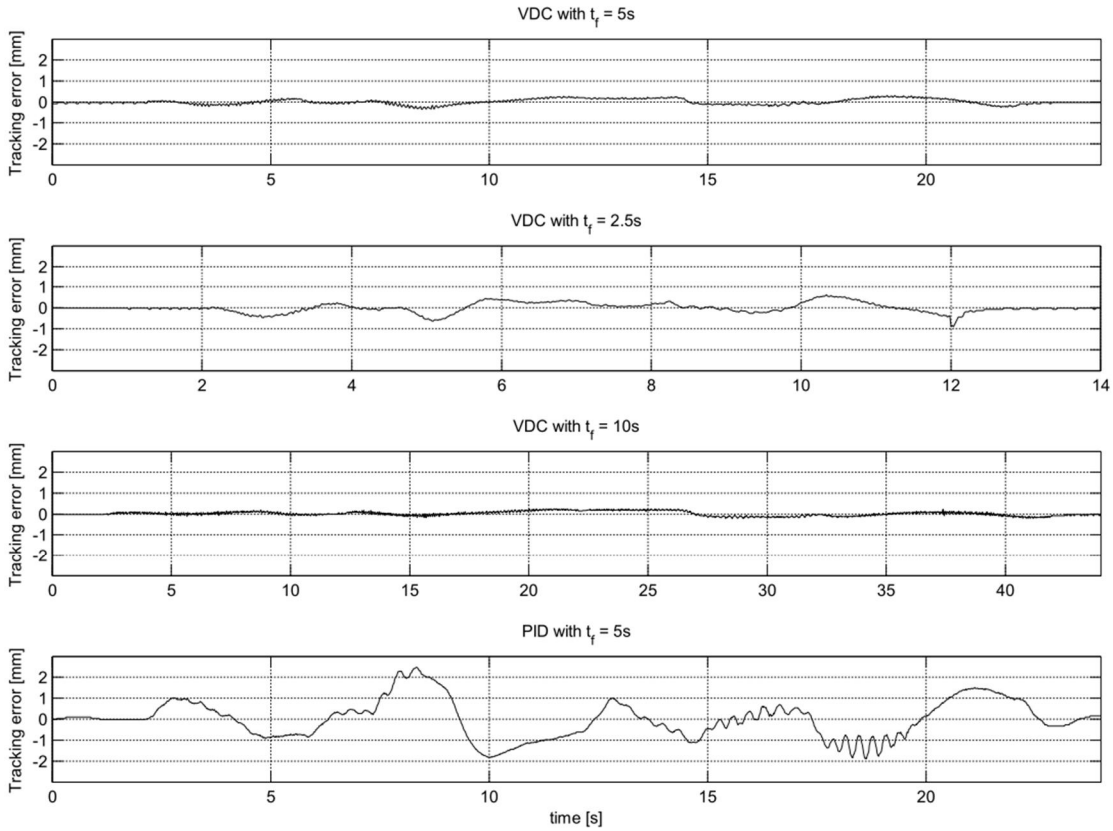

Figure 23: Cylinder 1 piston position tracking errors with VDC- and PID-controller.

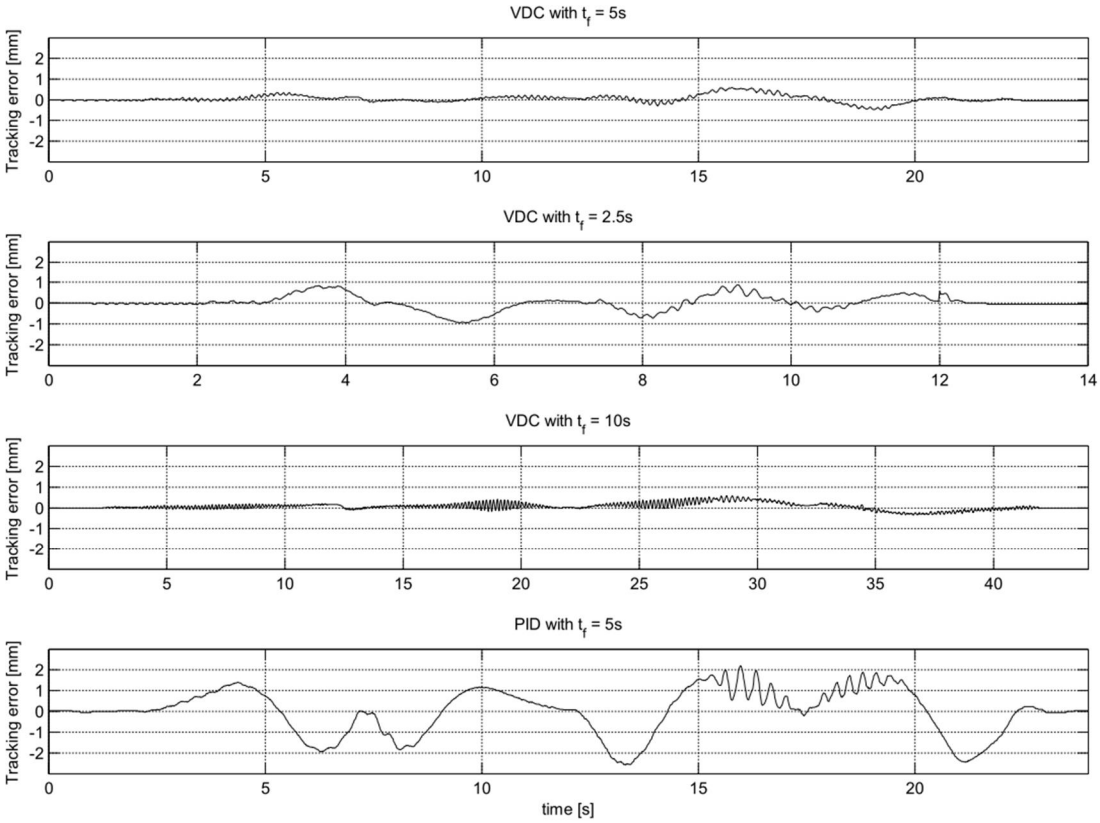

Figure 24: Cylinder 2 piston position tracking errors with VDC- and PID-controller.

The maximum piston position tracking errors during the Cartesian trajectory are given in Table 2:

Table 2: The maximum piston position tracking errors during driven Cartesian position trajectories.

	Maximum piston position tracking error for cylinder 1.	Maximum piston position tracking error for cylinder 2.
VDC t_{f5}	0.351 mm	0.585 mm
VDC $t_{f2.5}$	0.909 mm	0.960 mm
VDC t_{f10}	0.247 mm	0.587 mm
PID t_{f5}	2.471 mm	2.579 mm

As from Figure 23, Figure 24 and Table 2 can be seen, under the nominal Cartesian transition time t_{f5} roughly 7 times better piston position tracking ability for cylinder 1 was achieved with VDC-controller compared to PID-controller. Piston position tracking ability for cylinder 2 was about 4.4 times better with VDC-controller compared to PID-controller.

As aforementioned, PID-controller lost stability in attempts to drive Cartesian motion trajectory under Cartesian transition times $t_{f2.5}$ and t_{f10}. As from Figure 23 and Figure 24 can be seen, a stability was easily maintained with VDC-controller under different Cartesian transition times.

By comparing achieved VDC-controller results, one salience was that under Cartesian transition times t_{f5} and t_{f10}, much better results was achieved with cylinder 1

compared to cylinder 2. The difference between these cylinders can be explained with some problems in dynamical behavior of cylinder 2. It was noticed that around the operational piston position of 0.175 m, the piston position error of cylinder 2 seems to be increasing. This feature can be seen quite well from Figure 24 in the first graph (VDC t_{f5}) by looking behavior of cylinder 2 between time span 15s – 20s and from third graph (VDC t_{f10}) between time span 27.5s – 37.5. Note also that PID-controller had some problems around this operational piston position (see Figure 24, graph PID t_{f5} and time span 15s – 20s).

In Figure 25 are illustrated measured piston velocity trajectories with VDC- and PID-controller. In below figure required (or in case of PID desired) velocity profiles are given with black line and measured piston velocities are given red (cylinder 1) or magenta (cylinder 2) line.

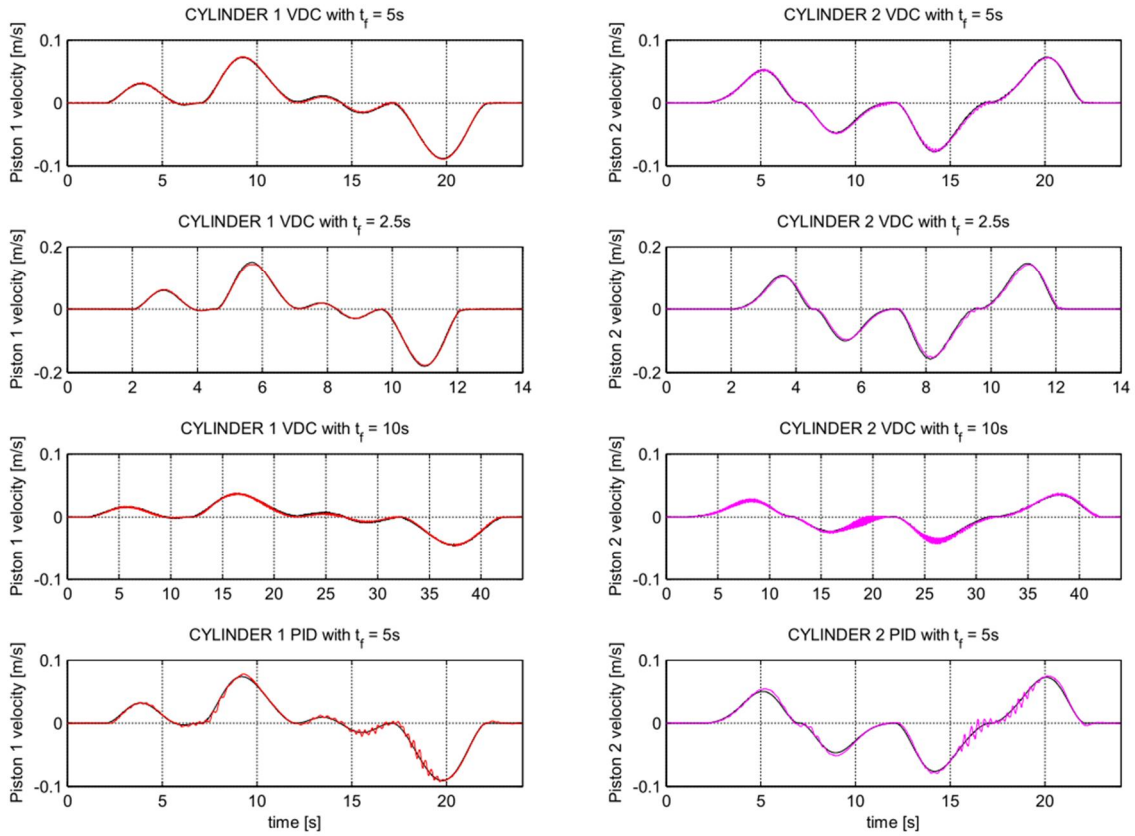

Figure 25: Measured piston velocity trajectories with VDC- and PID-controller.

In Figure 26 and Figure 27 are illustrated piston velocity tracking errors for cylinder 1 and cylinder 2, respectively. Note that with VDC-controller piston velocity tracking errors were measured from required piston velocity[7], defined in (3.29), whereas with PID-controller piston velocity tracking errors were measured from desired piston velocity trajectory given in Figure 22.

[7] In position control implementation, defined in (3.29), a desired piston velocity is incorporated into required piston velocity and it serves the reference trajectory of a velocity, given in Figure 22, with respect to time.

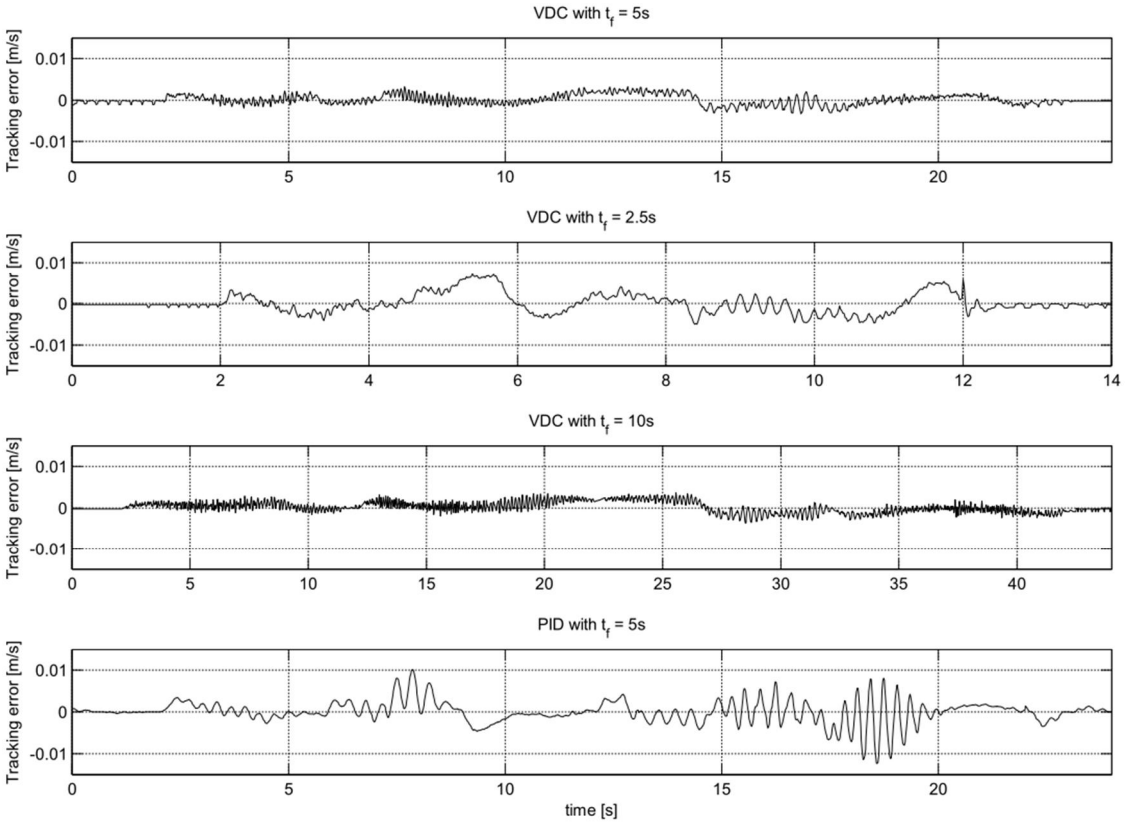

Figure 26: Cylinder 1 piston velocity tracking errors with VDC- and PID-controller.

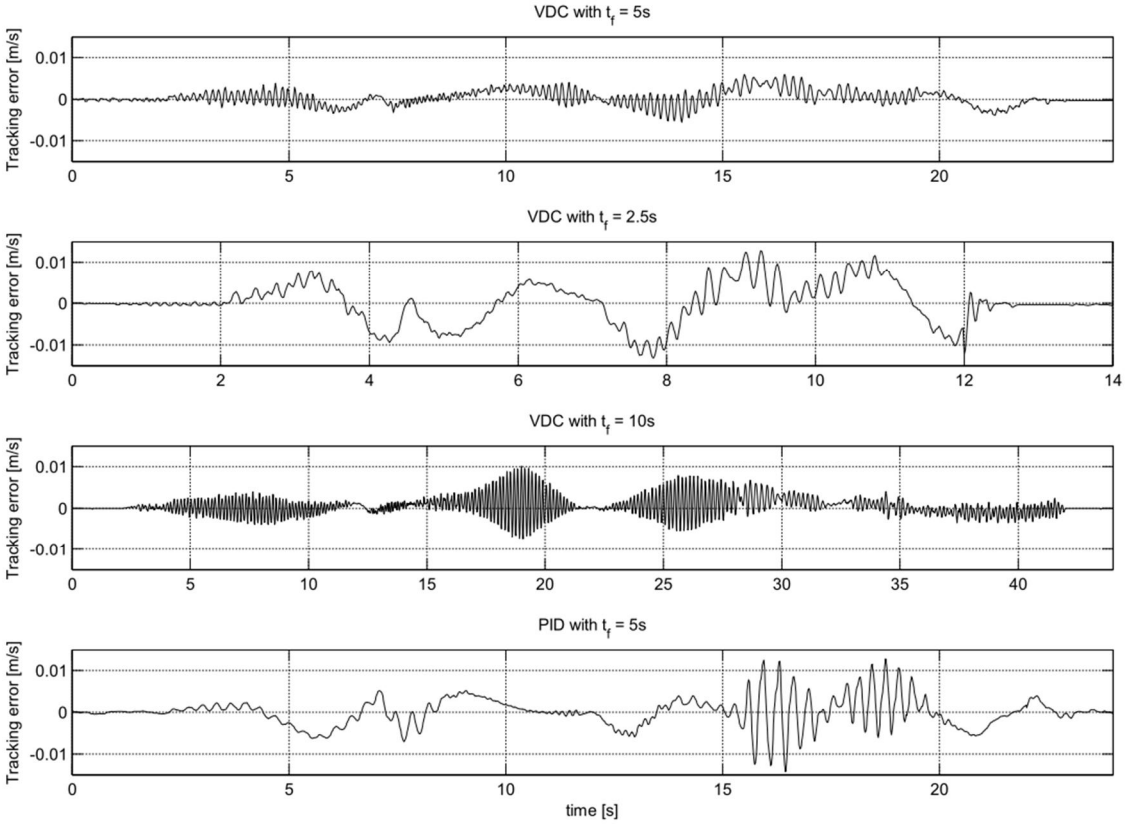

Figure 27: Cylinder 2 piston velocity tracking errors with VDC- and PID-controller.

The maximum piston velocity tracking errors during the driven Cartesian trajectories are given in Table 3.

Table 3: The maximum piston velocity tracking errors during driven Cartesian motion trajectories.

	Maximum piston velocity tracking error for cylinder 1.	Maximum piston velocity tracking error for cylinder 2.
VDC t_{f5}	3.35 mm/s	5.99 mm/s
VDC $t_{f2.5}$	7.15 mm/s	13.15 mm/s
VDC t_{f10}	3.69 mm/s	10.14 mm/s
PID t_{f5}	10.70 mm/s	14.54 mm/s

By looking cylinder 2 measured piston velocity trajectory with VDC and under t_{f10} (Figure 25, third row, second column) and cylinder 2 piston velocity tracking error with VDC and under t_{f10} (Figure 27, third plot), some high frequency oscillation can be seen. This implies that slightly smaller VDC-controller gains are needed, if studied manipulator is wanted to driven at smaller velocities than t_{f10} provides. From Figure 25 can be also seen that PID-controller was tuned quite near to asymptotic stability as some oscillation occurs at the end of trajectory.

In Figure 28 is illustrated a measured end-effector velocities in Cartesian space during driven Cartesian path for both VDC- and PID-controller under different Cartesian transition times. Given end-effector velocities were calculated from measured piston velocities, given in Figure 25. Similar to Figure 22, the time spans of different transition times in Figure 28 are scaled to be same for convenience.

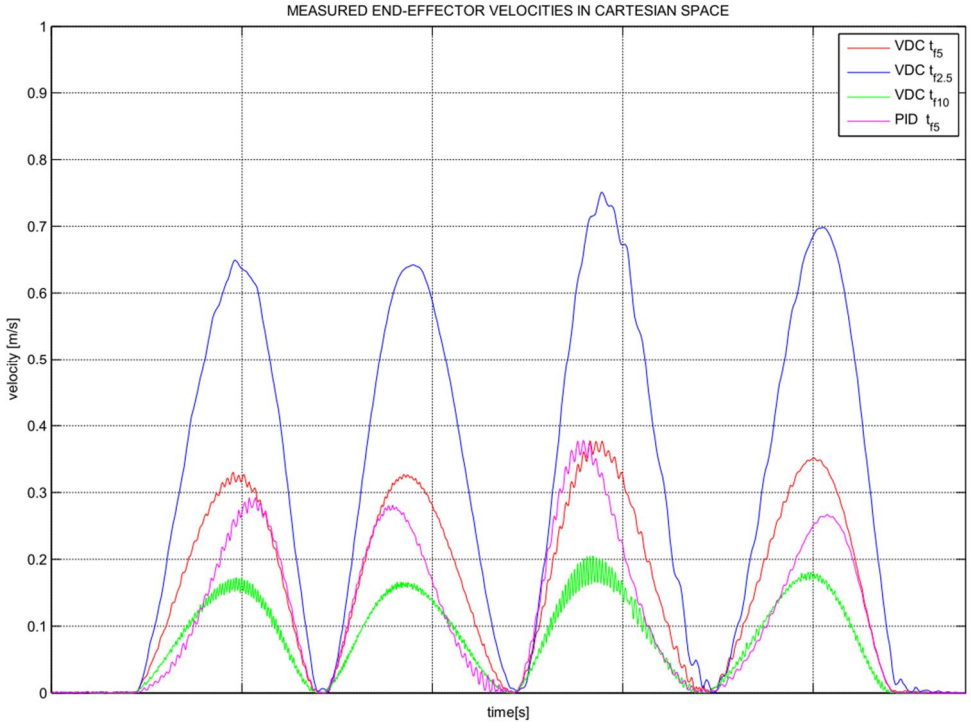

Figure 28: Measured end-effector velocities in Cartesian space with VDC- and PID-controller.

As from Figure 28 can be seen, under the nominal Cartesian transition time t_{f5} the maximum end-effector velocity in Cartesian space was about 0.38 m/s. Under the Cartesian transition time $t_{f2.5}$, the maximum end-effector velocity of about 0.75 m/s in Cartesian space was achieved.

In Figure 29 there are illustrated required and measured piston forces with VDC-controller under nominal Cartesian transition time t_{f5} for both cylinder 1 and cylinder 2. Piston forces with PID-controller were not measured as force feedback wasn't incorporated into PID control law. As from Figure 29 can be seen, measured piston force tracks quite well required piston force in both cylinder 1 and cylinder 2 case. However, peak piston force tracking error for both cylinders were around 7.5 kN (see Appendix I, Figure 40). In consequence of this, piston force error feedback gains k_{fp} in cylinder control equation (5.152) were needed to design quite small for both cylinders to maintain stability. Information given by Figure 29 reveals that there is still some potential to improve performance of VDC-controller by adjusting uncertain parameters of *rigid links* and *objects* defined in (B.17). This can be done by incorporating parameter adaptation, given in (Zhu 2010, p.32), into VDC control equations.

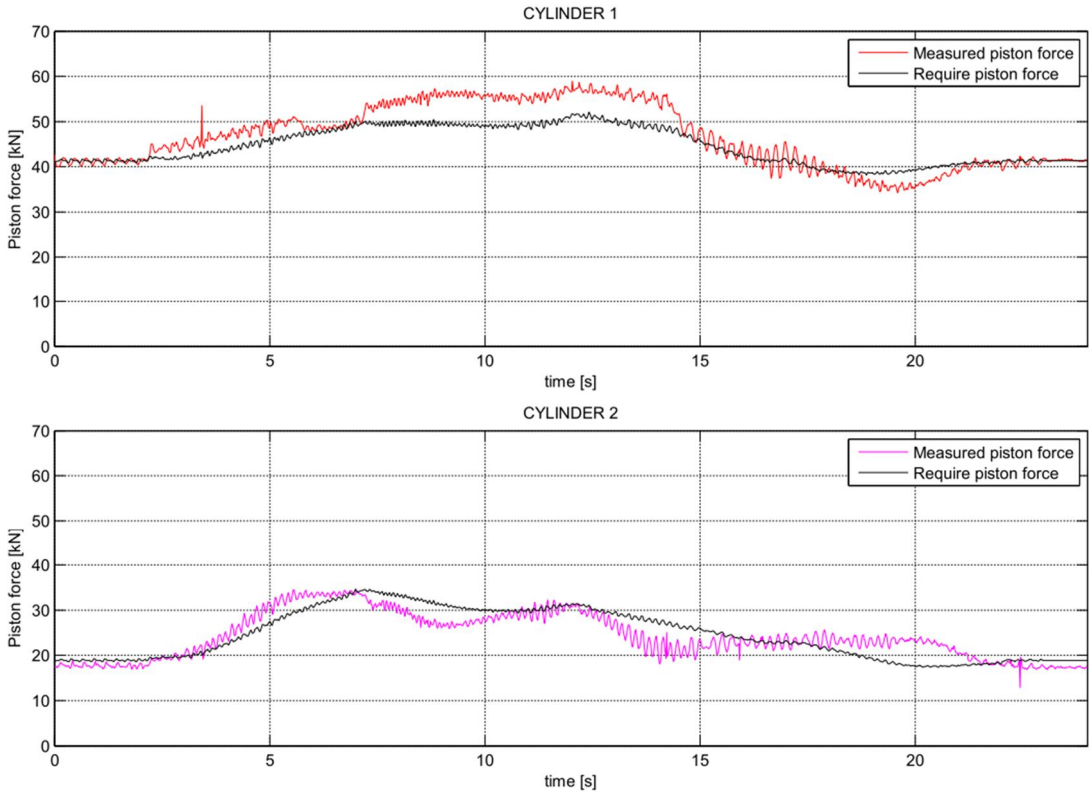

Figure 29: Required and measured piston forces with VDC-controller and Cartesian transition time of 5 s.

In Figure 30 and Figure 31 are illustrated measured valve control voltages for valve 1 and valve 2, respectively.

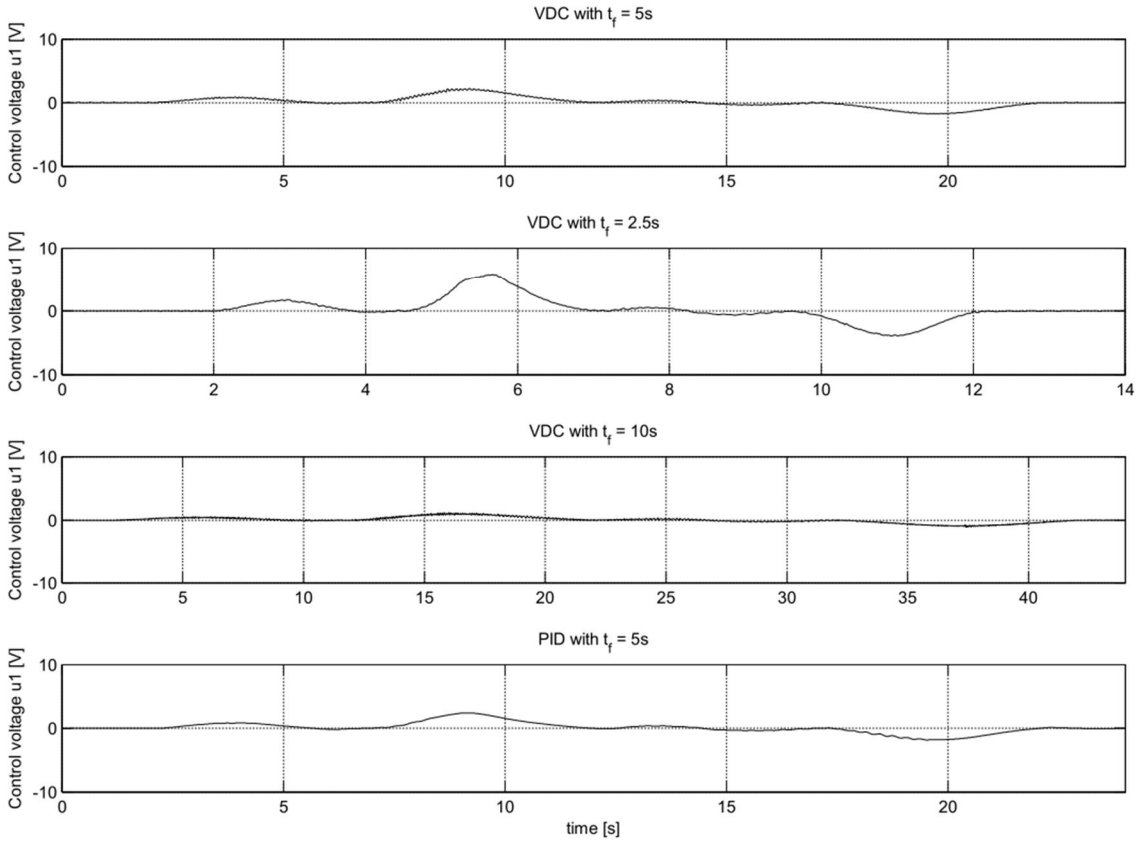

Figure 30: Measured control voltages of cylinder 1 control valve with VDC- and PID-controller.

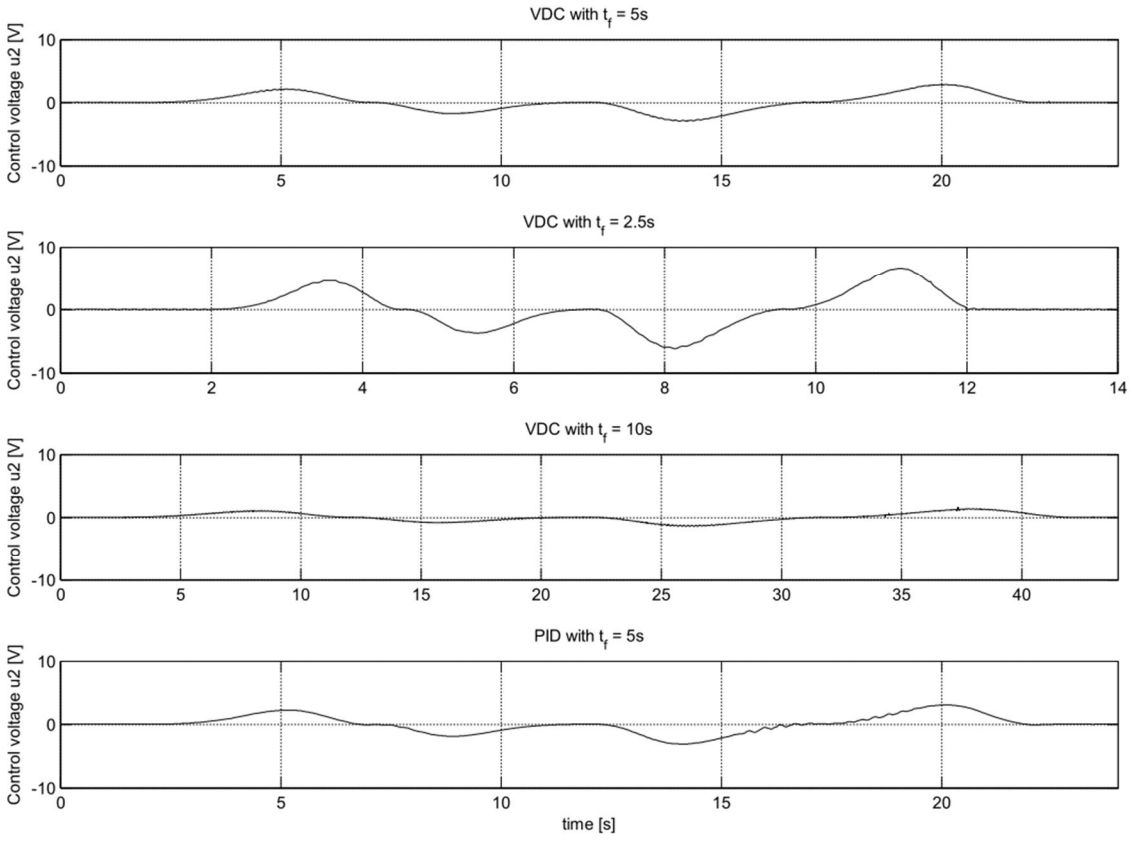

Figure 31: Measured control voltages of cylinder 2 control valve with VDC- and PID-controller.

As from Figure 30 and Figure 31 can be seen, a smooth control without unnecessary high frequency (and high amplitude) oscillation were achieved for VDC-controller under all applied Cartesian transition times. Figure 30 and Figure 31 also illustrates, that Cartesian transition time of $t_{f2.5}$ could considered to be near to performance limit of system as about 70 percentages (%) of valves capability was utilized. On the other hand, Cartesian transition time t_{f10} enabled only about 10 percentages (%) of valves capability. In view of above, an applied Cartesian motion trajectory with $t_{f2.5}$ can be considered to be fast in the view of system performance. On the other hand, Cartesian transition time t_{f10} can be considered to be a slow (in view of system performance) in which slow velocity friction, sensor noises and control valve non-linearities dominate. Thus, the performances of controllers were tested in very wide scale.

In studies of Zhu, e.g. (Zhu 2005) and (Zhu 2011), the ratio of the maximum position tracking error to the maximum velocity has been used as an indicator for the position tracking performance of a given robot. In (Zhu 2005), a hydraulic manipulator containing a very similar cylinder actuated joint (compared to joints studied in this thesis) was controlled with complete VDC-controller[8]. In (Zhu 2005), the ratio of the maximum position tracking error to the maximum velocity is reported to be 0.005 (s) for single hydraulically operated joint. In (Mattila 2000), the control of same hydraulic manipulator than in this thesis was studied and the ratio of the maximum position tracking error to the maximum velocity was about 0.0133 (s) for cylinder 1 and about 0.0300 for cylinder 2. In this thesis, for studied manipulator under a nominal Cartesian transition time t_{f5}, the ratio of the maximum position tracking error to the maximum velocity was calculated to be 0.0039 (s) for cylinder 1 and 0.0077 (s) for cylinder 2 and thus the achieved results can be seen very good. However, especially as parameter adaptation was not yet incorporated into VDC, the accuracy of used sensory system can be seen more or less questionable. Thus, more scientific evidences about performance and accuracy of used sensory system are required. Regardless of this, the performance comparisons between VDC- and PID-controller can be seen fully applicable.

During VDC and PID measurements no cavitations in cylinder chambers were detected. For further interest, more detailed information about accomplished measurements can be found in Appendix J, Appendix K, Appendix L and Appendix M. In Appendix J is documented measurements with VDC-controller under Cartesian transition time t_{f5}. In Appendix K is documented measurements with VDC-controller under Cartesian transition time $t_{f2.5}$. In Appendix K is documented measurements with VDC-controller under Cartesian transition time t_{f10}. In Appendix M is documented measurements with PID-controller under Cartesian transition time t_{f5}.

[8] In (Zhu 2005), the parameter adaptation was incorporated into control laws.

7 CONCLUSIONS AND FURTHER WORK

In this thesis, a new control theory, called Virtual Decomposition Control (VDC), was studied. The theory of VDC approach was successfully applied into studied hydraulic 2-DOF manipulator actuated with two hydraulic cylinders and the L_2 and L_∞ stability of subsystems were mathematically guaranteed leading to stability of entire system.

In experimental measurements the achieved results with VDC-controller were compared to corresponding results with PID-controller. Control of studied system was conducted in actuator space and the very same Cartesian motion trajectory was driven with both controllers. The defined Cartesian motion trajectory was driven with three different velocities, such that during fastest trajectory (with Cartesian transition time $t_{f2.5}$=2.5s) about 70 percentage of control valve capability were utilized and during slowest trajectory (with Cartesian transition time t_{f10}=10s) only about 10 percentage of valve capability were utilized. An applied Cartesian motion trajectory with $t_{f2.5}$ can be considered to be fast in the view of system performance. On the other hand, Cartesian transition time t_{f10} can be considered to be a slow (in view of system performance) in which slow velocity friction, sensor noises and control valve non-linearities dominate. Thus, the performances of controllers were tested in very wide scale.

In measurements both controllers (VDC and PID) were tuned under predominant conditions of nominal Cartesian transition time of t_{f5}=5s. VDC-controller was able to drive Cartesian motion trajectories with all three different Cartesian transition times without problems, whereas stability of PID-controller was lost under Cartesian transition times of $t_{f2.5}$ and t_{f10}. This implies that much better control robustness for VDC-controller (compared to PID-controller) was achieved. Stability limits of VDC-controller were not studied.

With VDC-controller, the piston position tracking errors for both cylinders were managed to kept under 1 mm even at fastest Cartesian transition time $t_{f2.5}$. On contrast, with PID-controller with 50 % slower Cartesian transition time t_{f5}, the maximum piston position tracking errors for both cylinders were around 2.5 mm. With VDC controller under Cartesian transition time t_{f10}, the maximum piston position tracking error for first cylinder of system was managed to kept under 0.25 mm. If performances of VDC- and PID-controller were compared under same Cartesian transition time t_{f5}, roughly 7 times better piston position tracking performance was achieved with VDC-controller (compared to PID-controller) for first cylinder of system. Corresponding results for second cylinder of system were about 4.4 times better with VDC-controller than PID-controller. Some problems with dynamical behavior cylinder 2 were noticed.

In studies of Zhu, e.g. (Zhu 2005) and (Zhu 2011), the ratio of the maximum position tracking error to the maximum velocity has been used as an indicator for the position tracking performance of a given robot. In (Zhu 2005), a hydraulic manipulator containing a very similar cylinder actuated joint (compared to joints studied in this thesis) was controlled with complete VDC-controller[9]. In (Zhu 2005), the ratio of the maximum position tracking error to the maximum velocity is reported to be 0.005 (s) for single hydraulically operated joint. In (Mattila 2000), the control of same hydraulic manipulator than in this thesis was studied and the ratio of the maximum position tracking error to the maximum velocity was about 0.0133 (s) for cylinder 1 and about 0.0300 for cylinder 2. In this thesis, for studied manipulator under a nominal Cartesian transition time t_{f5}, the ratio of the maximum position tracking error to the maximum velocity was calculated to be 0.0039 (s) for cylinder 1 and 0.0077 (s) for cylinder 2 and thus the achieved results can be seen very good. However, especially as parameter adaptation was not yet incorporated into VDC, the accuracy of used sensory system can be seen more or less questionable. Thus, more scientific evidences about performance and accuracy of used sensory system are required. Regardless of this, the performance comparisons between VDC- and PID-controller can be seen fully applicable.

In (Zhu 2005), an actual piston force was measured directly from piston with loadcell. In this thesis, the VDC was applied into a hydraulic system without using loadcells[10]. This was the first time in context of VDC and thus achieved results have novelty in this stand. The piston force computation from cylinder chamber pressures was proven to be practical method to compute piston forces in hydraulic VDC applications.

As a future work, similar measurements with enhanced angle sensory data will be required to do. Furthermore, as mention in section 6.4, even though measured piston force was tracking required piston force quite well, the correspondence between them can be likely improved by incorporating parameter adaptation into control equations. Parameter adaptation will be favorable to performed also other uncertain parameters defined in (5.145) and (5.155). Studies concerned to link flexibilities and contact with environment are still under evaluation.

[9] In (Zhu 2005), the parameter adaptation was incorporated into control laws.

[10] The actual piston forces were computed from cylinder chamber pressures according to equation (5.141).

REFERENCES

(Canudas 1995) **Canudas de Wit, C., *et all*. 1995.** A New Model for Control Systems with Friction. IEEE Transactions on Automatic Control. Vol. 40, No.3. (pp. 419 - 425).

(Craig 2005) **Craig, J. 2005.** Introduction to Robotics: Mechanics and Control. 3rd edition. Pearson/Prentice Hall.

(dSpace 2009) **dSpace. 2009.** Catalogue page of dSpace DS1103 PPC Controller Board. [Online] [Cited: 1.11.2012] http://www.dspace.de/shared/data/pdf/catalog2009/DS1103-PPC-ControllerBoard_dSPACE_Catalog_2009.pdf

(Harrison 1995) **Harrison, A.J.L, Stoten, D.P. 1995.** Generalized finite difference method for optimal estimation of derivatives in real-time control problems. Proceedings of the Institution of Mechanical Engineers. Vol. 209, (pp. 67-78)

(Huang 2010) **Huang, A-C, Chien, M-H. 2010.** Adaptive Control of Robot Manipulators: A Unified Regressor-Free Approach. World Scientific Publishing Company.

(Jazar 2010) **Jazar, R.N. 2010.** Theory of Applied Robotics: Kinematics, Dynamics, and Control. 2nd edition. Springer. (883 p.)

(Lewis 2004) **Lewis, F.L, Dawson, D.M., Abdallah C.T. 2004.** Robot Manipulator Control: Theory and Practise. 2nd edition. Marcel Dekker Publishing Company.

(Linjama 1996) **Linjama, M. 1995.** Mobilehydrauliikka. Chapter IV. IHA report 52. Tampere, Finland. ISBN 951-722-612-8. [in Finnish]

(Linjama 1998) **Linjama, M. 1998.** The Modeling and Actuator Space Control of Flexible Hydraulic Cranes. Acta Polytechnica Scandinavica. Mechanical Engineering Series No. 129.

(Mattila 2000) **Mattila, J. 2000.** On Energy-efficient Motion Control of Hydraulic Manipulators. Doctoral thesis. Tampere University of Technology. Publication 312. TTKK-Paino.

(Muhammad 2011) **Muhammad, A. 2011.** Impedance Control of Redundant Manipulators. Doctoral thesis. Tampere University of Technology. Publication 986. Uniprint TTY.

(Niksefat 1999) **Niksefat, N., Sepehri, M. 1999.** Robust Force Controller Design for a Hydraulic ctuator Based on Experimental Input-Output Data. Proceedings of the American Control Conference. San Diego, CA. pp. 3718-3722.

(Sciavicco 2001) **Sciavicco, L., Siciliano, B. 2001.** Modelling and control of robot manipulators. 2nd edition. Springer.

(Sirouspour 2001) **Sirouspour, M.R, Salcudean, S.E. 2001.** Nonlinear Control of Hydraulic Robots. IEEE Transactions on Robotics and Automation. Vol. 17, No.2. (pp. 173 - 182).

(Watton 1989) **Watton, J. 1989.** Fluid Power Systems: Modeling, Simulation, Analog and Microprocessor Control. Prentice-Hall. (490 p.)

(Zhu 1997) **Zhu, W-H., Xi, Y-G. *et al*. 1997.** Virtual Decomposition Based Control for Generalized High Dimensional Robotic Systems with Complicated Structures. IEEE Transactions on Robotics and Automation, Vol. 13, No. 3. (pp. 411- 436)

(Zhu 2002) **Zhu, W-H., De Schutter, J. 2002.** Experimental Verifications of Virtual-Decomposition-Based Motion/Force Control. IEEE Transactions on Robotics and Automation, Vol. 18, No. 3. (pp. 379- 386)

(Zhu 2005) **Zhu, W-H., Piedboeuf, J.C. 2005.** Adaptive output force tracking control of hydraulic cylinders with applications to robot manipulators. ASME J. Dynamic Syst. Measure. Contr. 127(2), (pp. 206- 217)

(Zhu 2010) **Zhu, W-H. 2010.** Virtual Decomposition Control: Toward Hyper Degrees of Freedom Robots. 1st edition. Springer-Verlag (STAR Series No. 60). (460 p.)

(Zhu 2011) **Zhu, W-H., Vukovich, G. 2011.** Virtual Decomposition control for Modular Robot Manipulators. Preprints of the 18th IFAC World Congress. (pp. 13486–13491). Available: http://www.nt.ntnu.no/users/skoge/prost/proceedings/ifac11-proceedings/data/html/papers/2233.pdf (10.4.2012)

(Ziegler 1942) **Ziegler, J.G., Nichols, N.B. 1942.** Optimum Settings for Automatic Controllers. Transactions of the ASME. Vol. 64. (pp.759-768)

APPENDIX A: REGRESSOR MATRIX AND PARAMETER VECTOR OF OBJECTS AND RIGID LINKS

In this appendix formulation for the regressor matrix $\boldsymbol{Y_A} \in \mathbb{R}^{6\times 13}$ and the parameter vector $\boldsymbol{\theta_A} \in \mathbb{R}^{13}$ of rigid body, to which frame $\{\mathbf{A}\}$ is attached as appeared in (2.19), is given.

According to (Zhu 2010, p.386-388), the non-zero elements in $\boldsymbol{Y_A} \in \mathbb{R}^{6\times 13}$ are listed as

$$y_A(1,1) = \frac{d}{dt}\left({}^A v_r\right)(1) + {}^A v(5)\,{}^A v_r(3) - {}^A v(6)\,{}^A v_r(2) + {}^A g(1) \quad \text{(A.1)}$$

$$y_A(1,2) = -{}^A v(5)\,{}^A v_r(5) - {}^A v(6)\,{}^A v_r(6) \quad \text{(A.2)}$$

$$y_A(1,3) = -\frac{d}{dt}\left({}^A v_r\right)(6) + {}^A v(5)\,{}^A v_r(4) \quad \text{(A.3)}$$

$$y_A(1,4) = \frac{d}{dt}\left({}^A v_r\right)(5) + {}^A v(6)\,{}^A v_r(4) \quad \text{(A.4)}$$

$$y_A(2,1) = \frac{d}{dt}\left({}^A v_r\right)(2) + {}^A v(6)\,{}^A v_r(1) - {}^A v(4)\,{}^A v_r(3) + {}^A g(2) \quad \text{(A.5)}$$

$$y_A(2,2) = \frac{d}{dt}\left({}^A v_r\right)(6) + {}^A v(4)\,{}^A v_r(5) \quad \text{(A.6)}$$

$$y_A(2,3) = -{}^A v(4)\,{}^A v_r(4) - {}^A v(6)\,{}^A v_r(6) \quad \text{(A.7)}$$

$$y_A(2,4) = -\frac{d}{dt}\left({}^A v_r\right)(4) + {}^A v(6)\,{}^A v_r(5) \quad \text{(A.8)}$$

$$y_A(3,1) = \frac{d}{dt}\left({}^A v_r\right)(3) + {}^A v(4)\,{}^A v_r(2) - {}^A v(5)\,{}^A v_r(1) + {}^A g(3) \quad \text{(A.9)}$$

$$y_A(3,2) = -\frac{d}{dt}\left({}^A v_r\right)(5) + {}^A v(4)\,{}^A v_r(6) \quad \text{(A.10)}$$

$$y_A(3,3) = \frac{d}{dt}\left({}^A v_r\right)(4) + {}^A v(5)\,{}^A v_r(6) \quad \text{(A.11)}$$

$$y_A(3,4) = -{}^A v(4)\,{}^A v_r(4) - {}^A v(5)\,{}^A v_r(5) \quad \text{(A.12)}$$

$$y_A(4,3) = y_A(3,1) \quad \text{(A.13)}$$

$$y_A(4,4) = -y_A(2,1) \quad \text{(A.14)}$$

$$y_A(4,6) = y_A(3,3) \quad \text{(A.15)}$$

$$y_A(4,7) = -y_A(2,4) \quad \text{(A.16)}$$

$$y_A(4,8) = y_A(3,2) \quad \text{(A.17)}$$

$$y_A(4,9) = -y_A(2,2) \quad \text{(A.18)}$$

$$y_A(4,10) = {}^A v(6)\,{}^A v_r(6) - {}^A v(5)\,{}^A v_r(5) \quad \text{(A.10)}$$

$$y_A(4,11) = \frac{d}{dt}\left({}^A v_r\right)(4) + {}^A v(5)\,{}^A v_r(6) - {}^A v(6)\,{}^A v_r(5) \quad \text{(A.20)}$$

$$y_A(4,12) = -{}^A v(6)\,{}^A v_r(5) \quad \text{(A.21)}$$

$$y_A(4,13) = {}^A v(5)\,{}^A v_r(6) \quad \text{(A.22)}$$

$$y_A(5,2) = -y_A(3,1) \quad \text{(A.23)}$$

$$y_A(5,4) = y_A(1,1) \tag{A.24}$$
$$y_A(5,5) = -y_A(3,2) \tag{A.25}$$
$$y_A(5,7) = y_A(1,4) \tag{A.26}$$
$$y_A(5,8) = -y_A(3,3) \tag{A.27}$$
$$y_A(5,9) = {}^{A}v(4)\,{}^{A}v_r(4) - {}^{A}v(6)\,{}^{A}v_r(6) \tag{A.28}$$
$$y_A(5,10) = y_A(1,3) \tag{A.29}$$
$$y_A(5,11) = {}^{A}v(6)\,{}^{A}v_r(4) \tag{A.30}$$
$$y_A(5,12) = \frac{d}{dt}\left({}^{A}v_r\right)(5) + {}^{A}v(6)\,{}^{A}v_r(4) - {}^{A}v(4)\,{}^{A}v_r(6) \tag{A.31}$$
$$y_A(5,13) = -{}^{A}v(4)\,{}^{A}v_r(6) \tag{A.32}$$
$$y_A(6,2) = y_A(2,1) \tag{A.33}$$
$$y_A(6,3) = -y_A(1,1) \tag{A.34}$$
$$y_A(6,5) = y_A(2,2) \tag{A.35}$$
$$y_A(6,6) = -y_A(1,3) \tag{A.36}$$
$$y_A(6,8) = {}^{A}v(5)\,{}^{A}v_r(5) - {}^{A}v(4)\,{}^{A}v_r(4) \tag{A.37}$$
$$y_A(6,9) = y_A(2,4) \tag{A.38}$$
$$y_A(6,10) = -y_A(1,4) \tag{A.39}$$
$$y_A(6,11) = -{}^{A}v(5)\,{}^{A}v_r(4) \tag{A.40}$$
$$y_A(6,12) = {}^{A}v(4)\,{}^{A}v_r(5) \tag{A.41}$$
$$y_A(6,13) = \frac{d}{dt}\left({}^{A}v_r\right)(6) + {}^{A}v(4)\,{}^{A}v_r(5) - {}^{A}v(5)\,{}^{A}v_r(4) \tag{A.42}$$

where $y_A(j,k) \in \mathbb{R}$ denotes an element of $\boldsymbol{Y_A} \in \mathbb{R}^{6\times 13}$ at row j and column k for $j \in \{1,6\}$ and $k \in \{1,13\}$; three variables $\frac{d}{dt}\left({}^{A}v_r\right)(j) \in \mathbb{R}$, ${}^{A}v(j) \in \mathbb{R}$, and ${}^{A}v_r(j) \in \mathbb{R}$ denote the jth element of $\frac{d}{dt}\left({}^{A}\boldsymbol{V}_r\right) \in \mathbb{R}^6$, ${}^{A}\boldsymbol{V} \in \mathbb{R}^6$, and ${}^{A}\boldsymbol{V}_r \in \mathbb{R}^6$, respectively, for all $j \in \{1,6\}$; and ${}^{A}g(j) \in \mathbb{R}$ denotes the jth element ${}^{A}\boldsymbol{R_I}\,\boldsymbol{g} \in \mathbb{R}^3$ with $\boldsymbol{g} = [0 \quad 0 \quad 9.8]^T \in \mathbb{R}^3$ for all $j \in \{1,3\}$. (Zhu 2010, p.388)

The 13 elements of $\boldsymbol{\theta_A} \in \mathbb{R}^{13}$ are listed as

$$\theta_{A1} = m_A \tag{A.43}$$
$$\theta_{A2} = m_A\,{}^{A}r_{mx} \tag{A.44}$$
$$\theta_{A3} = m_A\,{}^{A}r_{my} \tag{A.45}$$
$$\theta_{A4} = m_A\,{}^{A}r_{mz} \tag{A.46}$$
$$\theta_{A5} = m_A\,{}^{A}r_{mx}^2 \tag{A.47}$$
$$\theta_{A6} = m_A\,{}^{A}r_{my}^2 \tag{A.48}$$
$$\theta_{A7} = m_A\,{}^{A}r_{mz}^2 \tag{A.49}$$
$$\theta_{A8} = m_A\,{}^{A}r_{mx}\,{}^{A}r_{my} - I_{Axy} \tag{A.50}$$
$$\theta_{A9} = m_A\,{}^{A}r_{mx}\,{}^{A}r_{mz} - I_{Axz} \tag{A.51}$$
$$\theta_{A10} = m_A\,{}^{A}r_{my}\,{}^{A}r_{mz} - I_{Ayz} \tag{A.52}$$
$$\theta_{A11} = I_{Axx} \tag{A.53}$$
$$\theta_{A12} = I_{Ayy} \tag{A.54}$$
$$\theta_{A13} = I_{Azz} \tag{A.55}$$

where θ_{Ak} denotes the *k*th element of $\boldsymbol{\theta_A} \in \mathbb{R}^{13}$ for all $k \in \{1,13\}$; m_A is the mass; ${}^A\boldsymbol{r}_m = \left[{}^A r_{mx},\ {}^A r_{my},\ {}^A r_{mz} \right]^T \in \mathbb{R}^3$ denotes a vector pointing from the origin of frame {**A**} toward the center of mass and expressed in frame {**A**}, and I_{Axx}, I_{Ayy}, I_{Azz}, I_{Axy}, I_{Axz}, and I_{Ayz} are elements of $\boldsymbol{I_A}$. (Zhu 2010, p.389)

APPENDIX B: DERIVATION OF REGRESSOR MATRIX AND PARAMETER VECTOR FOR 2-DOF SYSTEM

Since the regressor matrix depends on the joint position, velocities, and accelerations, it should be updated in every control cycle (Huang 2010, p.83). Due to this fact, it is very desirable to try design regressor matrices as elemental form as possible, as computation of the complex regressor matrices during each sampling period in the real-time realizations is very time consuming (Huang 2010, p.vii).

As mentioned in chapter 4, the studied system can provide only 2-DOF of motion. Basically this means that system can provide motion only in one certain defined plane. With an appropriate frame attachment (see Figure 17), all linear motions subject to any rigid bodies of system (*objects* and *rigid links*) can be restricted to occur only in *xy*-plane (along *x*-axis and *y*-axis) with respect to attached body frame {A} of rigid body. Furthermore, in this case all rotational motions subject to any rigid body of system can be occur only about z-axis with respect to attached body frame {A} of rigid body.

In view of aforementioned, all motions along z-axis $\left({}^{\boldsymbol{A}}v(3) \in \mathbb{R}\right)$, about *x*-axis $\left({}^{\boldsymbol{A}}v(4) \in \mathbb{R}\right)$ and about *y*-axis $\left({}^{\boldsymbol{A}}v(5) \in \mathbb{R}\right)$ are cancelled out from every linear/angular velocity vectors ${}^{\boldsymbol{A}}\boldsymbol{V} \in \mathbb{R}^6$ defined in (2.4) subjecting to

$$ {}^{\boldsymbol{A}}v(j) = 0, \qquad \text{for all} \quad j \in \{3,5\}. \tag{B.1} $$

Obviously, also all motions in required linear/angular velocity vectors ${}^{\boldsymbol{A}}\boldsymbol{V_r} \in \mathbb{R}^6$along *z*-axis $\left({}^{\boldsymbol{A}}v(3) \in \mathbb{R}\right)$, about *x*-axis $\left({}^{\boldsymbol{A}}v(4) \in \mathbb{R}\right)$ and about *y*-axis $\left({}^{\boldsymbol{A}}v(5) \in \mathbb{R}\right)$, are required to be zero. Also terms $\frac{d}{dt}\left({}^{\boldsymbol{A}}v_r\right)(3) \in \mathbb{R}$, $\frac{d}{dt}\left({}^{\boldsymbol{A}}v_r\right)(4) \in \mathbb{R}$, and $\frac{d}{dt}\left({}^{\boldsymbol{A}}v_r\right)(5) \in \mathbb{R}$ in derivative of required linear/angular velocity vector $\frac{d}{dt}\left({}^{\boldsymbol{A}}\boldsymbol{V}\right) \in \mathbb{R}^6$ will naturally take form of zero. These can be expressed as

$$ {}^{\boldsymbol{A}}v_r(j) = 0, \qquad \text{for all} \quad j \in \{3,5\} \tag{B.2} $$

$$ \frac{d}{dt}\left({}^{\boldsymbol{A}}v_r\right)(j) = 0, \quad \text{for all} \quad j \in \{3,5\}. \tag{B.3} $$

Similar to motion generation ability of studied system, it is quite obvious that studied 2-DOF system can generate forces only in certain plane. With an appropriate frame attachment (see Figure 17), all linear forces subject to any rigid bodies of system can be

restricted to occur only in *xy*-plane (along *x*-axis and *y*-axis) with respect to attached body frame $\{\mathbf{A}\}$ of rigid bodies. Furthermore, all moments subject to any rigid bodies of system can be occur only about *z*-axis with respect to attached body frame $\{\mathbf{A}\}$ of rigid body. In view of (2.14) and (2.19), all required net force/moment vectors ${}^{\boldsymbol{A}}\boldsymbol{F}_r^* \in \mathbb{R}^6$ of system can be computed through regressor matrix and parameter vector. Duo to fact, that for all $j \in \{3,5\}$ there are not required forces in ${}^{\boldsymbol{A}}f_r(j) \in \mathbb{R}$ elements of ${}^{\boldsymbol{A}}\boldsymbol{F}_r^* \in \mathbb{R}^6$ and these elements are fully described by *j*th row of regressor matrix, respectively, it can be written as

$$y_{\boldsymbol{A}}(j,k) = 0, \quad \text{for all } j \in \{3,5\}, \text{ and } k \in \{1,13\} \tag{B.4}$$

where $y_{\boldsymbol{A}}(j,k) \in \mathbb{R}$ denotes an element of $\boldsymbol{Y}_{\boldsymbol{A}} \in \mathbb{R}^{6\times 13}$ at row *j* and column *k*.

By substituting these zero elements defined in (B.1) - (B.4) into regressor matrix defined in Appendix A, the non-zero elements of $\boldsymbol{Y}_{\boldsymbol{A}} \in \mathbb{R}^{6\times 13}$ can be listed as

$$y_{\boldsymbol{A}}(1,1) = \frac{d}{dt}\left({}^{\boldsymbol{A}}v_r\right)(1) - {}^{\boldsymbol{A}}v(6)\,{}^{\boldsymbol{A}}v_r(2) + {}^{\boldsymbol{A}}g(1) \tag{B.4}$$
$$y_{\boldsymbol{A}}(1,2) = -{}^{\boldsymbol{A}}v(6)\,{}^{\boldsymbol{A}}v_r(6) \tag{B.5}$$
$$y_{\boldsymbol{A}}(1,3) = -\frac{d}{dt}\left({}^{\boldsymbol{A}}v_r\right)(6) \tag{B.6}$$
$$y_{\boldsymbol{A}}(2,1) = \frac{d}{dt}\left({}^{\boldsymbol{A}}v_r\right)(2) - {}^{\boldsymbol{A}}v(6)\,{}^{\boldsymbol{A}}v_r(1) + {}^{\boldsymbol{A}}g(2) \tag{B.7}$$
$$y_{\boldsymbol{A}}(2,2) = \frac{d}{dt}\left({}^{\boldsymbol{A}}v_r\right)(6) \tag{B.8}$$
$$y_{\boldsymbol{A}}(2,3) = -{}^{\boldsymbol{A}}v(6)\,{}^{\boldsymbol{A}}v_r(6) \tag{B.9}$$
$$y_{\boldsymbol{A}}(6,2) = y_{\boldsymbol{A}}(2,1) \tag{B.10}$$
$$y_{\boldsymbol{A}}(6,3) = -y_{\boldsymbol{A}}(1,1) \tag{B.11}$$
$$y_{\boldsymbol{A}}(6,5) = y_{\boldsymbol{A}}(2,2) \tag{B.12}$$
$$y_{\boldsymbol{A}}(6,6) = -y_{\boldsymbol{A}}(1,3) \tag{B.13}$$
$$y_{\boldsymbol{A}}(6,13) = \frac{d}{dt}\left({}^{\boldsymbol{A}}v_r\right)(6) \tag{B.14}$$

which can be put into matrix form as

$$\boldsymbol{Y}_A = \begin{bmatrix} y_{\boldsymbol{A}}(1,1) & y_{\boldsymbol{A}}(1,2) & y_{\boldsymbol{A}}(1,3) & 0 & 0 & 0 & 0\;0\;0\;0\;0\;0 & 0 \\ y_{\boldsymbol{A}}(1,2) & y_{\boldsymbol{A}}(2,2) & y_{\boldsymbol{A}}(2,3) & 0 & 0 & 0 & 0\;0\;0\;0\;0\;0 & 0 \\ 0 & 0 & 0 & 0 & 0 & 0 & 0\;0\;0\;0\;0\;0 & 0 \\ 0 & 0 & 0 & 0 & 0 & 0 & 0\;0\;0\;0\;0\;0 & 0 \\ 0 & 0 & 0 & 0 & 0 & 0 & 0\;0\;0\;0\;0\;0 & 0 \\ 0 & y_{\boldsymbol{A}}(6,2) & y_{\boldsymbol{A}}(6,3) & 0 & y_{\boldsymbol{A}}(6,5) & y_{\boldsymbol{A}}(6,6) & 0\;0\;0\;0\;0\;0 & y_{\boldsymbol{A}}(6,13) \end{bmatrix} \tag{B.15}$$

By taking a slight look of (B.15) and its corresponding parameter vector defined Appendix A, it is easy to notice that parameter vector elements $\theta_{\boldsymbol{A}n}$, for all $n \in \{4,7,8,9,10,11,12\}$, has no effect to required net force/moment vectors ${}^{\boldsymbol{A}}\boldsymbol{F}_r^* \in \mathbb{R}^6$ in studied 2-DOF case and they can be removed from parameter vector for avoiding unnecessary parameter estimation.

Removing of discussed elements will lead to new regressor matrix $\boldsymbol{Y}_{2\boldsymbol{A}} \in \mathbb{R}^{6\times 6}$ taking form of

$$\boldsymbol{Y}_{2\boldsymbol{A}} = \begin{bmatrix} y_{\boldsymbol{A}}(1,1) & y_{\boldsymbol{A}}(1,2) & y_{\boldsymbol{A}}(1,3) & 0 & 0 & 0 \\ y_{\boldsymbol{A}}(1,2) & y_{\boldsymbol{A}}(2,2) & y_{\boldsymbol{A}}(2,3) & 0 & 0 & 0 \\ 0 & 0 & 0 & 0 & 0 & 0 \\ 0 & 0 & 0 & 0 & 0 & 0 \\ 0 & 0 & 0 & 0 & 0 & 0 \\ 0 & y_{\boldsymbol{A}}(6,2) & y_{\boldsymbol{A}}(6,3) & y_{\boldsymbol{A}}(6,5) & y_{\boldsymbol{A}}(6,6) & y_{\boldsymbol{A}}(6,13) \end{bmatrix} \tag{B.16}$$

where elements $y_{\boldsymbol{A}}(j,k)$ are obtained from (B.4) – (B.14). Finally, the new corresponding parameter vector $\boldsymbol{\theta}_{2\boldsymbol{A}} \in \mathbb{R}^6$ can be given as

$$\boldsymbol{\theta}_{2\boldsymbol{A}} = \begin{bmatrix} m_{\boldsymbol{A}} \\ m_{\boldsymbol{A}}\, {}^{\boldsymbol{A}}r_{mx} \\ m_{\boldsymbol{A}}\, {}^{\boldsymbol{A}}r_{my} \\ m_{\boldsymbol{A}}\, {}^{\boldsymbol{A}}r_{mx}^2 \\ m_{\boldsymbol{A}}\, {}^{\boldsymbol{A}}r_{my}^2 \\ I_{\boldsymbol{A}zz} \end{bmatrix} \tag{B.17}$$

APPENDIX C: STRUCTURAL DIMENSIONS OF HIAB 031

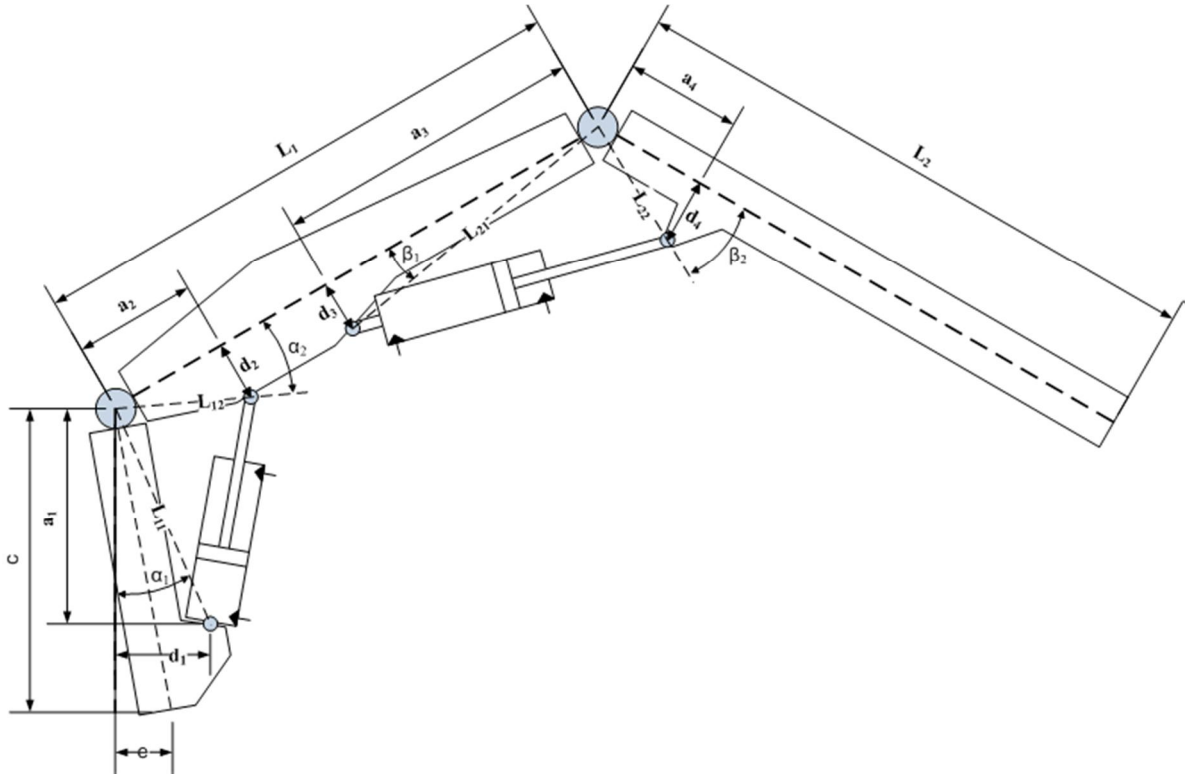

Figure 32: Structural dimension of HIAB 031

Numerical values for structural constant parameters of HIAB 031 are achieved from (Linjama 1996) as

L_1 = 1.6m	a_2 = 0.369m
L_2 = 1.689m	d_2 = 0.069m
d = 0.228m	a_3 = 1.131m
c = 0.957m	d_3 = 0.069m
a_1 = 0.953m	a_4 = 0.288m
d_1 = 0.404m	a_4 = 0.112m

and remaining structural dimensions can be computed from above as

$$L_{11} = \sqrt{{a_1}^2 + {d_1}^2} \qquad L_{12} = \sqrt{{a_2}^2 + {d_2}^2}$$

$$L_{21} = \sqrt{{a_3}^2 + {d_3}^2} \qquad L_{22} = \sqrt{{a_4}^2 + {d_4}^2}$$

$$\alpha_1 = \tan^{-1}\left(\frac{d_1}{a_1}\right) \qquad \alpha_2 = \tan^{-1}\left(\frac{d_2}{a_2}\right)$$

$$\beta_1 = \tan^{-1}\left(\frac{d_3}{a_3}\right) \qquad \beta_2 = \tan^{-1}\left(\frac{d_4}{a_4}\right)$$

APPENDIX D: DERIVATION OF LOAD DISTRIBUTION FACTORS

In this appendix an equations to calculate the load distribution factors α_3 and α_4 of *closed chain 2* are given. The load distribution factors α_1 and α_2 of *closed chain 1* can be obtained by similar manner by substituting respective *closed chain 1* equations in (D.1) – (D.18).

As the name implies, load distribution factors defines how the exerted force is distributed between rigid links. In our case, load distribution between two open chains is wanted to find out. In Figure 33 can be seen second *closed chain* of studied system.

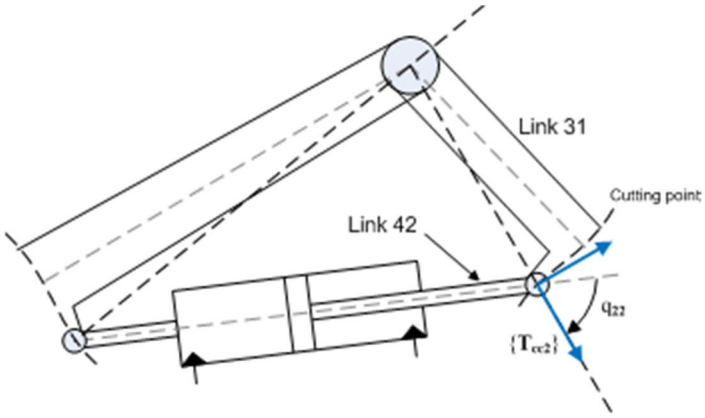

Figure 33: 2nd closed chain of studied system.

The force resultant ${}^{\boldsymbol{T}_{cc2}}\boldsymbol{F} \in \mathbb{R}^6$ exerted on the *cutting point 4* and expressed in frame $\{\boldsymbol{T}_{cc2}\}$ is known and can be computed in view of (5.39). Also *closed chain* angle q_{22} is known and defined in (5.8). Note that initially angle q_{22} will be given as negative.

In Figure 34 is illustrated a known force resultant ${}^{\boldsymbol{T}_{cc2}}\boldsymbol{F} \in \mathbb{R}^6$ in first quarter of frame $\{\boldsymbol{T}_{cc2}\}$. In view of Newton's third law of motion, there exist an equal but opposite reaction force $-{}^{\boldsymbol{T}_{cc2}}\boldsymbol{F} \in \mathbb{R}^6$ generated by *closed chain 2*.

The direction β of reaction force $-{}^{\boldsymbol{T}_{cc2}}\boldsymbol{F} \in \mathbb{R}^6$ can be computed as

$$\beta = \tan^{-1}\left(\frac{-{}^{Tcc2}F_y}{-{}^{Tcc2}F_x}\right) = \tan^{-1}\left(\frac{-{}^{Tcc2}\boldsymbol{F}(2)}{-{}^{Tcc2}\boldsymbol{F}(1)}\right) = \tan^{-1}\left(\frac{{}^{Tcc2}\boldsymbol{F}(2)}{{}^{Tcc2}\boldsymbol{F}(1)}\right) \quad \text{(D.1)}$$

where ${}^{T_{cc2}}\boldsymbol{F}(1)$ denotes the first element ${}^{T_{cc2}}\boldsymbol{F} \in \mathbb{R}^6$ and ${}^{T_{cc2}}\boldsymbol{F}(1)$ denotes the second element ${}^{T_{cc2}}\boldsymbol{F} \in \mathbb{R}^6$.

As from (D.1) and Figure 34 can be seen, the direction of force resultant ${}^{T_{cc2}}\boldsymbol{F} \in \mathbb{R}^6$ and respective reaction force $-{}^{T_{cc2}}\boldsymbol{F} \in \mathbb{R}^6$ occurs as positive in first and third quarters of frame $\{\boldsymbol{T}_{cc2}\}$. This comes due to fact that in these cases sign(${}^{T_{cc2}}\boldsymbol{F}(1)$) = sign(${}^{T_{cc2}}\boldsymbol{F}(2)$), which will lead to positive direction angle β.

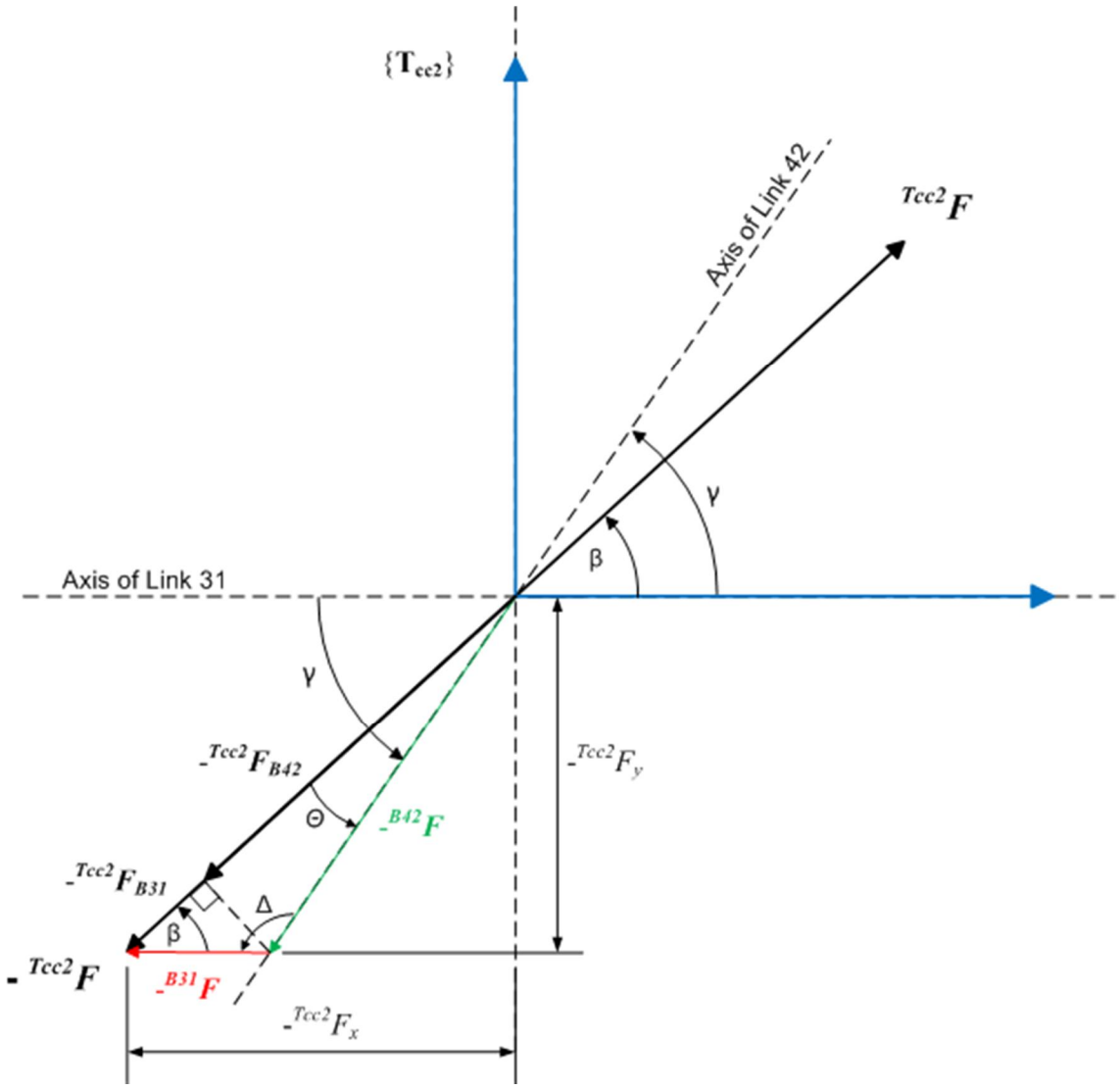

Figure 34: Forces in frame {T_{cc2}} with positive direction angle β.

Let first consider situations with positive direction angles β, as represented in Figure 34. For simplifying calculations, angle q_{22} is wanted to express in same direction as angle β. Thus, angle q_{22} is redefined as

$$\gamma = sign(\beta)|q_{22}| \tag{D.2}$$

The support forces, namely $-^{\boldsymbol{B}_{31}}\boldsymbol{F} \in \mathbb{R}^6$ and $-^{\boldsymbol{B}_{42}}\boldsymbol{F} \in \mathbb{R}^6$, generated by Link31 and Link42, respectively, can be computed with the law of sines as

$$-^{\boldsymbol{B}_{31}}\boldsymbol{F} = -\frac{\sin(\theta)}{\sin(\Delta)}\,^{\boldsymbol{T}_{cc2}}\boldsymbol{F} \tag{D.3}$$

$$-^{\boldsymbol{B}_{42}}\boldsymbol{F} = -\frac{\sin(\beta)}{\sin(\Delta)}\,^{\boldsymbol{T}_{cc2}}\boldsymbol{F}, \tag{D.4}$$

where the angles θ and Δ are defined as

$$\theta = \gamma - \beta \tag{D.5}$$
$$\Delta = \pi - \gamma \tag{D.6}$$

The components of support forces $-^{\boldsymbol{B}_{31}}\boldsymbol{F} \in \mathbb{R}^6$ and $-^{\boldsymbol{B}_{42}}\boldsymbol{F} \in \mathbb{R}^6$ parallel to reaction force $-^{\boldsymbol{T}_{cc2}}\boldsymbol{F} \in \mathbb{R}^6$, denoted as $-^{\boldsymbol{T}_{cc2}}\boldsymbol{F}_{\boldsymbol{B}_{31}} \in \mathbb{R}^6$ and $-^{\boldsymbol{T}_{cc2}}\boldsymbol{F}_{\boldsymbol{B}_{42}} \in \mathbb{R}^6$, respectively, can be computed as

$$-^{\boldsymbol{T}_{cc2}}\boldsymbol{F}_{\boldsymbol{B}_{31}} = -\cos(\beta)\,^{\boldsymbol{B}_{31}}\boldsymbol{F} \tag{D.7}$$
$$-^{\boldsymbol{T}_{cc2}}\boldsymbol{F}_{\boldsymbol{B}_{42}} = -\cos(\theta)\,^{\boldsymbol{B}_{42}}\boldsymbol{F} \tag{D.8}$$

On the other hand, force components $-^{\boldsymbol{T}_{cc2}}\boldsymbol{F}_{\boldsymbol{B}_{31}} \in \mathbb{R}^6$ and $-^{\boldsymbol{T}_{cc2}}\boldsymbol{F}_{\boldsymbol{B}_{42}} \in \mathbb{R}^6$ given in (D.6) and (D.7), respectively, can be obtained by product of load distribution factor and respective support force, as

$$-^{\boldsymbol{T}_{cc2}}\boldsymbol{F}_{\boldsymbol{B}_{31}} = -\alpha_3\,^{\boldsymbol{T}_{cc2}}\boldsymbol{F} \tag{D.9}$$
$$-^{\boldsymbol{T}_{cc2}}\boldsymbol{F}_{\boldsymbol{B}_{42}} = -\alpha_4\,^{\boldsymbol{T}_{cc2}}\boldsymbol{F} \tag{D.10}$$

By substituting (D.7) into (D.9) and (D.8) into (D.10), yields

$$^{\boldsymbol{T}_{cc2}}\boldsymbol{F}_{\boldsymbol{B}_{31}} = \cos(\beta)\frac{\sin(\theta)}{\sin(\Delta)}\,^{\boldsymbol{T}_{cc2}}\boldsymbol{F} \tag{D.11}$$

$$^{\boldsymbol{T}_{cc2}}\boldsymbol{F}_{\boldsymbol{B}_{42}} = \cos(\theta)\frac{\sin(\beta)}{\sin(\Delta)}\,^{\boldsymbol{T}_{cc2}}\boldsymbol{F}. \tag{D.12}$$

Now, the load distribution factors α_3 and α_4 can be solved with positive direction angles $\beta \geq 0$ by substituting (D.9) into (D.11) and (D.10) into (D.12), leading to

$$\alpha_3 = \cos(\beta)\frac{\sin(\theta)}{\sin(\Delta)} \quad , \beta \geq 0 \tag{D.13}$$

$$\alpha_4 = \cos(\theta)\frac{\sin(\beta)}{\sin(\Delta)} \quad , \beta \geq 0 \tag{D.14}$$

If the force resultant ${}^{T_{cc2}}\boldsymbol{F} \in \mathbb{R}^6$ occurs in second or fourth quarter of frame $\{\boldsymbol{T}_{cc2}\}$, the direction angle β defined in (E.1) will occur as negative. This comes due to fact, that in these cases sign(${}^{T_{cc2}}\boldsymbol{F}(1)$) ≠ sign(${}^{T_{cc2}}\boldsymbol{F}(2)$). The situation with negative direction angle is illustrated in Figure 35.

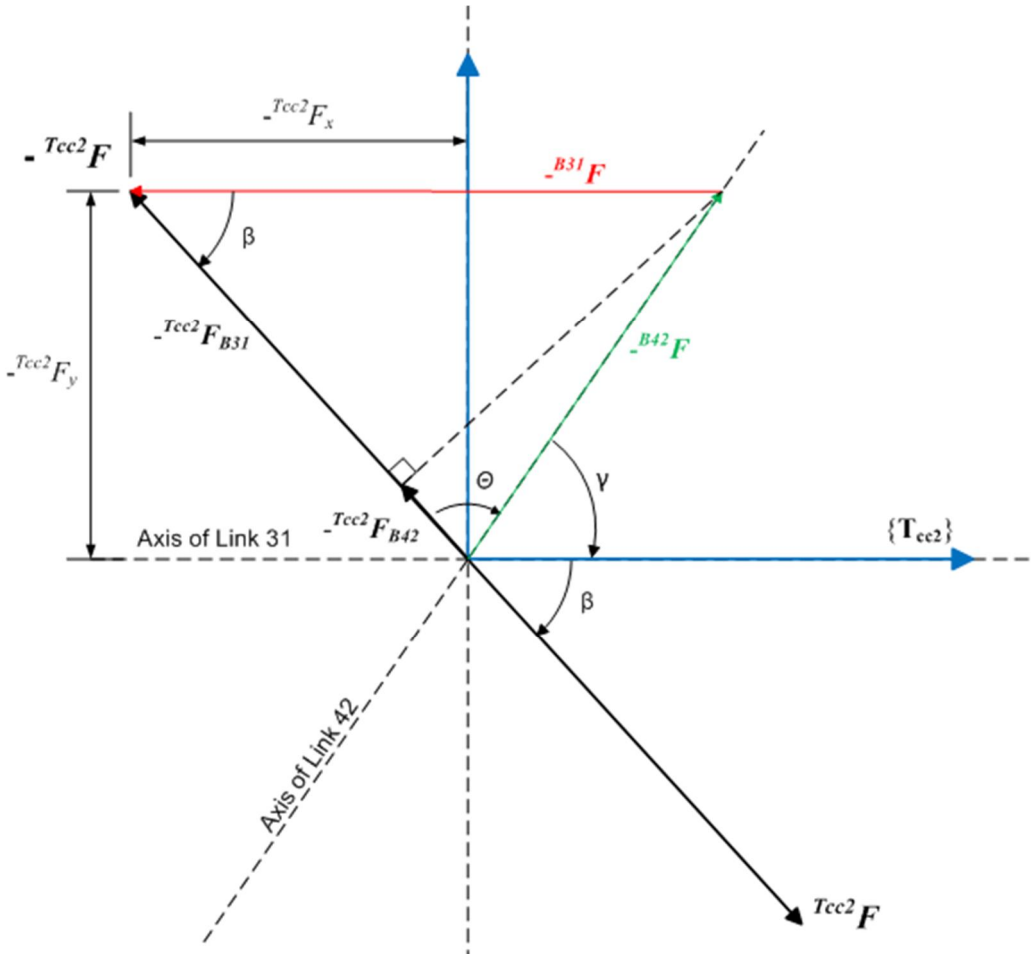

Figure 35: Forces in frame {T_{cc2}} with negative direction angle β.

Similar to (D.3) – (D.14), the load distribution factors α_3 and α_4 for negative direction angles $\beta < 0$, can derived to be in view of Figure 35 as

$$\alpha_3 = \cos(\beta)\frac{\sin(\theta)}{\sin(\gamma)}, \qquad \beta < 0 \tag{D.15}$$

$$\alpha_4 = \cos(\theta)\frac{\sin(\beta)}{\sin(\gamma)}, \qquad \beta < 0 \tag{D.16}$$

where the angle θ can computed as

$$\theta = -\pi - q_{22} - \beta \tag{D.17}$$

Finally, the load distribution factors α_3 and α_4 from an known arbitrary force resultant ${}^{\boldsymbol{T}_{cc2}}\boldsymbol{F} \in \mathbb{R}^6$, can be computed in view of (D.12) - (D.14) as

$$\alpha_3 = \begin{cases} \cos(\beta)\frac{\sin(\theta)}{\sin(\Delta)}, & if\ \beta \geq 0 \\ \cos(\beta)\frac{\sin(\theta)}{\sin(\gamma)}, & if\ \beta < 0 \end{cases} \tag{D.18}$$

$$\alpha_4 = \begin{cases} \cos(\theta)\frac{\sin(\beta)}{\sin(\Delta)}, & if\ \beta \geq 0 \\ \cos(\theta)\frac{\sin(\beta)}{\sin(\gamma)}, & if\ \beta < 0 \end{cases} \tag{D.19}$$

APPENDIX E: DERIVATION OF INTERNAL FORCE VECTOR ${}^{T}\boldsymbol{\eta}$

In this appendix a derivation to calculate internal force vectors ${}^{\boldsymbol{T}}\boldsymbol{\eta} \in \mathbb{R}^6$ are given. Internal force vector ${}^{\boldsymbol{T_{CC2}}}\boldsymbol{\eta} \in \mathbb{R}^6$ of *closed chain 2* is used as an illustrative example. The internal force vector ${}^{\boldsymbol{T_{CC1}}}\boldsymbol{\eta} \in \mathbb{R}^6$ of *closed chain 1* can be obtained by similar manners by substituting respective *closed chain 1* equations in (E.1) – (E.20).

In view of Assumption 1, the torque constraints at the three unactuated joints can be expressed as

$$\boldsymbol{z}_\tau^T {}^{\boldsymbol{T_4}}\boldsymbol{F} = 0 \tag{E.1}$$

$$\boldsymbol{z}_\tau^T {}^{\boldsymbol{B_{31}}}\boldsymbol{F} = 0 \tag{E.2}$$

$$\boldsymbol{z}_\tau^T {}^{\boldsymbol{B_{41}}}\boldsymbol{F} = 0 \tag{E.3}$$

After the load distribution factors α_3 and α_4 being specified, the three meaningful elements in ${}^{\boldsymbol{T_{CC2}}}\boldsymbol{\eta} \in \mathbb{R}^6$ (the two force elements in *x* and *y* and the moment element in *z* are determined by satisfying the constraints (E.1) - (E.3).

The moment element ${}^{\boldsymbol{T_{CC2}}}\eta_z$ of ${}^{\boldsymbol{T_{CC2}}}\boldsymbol{\eta}$ can be determined in view of constraint (E.1)

$$\boldsymbol{z}_\tau^T {}^{\boldsymbol{T_4}}\boldsymbol{F} = 0 \tag{E.4}$$

by using (5.46)

$$\boldsymbol{z}_\tau^T\left(\alpha_4 {}^{\boldsymbol{T_{CC2}}}\boldsymbol{F} - {}^{\boldsymbol{T_{CC2}}}\boldsymbol{\eta}\right) = 0 \tag{E.5}$$

$$\rightarrow \boldsymbol{z}_\tau^T {}^{\boldsymbol{T_{CC2}}}\boldsymbol{\eta} = \alpha_4 \boldsymbol{z}_\tau^T {}^{\boldsymbol{T_{CC2}}}\boldsymbol{F} \tag{E.6}$$

$$\rightarrow {}^{\boldsymbol{T_{CC2}}}\eta_z = \alpha_4 \boldsymbol{z}_\tau^T {}^{\boldsymbol{T_{CC2}}}\boldsymbol{F} \tag{E.7}$$

Now, note the fact that frames $\{\boldsymbol{T}_{CC2}\}$ and $\{\boldsymbol{B}_{31}\}$ are set to be coincide (see Figure 13). Thus, the effect of force element ${}^{\boldsymbol{T_{CC2}}}\eta_x$ to produce torque in frame $\{\boldsymbol{B_{31}}\}$ is cancelled out and the force element ${}^{\boldsymbol{T_{CC2}}}\eta_y$ can determined through (E.2) by using (5.41)(5.45) and (5.47) as

$$\boldsymbol{z}_\tau^T {}^{\boldsymbol{B_{31}}}\boldsymbol{F} = 0 \tag{E.8}$$

$$\rightarrow \boldsymbol{z}_\tau^T \left({}^{\boldsymbol{B_{31}}}\boldsymbol{F}^* + {}^{\boldsymbol{B_{31}}}\boldsymbol{U}_{\boldsymbol{T_3}} {}^{\boldsymbol{T_3}}\boldsymbol{F} \right) = 0 \tag{E.9}$$

$$\rightarrow {}^{\boldsymbol{B_{31}}}\boldsymbol{F}^* + {}^{\boldsymbol{B_{31}}}\boldsymbol{U}_{\boldsymbol{T_3}} \left(\alpha_3 {}^{\boldsymbol{T_{CC2}}}\boldsymbol{F} + {}^{\boldsymbol{T_{CC2}}}\boldsymbol{\eta} \right) = 0 \tag{E.10}$$

$$\rightarrow {}^{\boldsymbol{B_{31}}}\boldsymbol{U}_{\boldsymbol{T_3}} {}^{\boldsymbol{T_{CC2}}}\boldsymbol{\eta} = -{}^{\boldsymbol{B_{31}}}\boldsymbol{F}^* - \alpha_3 {}^{\boldsymbol{B_{31}}}\boldsymbol{U}_{\boldsymbol{T_3}} {}^{\boldsymbol{T_{CC2}}}\boldsymbol{F} \tag{E.11}$$

Consider the fact that force/moment vectors ${}^{\boldsymbol{B_{31}}}\boldsymbol{F}^*$ and ${}^{\boldsymbol{T_{CC2}}}\boldsymbol{F}$, load distribution factor α_3 and transformation matrix ${}^{\boldsymbol{B_{31}}}\boldsymbol{U}_{\boldsymbol{T_3}}$ are known. Now, the equation (E.11) can be written in form of

$$\begin{bmatrix} {}^{\boldsymbol{B_{31}}}\boldsymbol{R}_{\boldsymbol{T_3}} & \boldsymbol{0}_{3\times 3} \\ \left({}^{\boldsymbol{B_{31}}}\boldsymbol{r}_{\boldsymbol{B_{31}T_3}} \times \right) {}^{\boldsymbol{B_{31}}}\boldsymbol{R}_{\boldsymbol{T_3}} & {}^{\boldsymbol{B_{31}}}\boldsymbol{R}_{\boldsymbol{T_3}} \end{bmatrix} \begin{bmatrix} {}^{\boldsymbol{T_{CC2}}}\eta_x \\ {}^{\boldsymbol{T_{CC2}}}\eta_y \\ 0 \\ 0 \\ 0 \\ {}^{\boldsymbol{T_{CC2}}}\eta_z \end{bmatrix} = \begin{bmatrix} F_x \\ F_y \\ 0 \\ 0 \\ 0 \\ M_z \end{bmatrix} \tag{E.12}$$

$$\rightarrow \begin{bmatrix} u_{11} & u_{12} & 0 & 0 & 0 & 0 \\ u_{21} & u_{22} & 0 & 0 & 0 & 0 \\ 0 & 0 & 1 & 0 & 0 & 0 \\ 0 & 0 & 0 & u_{44} & u_{45} & 0 \\ 0 & 0 & u_{53} & u_{54} & u_{55} & 0 \\ 0 & u_{62} & 0 & 0 & 0 & 1 \end{bmatrix} \begin{bmatrix} {}^{\boldsymbol{T_{CC2}}}\eta_x \\ {}^{\boldsymbol{T_{CC2}}}\eta_y \\ 0 \\ 0 \\ 0 \\ {}^{\boldsymbol{T_{CC2}}}\eta_z \end{bmatrix} = \begin{bmatrix} F_x \\ F_y \\ 0 \\ 0 \\ 0 \\ M_z \end{bmatrix} \tag{E.13}$$

Note, that in (E.13) elements u_{61} and u_{63} will have form of zero, indefinitely, due to appropriate frame attachment (lengths from $\{\boldsymbol{B}_{31}\}$ to $\{\boldsymbol{T}_3\}$ along *y*- and *z*-axis are zero). Thus, the force element ${}^{\boldsymbol{T_{CC2}}}\eta_y$ can be solved from (E.13) by using the last row of ${}^{\boldsymbol{B_{31}}}\boldsymbol{U}_{\boldsymbol{T_3}} \in \mathbb{R}^{6\times 6}$ as

$$u_{62} {}^{\boldsymbol{T_{CC2}}}\eta_y + {}^{\boldsymbol{T_{CC2}}}\eta_z = M_z \tag{E.14}$$

$$\rightarrow {}^{\boldsymbol{T_{CC2}}}\eta_y = \frac{M_z - {}^{\boldsymbol{T_{CC2}}}\eta_z}{u_{62}} \tag{E.15}$$

Consider the fact that force elements ${}^{\boldsymbol{T_{CC2}}}\eta_z$ and ${}^{\boldsymbol{T_{CC2}}}\eta_y$ are now known. The force element ${}^{\boldsymbol{T_{CC2}}}\eta_x$ can be solved through (E.3) by using (5.46), (5.49) and (5.50) as

$$\boldsymbol{z}_\tau^T {}^{\boldsymbol{B_{41}}}\boldsymbol{F} = 0 \tag{E.16}$$

$$\rightarrow \boldsymbol{z}_\tau^T \left({}^{\boldsymbol{B_{41}}}\boldsymbol{F}^* + {}^{\boldsymbol{B_{41}}}\boldsymbol{U}_{\boldsymbol{B_{42}}} {}^{\boldsymbol{B_{42}}}\boldsymbol{F} \right) = 0 \tag{E.17}$$

$$\rightarrow {}^{\boldsymbol{B_{41}}}\boldsymbol{F}^* + {}^{\boldsymbol{B_{41}}}\boldsymbol{U}_{\boldsymbol{B_{42}}} \left({}^{\boldsymbol{B_{42}}}\boldsymbol{F}^* + {}^{\boldsymbol{B_{42}}}\boldsymbol{U}_{\boldsymbol{T_4}} {}^{\boldsymbol{T_4}}\boldsymbol{F} \right) = 0 \tag{E.18}$$

$$\rightarrow {}^{\boldsymbol{B_{41}}}\boldsymbol{F}^* + {}^{\boldsymbol{B_{41}}}\boldsymbol{U}_{\boldsymbol{B_{42}}} {}^{\boldsymbol{B_{42}}}\boldsymbol{F}^* + {}^{\boldsymbol{B_{41}}}\boldsymbol{U}_{\boldsymbol{B_{42}}} {}^{\boldsymbol{B_{42}}}\boldsymbol{U}_{\boldsymbol{T_4}} \left(\alpha_4 {}^{\boldsymbol{T_{CC2}}}\boldsymbol{F} - {}^{\boldsymbol{T_{CC2}}}\boldsymbol{\eta} \right) = 0 \tag{E.16}$$

$$\rightarrow {}^{B_{41}}\boldsymbol{U}_{B_{42}}\,{}^{B_{42}}\boldsymbol{U}_{T_4}\,{}^{T_{CC2}}\boldsymbol{\eta} = {}^{B_{41}}\boldsymbol{F}^{*} + {}^{B_{41}}\boldsymbol{U}_{B_{42}}\,{}^{B_{42}}\boldsymbol{F}^{*} + \alpha_4\,{}^{B_{41}}\boldsymbol{U}_{B_{42}}\,{}^{B_{42}}\boldsymbol{U}_{T_4}\,{}^{T_{CC2}}\boldsymbol{F} \quad \text{(E.17)}$$

Again, the force/moment vectors ${}^{B_{41}}\boldsymbol{F}^{*}$, ${}^{B_{42}}\boldsymbol{F}^{*}$, ${}^{T_{CC2}}\boldsymbol{F}$, load distribution factor α_4, and transformation matrices ${}^{B_{41}}\boldsymbol{U}_{B_{42}}$ and ${}^{B_{42}}\boldsymbol{U}_{T_4}$ are known. Now, the equation (E.17) can written in form of

$$\begin{bmatrix} u_{11} & u_{12} & 0 & 0 & 0 & 0 \\ u_{21} & u_{22} & 0 & 0 & 0 & 0 \\ 0 & 0 & 1 & 0 & 0 & 0 \\ 0 & 0 & u_{43} & u_{44} & u_{45} & 0 \\ 0 & 0 & u_{53} & u_{54} & u_{55} & 0 \\ u_{61} & u_{62} & 0 & 0 & 0 & 1 \end{bmatrix} \begin{bmatrix} {}^{T_{CC2}}\eta_x \\ {}^{T_{CC2}}\eta_y \\ 0 \\ 0 \\ 0 \\ {}^{T_{CC2}}\eta_z \end{bmatrix} = \begin{bmatrix} F_x \\ F_y \\ 0 \\ 0 \\ 0 \\ M_z \end{bmatrix} \quad \text{(E.18)}$$

Finally, the force element ${}^{T_{CC2}}\eta_x$ can be solved from (E.18) by using the last row of ${}^{B_{41}}\boldsymbol{U}_{B_{42}}\,{}^{B_{42}}\boldsymbol{U}_{T_4} \in \mathbb{R}^{6\times 6}$ as

$$u_{61}\,{}^{T_{CC2}}\eta_x + u_{62}\,{}^{T_{CC2}}\eta_y + {}^{T_{CC2}}\eta_z = M_z \quad \text{(E.19)}$$

$$\rightarrow {}^{T_{CC2}}\eta_x = \frac{M_z - {}^{T_{CC2}}\eta_z - u_{62}\,{}^{T_{CC2}}\eta_y}{u_{61}} \quad \text{(E.20)}$$

APPENDIX F: APPLIED FRICTION MODEL FOR CYLINDERS

According to (Zhu 2005) a suitable friction model is necessary for achieving a good output force control of cylinder. This comes due to fact that the piston friction makes a large difference between the output force and the chamber pressure force.

A friction model proposed in (Zhu 2010, p.181) and represented in (Zhu 2005) is used to model cylinder piston frictions in both cylinders of HIAB 031.

A Coulomb-viscous friction model with dc offset

$$f_{\mu c} = k_{cp} g(z, z_{ss}) \mathcal{S}(z) - k_{cn} g(-z, z_{ss}) \mathcal{S}(-z) + k_0 + \left[k_{vp} \mathcal{S}(\dot{x}) + k_{vn} \mathcal{S}(-\dot{x})\right] \phi(\dot{x}) \dot{x} \quad \text{(F.1)}$$

is used as part of the friction model devoted to sliding motion, where $\mathcal{S}$ is a selective function defined as

$$\mathcal{S}(x) \triangleq \begin{cases} 1, & if\ x > 0 \\ 0, & if\ x \leq 0 \end{cases} \quad \text{(F.2)}$$

$g(z, z_{ss})$ is a differentiable function defined as

$$g(z, z_{ss}) \triangleq \begin{cases} 1, & if\ z \geq z_{ss} \\ \frac{z}{z_{ss}}, & if\ 0 < z < z_{ss} \\ 0, & if\ z \leq 0 \end{cases} \quad \text{(F.3)}$$

with $z_{ss} > 0$ being a constant, z denotes the average deformation of bristles in friction model described in (Canudas 1995), where the derivative of z is governed by

$$\dot{z} = \dot{x} - \frac{|\dot{x}|}{z_{ss}} z \quad \text{(F.4)}$$

where $\dot{x}$ denotes the piston velocity. In (F.1), the first two terms on the right-hand side are devoted to the Coulomb friction, the constant k_0 denotes a dc offset, and the last term in the right-hand side is devoted to the Stribeck and viscous friction with which $\phi(\dot{x})$ is a bounded and differentiable function characterizing the profile of the Stribeck and viscous friction.

Similar to (Zhu 2005), the $\phi(\dot{x})$ is chosen as

$$\phi(\dot{x}) = -1 \tag{F.5}$$

to accommodate the Stribeck effect only, since the operational velocity cylinder is very low. Parameters k_{cp} and k_{vp} correspond to the positive piston velocity $\dot{x}$, and k_{cn} and k_{vn} correspond the negative piston velocity $\dot{x}$.

Based on the experimental observations, it is found that the friction force in presliding motion is a function of the output force. The mathematical formulation can be expressed as

$$f_{\mu s} = [k_{fp}\mathcal{S}(F_{out}) + k_{fn}\mathcal{S}(-F_{out})]\varphi(F_{out}) \tag{F.6}$$

where F_{out} denotes the output force, and k_{fp} and k_{fn} are two positive constraints associated with positive and negative output forces, respectively, and $\varphi(F_{out})$ is a monotonic function defined as

$$\varphi(F_{out}) = \frac{F_{out}}{1+\delta|F_{out}|} \tag{F.7}$$

with $\delta > 0$ being a constant.

Finally, the total piston friction force is represented as

$$f_f = [1 - \mathcal{L}(t)]f_{\mu c} + \mathcal{L}(t)f_{\mu s} \tag{F.8}$$

where $\mathcal{L}(t) \in [0,1]$ is a differentiable switching function that ensures a smooth transition between sliding motion and presliding motion with $\mathcal{L}(t) \to 1$ for presliding motion and $\mathcal{L}(t) \to 0$ for sliding motion. In view of (Zhu 2005), the applied switching function of friction model is selected to be

$$\mathcal{L}(t) = \frac{1}{1+(\delta_1 \ddot{\tilde{x}}(t))^3} \tag{F.9}$$

with

$$\ddot{\tilde{x}}(t) = 10\big(|\dot{x}(t)| - \dot{\tilde{x}}(t)\big) \tag{F.10}$$

where $\delta_1 > 0$ is a constant and $\dot{\tilde{x}}(t) \geq 0$ if $\dot{\tilde{x}}(0) = 0$.

In view of (Zhu 2010, p.181), the selected friction model defined in (F.8) is wanted to represent in linear parameterizised form as

$$f_f = \boldsymbol{Y}_f \boldsymbol{\theta}_f. \tag{F.11}$$

The regressor matrix $\boldsymbol{Y}_f$ in (F.11) can be written as

$$\boldsymbol{Y}_f = \begin{bmatrix} \big(1-\mathcal{L}(t)\big)g(z,z_{ss})\mathcal{S}(z) \\ -\big(1-\mathcal{L}(t)\big)g(-z,z_{ss})\mathcal{S}(-z) \\ \big(1-\mathcal{L}(t)\big) \\ \big(1-\mathcal{L}(t)\big)\mathcal{S}(\dot{x})\phi(\dot{x})\dot{x} \\ \big(1-\mathcal{L}(t)\big)\mathcal{S}(-\dot{x})\phi(\dot{x})\dot{x} \\ \mathcal{S}(F_d)\mathcal{L}(t)\varphi(F_d) \\ \mathcal{S}(-F_d)\mathcal{L}(t)\varphi(F_d) \end{bmatrix}^T \in \mathbb{R}^{1\times 7}, \tag{F.12}$$

where F_d denotes the desired output force, and the parameter vector $\boldsymbol{\theta}_f$ is defined as

$$\boldsymbol{\theta}_f = \begin{bmatrix} k_{cp} & k_{cn} & k_0 & k_{vp} & k_{vn} & k_{fp} & k_{fn} \end{bmatrix}^T \in \mathbb{R}^7 \tag{F.13}$$

(Zhu 2005).

The following parameters were used in an applied friction model $k_{cp} = k_{cn} = 500\ N$, $k_0 = 0$, $k_{vp} = k_{vn} = -2000\ N/(m/s)$ and $k_{fp} = k_{fn} = 800\ N$. Given friction parameters are extracted from (Linjama 1996), where same system (HIAB 031) in different context was studied. Friction profiles with given parameters are illustrated in Figure 36.

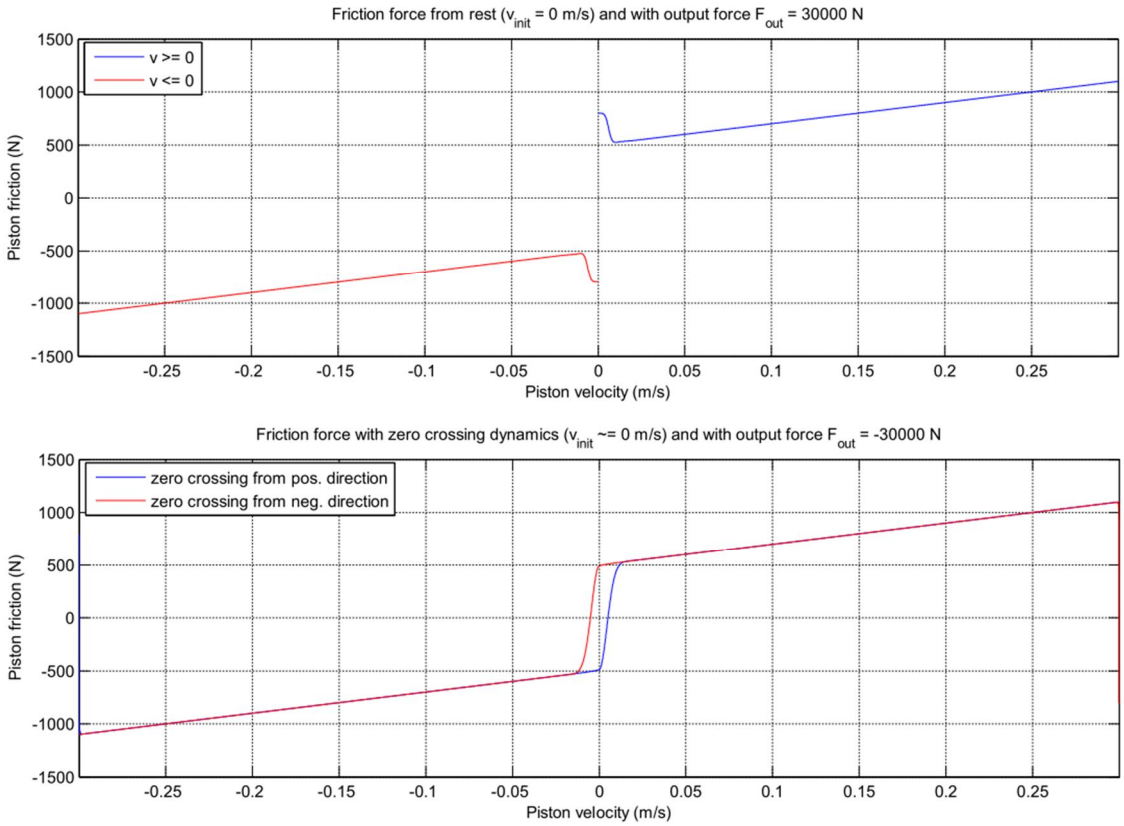

Figure 36: Friction force profiles with applied parameters and with output force F_{out} = 30000 N.

APPENDIX G: VIRTUAL STABILITY OF STUDIED HYDRAULIC MANIPULATOR

In this appendix the *virtual stability* with respect to *zero-mass object*, *object 1*, *object 2*, *open chain 1 and* open *chain 3* will be presented. All Equations, Theorems, Lemmas and Proofs of this chapter are applied in view of (Zhu 2010. pp.177-181).

In view of (3.15) the non-negative accompanying function of *object 2* can be selected as

$$v_{O_2} = \frac{1}{2}\left({}^{O_2}\mathbf{V_r} - {}^{O_2}\mathbf{V}\right)^{\mathrm{T}}\mathbf{M}_{O_2}\left({}^{O_2}\mathbf{V_r} - {}^{O_2}\mathbf{V}\right) \tag{G.1}$$

and in view of (3.16) the derivative of (G.1) is

$$\begin{aligned}\dot{v}_{O_2} \leq & -\left({}^{O_2}\mathbf{V_r} - {}^{O_2}\mathbf{V}\right)^{\mathrm{T}}\mathbf{K}_{O_2}\left({}^{O_2}\mathbf{V_r} - {}^{O_2}\mathbf{V}\right) \\ & +\left({}^{O_2}\mathbf{V_r} - {}^{O_2}\mathbf{V}\right)^{\mathrm{T}}\left({}^{O_2}\mathbf{F}_{\mathrm{r}}^{*} - {}^{O_2}\mathbf{F}^{*}\right)\end{aligned} \tag{G.2}$$

Theorem 5.1. *The object 2 described by (5.35) - (5.37), combined with its respective control equations (5.95) and (5.97), is virtually stable with its affiliated vector* ${}^{O_2}\boldsymbol{V_r} - {}^{O_2}\boldsymbol{V}$ *being a virtual function in both* L_2 *and* L_∞*, in the sense of Definition 2.*10.

Proof: It follows from (5.35), (5.55), (5.95), (5.106), and (2.21) that

$$\begin{aligned}&\left({}^{O_2}\boldsymbol{V_r} - {}^{O_2}\boldsymbol{V}\right)^{T}\left({}^{O_2}\boldsymbol{F}_r^{*} - {}^{O_2}\boldsymbol{F}^{*}\right) \\ &\quad = \left({}^{O_2}\boldsymbol{V_r} - {}^{O_2}\boldsymbol{V}\right)^{T}{}^{O_2}\boldsymbol{U}_{T_3}\left({}^{T_3}\boldsymbol{F}_r - {}^{T_3}\boldsymbol{F}\right) \\ &\qquad +\left({}^{O_2}\boldsymbol{V_r} - {}^{O_2}\boldsymbol{V}\right)^{T}{}^{O_2}\boldsymbol{U}_{T_4}\left({}^{T_4}\boldsymbol{F}_r - {}^{T_4}\boldsymbol{F}\right) \\ &\qquad -\left({}^{O_2}\boldsymbol{V_r} - {}^{O_2}\boldsymbol{V}\right)^{T}{}^{O_2}\boldsymbol{U}_{G}\left({}^{G}\boldsymbol{F}_r - {}^{G}\boldsymbol{F}\right) \\ &\quad = p_{T_3} + p_{T_4} - p_{G}\end{aligned} \tag{G.3}$$

Consider the fact that *object 2* has all *driven cutting points* associated with frames $\{\boldsymbol{T}_3\}$ and $\{\boldsymbol{T}_4\}$. Substituting (G.3) into (G.2) and using (G.1) and Definition 2.10. completes the proof.

■

Theorem 5.2. *The open chain 3 described by (5.28), (5.29), (5.40), (5.41), (5.48), (5.47), and (E.2), combined with its respective control equations (5.88), (5.89), (5.102), (5.103), (5.111), (5.110), and* (E.2)*, is a virtually stable with its affiliated vectors* $^{B_3}\boldsymbol{V_r} - {}^{B_3}\boldsymbol{V}$ *and* $^{B_{31}}\boldsymbol{V_r} - {}^{B_{31}}\boldsymbol{V}$ *being virtual function in both* L_2 *and* L_∞*, in the sense of Definition 2.*10.

Proof: Select the non-negative accompanying function of the *open chain 3* as

$$v_3 = v_{B_3} + v_{B_{31}} \tag{G.4}$$

where

$$v_{B_3} = \frac{1}{2}\left({}^{B_3}\mathbf{V_r} - {}^{B_3}\mathbf{V}\right)^{\mathrm{T}}\mathbf{M}_{B_3}\left({}^{B_3}\mathbf{V_r} - {}^{B_3}\mathbf{V}\right) \tag{G.5}$$

$$v_{B_{31}} = \frac{1}{2}\left({}^{B_{31}}\mathbf{V_r} - {}^{B_{31}}\mathbf{V}\right)^{\mathrm{T}}\mathbf{M}_{B_{31}}\left({}^{B_{31}}\mathbf{V_r} - {}^{B_{31}}\mathbf{V}\right) \tag{G.6}$$

are the two non-negative accompanying functions assigned to the two rigid links affiliated with the *open chain 3*.

With appropriate frame substitution, it follows from (5.40), (5.41), (5.102), (5.103), and Lemma 3.1. that

$$\begin{aligned}\dot{v}_{B_3} \le & -\left({}^{B_3}\boldsymbol{V_r} - {}^{B_3}\boldsymbol{V}\right)^T\boldsymbol{K}_{B_3}\left({}^{B_3}\boldsymbol{V_r} - {}^{B_3}\boldsymbol{V}\right)\\ & +\left({}^{B_3}\boldsymbol{V_r} - {}^{B_3}\boldsymbol{V}\right)^T\left({}^{B_3}\boldsymbol{F}_r^* - {}^{B_3}\boldsymbol{F}^*\right)\end{aligned} \tag{G.7}$$

$$\begin{aligned}\dot{v}_{B_{31}} \le & -\left({}^{B_{31}}\boldsymbol{V_r} - {}^{B_{31}}\boldsymbol{V}\right)^T\boldsymbol{K}_{B_{31}}\left({}^{B_{31}}\boldsymbol{V_r} - {}^{B_{31}}\boldsymbol{V}\right)\\ & +\left({}^{B_{31}}\boldsymbol{V_r} - {}^{B_{31}}\boldsymbol{V}\right)^T\left({}^{B_{31}}\boldsymbol{F}_r^* - {}^{B_{31}}\boldsymbol{F}^*\right)\end{aligned} \tag{G.8}$$

In view of (2.21), (5.28), (5.29), (5.48), (5.47), (E.2), (5.88), (5.89), (5.111), (5.110), and (5.127), it results in

$$\left({}^{B_3}\boldsymbol{V_r} - {}^{B_3}\boldsymbol{V}\right)^T\left({}^{B_3}\boldsymbol{F}_r^* - {}^{B_3}\boldsymbol{F}^*\right) = p_{B_3} - p_{B_{31}} \tag{G.9}$$

$$\left({}^{B_{31}}\boldsymbol{V_r} - {}^{B_{31}}\boldsymbol{V}\right)^T\left({}^{B_{31}}\boldsymbol{F}_r^* - {}^{B_{31}}\boldsymbol{F}^*\right) = p_{B_{31}} - p_{T_3} \tag{G.10}$$

Substituting (G.9) and (G.10) into (G.7) and (G.8) yields

$$\begin{aligned}\dot{v}_3 = & \dot{v}_{B_3} + \dot{v}_{B_{31}}\\ \le & -\left({}^{B_3}\boldsymbol{V_r} - {}^{B_3}\boldsymbol{V}\right)^T\boldsymbol{K}_{B_3}\left({}^{B_3}\boldsymbol{V_r} - {}^{B_3}\boldsymbol{V}\right)\\ & -\left({}^{B_{31}}\boldsymbol{V_r} - {}^{B_{31}}\boldsymbol{V}\right)^T\boldsymbol{K}_{B_{31}}\left({}^{B_{31}}\boldsymbol{V_r} - {}^{B_{31}}\boldsymbol{V}\right)\\ & + p_{B_3} - p_{T_3}.\end{aligned} \tag{G.11}$$

Consider the fact that *open chain 3* has one *driving cutting point* associated with frame $\{\boldsymbol{T}_3\}$ and one *driven cutting point* associated with frame $\{\boldsymbol{B}_3\}$. Using (G.4) - (G.6), (G.11) and Definition 2.10. completes the proof.

■

Lemma 5.1. *The open chain 4 described by (5.30)-(5.32), (5.41), (5.42), (5.49), (5.50), (5.53), and (E.1), (E.3) and combined with its respective control equations (5.90)-*(5.92)*, (5.104), (5.105), (5.112), (5.113), (5.124),* (5.126)*, and* (5.128)*, is a virtually stable with its affiliated vectors.*

Let

$$v_4 = v_{\boldsymbol{B}_{41}} + v_{\boldsymbol{B}_{42}} \tag{G.12}$$

be the non-negative accompanying functions assigned to the open chain 4, where

$$v_{\boldsymbol{B}_{41}} = \frac{1}{2}\left({}^{\boldsymbol{B}_{41}}\mathbf{V}_{\mathbf{r}} - {}^{\boldsymbol{B}_{41}}\mathbf{V}\right)^{\mathrm{T}}\mathbf{M}_{\boldsymbol{B}_{41}}\left({}^{\boldsymbol{B}_{41}}\mathbf{V}_{\mathbf{r}} - {}^{\boldsymbol{B}_{41}}\mathbf{V}\right) \tag{G.13}$$

$$v_{\boldsymbol{B}_{42}} = \frac{1}{2}\left({}^{\boldsymbol{B}_{42}}\mathbf{V}_{\mathbf{r}} - {}^{\boldsymbol{B}_{42}}\mathbf{V}\right)^{\mathrm{T}}\mathbf{M}_{\boldsymbol{B}_{42}}\left({}^{\boldsymbol{B}_{42}}\mathbf{V}_{\mathbf{r}} - {}^{\boldsymbol{B}_{42}}\mathbf{V}\right) \tag{G.14}$$

are the two non-negative accompanying functions assigned to the two rigid bodies (cylinder 2 piston rod and cylinder 2 base) affiliated with the open chain 4. Then, the time derivative of (G.12) *can be expressed as*

$$\begin{aligned}\dot{v}_4 &= \dot{v}_{\boldsymbol{B}_{41}} + \dot{v}_{\boldsymbol{B}_{42}} \\ &\leq -\left({}^{\boldsymbol{B}_{41}}\boldsymbol{V}_{\boldsymbol{r}} - {}^{\boldsymbol{B}_{41}}\boldsymbol{V}\right)^{T}\boldsymbol{K}_{\boldsymbol{B}_{41}}\left({}^{\boldsymbol{B}_{41}}\boldsymbol{V}_{\boldsymbol{r}} - {}^{\boldsymbol{B}_{41}}\boldsymbol{V}\right) \\ &\quad -\left({}^{\boldsymbol{B}_{42}}\boldsymbol{V}_{\boldsymbol{r}} - {}^{\boldsymbol{B}_{42}}\boldsymbol{V}\right)^{T}\boldsymbol{K}_{\boldsymbol{B}_{42}}\left({}^{\boldsymbol{B}_{42}}\boldsymbol{V}_{\boldsymbol{r}} - {}^{\boldsymbol{B}_{42}}\boldsymbol{V}\right) \\ &\quad +p_{\boldsymbol{B}_4} - p_{\boldsymbol{T}_4} + (\dot{x}_{4r} - \dot{x}_{4r})(f_{c2r} - f_{c2})\end{aligned} \tag{G.15}$$

where $p_{\boldsymbol{B}_2}$ and $p_{\boldsymbol{T}_2}$ denote the two virtual flows by Definition 2.9. at the two cutting points of the open chain 4.

Proof: Similar to (G.7) and (G.8), it follows from (5.41), (5.42), (5.104), (5.105), and Lemma 3.1. that

$$\begin{aligned}\dot{v}_{\boldsymbol{B}_{41}} &\leq -\left({}^{\boldsymbol{B}_{41}}\boldsymbol{V}_{\boldsymbol{r}} - {}^{\boldsymbol{B}_{41}}\boldsymbol{V}\right)^{T}\boldsymbol{K}_{\boldsymbol{B}_{41}}\left({}^{\boldsymbol{B}_{41}}\boldsymbol{V}_{\boldsymbol{r}} - {}^{\boldsymbol{B}_{41}}\boldsymbol{V}\right) \\ &\quad +\left({}^{\boldsymbol{B}_{41}}\boldsymbol{V}_{\boldsymbol{r}} - {}^{\boldsymbol{B}_{41}}\boldsymbol{V}\right)^{T}\left({}^{\boldsymbol{B}_{41}}\boldsymbol{F}_{r}^{*} - {}^{\boldsymbol{B}_{41}}\boldsymbol{F}^{*}\right)\end{aligned} \tag{G.16}$$

$$\begin{aligned}\dot{v}_{\boldsymbol{B}_{42}} &\leq -\left({}^{\boldsymbol{B}_{42}}\boldsymbol{V}_{\boldsymbol{r}} - {}^{\boldsymbol{B}_{42}}\boldsymbol{V}\right)^{T}\boldsymbol{K}_{\boldsymbol{B}_{42}}\left({}^{\boldsymbol{B}_{42}}\boldsymbol{V}_{\boldsymbol{r}} - {}^{\boldsymbol{B}_{42}}\boldsymbol{V}\right) \\ &\quad +\left({}^{\boldsymbol{B}_{42}}\boldsymbol{V}_{\boldsymbol{r}} - {}^{\boldsymbol{B}_{42}}\boldsymbol{V}\right)^{T}\left({}^{\boldsymbol{B}_{42}}\boldsymbol{F}_{r}^{*} - {}^{\boldsymbol{B}_{42}}\boldsymbol{F}^{*}\right)\end{aligned} \tag{G.17}$$

hold.

In view of (2.21), (5.30) - (5.32), (5.49), (5.50), (5.53), (E.1), (5.90) - (5.92), (5.112), (5.113), (5.124), (5.126),and (5.128), it result in

$$\begin{aligned}\left({}^{\boldsymbol{B}_{41}}\boldsymbol{V}_{\boldsymbol{r}}-{}^{\boldsymbol{B}_{41}}\boldsymbol{V}\right)^{T}\left({}^{\boldsymbol{B}_{41}}\boldsymbol{F}_{r}^{*}-{}^{\boldsymbol{B}_{41}}\boldsymbol{F}^{*}\right)&\\ =p_{\boldsymbol{B}_{4}}-p_{\boldsymbol{B}_{42}}+(\dot{x}_{4r}-\dot{x}_{4r})(f_{c2r}-f_{c2})&\qquad\text{(G.18)}\\ \left({}^{\boldsymbol{B}_{42}}\boldsymbol{V}_{\boldsymbol{r}}-{}^{\boldsymbol{B}_{42}}\boldsymbol{V}\right)^{T}\left({}^{\boldsymbol{B}_{42}}\boldsymbol{F}_{r}^{*}-{}^{\boldsymbol{B}_{42}}\boldsymbol{F}^{*}\right)&\\ =p_{\boldsymbol{B}_{42}}-p_{\boldsymbol{T}_{4}}&\qquad\text{(G.19)}\end{aligned}$$

Finally, Substituting (G.18) and (G.19) into (G.16) and (G.17) yields (G.15).

■

In view of (3.15) the non-negative accompanying function of *object 1* can be selected as

$$v_{\boldsymbol{O}_1}=\tfrac{1}{2}\left({}^{\boldsymbol{O}_1}\mathbf{V}_{\mathbf{r}}-{}^{\boldsymbol{O}_1}\mathbf{V}\right)^{\mathrm{T}}\mathbf{M}_{\boldsymbol{O}_1}\left({}^{\boldsymbol{O}_1}\mathbf{V}_{\mathbf{r}}-{}^{\boldsymbol{O}_1}\mathbf{V}\right)\qquad\text{(G.20)}$$

and in view of (3.16) the derivative of (G.20) is

$$\begin{aligned}\dot{\mathrm{v}}_{\boldsymbol{O}_1}\leq&-\left({}^{\boldsymbol{O}_1}\mathbf{V}_{\mathbf{r}}-{}^{\boldsymbol{O}_1}\mathbf{V}\right)^{\mathrm{T}}\mathbf{K}_{\boldsymbol{O}_1}\left({}^{\boldsymbol{O}_1}\mathbf{V}_{\mathbf{r}}-{}^{\boldsymbol{O}_1}\mathbf{V}\right)\\&+\left({}^{\boldsymbol{O}_1}\mathbf{V}_{\mathbf{r}}-{}^{\boldsymbol{O}_1}\mathbf{V}\right)^{\mathrm{T}}\left({}^{\boldsymbol{O}_1}\mathbf{F}_{\mathrm{r}}^{*}-{}^{\boldsymbol{O}_1}\mathbf{F}^{*}\right)\qquad\text{(G.21)}\end{aligned}$$

Theorem 5.3. *The object 1 described by* (5.26), (5.54) *and* (5.55), *combined with its respective control equations* (5.86) *and* (5.96), *is virtually stable with its affiliated vector* ${}^{\boldsymbol{O}_1}\boldsymbol{V}_{\boldsymbol{r}}-{}^{\boldsymbol{O}_1}\boldsymbol{V}$ *being a virtual function in both* L_2 *and* L_∞, *in the sense of Definition 2*.10.

Proof: It follows from (5.26), (5.37), (5.86), (5.115), and (2.21) that

$$\begin{aligned}\left({}^{\boldsymbol{O}_1}\boldsymbol{V}_{\boldsymbol{r}}-{}^{\boldsymbol{O}_1}\boldsymbol{V}\right)^{T}\left({}^{\boldsymbol{O}_1}\boldsymbol{F}_{r}^{*}-{}^{\boldsymbol{O}_1}\boldsymbol{F}^{*}\right)&\\ =\left({}^{\boldsymbol{O}_1}\boldsymbol{V}_{\boldsymbol{r}}-{}^{\boldsymbol{O}_1}\boldsymbol{V}\right)^{T}{}^{\boldsymbol{O}_1}\boldsymbol{U}_{\boldsymbol{T}_1}\left({}^{\boldsymbol{T}_1}\boldsymbol{F}_{r}-{}^{\boldsymbol{T}_1}\boldsymbol{F}\right)&\\ +\left({}^{\boldsymbol{O}_1}\boldsymbol{V}_{\boldsymbol{r}}-{}^{\boldsymbol{O}_1}\boldsymbol{V}\right)^{T}{}^{\boldsymbol{O}_1}\boldsymbol{U}_{\boldsymbol{T}_2}\left({}^{\boldsymbol{T}_3}\boldsymbol{F}_{r}-{}^{\boldsymbol{T}_3}\boldsymbol{F}\right)&\\ -\left({}^{\boldsymbol{O}_2}\boldsymbol{V}_{\boldsymbol{r}}-{}^{\boldsymbol{O}_2}\boldsymbol{V}\right)^{T}{}^{\boldsymbol{O}_2}\boldsymbol{U}_{\boldsymbol{B}_3}\left({}^{\boldsymbol{B}_3}\boldsymbol{F}_{r}-{}^{\boldsymbol{B}_3}\boldsymbol{F}\right)&\\ -\left({}^{\boldsymbol{O}_2}\boldsymbol{V}_{\boldsymbol{r}}-{}^{\boldsymbol{O}_2}\boldsymbol{V}\right)^{T}{}^{\boldsymbol{O}_2}\boldsymbol{U}_{\boldsymbol{B}_4}\left({}^{\boldsymbol{B}_4}\boldsymbol{F}_{r}-{}^{\boldsymbol{B}_4}\boldsymbol{F}\right)&\\ =p_{\boldsymbol{T}_1}+p_{\boldsymbol{T}_2}-p_{\boldsymbol{B}_3}-p_{\boldsymbol{B}_4}&\qquad\text{(G.22)}\end{aligned}$$

Consider the fact that *object 1* has all its *driving cutting points* associated with frames $\{\boldsymbol{B}_3\}$ and $\{\boldsymbol{B}_4\}$ and all its *driven cutting points* associated with frames $\{\boldsymbol{T}_1\}$ and $\{\boldsymbol{T}_2\}$. Substituting (G.22) into (G.21) and using (G.20) and Definition 2.10. complete the proof.

■

Theorem 5.4. *The open chain 1 described by (5.17), (5.18), (5.57), (5.58), (5.64), (5.65), and* (E.2)*, combined with its respective control equations (5.79), (5.80), (5.98), (5.99), (5.119), (5.120), and* (5.130)*, is a virtually stable with its affiliated vectors* ${}^{\boldsymbol{B}_1}\boldsymbol{V}_{\boldsymbol{r}} - {}^{\boldsymbol{B}_1}\boldsymbol{V}$ *and* ${}^{\boldsymbol{B}_{11}}\boldsymbol{V}_{\boldsymbol{r}} - {}^{\boldsymbol{B}_{11}}\boldsymbol{V}$ *being virtual function in both* L_2 *and* L_∞*, in the sense of Definition 2.*10.

Proof: Select the non-negative accompanying function of the *open chain 1* as

$$v_1 = v_{\boldsymbol{B}_1} + v_{\boldsymbol{B}_{11}} \tag{G.23}$$

where

$$v_{\boldsymbol{B}_1} = \frac{1}{2}\left({}^{\boldsymbol{B}_1}\mathbf{V}_{\mathbf{r}} - {}^{\boldsymbol{B}_1}\mathbf{V}\right)^{\mathrm{T}}\mathbf{M}_{\boldsymbol{B}_1}\left({}^{\boldsymbol{B}_1}\mathbf{V}_{\mathbf{r}} - {}^{\boldsymbol{B}_1}\mathbf{V}\right) \tag{G.24}$$

$$v_{\boldsymbol{B}_{11}} = \frac{1}{2}\left({}^{\boldsymbol{B}_{11}}\mathbf{V}_{\mathbf{r}} - {}^{\boldsymbol{B}_{11}}\mathbf{V}\right)^{\mathrm{T}}\mathbf{M}_{\boldsymbol{B}_{11}}\left({}^{\boldsymbol{B}_{11}}\mathbf{V}_{\mathbf{r}} - {}^{\boldsymbol{B}_{11}}\mathbf{V}\right) \tag{G.25}$$

are the two non-negative accompanying functions assigned to the two rigid links affiliated with the *open chain 1*.

With appropriate frame substitution, it follows from (5.57), (5.58), (5.98), (5.99) and Lemma 3.1. that

$$\begin{aligned}\dot{v}_{\boldsymbol{B}_1} \le &-\left({}^{\boldsymbol{B}_1}\boldsymbol{V}_{\boldsymbol{r}} - {}^{\boldsymbol{B}_1}\boldsymbol{V}\right)^T\boldsymbol{K}_{\boldsymbol{B}_1}\left({}^{\boldsymbol{B}_1}\boldsymbol{V}_{\boldsymbol{r}} - {}^{\boldsymbol{B}_1}\boldsymbol{V}\right)\\ &+\left({}^{\boldsymbol{B}_1}\boldsymbol{V}_{\boldsymbol{r}} - {}^{\boldsymbol{B}_3}\boldsymbol{V}\right)^T\left({}^{\boldsymbol{B}_1}\boldsymbol{F}_r^* - {}^{\boldsymbol{B}_1}\boldsymbol{F}^*\right)\end{aligned} \tag{G.26}$$

$$\begin{aligned}\dot{v}_{\boldsymbol{B}_{11}} \le &-\left({}^{\boldsymbol{B}_{11}}\boldsymbol{V}_{\boldsymbol{r}} - {}^{\boldsymbol{B}_{11}}\boldsymbol{V}\right)^T\boldsymbol{K}_{\boldsymbol{B}_{11}}\left({}^{\boldsymbol{B}_{11}}\boldsymbol{V}_{\boldsymbol{r}} - {}^{\boldsymbol{B}_{11}}\boldsymbol{V}\right)\\ &+\left({}^{\boldsymbol{B}_{11}}\boldsymbol{V}_{\boldsymbol{r}} - {}^{\boldsymbol{B}_{11}}\boldsymbol{V}\right)^T\left({}^{\boldsymbol{B}_{11}}\boldsymbol{F}_r^* - {}^{\boldsymbol{B}_{11}}\boldsymbol{F}^*\right)\end{aligned} \tag{G.27}$$

In view of (2.21), (5.17), (5.18), (5.64), (5.65), (E.2), (5.79), (5.80), (5.119), (5.120), and (5.130) it results in

$$\left({}^{\boldsymbol{B}_1}\boldsymbol{V}_{\boldsymbol{r}} - {}^{\boldsymbol{B}_1}\boldsymbol{V}\right)^T\left({}^{\boldsymbol{B}_1}\boldsymbol{F}_r^* - {}^{\boldsymbol{B}_1}\boldsymbol{F}^*\right) = p_{\boldsymbol{B}_1} - p_{\boldsymbol{B}_{11}} \tag{G.28}$$

$$\left({}^{\boldsymbol{B}_{11}}\boldsymbol{V}_{\boldsymbol{r}} - {}^{\boldsymbol{B}_{11}}\boldsymbol{V}\right)^T\left({}^{\boldsymbol{B}_{11}}\boldsymbol{F}_r^* - {}^{\boldsymbol{B}_{11}}\boldsymbol{F}^*\right) = p_{\boldsymbol{B}_{11}} - p_{\boldsymbol{T}_1} \tag{G.29}$$

Substituting (G.28) and (G.29) into (G.26) and (G.27) yields

$$\begin{aligned}\dot{v}_1 &= \dot{v}_{\boldsymbol{B}_1} + \dot{v}_{\boldsymbol{B}_{11}} \\ &\leq -\left({}^{\boldsymbol{B}_1}\boldsymbol{V}_{\boldsymbol{r}} - {}^{\boldsymbol{B}_1}\boldsymbol{V}\right)^T \boldsymbol{K}_{\boldsymbol{B}_1}\left({}^{\boldsymbol{B}_1}\boldsymbol{V}_{\boldsymbol{r}} - {}^{\boldsymbol{B}_1}\boldsymbol{V}\right) \\ &\quad -\left({}^{\boldsymbol{B}_{11}}\boldsymbol{V}_{\boldsymbol{r}} - {}^{\boldsymbol{B}_{11}}\boldsymbol{V}\right)^T \boldsymbol{K}_{\boldsymbol{B}_{11}}\left({}^{\boldsymbol{B}_{11}}\boldsymbol{V}_{\boldsymbol{r}} - {}^{\boldsymbol{B}_{11}}\boldsymbol{V}\right) \\ &\quad +p_{\boldsymbol{B}_1} - p_{\boldsymbol{T}_1}. \end{aligned} \tag{G.30}$$

Consider the fact that *open chain 1* has one *driving cutting point* associated with frame $\{\boldsymbol{T}_1\}$ and one *driven cutting point* associated with frame $\{\boldsymbol{B}_1\}$. Using (G.23) - (G.25), (G.30) and Definition 2.10. completes the proof.

■

Lemma 5.2. *The open chain 2 described by* (5.19)-(5.21), (5.59), (5.60), (5.66), (5.67),(5.70), (E.1), *and* (E.3) *and combined with its respective control equations* (5.81)-(5.83), (5.100), (5.101), (5.121), (5.122), (5.125), (5.129), *and* (5.131), *is a virtually stable with its affiliated vectors*

Let

$$v_2 = v_{\boldsymbol{B}_{21}} + v_{\boldsymbol{B}_{22}} \tag{G.31}$$

be the non-negative accompanying functions assigned to the fourth open chain, where

$$v_{\boldsymbol{B}_{21}} = \frac{1}{2}\left({}^{\boldsymbol{B}_{21}}\mathbf{V}_{\mathbf{r}} - {}^{\boldsymbol{B}_{21}}\mathbf{V}\right)^{\mathrm{T}} \mathbf{M}_{\boldsymbol{B}_{21}}\left({}^{\boldsymbol{B}_{21}}\mathbf{V}_{\mathbf{r}} - {}^{\boldsymbol{B}_{21}}\mathbf{V}\right) \tag{G.32}$$

$$v_{\boldsymbol{B}_{22}} = \frac{1}{2}\left({}^{\boldsymbol{B}_{22}}\mathbf{V}_{\mathbf{r}} - {}^{\boldsymbol{B}_{22}}\mathbf{V}\right)^{\mathrm{T}} \mathbf{M}_{\boldsymbol{B}_{22}}\left({}^{\boldsymbol{B}_{22}}\mathbf{V}_{\mathbf{r}} - {}^{\boldsymbol{B}_{22}}\mathbf{V}\right) \tag{G.33}$$

are the two non-negative accompanying functions assigned to the two rigid bodies (cylinder 1 piston rod and cylinder 1 base) affiliated with the open chain 2. Then, the time derivative of (G.31) *can be expressed as*

$$\begin{aligned}\dot{v}_2 &= \dot{v}_{\boldsymbol{B}_{21}} + \dot{v}_{\boldsymbol{B}_{22}} \\ &\leq -\left({}^{\boldsymbol{B}_{21}}\boldsymbol{V}_{\boldsymbol{r}} - {}^{\boldsymbol{B}_{21}}\boldsymbol{V}\right)^T \boldsymbol{K}_{\boldsymbol{B}_{21}}\left({}^{\boldsymbol{B}_{21}}\boldsymbol{V}_{\boldsymbol{r}} - {}^{\boldsymbol{B}_{21}}\boldsymbol{V}\right) \\ &\quad -\left({}^{\boldsymbol{B}_{22}}\boldsymbol{V}_{\boldsymbol{r}} - {}^{\boldsymbol{B}_{22}}\boldsymbol{V}\right)^T \boldsymbol{K}_{\boldsymbol{B}_{22}}\left({}^{\boldsymbol{B}_{22}}\boldsymbol{V}_{\boldsymbol{r}} - {}^{\boldsymbol{B}_{22}}\boldsymbol{V}\right) \\ &\quad +p_{\boldsymbol{B}_2} - p_{\boldsymbol{T}_2} + (\dot{x}_{1r} - \dot{x}_{1r})(f_{c1r} - f_{c1}) \end{aligned} \tag{G.34}$$

where $p_{\boldsymbol{B}_2}$ and $p_{\boldsymbol{T}_2}$ denote the two virtual flows by Definition 2.9. at the two cutting points of the open chain 2.

Proof: It follows from (5.59), (5.60), (5.100), (5.101), and Lemma 3.1. that

$$\dot{v}_{\boldsymbol{B}_{21}} \leq -\left({}^{\boldsymbol{B}_{21}}\boldsymbol{V}_{\boldsymbol{r}} - {}^{\boldsymbol{B}_{21}}\boldsymbol{V}\right)^{T} \boldsymbol{K}_{\boldsymbol{B}_{21}} \left({}^{\boldsymbol{B}_{21}}\boldsymbol{V}_{\boldsymbol{r}} - {}^{\boldsymbol{B}_{21}}\boldsymbol{V}\right) + \left({}^{\boldsymbol{B}_{21}}\boldsymbol{V}_{\boldsymbol{r}} - {}^{\boldsymbol{B}_{21}}\boldsymbol{V}\right)^{T} \left({}^{\boldsymbol{B}_{21}}\boldsymbol{F}_{r}^{*} - {}^{\boldsymbol{B}_{21}}\boldsymbol{F}^{*}\right) \tag{G.35}$$

$$\dot{v}_{\boldsymbol{B}_{22}} \leq -\left({}^{\boldsymbol{B}_{22}}\boldsymbol{V}_{\boldsymbol{r}} - {}^{\boldsymbol{B}_{22}}\boldsymbol{V}\right)^{T} \boldsymbol{K}_{\boldsymbol{B}_{22}} \left({}^{\boldsymbol{B}_{22}}\boldsymbol{V}_{\boldsymbol{r}} - {}^{\boldsymbol{B}_{22}}\boldsymbol{V}\right) + \left({}^{\boldsymbol{B}_{22}}\boldsymbol{V}_{\boldsymbol{r}} - {}^{\boldsymbol{B}_{22}}\boldsymbol{V}\right)^{T} \left({}^{\boldsymbol{B}_{22}}\boldsymbol{F}_{r}^{*} - {}^{\boldsymbol{B}_{22}}\boldsymbol{F}^{*}\right) \tag{G.36}$$

hold.

In view of (2.21), (5.19)-(5.21), (5.66), (5.67), (5.70), (E.1), (E.3), (5.81)-(5.83), (5.121), (5.122), (5.125), (5.129), and (5.131) it result in

$$\left({}^{\boldsymbol{B}_{21}}\boldsymbol{V}_{\boldsymbol{r}} - {}^{\boldsymbol{B}_{21}}\boldsymbol{V}\right)^{T} \left({}^{\boldsymbol{B}_{21}}\boldsymbol{F}_{r}^{*} - {}^{\boldsymbol{B}_{21}}\boldsymbol{F}^{*}\right) = p_{\boldsymbol{B}_{2}} - p_{\boldsymbol{B}_{22}} + (\dot{x}_{1r} - \dot{x}_{1r})(f_{c1r} - f_{c1}) \tag{G.37}$$

$$\left({}^{\boldsymbol{B}_{22}}\boldsymbol{V}_{\boldsymbol{r}} - {}^{\boldsymbol{B}_{22}}\boldsymbol{V}\right)^{T} \left({}^{\boldsymbol{B}_{22}}\boldsymbol{F}_{r}^{*} - {}^{\boldsymbol{B}_{22}}\boldsymbol{F}^{*}\right) = p_{\boldsymbol{B}_{22}} - p_{\boldsymbol{T}_{2}} \tag{G.38}$$

Finally, substituting (G.37) and (G.38) into (G.35) and (G.36) yields (G.34).

■

Theorem 5.5. *The zero-mass object described by* (5.16) *and* (5.69)*, combined with the control equations* (5.78) *and* (5.123)*, is virtually stable in the sense of Definition 2.*10.

Proof: it follows from (5.69) and (5.123) that

$${}^{\boldsymbol{B}_{cc1}}\boldsymbol{F}_{r} - {}^{\boldsymbol{B}_{cc1}}\boldsymbol{F} = \left({}^{\boldsymbol{B}_{1}}\boldsymbol{F}_{r} - {}^{\boldsymbol{B}_{1}}\boldsymbol{F}\right) + \left({}^{\boldsymbol{B}_{2}}\boldsymbol{F}_{r} - {}^{\boldsymbol{B}_{2}}\boldsymbol{F}\right) \tag{G.39}$$

holds.

Let the non-negative accompanying function be zero. Premultiplying (G.39) by $\left({}^{\boldsymbol{B}_{cc1}}\boldsymbol{V}_{r} - {}^{\boldsymbol{B}_{cc1}}\boldsymbol{V}\right)^{T}$ and using (2.21), (5.16) , and (5.78) yields

$$0 = p_{\boldsymbol{B}_{cc1}} - p_{\boldsymbol{B}_{1}} - p_{\boldsymbol{B}_{2}} \tag{G.40}$$

which proves the theorem in view of Definition 2.10.

■

Above Theorems 5.1 - 5.5 ensure that the *virtual stability* of *object 2, object 1, zero-mass object, open chain 3,* and *open chain 1*. However, appearance of $(\dot{x}_{2r} - \dot{x}_{2r})(f_{c2r} - f_{c2})$ and $(\dot{x}_{1r} - \dot{x}_{1r})(f_{c1r} - f_{c1})$ in the right-hand side of (G.15) and (G.34), respectively, prevents the virtual stability of the *open chain 4* and *open chain 2* from being held. These terms will be addressed in the next Appendix H.

APPENDIX H: VIRTUAL STABILITY OF HYDRAULIC ACTUATOR ASSEMBLY

In this appendix the *virtual stability* with respect to hydraulic actuator (*open chain 2 and open chain 4)* will be presented. Due to similar kinematic structures, equations concerned to cylinder 1 can be directly applied to cylinder 2 by replacing *open chain 2* equations and frames $\{\boldsymbol{B}_{21}\}$ and $\{\boldsymbol{B}_{22}\}$ to respective *open chain 4* equations and frames $\{\boldsymbol{B}_{41}\}$ and $\{\boldsymbol{B}_{42}\}$. All Equations, Theorems, Lemmas and Proofs of this chapter are taken directly from (Zhu 2010. pp.185-187).

Lemma 5.3. *Consider the hydraulic cylinder 1 dynamic described by* (F.8), (F.11), (5.142), (5.143) *and combined with the control equations* (5.151), (5.153), (5.154) *and* (5.155)*. The time derivative of non-negative accompanying function of the cylinder 1 (open chain 2)*

$$v_c = \frac{1}{2\beta}\left(f_{pr} - f_p\right)^2 \tag{H.1}$$

is

$$\dot{v}_c \leq -k_{fp}\left(f_{pr} - f_p\right)^2 - k_x(f_{cr} - f_c)(\dot{x}_r - \dot{x}) \tag{H.2}$$

Theorem 5.6. *The open chain 2 described by* (5.19) – (5.21), (5.59), (5.60), (5.66), (5.67),(5.70), (E.1), (E.3), (F.8), (F.11), (5.142) *and* (5.143) *combined with the control equations* (5.81) – (5.83), (5.100), (5.101), (5.121), (5.122), (5.125), (5.129), (5.131), (5.151), (5.153), (5.154) *and* (5.155) *is a virtually stable with its affiliated vectors and variables* ${}^{\boldsymbol{B}_{21}}\boldsymbol{V}_{\boldsymbol{r}} - {}^{\boldsymbol{B}_{21}}\boldsymbol{V}$, ${}^{\boldsymbol{B}_{22}}\boldsymbol{V}_{\boldsymbol{r}} - {}^{\boldsymbol{B}_{22}}\boldsymbol{V}$ *and* $f_{pr} - f_p$ *being virtual functions in both* L_2 *and* L_∞*, in sense of Definition 2.*10.

Proof: The proof follows directly from Lemmas 5.2 and 5.3. Define the non-negative accompanying function of the *open chain 2* as

$$v_{oc2} = v_2 + \frac{v_c}{k_x} \tag{H.3}$$

where v_2 and v_{c1} are defined by (G.31) and (H.1), respectively. It follows from (G.34) and (H.2) that

$$\begin{aligned}\dot{v}_{oc2} &= \dot{v}_2 + \frac{\dot{v}_c}{k_x} \\ &\leq -\left({}^{\boldsymbol{B}_{21}}\boldsymbol{V}_{\boldsymbol{r}} - {}^{\boldsymbol{B}_{21}}\boldsymbol{V}\right)^T \boldsymbol{K}_{\boldsymbol{B}_{21}} \left({}^{\boldsymbol{B}_{21}}\boldsymbol{V}_{\boldsymbol{r}} - {}^{\boldsymbol{B}_{21}}\boldsymbol{V}\right) \\ &\quad -\left({}^{\boldsymbol{B}_{22}}\boldsymbol{V}_{\boldsymbol{r}} - {}^{\boldsymbol{B}_{22}}\boldsymbol{V}\right)^T \boldsymbol{K}_{\boldsymbol{B}_{22}} \left({}^{\boldsymbol{B}_{22}}\boldsymbol{V}_{\boldsymbol{r}} - {}^{\boldsymbol{B}_{22}}\boldsymbol{V}\right) \\ &\quad -\frac{k_{fp}}{k_x}\left(f_{pr} - f_p\right)^2 + p_{\boldsymbol{B}_2} - p_{\boldsymbol{T}_2} \end{aligned} \tag{H.4}$$

holds.

Consider the fact that *open chain 2* has one *driving cutting point* associated with frame $\{\boldsymbol{T}_2\}$ and one *driven cutting point* associated with frame $\{\boldsymbol{T}_2\}$. Using (G.31), (H.1), (H.3), (H.4) and Definition 2.10. completed the proof.

■

Theorems 5.1 – 5.6 ensure that all *objects* and *open chains* of assembly combined with their respective control equations are *virtually stable* in the sense of Definition 2.10. Therefore, the complete hydraulically actuated manipulator (HIAB 031) is virtually stable, in view of Lemma 2.1.

APPENDIX I: AN APPLIED PARAMETER VECTORS FOR STUDID SYSTEM

Parameter Vectors of Rigid Bodies:

As mentioned in section 6.1, parameters of all parameter vectors of studied system were computed by utilizing SolidWorks 3D CAD program. As from Appendix B can be seen, a parameter vector $\boldsymbol{\theta}_{2A} \in \mathbb{R}^6$ of rigid body can be given by solving four parameters related to rigid body. These parameters are:

m_A Mass of rigid body

${}^{A}r_{mx}$ Distance from body frame $\{\boldsymbol{A}\}$ to the center of mass along *x*-axis and expressed in body frame $\{\boldsymbol{A}\}$.

${}^{A}r_{my}$ Distance from body frame $\{\boldsymbol{A}\}$ to the center of mass along *y*-axis and expressed in body frame $\{\boldsymbol{A}\}$.

I_{Azz} Moment of inertia around the center of mass about *z*-axis and axpressed in body frame $\{\boldsymbol{A}\}$.

Computed parameters for all rigid bodies are given in Table 4. For additional information about rigid bodies and body frames, see Figure 12, Figure 13, Figure 14 and Figure 15.

Table 4: Computed parameter for rigid bodies.

Rigid Body	Body frame	m_A [kg]	${}^{A}r_{mx}$ [m]	${}^{A}r_{my}$ [m]	I_{Azz} [kg·m^2]
Link$_1$	$\{\boldsymbol{B}_1\}$	20.0570	0.4421	0.1023	3.2254
Link$_{11}$	$\{\boldsymbol{B}_{11}\}$	18.7600	0.1786	0.1237	1.2397
Link$_{21}$	$\{\boldsymbol{B}_{21}\}$	17.3599	0.3580	0	3.1306
Link$_{22}$	$\{\boldsymbol{B}_{22}\}$	10.3500	0.3300	0	1.6832
Object 1	$\{\boldsymbol{O}_1\}$	6.2278	0	0	0.0655
Link$_3$	$\{\boldsymbol{B}_3\}$	55.1400	0.5380	0.1065	22.7132
Link$_{31}$	$\{\boldsymbol{B}_{31}\}$	9.5960	0.1388	0.0768	0.3830
Link$_{41}$	$\{\boldsymbol{B}_{41}\}$	17.3599	0.3580	0	3.1306
Link$_{42}$	$\{\boldsymbol{B}_{42}\}$	10.3500	0.3300	0	1.6832
Object 2	$\{\boldsymbol{O}_2\}$	575.000	0	0	81.0880

In view of (B.17) and Table 4, the parameter vectors for each rigid body can be computed as

$$\boldsymbol{\theta}_{2A} = \begin{bmatrix} m_A & m_A\,{}^{A}r_{mx} & m_A\,{}^{A}r_{my} & m_A\,{}^{A}r_{mx}^2 & m_A\,{}^{A}r_{my}^2 & I_{Azz} \end{bmatrix}^{T}$$

Note, that ${}^{A}r_{mx}$ and ${}^{A}r_{my}$ for body frames $\{O_1\}$ and $\{O_2\}$ are zero because these frames are set to be located at the center of masses of Object 1 and Object 2, respectively. The measured distances from frame $\{T_{cc1}\}$ to $\{O_1\}$ were:

$${}^{T_{cc1}}r_{O_{1\_x}} = 0.0232\ \text{m}$$
$${}^{T_{cc1}}r_{O_{1\_y}} = 0.1490\ \text{m}$$

Similar, the measured distances from frame $\{T_{cc2}\}$ to $\{O_2\}$ were:

$${}^{T_{cc2}}r_{O_{2\_x}} = 1.2178\ \text{m}$$
$${}^{T_{cc2}}r_{O_{2\_y}} = 0.6110\ \text{m}$$

Above dimensions were needed in computations of transformation matrices ${}^{T_{cc1}}U_{O_1} \in \mathbb{R}^{6\times6}$ and ${}^{T_{cc2}}U_{O_2} \in \mathbb{R}^{6\times6}$.

Valve Flow Coefficient Parameter Vectors:

The valve flow coefficient parameter vector $\boldsymbol{\theta}_v \in \mathbb{R}^4$ defined in (5.145) contains four flow coefficient parameters for each valve control edge. Preliminary values for these parameters were first extracted from manufacturer's datasheet. Then, fine tuned values for these parameters were found out during test measures by changing values as long as best the correspondence between required velocity and measured velocity were found. Applied values for both control valves are given in Table 5.

Table 5: An applied parameters into valve flow coefficient parameter vectors.

	Parameter	Applied value $\left[\frac{m^3}{s\cdot V\cdot\sqrt{Pa}}\right]$
Valve 1	c_{p1}	$6.20\cdot10^{-8}$
	c_{n1}	$6.20\cdot10^{-8}$
	c_{p2}	$6.20\cdot10^{-8}$
	c_{n2}	$6.20\cdot10^{-8}$
Valve 2	c_{p1}	$3.55\cdot10^{-8}$
	c_{n1}	$3.55\cdot10^{-8}$
	c_{p2}	$3.55\cdot10^{-8}$
	c_{n2}	$3.55\cdot10^{-8}$

Parameter Vector of Cylinder Control:

The cylinder control parameter vector $\boldsymbol{\theta}_c \in \mathbb{R}^3$ defined in (5.155) contains three different parameters β denoting the effective bulk modulus, A_A denoting the area cylinder chamber A and A_B denoting the area cylinder chamber B (see Figure 18). Following values for parameters in parameter vectors for cylinder 1 and cylinder 2 were used.

Table 6: An applied parameters into cylinder control parameter vectors.

	β [MPa]	A_A [m^2]	A_B[m^2]
Cylinder 1	1100	$5.026 \cdot 10^{-3}$	$3.436 \cdot 10^{-3}$
Cylinder 2	1100	$5.026 \cdot 10^{-3}$	$3.436 \cdot 10^{-3}$

APPENDIX J: MEASURED VDC-CONTROLLER RESULTS WITH CARTESIAN TRANSITION TIME OF 5 s.

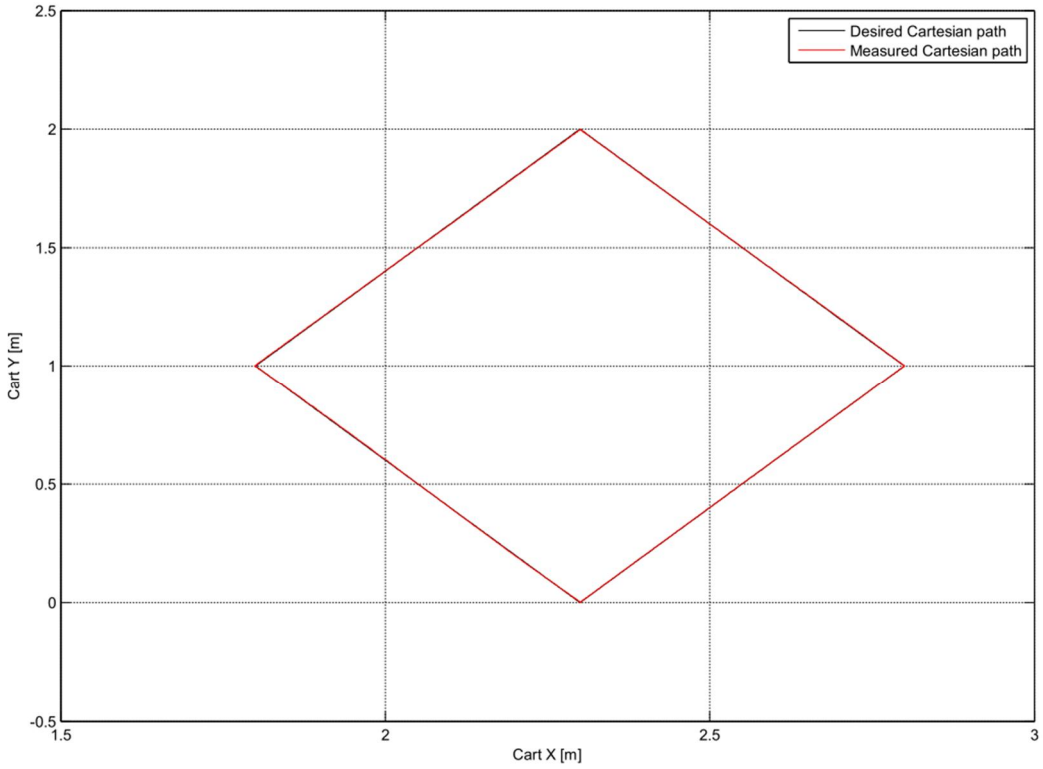

Figure 37: Desired and measured Cartesian paths with VDC-controller under Cartesian transition time of 5 s.

The Cartesian position tracking error in Figure 38 is given in the view of equation (J.1).

$$err = \sqrt{(X_{des} - X)^2 + (Y_{des} - Y)^2} \tag{J.1}$$

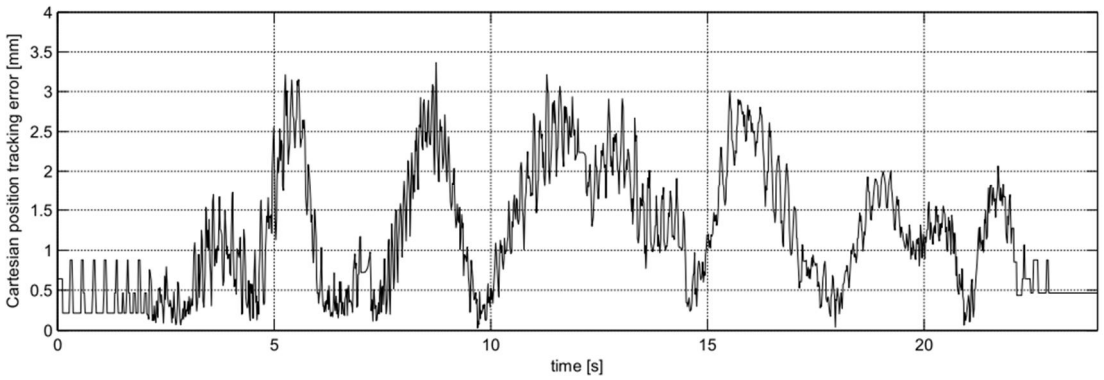

Figure 38: Cartesian position tracking error with VDC-controller under Cartesian transition time of 5 s.

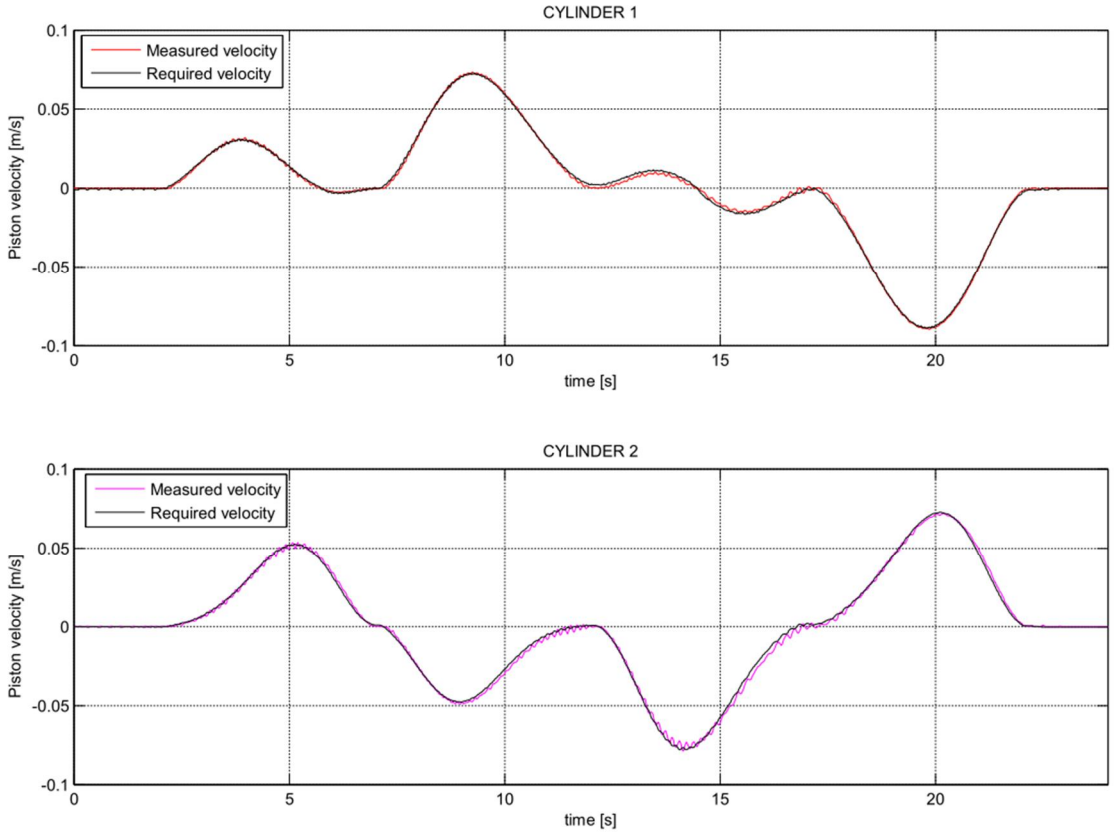

Figure 39: Required and measured piston velocity trajectories with VDC-controller under Cartesian transition time of 5 s.

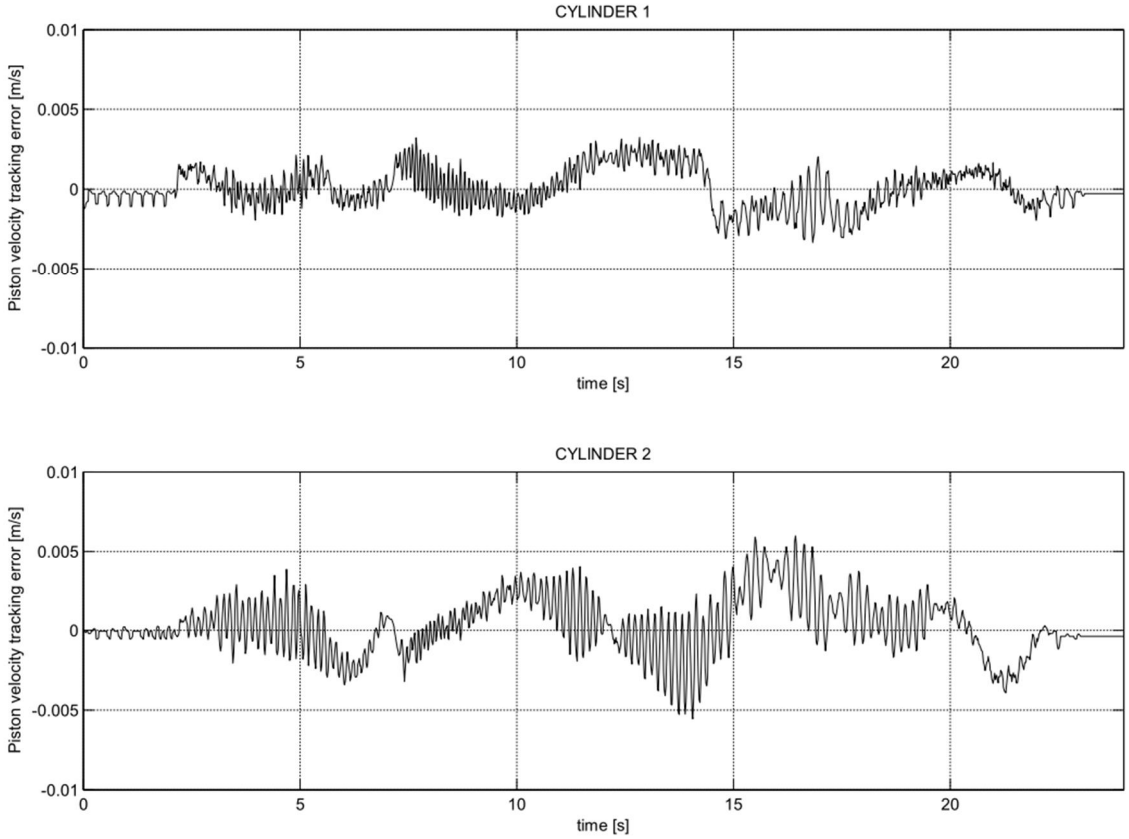

Figure 40: Piston velocity tracking errors with VDC-controller under Cartesian transition time of 5 s.

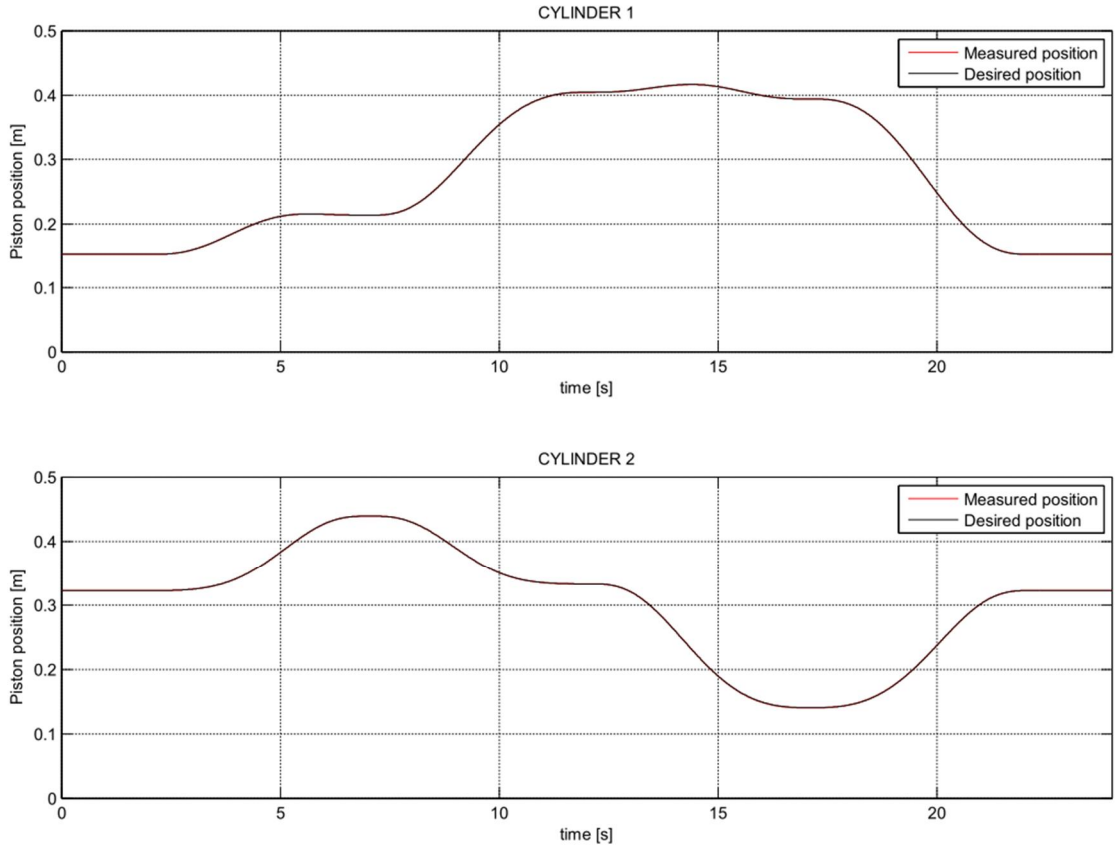

Figure 41: Desired and measured piston position trajectories with VDC-controller under Cartesian transition time of 5 s.

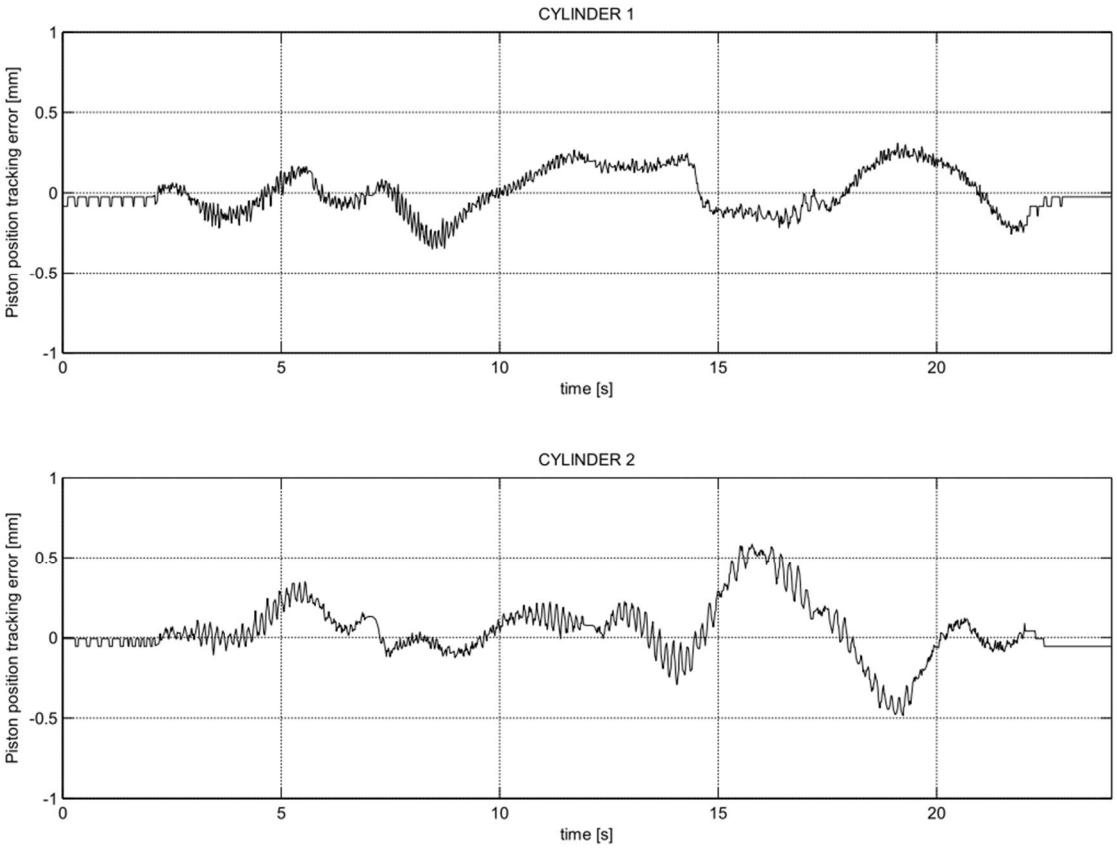

Figure 42: Piston position tracking errors with VDC-controller under Cartesian transition time of 5 s.

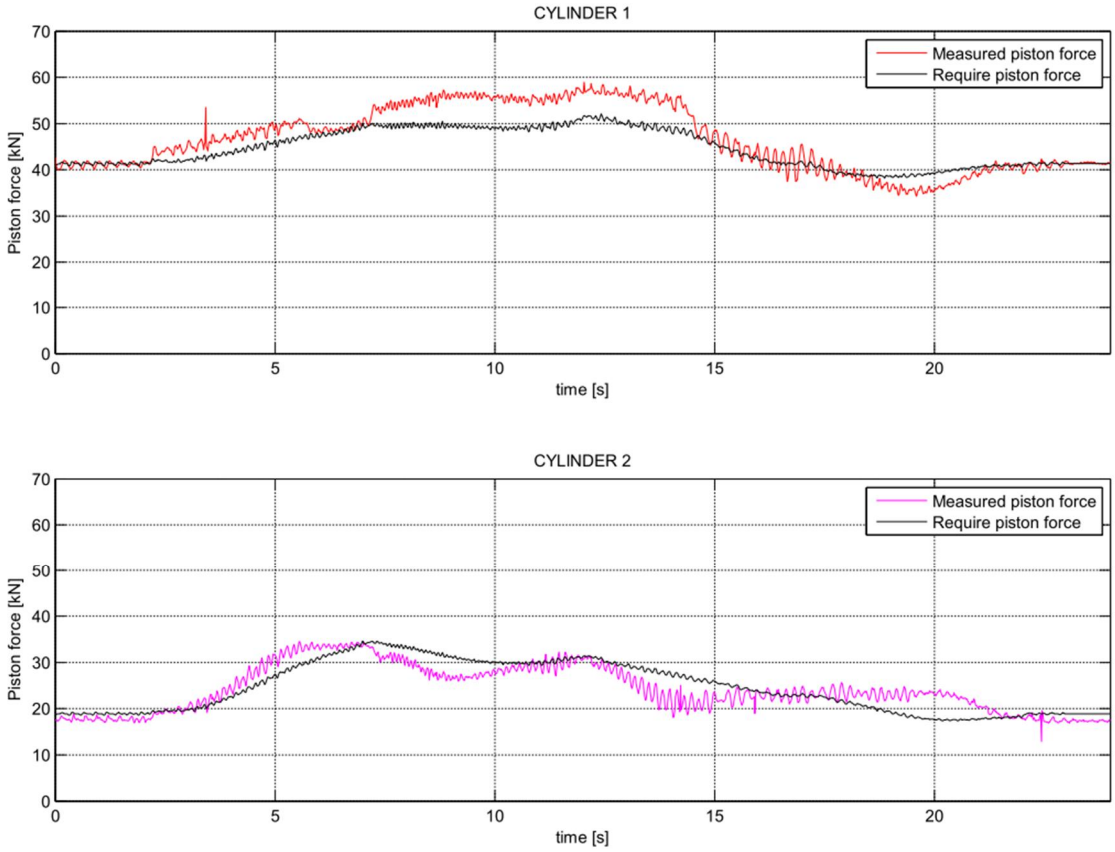

Figure 43: Required and measured piston forces with VDC-controller under Cartesian transition time of 5 s.

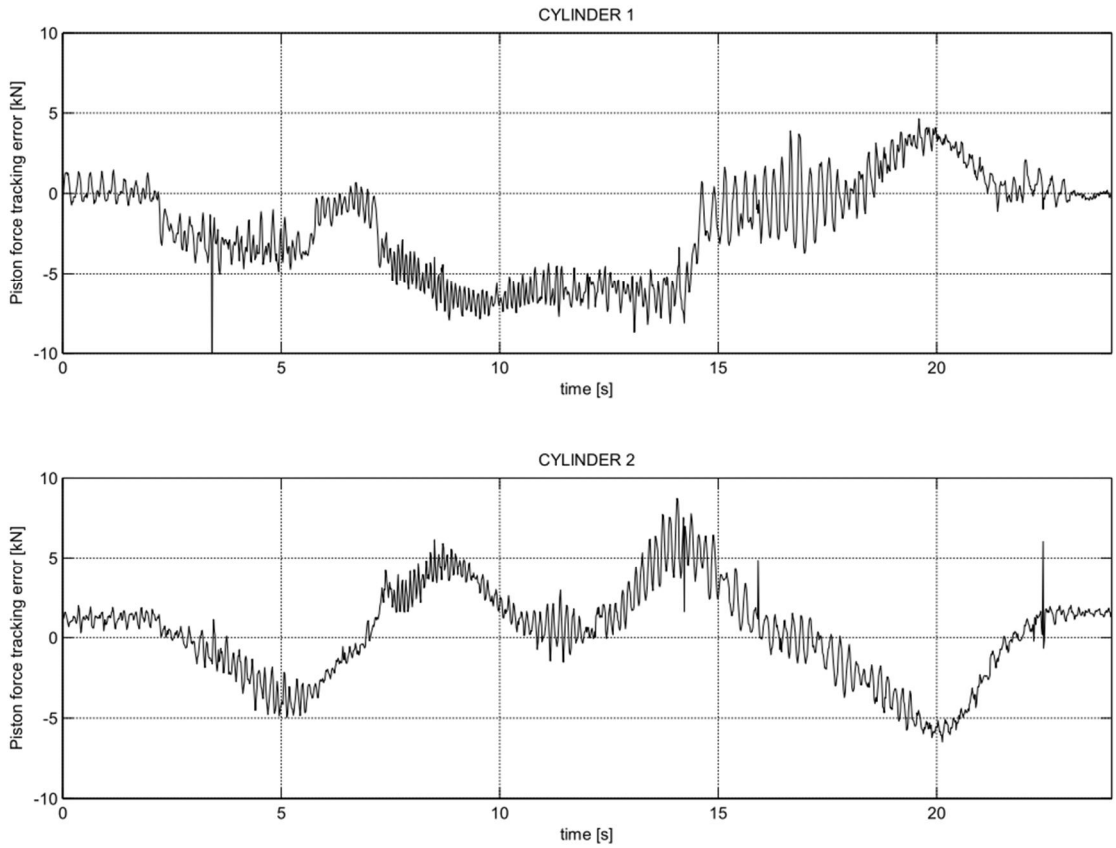

Figure 44: Piston force tracking errors with VDC-controller under Cartesian transition time of 5 s.

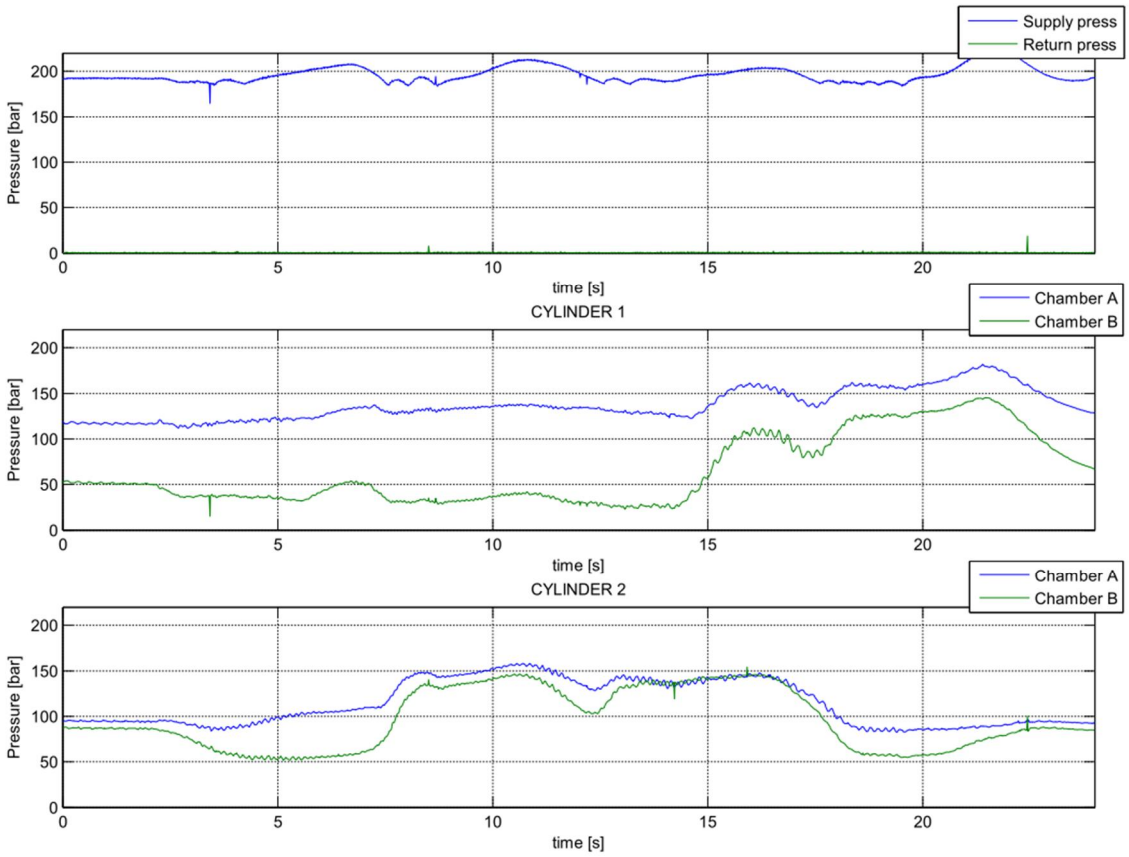

Figure 45: System pressures during with VDC-controller under Cartesian transition time of 5 s.

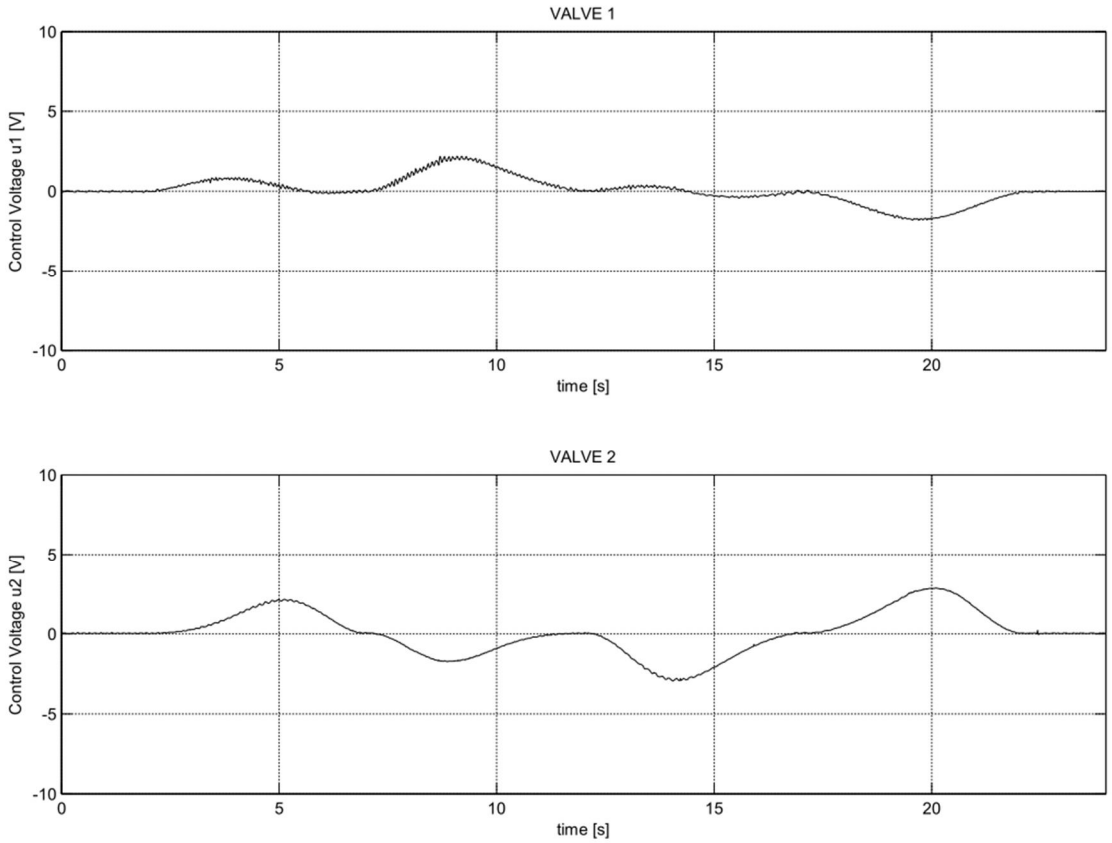

Figure 46: Valve control voltages with VDC-controller under Cartesian transition time of 5 s.

APPENDIX K: MEASURED VDC-CONTROLLER RESULTS WITH CARTESIAN TRANSITION TIME OF 2.5 s.

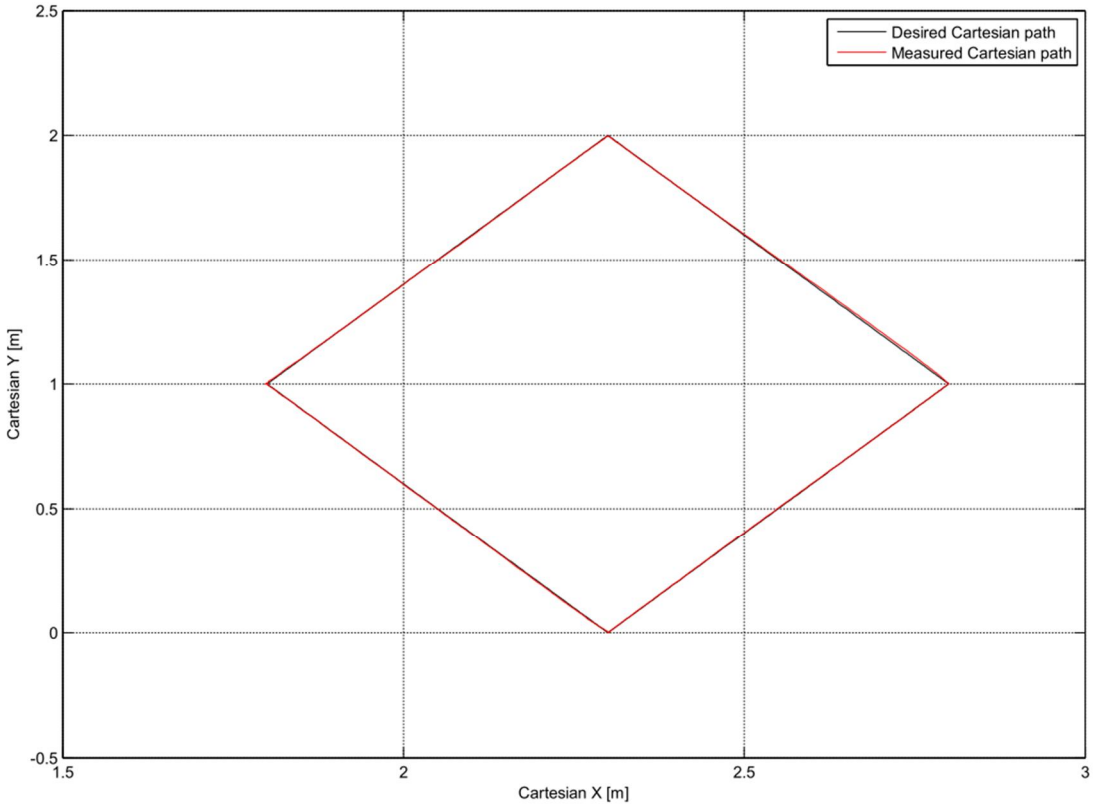

Figure 47: Desired and measured Cartesian paths with VDC-controller under Cartesian transition time of 2.5s.

The Cartesian position tracking error in Figure 48 is given in the view of equation (J.1).

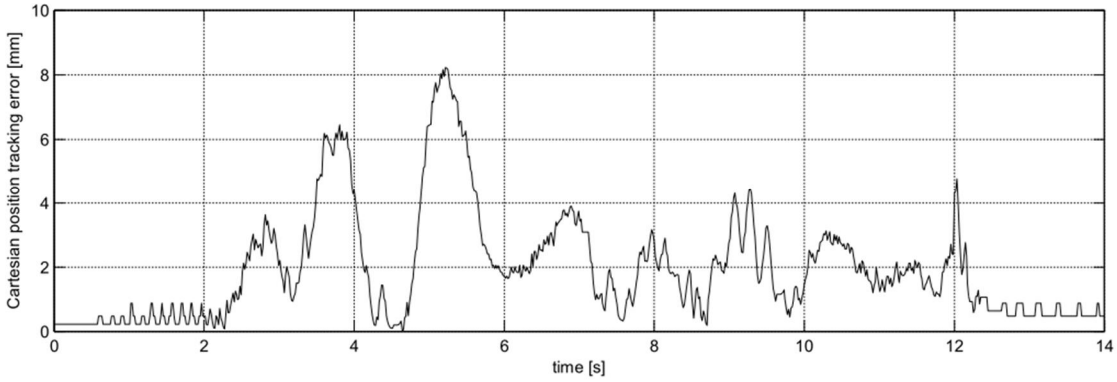

Figure 48: Cartesian position tracking error with VDC-controller under Cartesian transition time of 2.5 s.

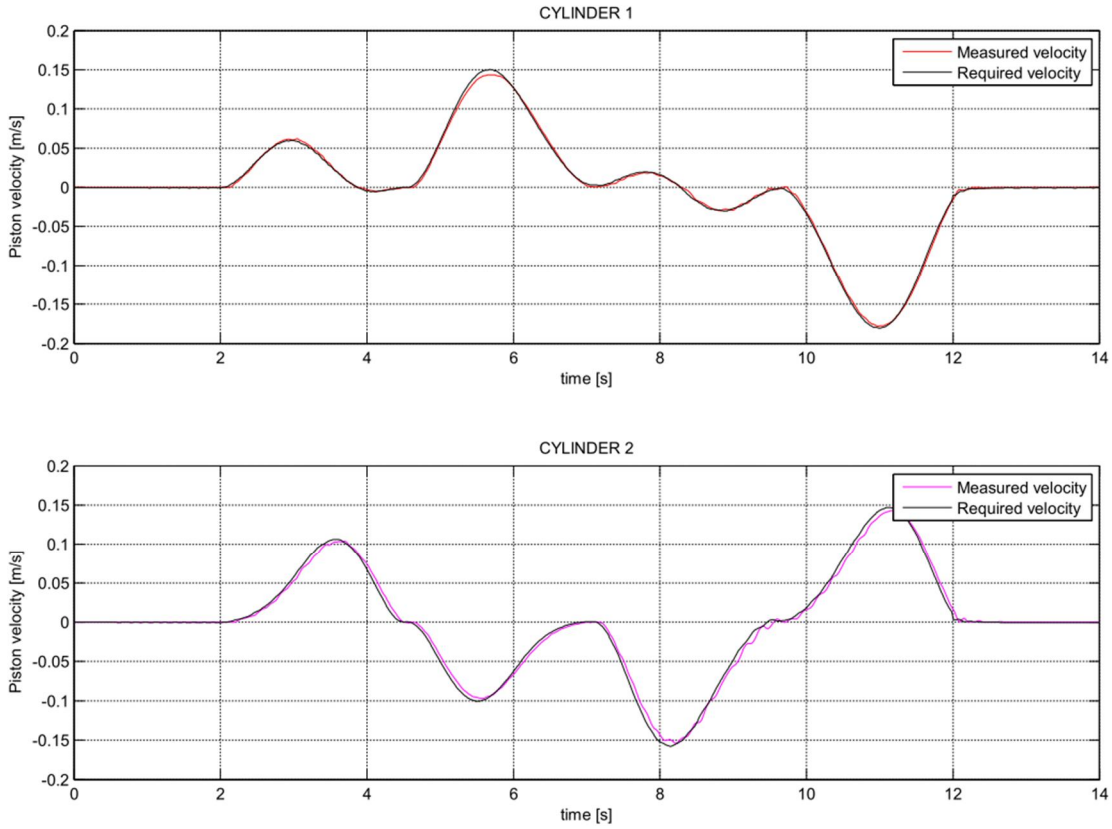

Figure 49: Required and measured piston velocity trajectories with VDC-controller under Cartesian transition time of 2.5s.

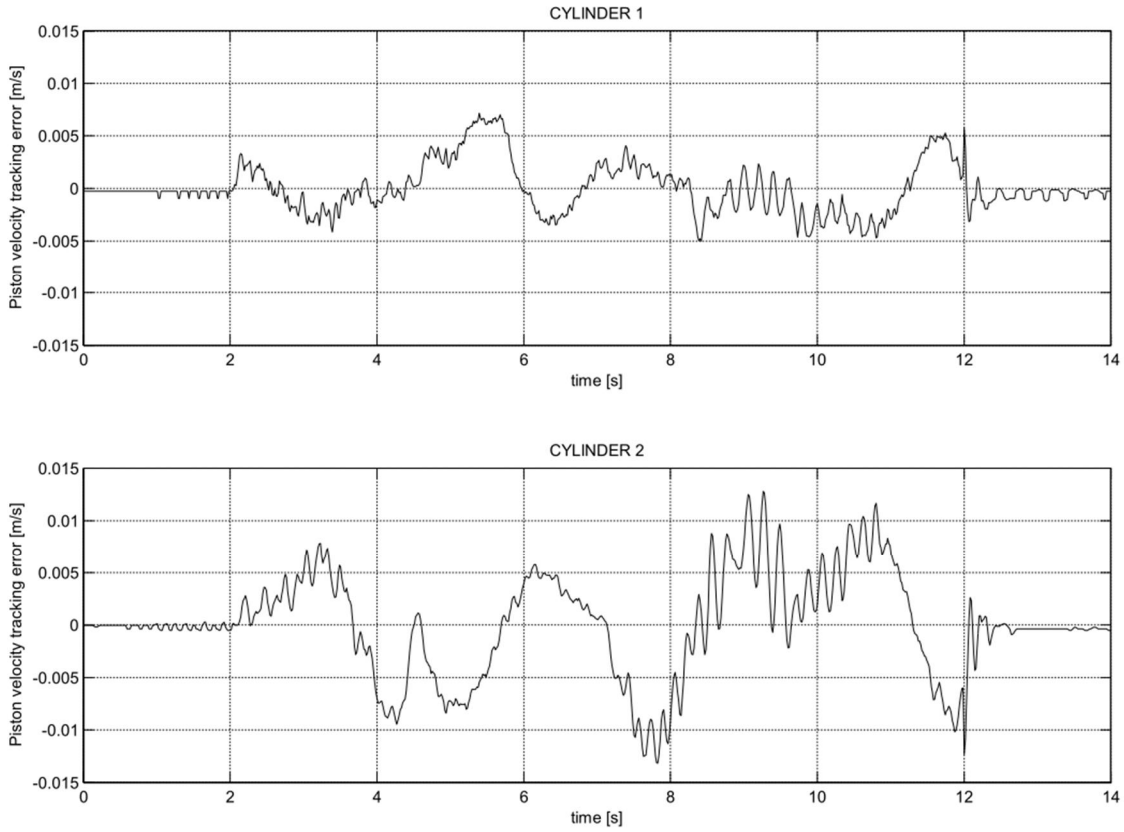

Figure 50: Piston velocity tracking errors with VDC-controller under Cartesian transition time of 2.5s

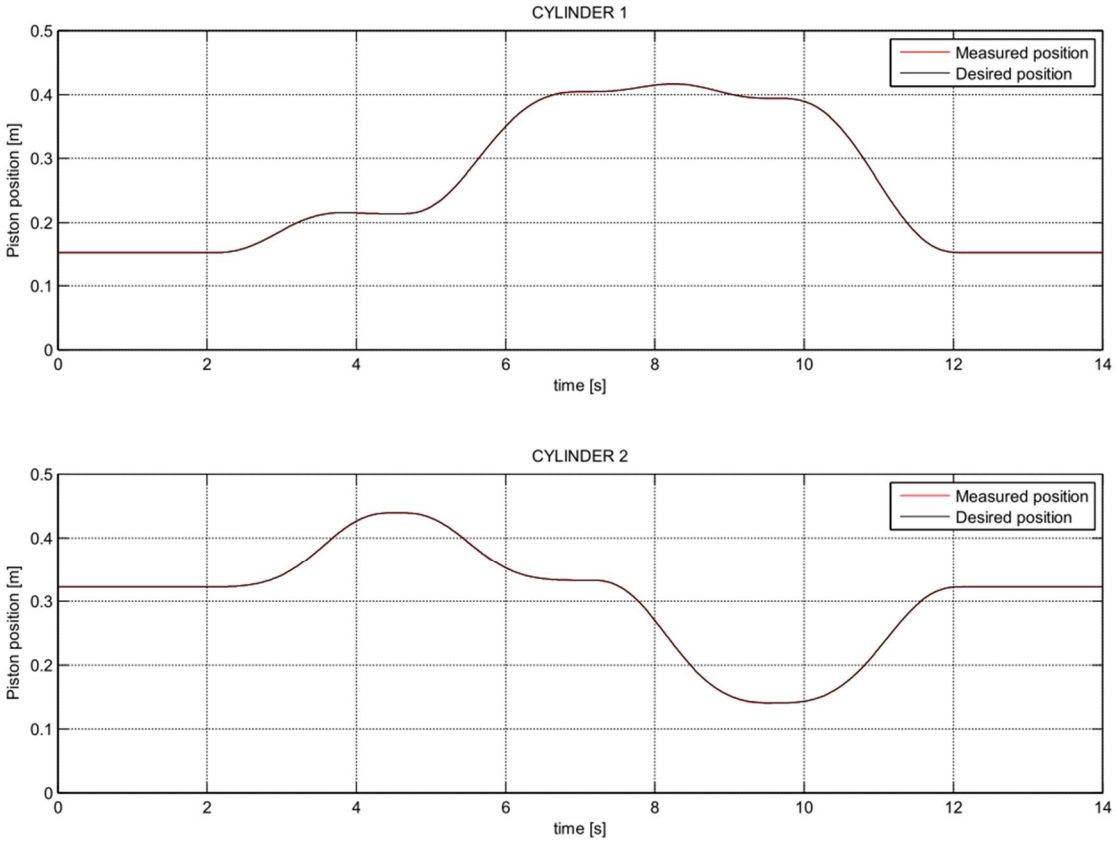

Figure 51: Desired and measured piston position trajectories with VDC-controller under Cartesian transition time of 2.5s.

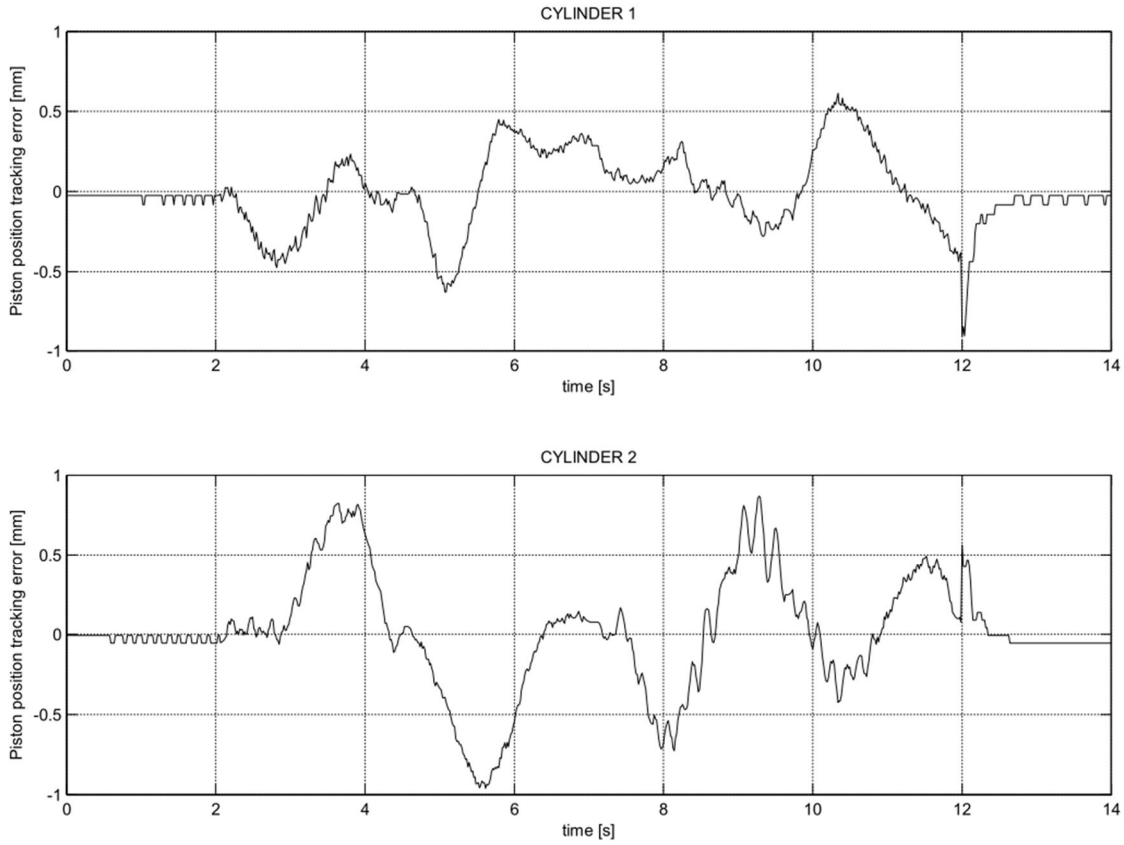

Figure 52: Piston position tracking errors with VDC-controller under transition time of 2.5s.

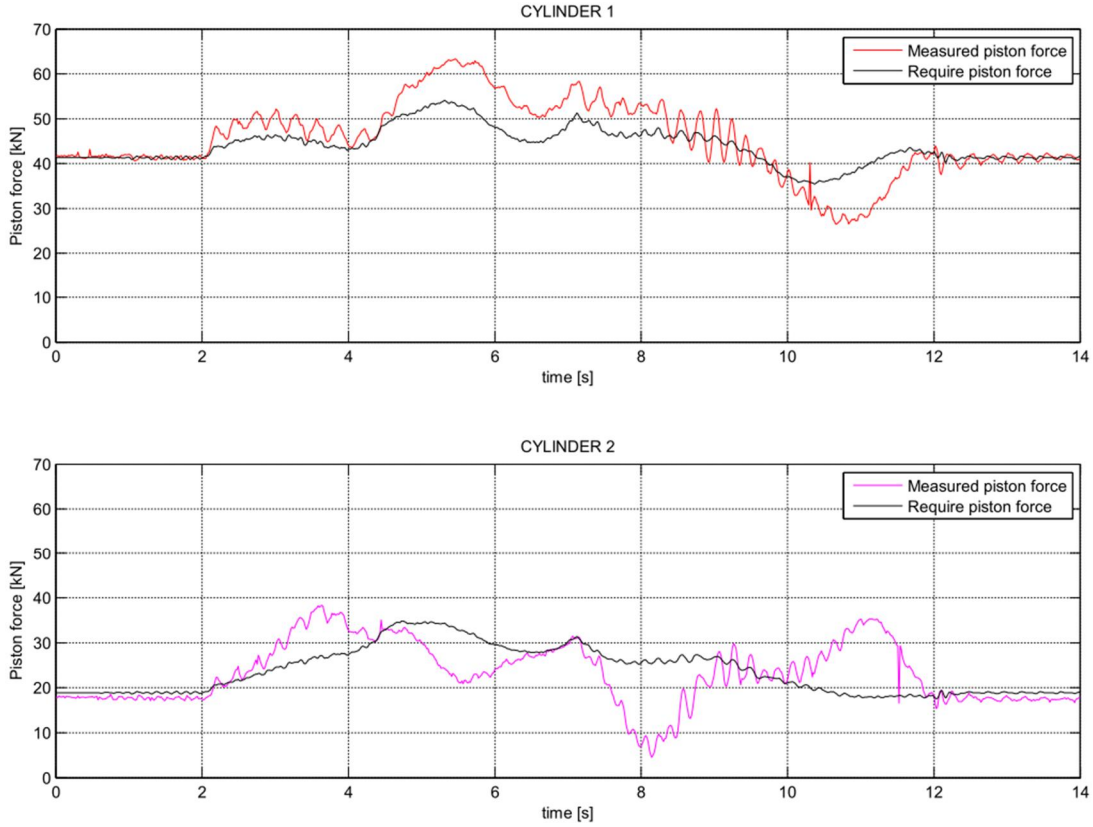

Figure 53: Required and measured piston forces with VDC-controller under Cartesian transition of 2.5s.

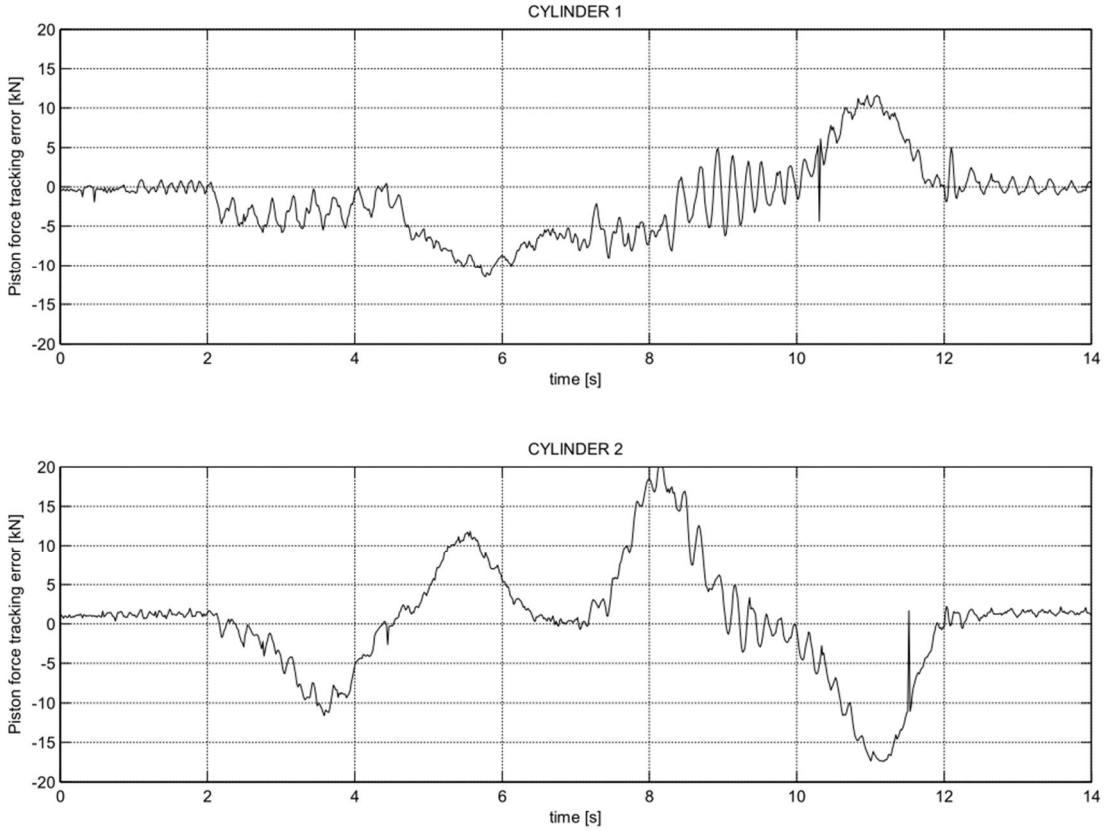

Figure 54: Piston force tracking errors with VDC-controller under Cartesian transition time of 2.5s.

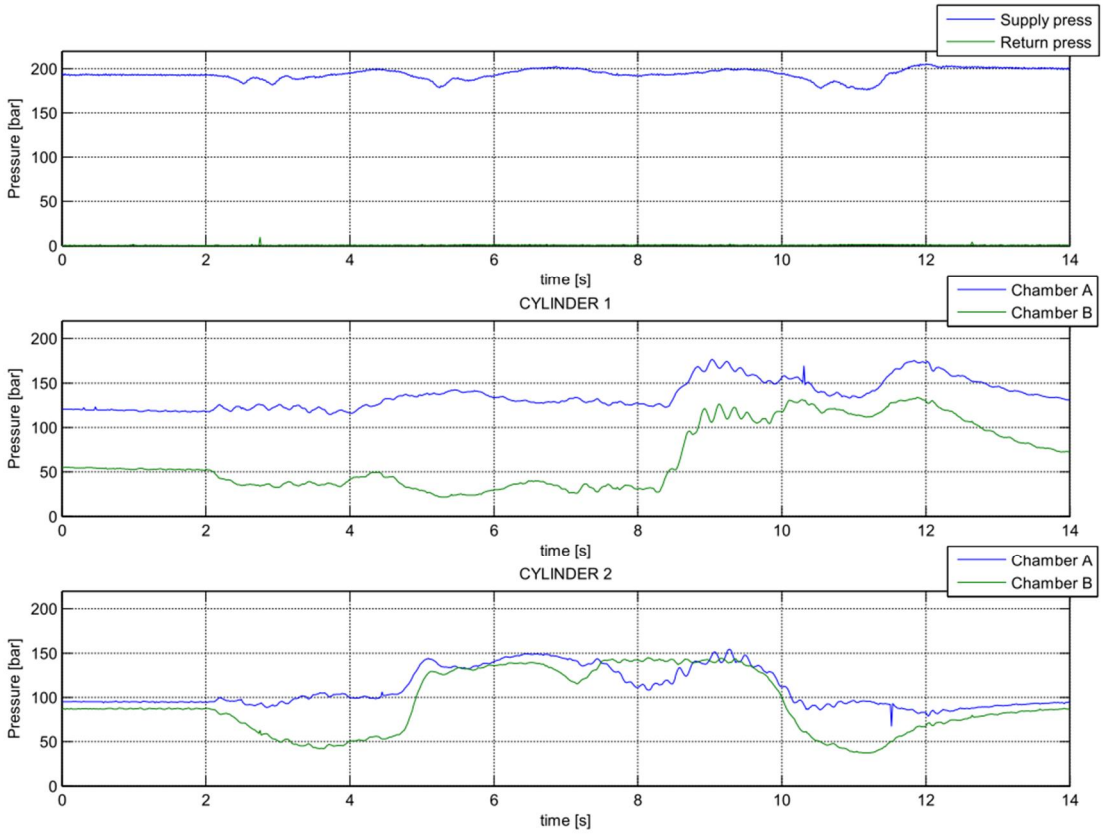

Figure 55: System pressures with VDC-controller under Cartesian transition time of 2.5s.

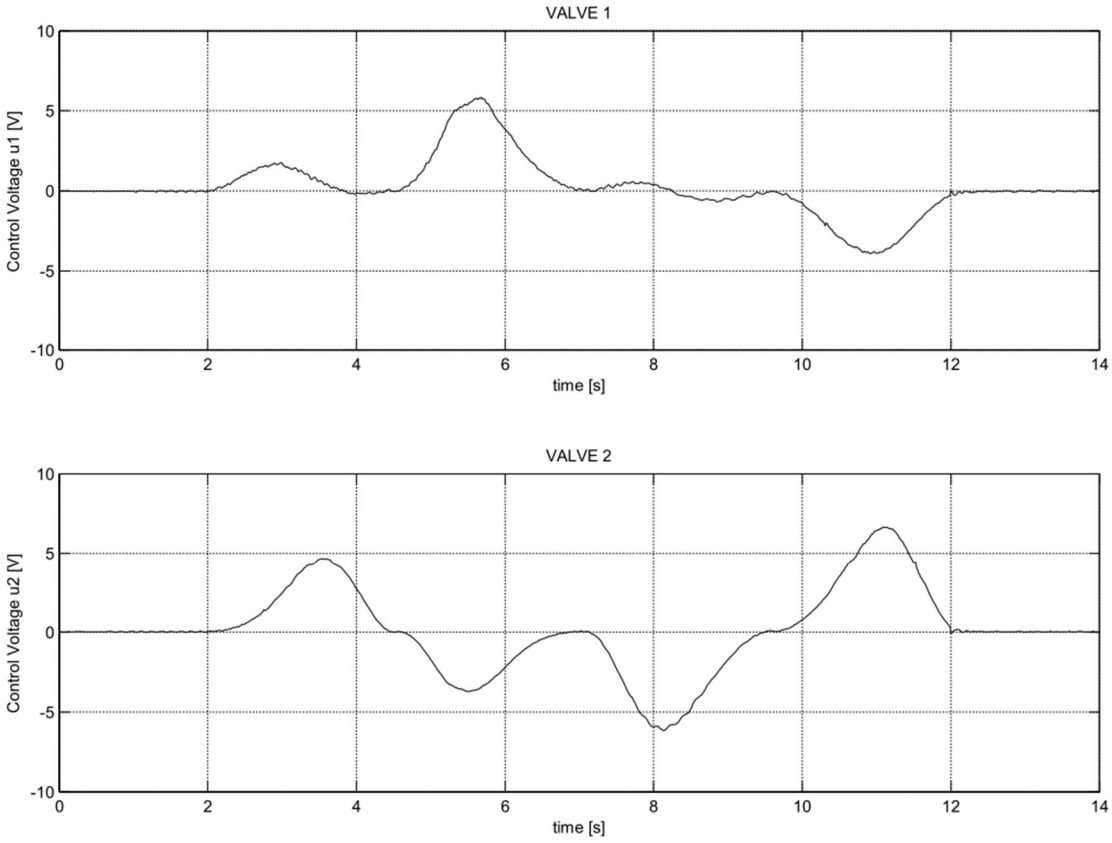

Figure 56: Valve control voltages with VDC-controller under transition time of 2.5s.

APPENDIX L: MEASURED VDC-CONTROLLER RESULTS WITH CARTESIAN TRANSITION TIME OF 10 s.

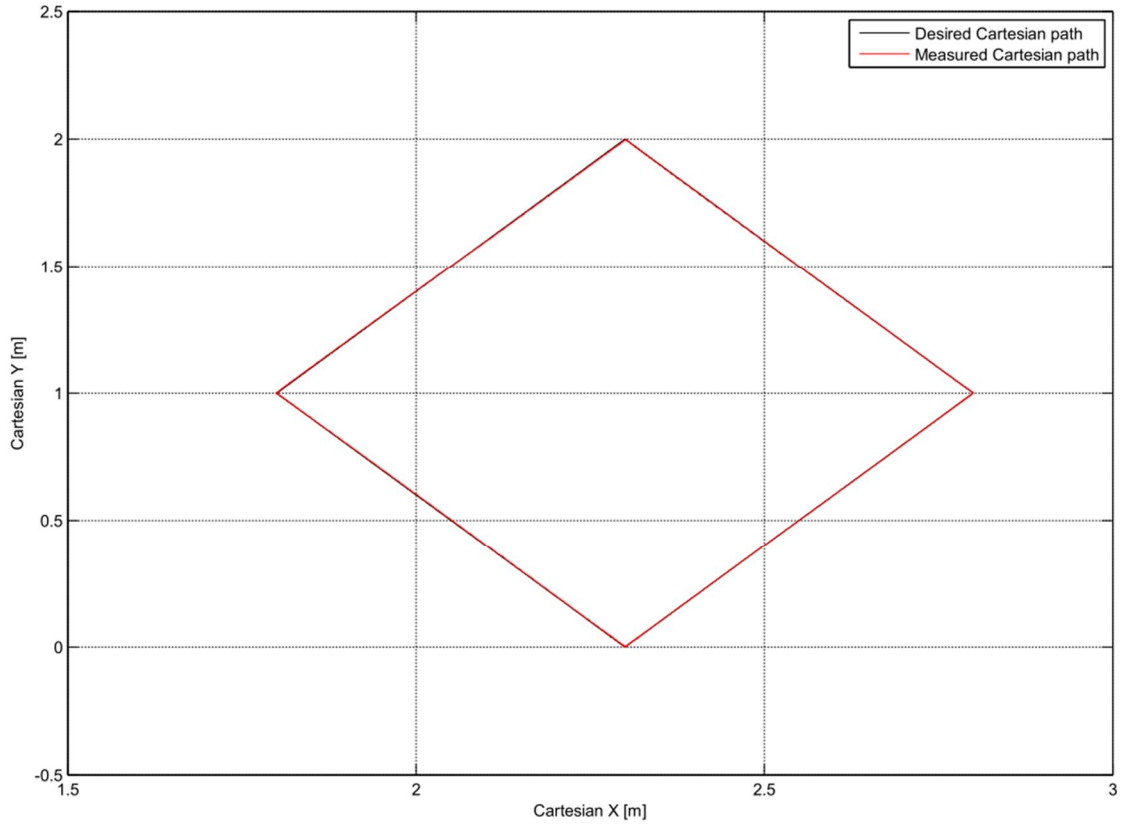

Figure 57: Desired and measured Cartesian paths with VDC-controller under Cartesian transition time of 10s.

The Cartesian position tracking error in Figure 58 is given in the view of equation (J.1).

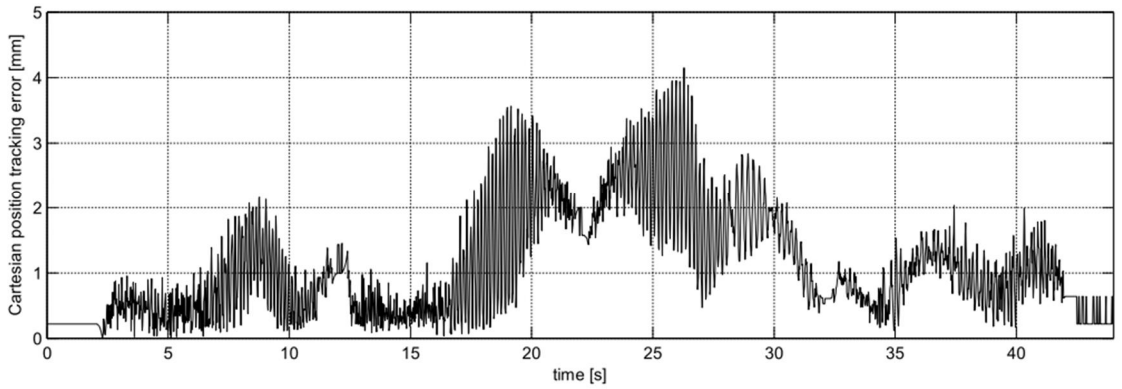

Figure 58: Cartesian position tracking error with VDC-controller under Cartesian transition time of 10s.

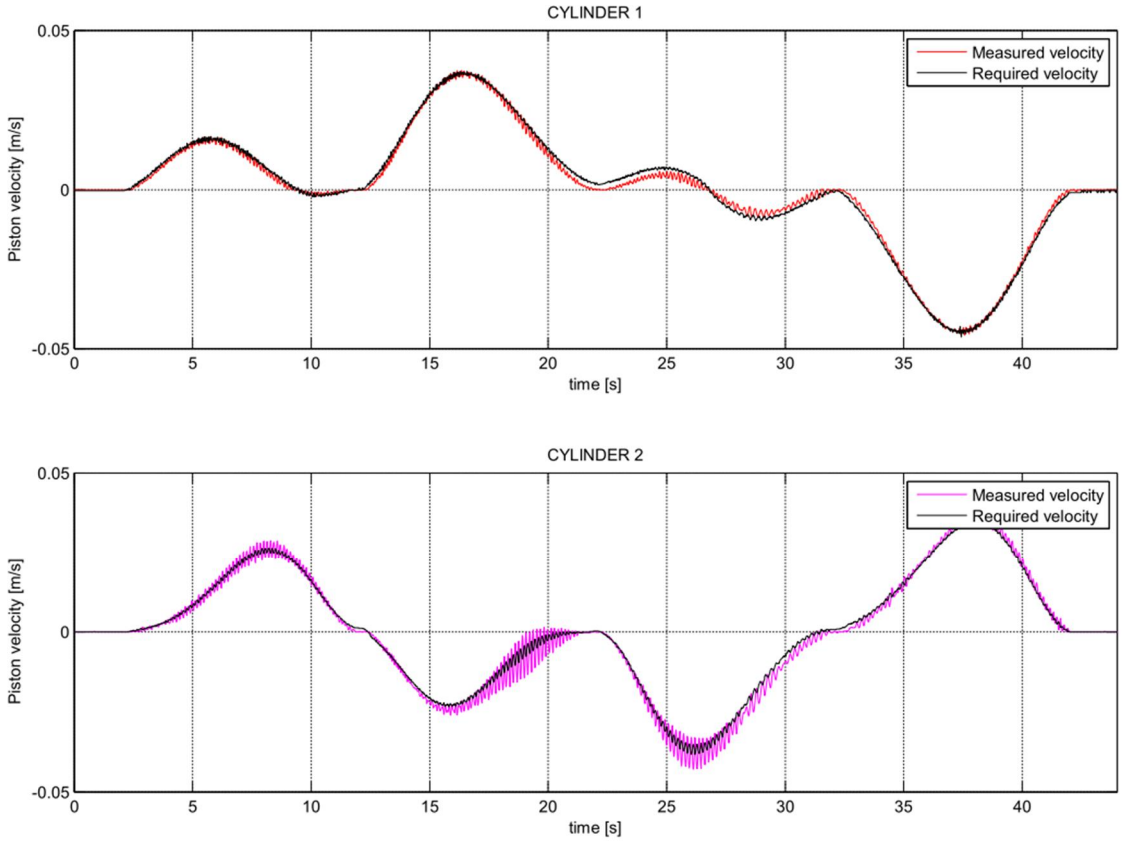

Figure 59: Required and measured piston velocity trajectories with VDC-controller under Cartesian transition time of 10s.

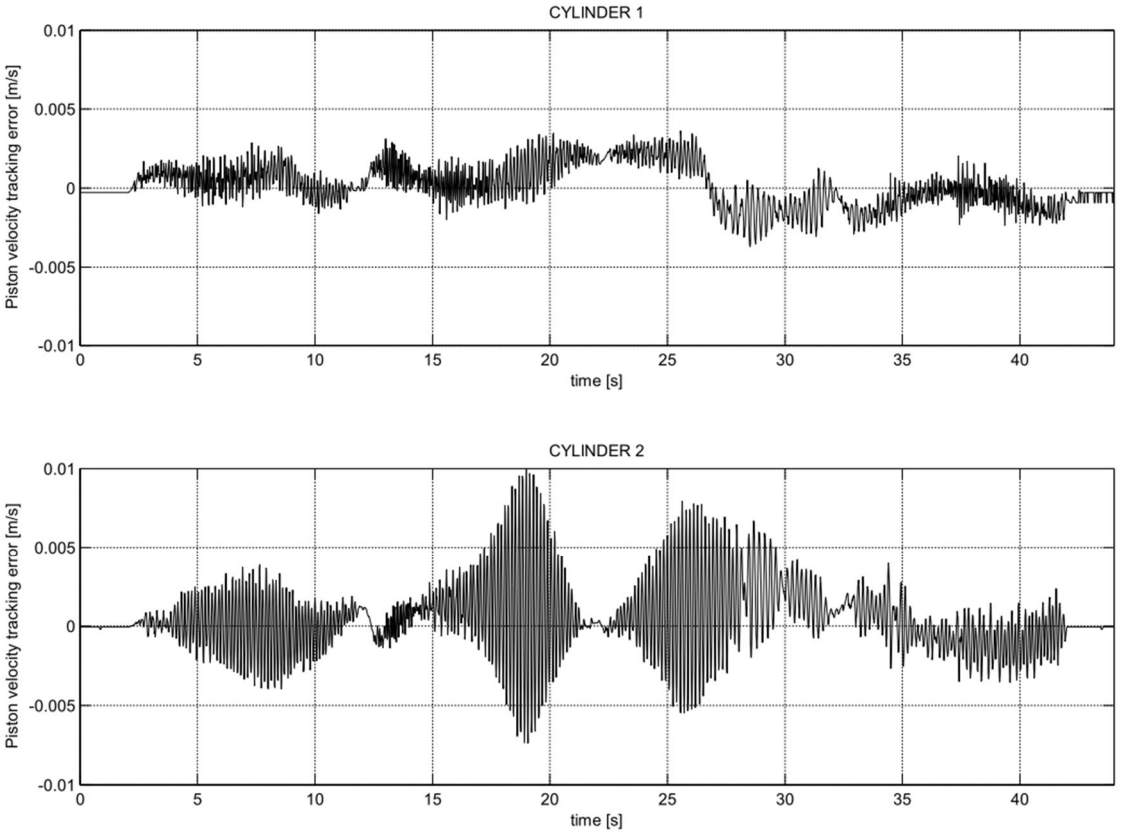

Figure 60: Piston velocity tracking errors with VDC-controller under Cartesian transition time of 10s.

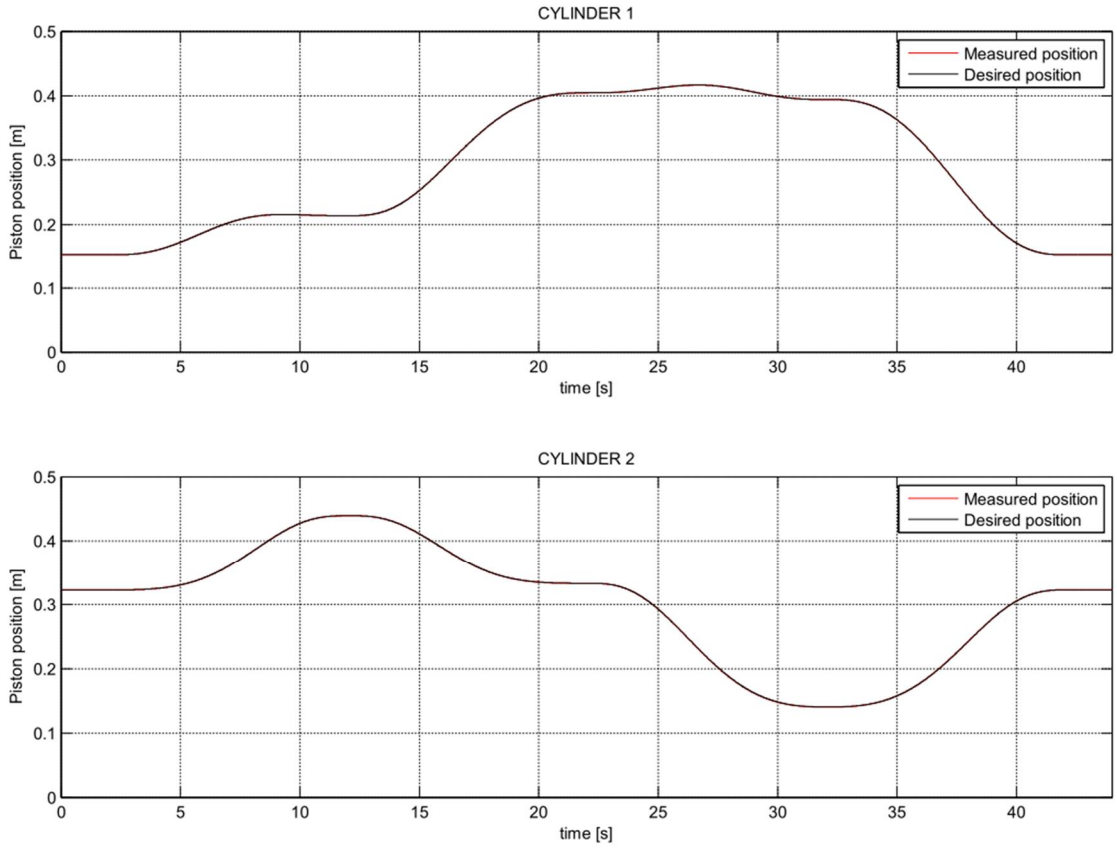

Figure 61: desired and measured piston position trajectories with VDC-controller under Cartesian transiton time of 10s.

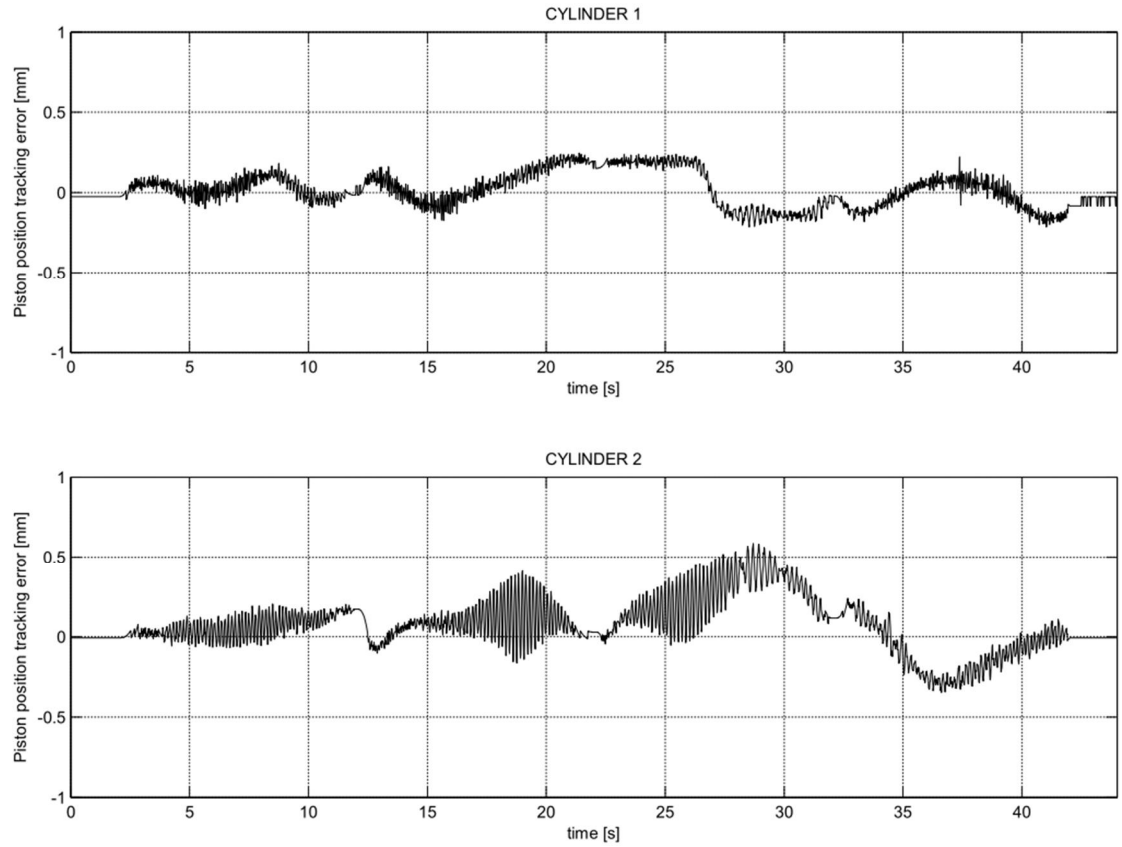

Figure 62: Piston position tracking errors with VDC-controller under Cartesian transition time of 10s.

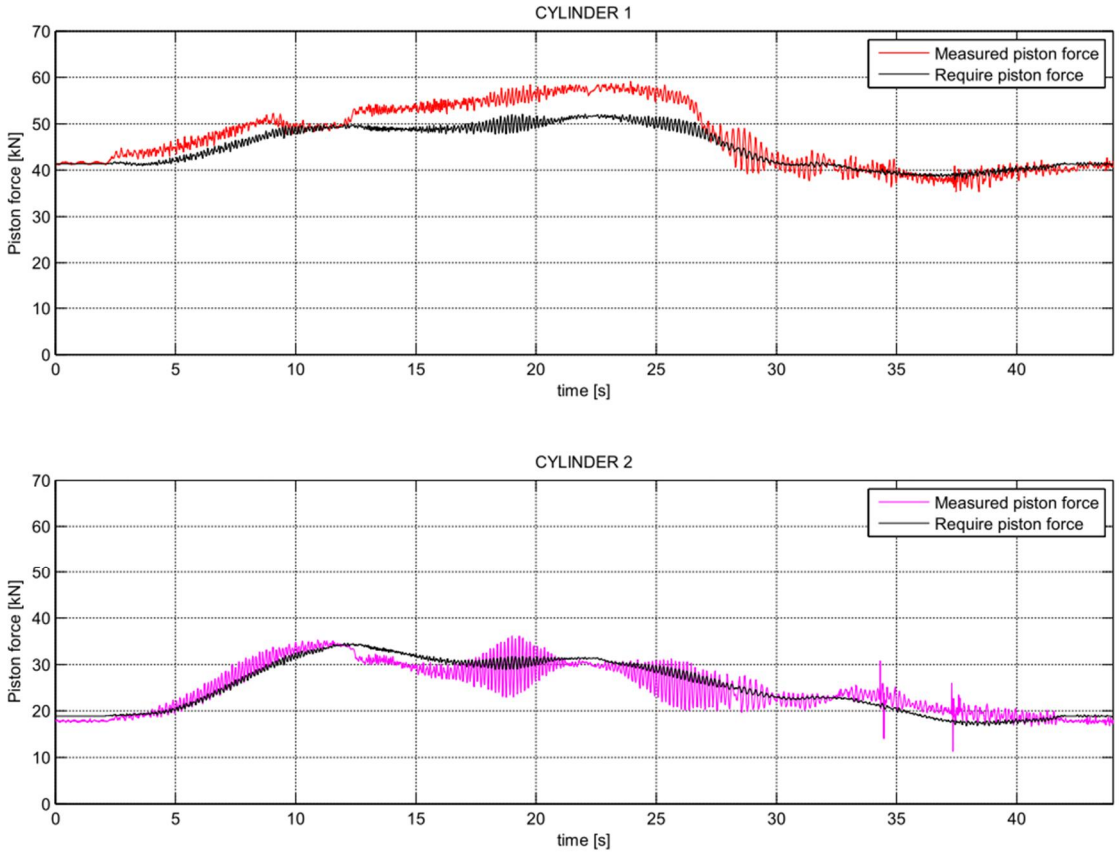

Figure 63: Required and measured piston forces with VDC-controller under Cartesian transition time of 10s.

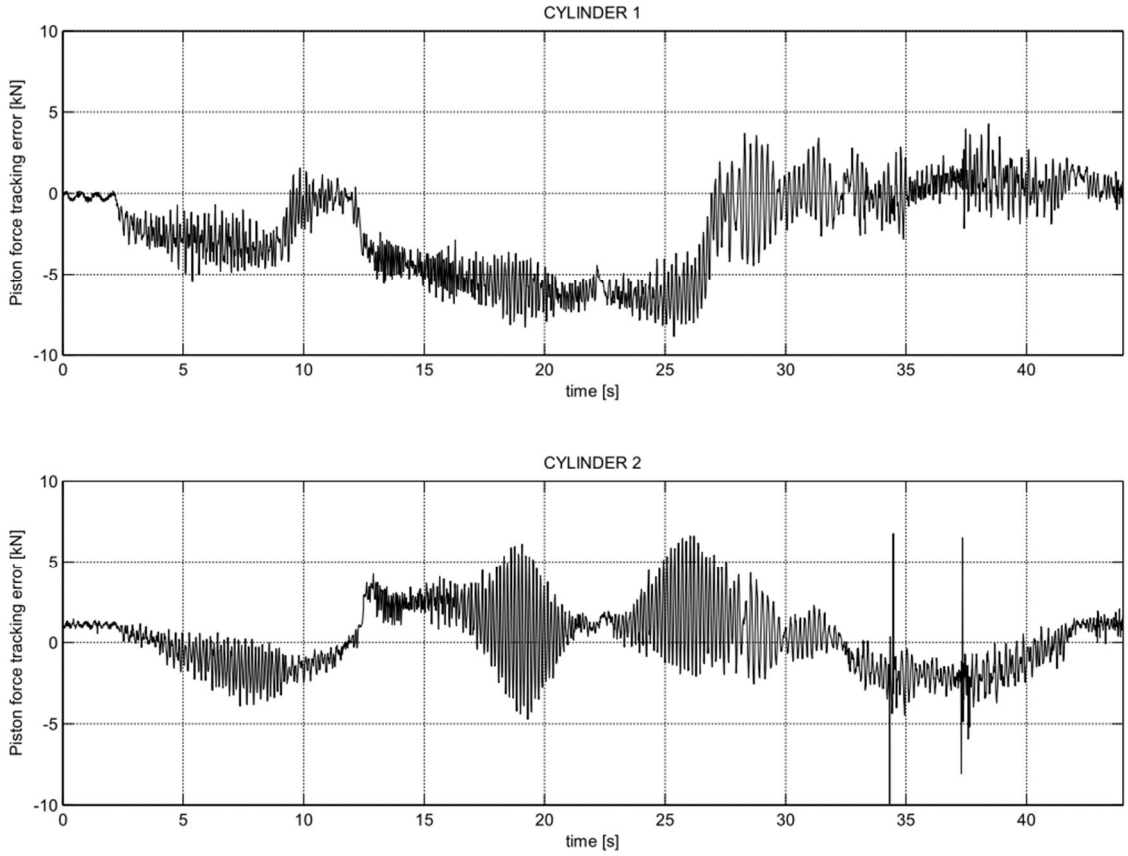

Figure 64: Piston force tracking errors with VDC-controller under Cartesian transition time of 10s.

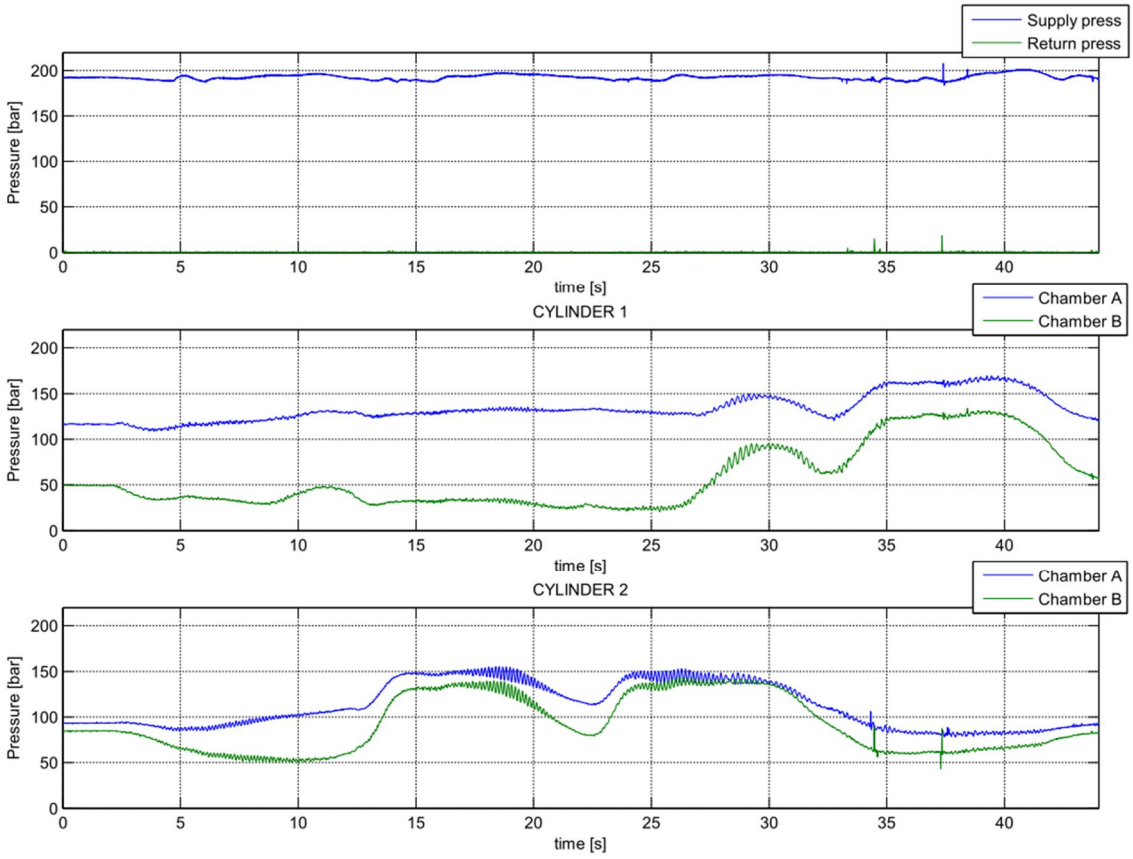

Figure 65: System pressures with VDC-controller under Cartesian transition time of 10s.

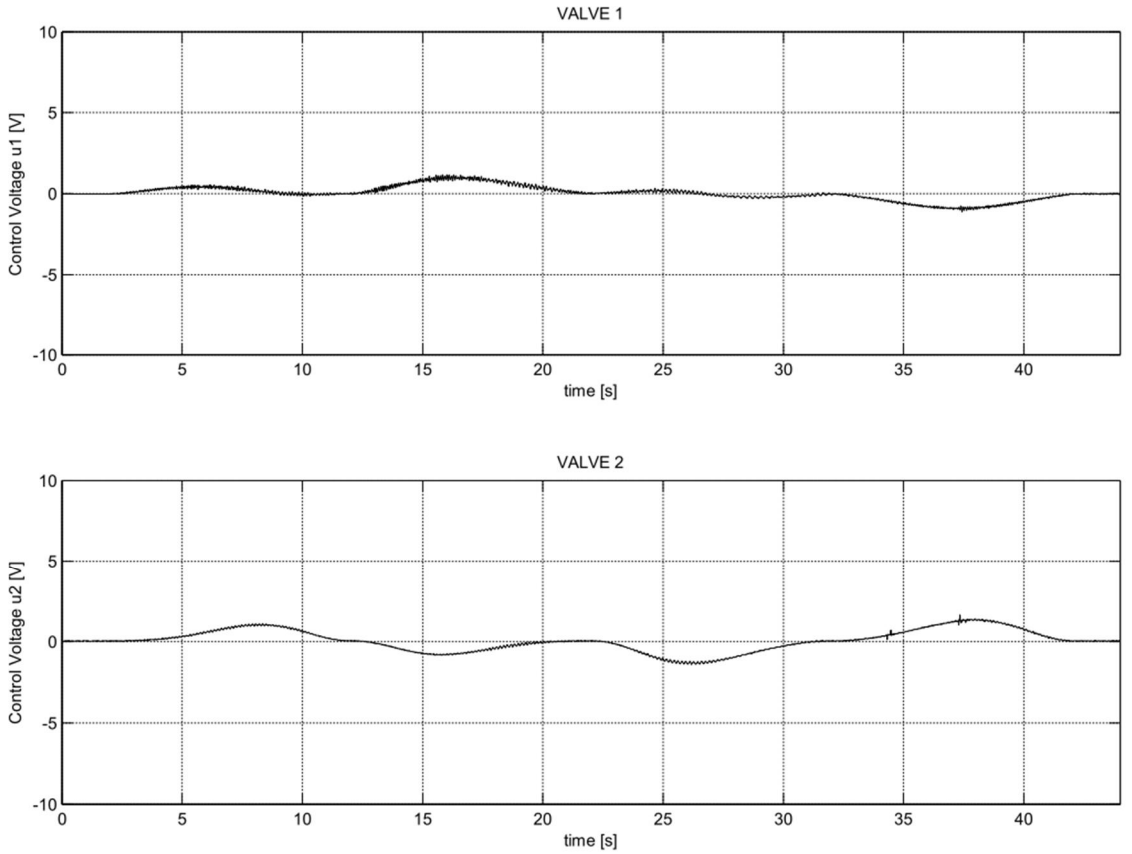

Figure 66: Valve control voltages with VDC-controller under Cartesian transition time of 10s.

APPENDIX M: MEASURED PID-CONTROLLER RESULTS WITH CARTESIAN TRANSITION TIME OF 5 s.

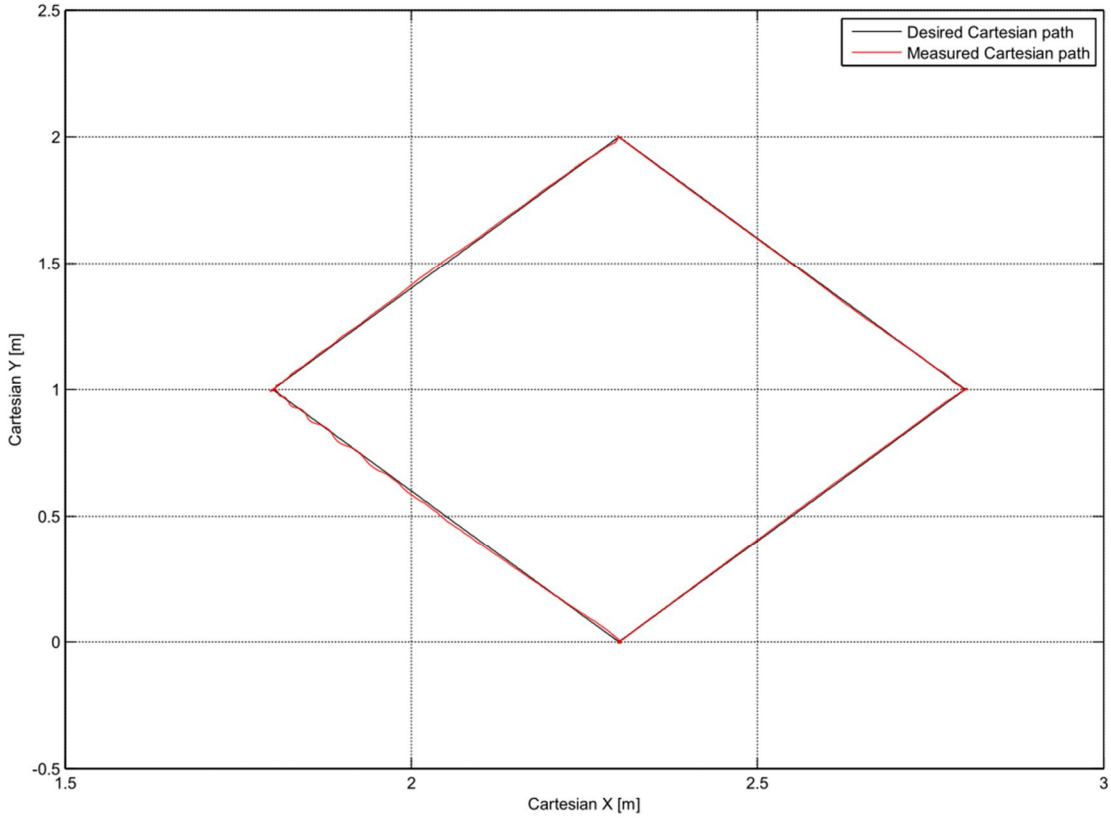

Figure 67: Desired and measured Cartesian paths with PID-controller under Cartesian transition time of 5 s.

The Cartesian position tracking error in Figure 68 is given in the view of equation (J.1).

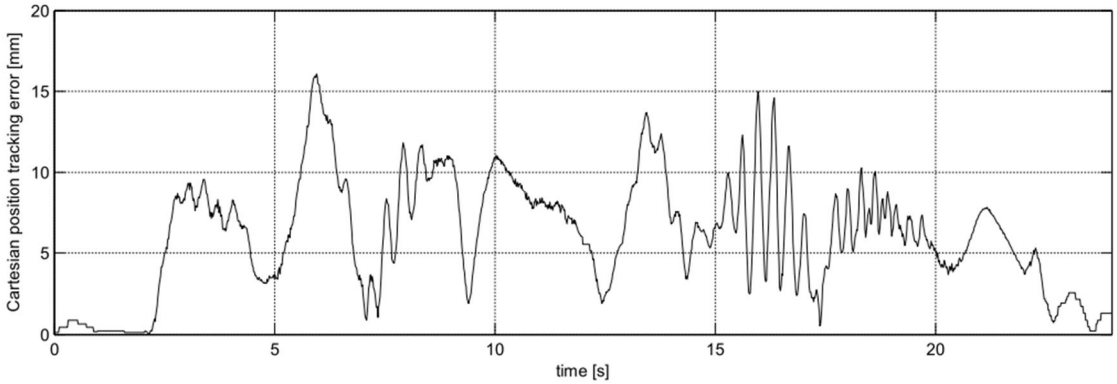

Figure 68: Cartesian position tracking error with PID-controller under Cartesian transition time of 5 s.

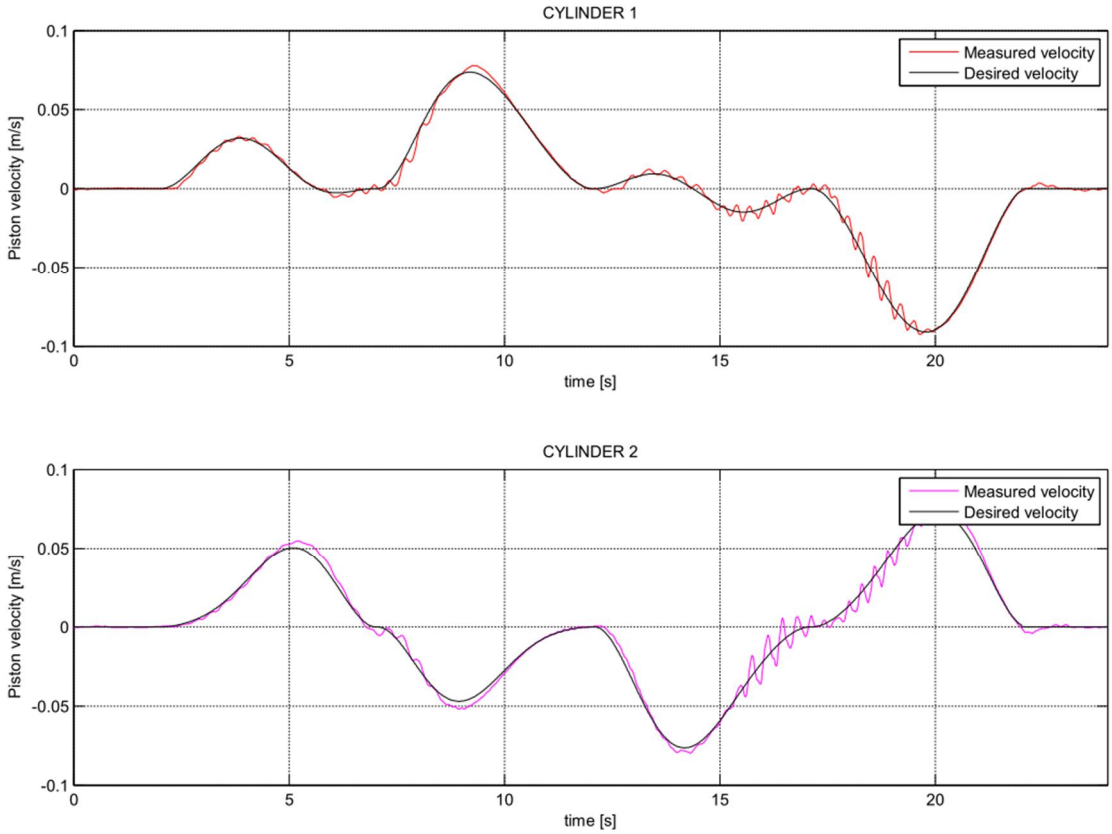

Figure 69: Desired and measured piston velocity trajectories with PID-controller under Cartesian transition time of 5 s.

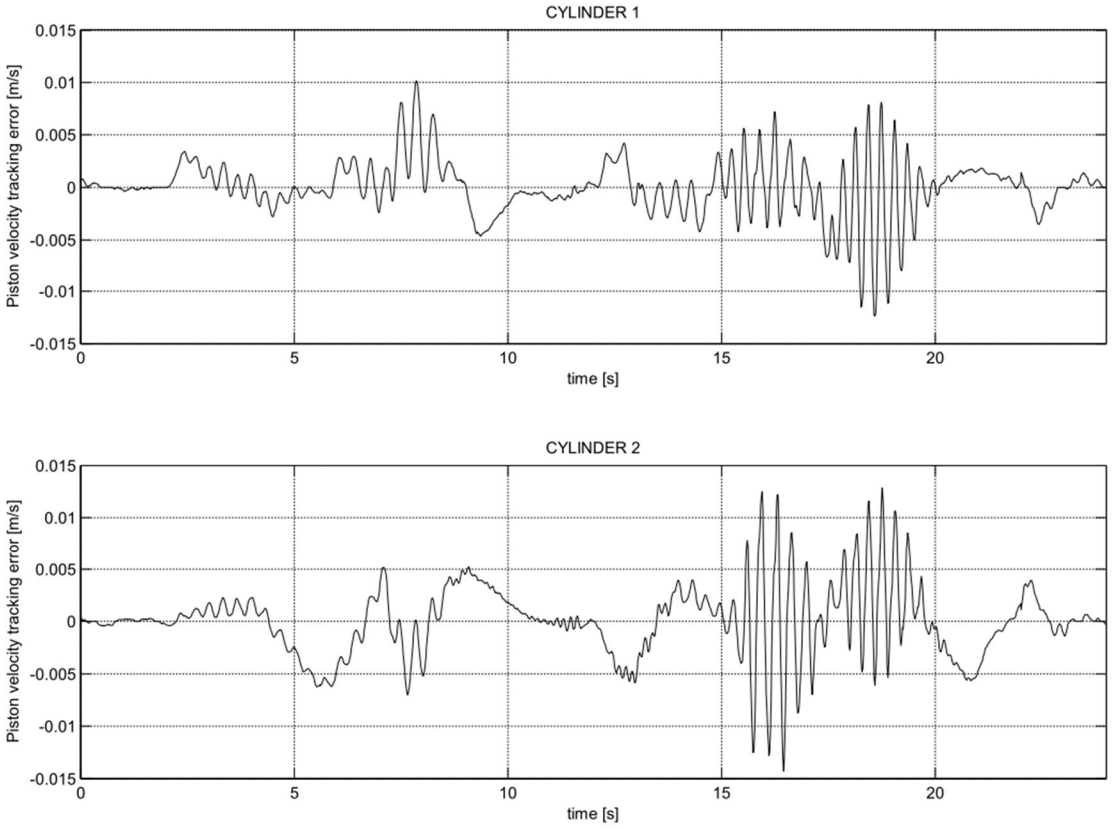

Figure 70: Velocity tracking errors with PID-controller under Cartesian transition time of 5 s.

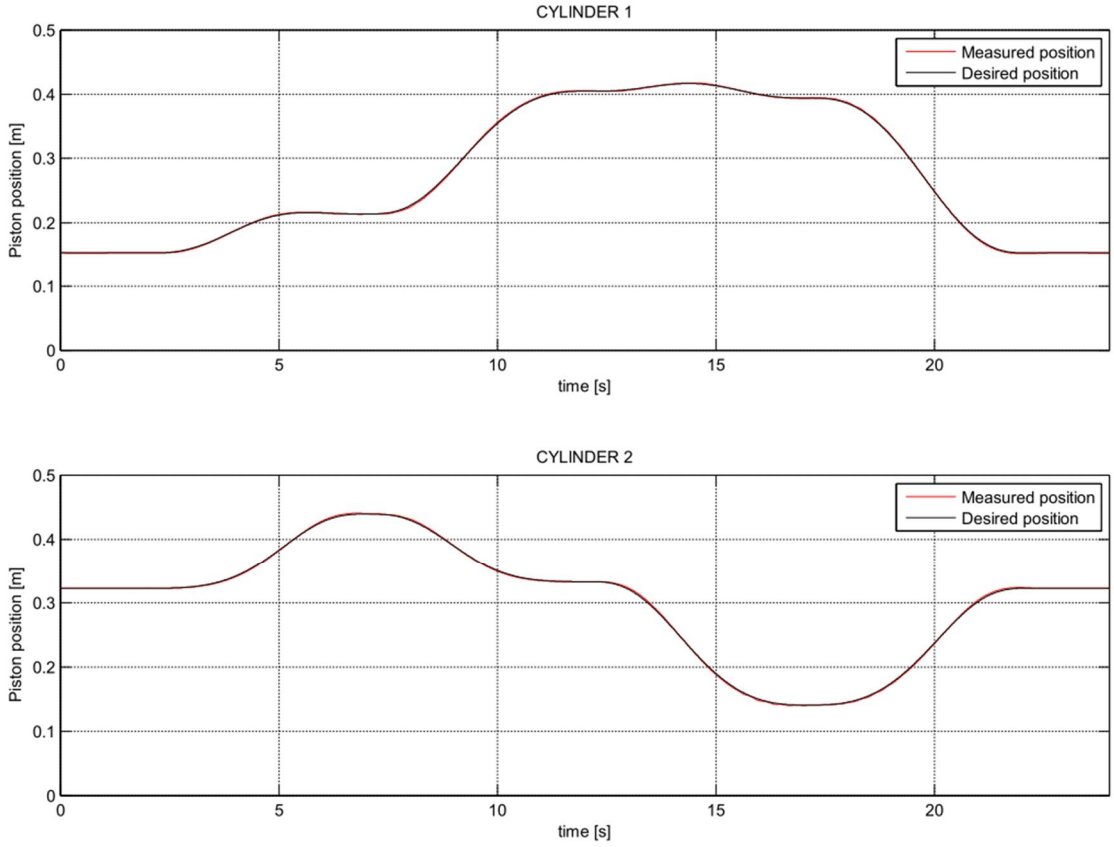

Figure 71: Desired and measured piston position trajectories with PID-controller under Cartesian transition time of 5 s.

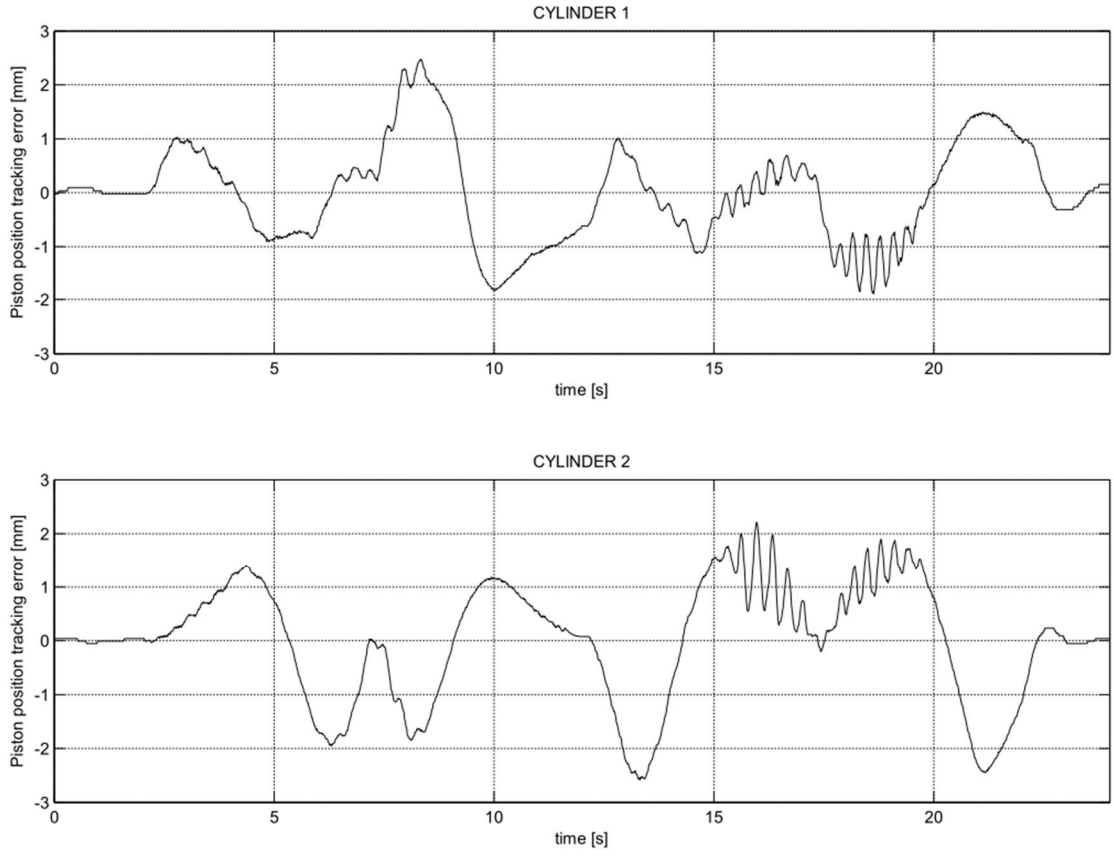

Figure 72: Piston position tracking errors with PID-controller under Cartesian transition time of 5 s.

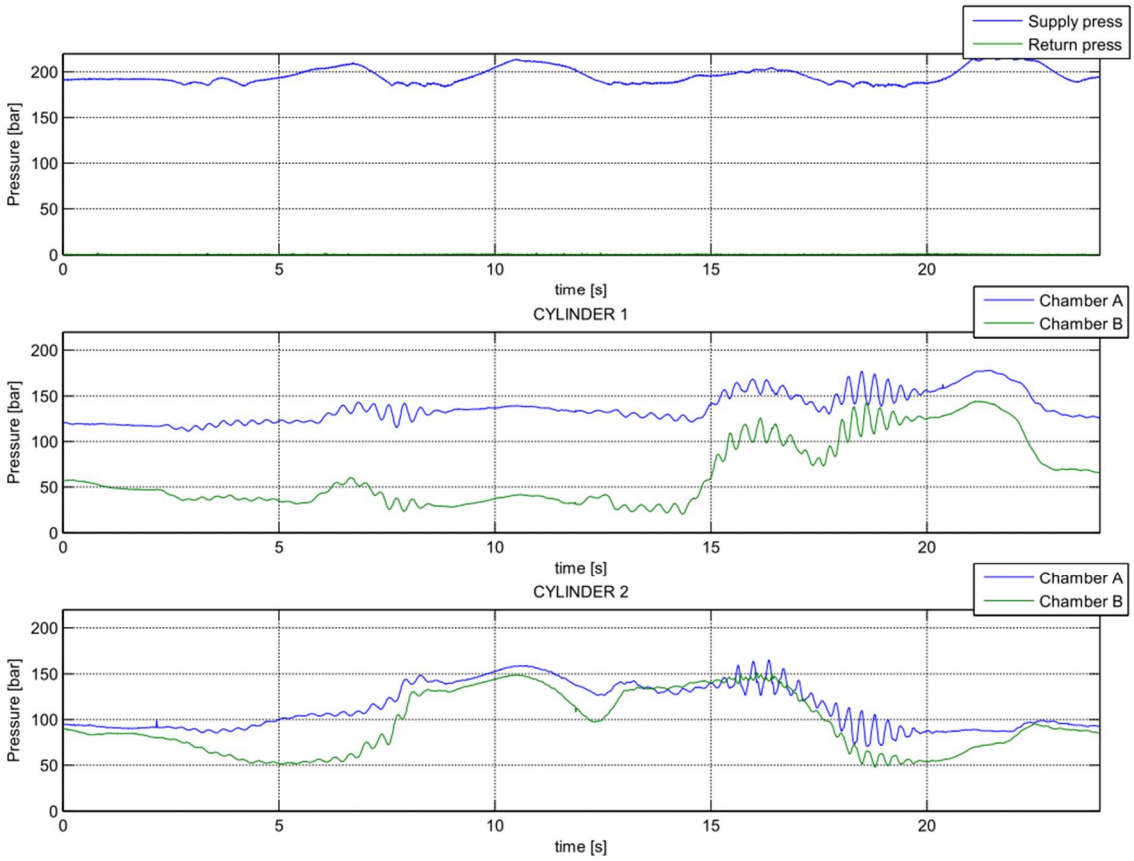

Figure 73: System pressures during Cartesian drive with PID-controller under Cartesian transition time of 5 s.

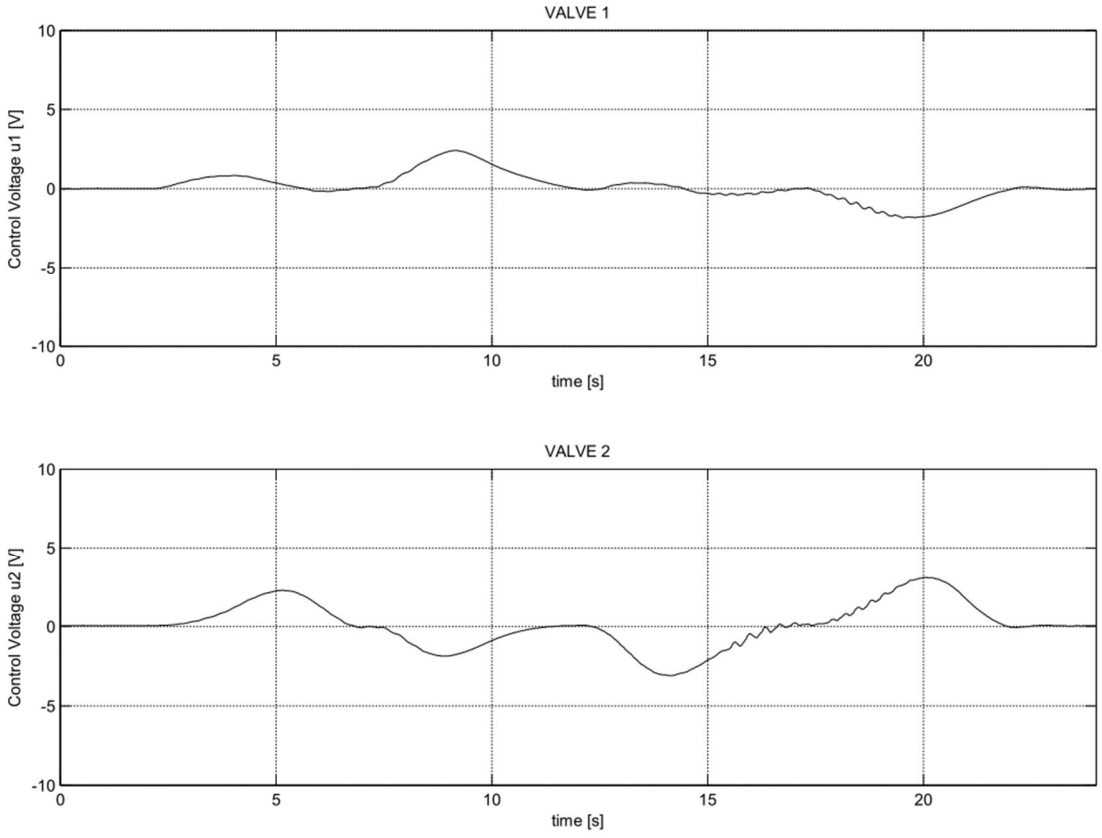

Figure 74: Valve control voltages with PID-controller under Cartesian transition time of 5 s.